

EVALUATION OF NEW TECHNOLOGIES TO SUPPORT ASSET MANAGEMENT OF METRO SYSTEMS

GUNASINGAM RAVINDRAN

**Department of Civil, Environmental and Geomatic Engineering
Faculty of Engineering Science, University College London - U.K**

**A thesis submitted in partial fulfilment of the requirements for the award
of the degree Doctor of Engineering (Eng.D) at the
University of College London**

August 2020

© Gunasingam Ravindran

Declaration of Authorship

I, Gunasingam Ravindran, confirm that the work presented in this thesis is my own. Where information has been derived from other sources, I confirm that this has been indicated in the thesis.

Signed

Date

Abstract

Since 1930, London Underground Limited (LUL) has performed visual inspections to understand the condition of the physical assets such as tunnels, bridges and structures. The major problem with this kind of inspection is the lack in quality of the data, as it depends on the ability of the inspector to assess and interpret the condition of the asset both accurately and with repeatability. In addition, data collection is time-consuming and, therefore, costly when the whole of the metro network needs to be regularly inspected and there are limited periods when access is available. The problems associated with access to the infrastructure have increased significantly with the implementation of the night tube and will increase further as the night tube is extended over the next 5 to 10 years. To determine the condition of metro assets and to predict the need for intervention, monitoring the changes in the assets' condition is key to any further evaluation and maintenance planning.

This thesis presents the outcomes of using new technologies such as Thermography, Kinematic and Static Laser Scanning, Close-Range Photogrammetry and Total Station to measure defects, such as water seepage, mortar loss in joints, lining face loss (in brick tunnels), cracks, corrosion, voids, cavities and spalls. Each technique is explored through three case studies that evaluate the performance and limitation in the determination of the asset condition.

The first case study was performed to compare and contrast the use of Euroconsult's high definition laser survey against a Principal Inspection Report to determine the level of consistency in predicting the asset condition. During this case study, reports from laser surveys and principal inspections of brick tunnels and covered ways were compared. This analysis showed that a direct comparison between the two inspections is not appropriate because the laser inspection does not capture all the defects mentioned in the Engineering Standard S1060. It also showed that to close the gap between the laser survey and visual inspection, laser surveys would have to be performed every year in brick tunnels and then compare any changes in asset condition with that from the previous scan.

The second case study was performed using Infrared Thermography (IRT) to identify water seepage in the brick tunnels as well as test the system in a configuration that would allow the survey to be done from an engineering train. A set of calibration tests were performed in the lab and later the technique was trialled on an engineering train. The results showed that it is possible to measure the level of moisture on specific parts of the lining and that the comparison of surveys performed at different times can allow asset managers

to react before a seepage is established, potentially reducing the risk of system disruption caused by water ingress in tunnels. The data also revealed that this technique could be used for other purposes, such as examining the condition of other assets such as brackets, cable supports and broken light bulbs.

The third case study was performed using a Terrestrial Laser Scanner, Close-Range Photogrammetry and Total Station Survey to identify defects in structures. In order to test these technologies, a wing wall, located on the north-east wing of the HC3 underbridge at Ladbroke Grove Station, was chosen. This case study demonstrated that LUL can easily implement this type of technology to inspect rapidly their buildings and structures, being able to identify defects and monitor their assets for translation, rotation and changes in shape during changes in loading or the decay of the structure (insidious decline) and the construction of nearby assets.

In this research, a large volume of data was captured, and further work is needed in order to manage the data using 'big data' concepts. Although it may not be possible to fully understand the insidious decline of an asset, the use of these techniques allows us to better understand how a civil asset behaves, potentially reducing the amount of reactive maintenance to a minimum, consequently reducing service costs and falls in revenue due to disruptions in the system. To successfully analyse the data from new technologies a combination of skills is required and different or retrained personal will be needed.

Impact Statement

This research work addressed the problem currently faced by London Underground Limited and other metro operators around the world when inspecting their ageing assets. The deterioration and deformation of these assets are currently monitored by regular visual inspections, supported by some form of measurement. The major problem with this kind of inspection is the quality and repeatability of the data as it depends on the ability of the inspector to interpret the information obtained.

This research investigated the application of new methods to the inspection of metro infrastructures, such as Infrared Thermography, Close-Range Photogrammetry and Laser scanner. It also developed a standard approach to the use of these technologies to automate or semi-automate the visual inspections. Leveraging advances in monitoring equipment and sensors to more efficiently perform these activities and enable the capture of reliable and detailed condition data and defects. The use of these technologies will reduce the amount of time taken to perform these activities consequently reducing the track access time required, consequently reducing the resources required and enabling a cost reduction to be achieved. Further benefits will be exploited using the new technologies as the organisation will be able to utilise data not previously available and/or to a higher level of accuracy. This will be a key enabler to move towards more predictive maintenance regimes.

Also, during this research, infrared thermography was used to investigate water seepage in tunnels. Improvements to the management of seepage will lead to performance improvements and cost reductions through the consolidation of information and data sources. The new capability will enable more effective co-ordination with other information and/or asset owners, where the cause of the seepage is from a 3rd Party.

During this research, a methodology was developed using Close Range Photogrammetry and Terrestrial Laser Scanner to identify defects in structures. A case study demonstrated that any infrastructure owner can easily implement this type of technology to inspect rapidly their buildings and structures, be able to identify defects and monitor their assets decay.

The work carried out in this research recommends the use of digital condition data throughout the data management process. This enhances the capability of other infrastructure owners to more effectively and efficiently manage ageing civils assets by enabling Predictive Maintenance (PM) techniques to be implemented.

Acknowledgement

I wish to express my deep gratitude to my academic supervisors' Dr Pedro Ferreira and Prof. Anthony Swain and industrial supervisor Dr Fiona Thomson (London Underground) for their continuous support and encouragement throughout my Eng.D program. Their advice and guidance were essential for the completion of this thesis.

Special thanks are extended to Mr Ash Parmar and Mr Adrian Lintott (London Underground) for their help to organise site trials. I would like to thank Mr Nick Burgess (London Underground) for sharing his knowledge in brick tunnel inspection.

Thanks go to Mr Ben Boorman (UCL) for his support during the lab test work.

Finally, I would like to dedicate this thesis to my wife and my daughter there will never be enough words to express my gratitude for everything you've done for me. I wouldn't be here without your endless love and support (both emotional and financial).

I would like to thank the Engineering Physical Sciences Research Council (EPSRC) and London Underground Limited (LUL) for funding my studies.

Contents

Abstract	v
Impact Statement	viii
Acknowledgement	x
List of Figures	xxi
List of Tables	xxxii
List of Acronyms	xxxvi
Chapter 1. Introduction	1
1.1 Project Background	4
1.2 Research Objectives	6
1.3 Research Methodology	7
1.4 Thesis Outline	8
Chapter 2. Infrastructure Asset Management and Gap Analysis	11
2.1 Introduction	11
2.2 Asset Management Policy, Strategy & Objectives	12
2.3 Asset Management Policy	12
2.4 Asset Management Strategy (AMS)	13
2.4.1 Asset Management Objectives	13
2.5 Asset Management Information System	14
2.5.1 Asset Information Requirements	14
2.6 Asset Data Collection	15
2.7 Asset Failure Mode	16
2.7.1 Failure Treatment Strategies	18
2.8 Whole life value	18
2.9 London Underground Asset Management	20
2.9.1 LUL Vision	20

2.9.2	LUL Civils Assets Strategy	20
2.10	LUL Asset Life Cycle	20
2.11	LUL Asset Maintenance Regimes	21
2.12	LUL Inspection.....	22
2.12.1	Principal Inspection	24
2.12.2	Special Inspection	24
2.12.3	Inspections for Analytical Assessment	24
2.13	Planned Preventive and Corrective Maintenance.....	27
2.14	Predictive and Preventive Maintenance	28
2.15	Gap Analysis: LUL Civil Infrastructure Asset Management	29
2.15.1	Introduction	29
2.15.2	Current Conditions of the LUL's Assets.....	29
2.15.3	Gap Identification	31
2.15.4	Factors Responsible for the GAP	33
2.15.5	The Future State	33
2.15.6	Remedies, Actions and Proposals.....	34
Chapter 3. Case Study - Brick Tunnels - Defects Comparison and Change Detection		36
3.1	Introduction.....	36
3.2	Literature Review.....	38
3.2.1	Tunnel Inspection Methods	41
3.3	Requirements of a Brick Tunnel Inspection	44
3.3.1	The standard for the Inspection of Bridges and Structures- S1060	45
3.3.2	The Management System Work Instructions Inspecting Brick Tunnels W2822.....	47
3.3.3	Completion of Brick Tunnel Inspection Charts	47

3.3.4	The Management System Work Instructions- W2909- Producing A Brick Tunnel Inspection Chart.	48
3.4	Changes in Condition of an Asset	49
3.4.1	Water Seepage / Ingress.....	49
3.4.2	Bulging	50
3.4.3	Drummy/Hollow Brickwork	51
3.4.4	Efflorescence	51
3.4.5	Fractures and Cracks.....	52
3.4.6	Hairline and Dimension	53
3.4.7	Joint Loss	53
3.4.8	Leached Deposits and Surface Deposits	54
3.4.9	Spalling and Missing Brick Works	54
3.4.10	Repairs.....	55
3.4.11	Intrusive Vegetation.....	55
3.4.12	Wet or Damp Areas.....	56
3.5	Selection of Appropriate Technologies	57
3.6	Scanning System Description.....	60
3.7	Tunnelling System Description	63
3.7.1	Principles of the survey system (3D-camera-laser units)	65
3.7.2	Acquisition and synchronization software.....	66
3.7.3	Data provided by the Tunnelling System.....	66
3.7.4	LIDAR System Description.....	67
3.7.5	Visible infrared cameras.....	68
3.8	Raw Data Analysis	69
3.8.1	Evaluation of tunnels conditions using laser survey	70
3.9	Principal Inspection (Visual Inspection)	74
3.10	Inspection Frequency	79

3.11	Euroconsult's Laser Scanner First Inspection 2014.....	80
3.11.1	Description of the Laser Survey	80
3.11.2	Laser Scanning Inspection	81
3.11.3	Data Analysis	85
3.11.4	Comparison of Visual Inspection and Laser Scanner Inspection of Assets	89
3.12	Comparison of defects identified by the Visual Inspection and the Laser Inspection	114
3.12.1	Principal Inspection process.....	114
3.12.2	Defects Identified by Euroconsult high definition laser scanning system	117
3.12.3	Comparison of defects	117
3.12.4	Joint loss	119
3.12.5	Dampness/water ingress.....	120
3.12.6	Lining face loss/Spalling.....	121
3.12.7	Cracks/Fractures.....	122
3.13	Description of Euroconsult's Laser Scanner Second Inspection 2015	123
3.14	Laser Survey Flow Chart	125
3.15	Condition Survey	127
3.16	Laser scanning scores comparison between 2014 and 2015 inspection	127
3.17	TUNNEL 6	137
3.17.1	Lining Face Loss	138
3.17.2	Mortar Loss in Joints	139
3.18	TUNNEL 17	140
3.18.1	Damp patch.....	142
3.18.2	Cracking.....	147

3.18.3	Mortar loss in joints	148
3.18.4	Lining face loss.....	149
3.18.5	Brackets and Deflector plates	152
3.19	TUNNEL 53	154
3.19.1	Cracking	155
3.19.2	Mortar loss in joints	157
3.19.3	Face loss/ spalling.....	161
3.19.4	Damp patches	162
3.19.5	Repaired area	163
3.20	TUNNEL 56	164
3.20.1	Seepage/ Damp patches.....	165
3.20.2	Mortar loss in Joint	167
3.21	Tunnel 72.....	168
3.22	Ranges of Interpretative Variability for Each Inspection	169
3.23	Evaluation of Laser and Visual Inspection performance against requirements	171
3.24	Requirements for Replacing Existing Methodology	182
3.24.1	Organisational Change Processes	182
3.24.2	Changes to Standards.....	182
3.24.3	IM Support and Resources Needed	183
3.25	Advantage and Limitation of Technology.....	183
3.25.1	Advantages	183
3.25.2	Limitations	186
3.26	Integration of Different Technologies with Laser Survey	187
3.27	Conclusions	188
Chapter 4. Application Of Infrared Thermography		191
4.1	Introduction.....	191

4.2	Literature Review.....	191
4.2.1	Fundamentals of Infrared Thermography	191
4.2.2	Active and Passive Thermography.....	194
4.2.3	Detection of Moisture by Infrared Thermography	196
4.3	Laboratory Testing.....	198
4.3.1	Sensors Calibration.....	198
4.3.2	Humidity Sensor Calibration.....	199
4.3.3	Check for the Temperature Sensors	203
4.4	Experiment # 1 Set-Up	205
4.4.1	Thermal Imaging Camera.....	207
4.4.2	Data Acquisition	207
4.4.3	Data Analysis	207
4.4.4	Experiment # 1 Conclusion	222
4.5	Experiment # 2 Set-Up	223
4.5.1	Data Analysis	225
4.5.2	Experiment #2 Conclusions.....	242
4.6	Thermography Site Trial	243
4.6.1	Introduction	243
4.6.2	Water Ingress/Seepage into London Underground Assets	243
4.7	Scanning Methodology	245
4.8	Method- Detection of Water Seepage/Ingress.....	246
4.9	Data Analysis.....	247
4.10	Tunnel 58 (TL58).....	248
4.11	Tunnel 41 (TL 41).....	254
4.12	Tunnel (TL 77).....	259
4.13	Thermography Site Trial Conclusion	263

Chapter 5. Case Study - HC3 Underbridge North East Wing Wall Monitoring	265
5.1 Introduction.....	265
5.2 Structural Health Monitoring (SHM).....	266
5.3 Site Location and Description of Structures.....	270
5.3.1 Principal Inspection Report	273
5.4 Geology and Reason for Monitoring	273
5.5 Total Station Survey	275
5.5.1 Targets	276
5.5.2 Reference framework.....	277
5.5.3 Total Station Monitoring Setup	278
5.6 Terrestrial Laser Scanner (TLS)	280
5.6.1 Principles of Laser Scanning.....	283
5.6.2 Error sources of laser scanning points	286
5.6.3 TLS Survey Planning.....	288
5.6.4 TLS Instrumentation	288
5.6.5 TLS Data Collection	290
5.6.6 Registration and Geo-Referencing	292
5.6.7 Cyclone - Data Processing.....	292
5.7 Close Range Photogrammetry (CRP)	295
5.7.1 Digital Camera.....	298
5.7.2 Artificial Target Selection.....	299
5.7.3 Photogrammetry Data Capturing.....	300
5.7.4 Data Processing.....	302
5.7.5 Camera calibration	302
5.8 Change Detection and Deformation Analysis	305
5.8.1 Point-to-point-based deformation	306

5.8.2	Point-to-surface-based deformation	306
5.8.3	Surface to surface-based deformation	307
5.9	Data Analysis and Results.....	307
5.9.1	Comparison between Total Station (TS), Terrestrial Laser Scanner (TLS) and Close-Range Photogrammetry (CRP)	307
5.10	Point Cloud Comparison in Cloud Compare	314
5.11	TLS and CRP results.....	315
5.11.1	TLS Results.....	316
5.11.2	CRP Results.....	322
5.12	Further Analysis of Terrestrial Laser Scanner (TLS) and Close-Range Photogrammetry (CRP) data	330
5.12.1	Comparison of movements between top, middle and bottom strips of wall	333
5.12.2	Comparing Terrestrial Laser scanner and Close-Range Photogrammetry point clouds	335
5.12.3	Comparison between the first and last epoch of laser scanner and photogrammetry.....	336
5.13	Conclusion.....	339
Chapter 6. Conclusions and Future work.....		341
6.1	Introduction.....	341
6.2	Conclusions.....	341
6.3	Future work.....	343
References and Bibliography		348
Appendix A:- Tunnel laser survey with severity scores- Euroconsult		367
Appendix B:- Summary of Scores laser survey (2014) and visual inspection		369
Appendix C:- Tunnel Chart- Tunnel 26.....		376
Appendix D:- Incidents identified by the laser survey for TL 26.....		377

List of Figures

Figure 2-1 Decision required throughout asset lifecycle	21
Figure 2-2 Water Ingress; harmless drip (A1)	25
Figure 2-3 Water ingress; Rail Corrosion, Signalling fault (A4)	25
Figure 2-4 Water ingress; short circuit – earth fault or Burning (A2)	26
Figure 2-5 Acidic soil (B4)	26
Figure 2-6 Soil ingress (C4)	26
Figure 2-7 Corrosion (B3)	27
Figure 2-8 Overstress (B2)	27
Figure 3-1 Inspection using an impact hammer	42
Figure 3-2 ROBO-SPECT System - Concept	43
Figure 3-3 Active water seepage (TL 14, LUL 2011)	50
Figure 3-4 Bulging (Mckibbins et.al, 2009).....	50
Figure 3-5 Efflorescence to a brick tunnel(TL27, 2011)	52
Figure 3-6 Fractures and Cracks	52
Figure 3-7 Hairline crack (Technical user manual, 2009).....	53
Figure 3-8 Joint loss (TL60, 2012)	53
Figure 3-9 Leached deposits (TL56, LUL 2013).....	54
Figure 3-10 Spalling and missing brick works (W2822, 2014)	55
Figure 3-11 Repaired work (TL14, LUL 2011)	55
Figure 3-12 Intrusive vegetation (TL10, LUL 2011).....	56
Figure 3-13 Wet or damp area (TL14, 2011)	57
Figure 3-14 Schematic diagram of the cameras mounted on the flat trolley (Euroconsult, 2014).....	61
Figure 3-15 View of the side sensors that inspect the sidewalls (Euroconsult, 2014).....	62
Figure 3-16 Tunnel scanning sensor Deployment (Laurent, 2014)	63
Figure 3-17 Laser-camera units/laser line projector and digital scanning camera (Euroconsult, 2016).....	64
Figure 3-18 The odometer(Euroconsult, 2016)	65
Figure 3-19 Principles of the survey system (3D-camera-laser units).....	66
Figure 3-20 Resolution Vs Inspection speed (Laurent, 2014)	67
Figure 3-21 Mortar loss in joints- 3D segment re-construction.....	67

Figure 3-22 Point cloud of the underground tunnel(Euroconsult, 2016)	68
Figure 3-23 Set of illuminators and Infrared Cameras(Euroconsult, 2016) ..	68
Figure 3-24 Data acquired in complete darkness.....	69
Figure 3-25 Division of tunnels for visual inspection(Network Rail, 2014)....	78
Figure 3-26 Metal frame with six sensors on a flat wagon	81
Figure 3-27 Tunnel Defects Key	82
Figure 3-28 Number of Assets Vs percentage difference	86
Figure 3-29 Laser Survey vs Visual Inspection Rating of 112 assets in the SSL	87
Figure 3-30 General view of the covered way 15(LUL, 2011)	90
Figure 3-31 North abutment 1mm open horizontal fracture(LUL, 2011).....	90
Figure 3-32 General view of tunnel 17 (LUL, 2011)	94
Figure 3-33 Laser inspection water seepage -TL17.....	94
Figure 3-34 Visual inspection water seepage – TL17 (LUL, 2011)	95
Figure 3-35 Laser inspection Mortar loss in joints- TL17 (LUL, 2011).....	95
Figure 3-36 Visual inspection Mortar loss in joints – TL17, LUL 2013	96
Figure 3-37 Laser inspection Dampness TL-17	96
Figure 3-38 Visual inspection water seepage tunnel chart TL-17(LUL, 2011)	97
Figure 3-39 Face loss in the arch soffit-TL17.....	97
Figure 3-40 General view of the tunnel TL 56 (LUL, 2011)	99
Figure 3-41 Laser Inspection Dampness- TL56.....	100
Figure 3-42 Visual Inspection Wet area TL56 (LUL, 2011)	100
Figure 3-43 Laser Inspection Face and Joint loss- TL56	101
Figure 3-44 Visual Inspection Face and Joint loss- TL56 (LUL, 2011).....	101
Figure 3-45 Laser inspection Repaired area-TL56.....	102
Figure 3-46 Visual Inspection Repaired area - TL56 (LUL, 2011).....	102
Figure 3-47 Laser Inspection Re-pointing work - TL56	103
Figure 3-48 Visual Inspection Re-pointing work- TL56 (LU, 2011).....	103
Figure 3-49 TL60 view from Bayswater station end (LUL, 2011)	105
Figure 3-50 Laser Inspection Joint loss - TL60	106
Figure 3-51 Visual Inspection Joint loss- TL60 (LUL, 2011)	106
Figure 3-52 Laser inspection Dampness- TL60	106
Figure 3-53 Visual inspection Water Seepage -TL60 (LUL, 2011).....	107

Figure 3-54 General View of CW61 (LUL, 2011)	109
Figure 3-55 General view facing East to the West end of the tunnel (LUL, 2012)	111
Figure 3-56 Laser Inspection Dampness- TL53.....	112
Figure 3-57 Visual Inspection Active Seepage- TL53 (LUL, 2011)	112
Figure 3-58 Standard defect notation masonry structures and structural components (S1060, 2011).....	115
Figure 3-59 London Underground Inspection Tunnel Chart.....	116
Figure 3-60 Rotamag tower set-up used for visual inspection (Permaquip, 2016).....	116
Figure 3-61 Tunnel 17 (D104 / TL17) visual inspection chart	118
Figure 3-62 Dampness show in laser inspection 2014.....	118
Figure 3-63 Joint loss identified by the Laser Survey 2014.....	119
Figure 3-64 Joint Loss comparison between visual inspection and Laser Inspection	120
Figure 3-65 Dampness Comparison between Visual Inspection and Laser inspection.....	121
Figure 3-66 Lining face loss comparison between Visual Inspection and Laser Inspection	122
Figure 3-67 Cracking Laser Inspection	123
Figure 3-68 Laser scanning inspected section in the District Line	124
Figure 3-69 Laser scanning inspected section in the Metropolitan Line.....	125
Figure 3-70 Euroconsult's Laser Scanner Workflow	126
Figure 3-71 Comparison of tunnel scores between 2014 and 2015 Laser inspection.....	129
Figure 3-72 Comparison of cracking between 2014 and 2015 Laser inspection	131
Figure 3-73 Comparison of damp patches between 2014 and 2015 Laser inspection.....	132
Figure 3-74 Comparison of Joint Loss between 2014 and 2015 Laser inspection.....	133
Figure 3-75 Comparison of face loss between 2014 and 2015 Laser inspection	135
Figure 3-76 TL6 lining face loss at chainage 3- 2015 Laser inspection	139

Figure 3-77 TL 6 Scattered mortar loss in joints at chainage 4- 2015 Laser inspection.....	140
Figure 3-78 TL17- active water seepage at chainage 77, from the arch springer to track level- visual inspection 2013	142
Figure 3-79 TL17 water seepage at chainage 77 -2015 Laser Inspection .	143
Figure 3-80 TL17 no water seepage at chainage 77-2014 Laser Inspection	143
Figure 3-81 TL 17 area of damp patches at chainage 102 2014 and 2015 Laser Inspection.....	144
Figure 3-82 TL 17 area of damp patch at chainage 164 2014 and 2015 Laser Inspection	146
Figure 3-83 TL 17 area of a damp patch at chainage 87 2014 and 2015 Laser Inspection	147
Figure 3-84 TL17 transverse and diagonal cracks at chainage 101 2014 inspection.....	148
Figure 3-85 TL17 mortar loss in joints at chainage 100 2014 and 2015 Laser Inspection	149
Figure 3-86 TL17 lining face loss at chainage100 2014 Laser inspection..	150
Figure 3-87 TL17 lining face loss at chainage100 -2015 Laser inspection ..	151
Figure 3-88 Spalling North abutment at chainage 513m from West Visual Inspection-2013	151
Figure 3-89 TL17 no spalling around recess area at chainage 513m	152
Figure 3-90 Deflector plates.....	153
Figure 3-91 Cable brackets.....	153
Figure 3-92 TL53 vertical crack at south abutment 581m from west visual inspection.....	155
Figure 3-93 Vertical crack at South abutment 581m from West-2014 Laser inspection.....	156
Figure 3-94 Vertical crack at South abutment 581m from West-2015 Laser inspection.....	157
Figure 3-95 TL53 mortar loss in joints.....	158
Figure 3-96 Mortar loss in joints, (enlarged)	158
Figure 3-97 TL53 mortar loss in joints- profile.....	159
Figure 3-98 TL 53 Locations of mortar loss in joints at chainage 220 2014 Laser inspection.....	160

Figure 3-99 TL53 face loss at chainage 470 2015 Laser survey	161
Figure 3-100 TL53 face loss at chainage 470 visual inspection.....	162
Figure 3-101 TL53 active water seepage at north abutment chainage between 95m and 100m West.....	162
Figure 3-102 TL53 water seepage between chainage 95m and 100m	163
Figure 3-103 TL53 repaired area	164
Figure 3-104 TL56 water seepage at 2014 scan.....	166
Figure 3-105 TL56 no water seepage at 2015 scan.....	166
Figure 3-106 TL56 visual inspection wet area (LUL, 2011).....	166
Figure 3-107 TL56 mortar loss in joints at chainage 100m south sidewall visual inspection, 2013	167
Figure 3-108 TL56 mortar loss in joints at chainage 100 2014 laser inspection	168
Figure 3-109 Defects along tunnel 26	185
Figure 3-110 Visual Image and Thermal Image can be viewed in parallel .	187
Figure 4-1 Electromagnetic Spectrum (Barreira <i>et al.</i> 2012).....	192
Figure 4-2 Calibration using Potassium Sulphate	200
Figure 4-3 Calibration using Sodium Bromide.....	201
Figure 4-4 Calibration using Sodium Chloride.....	201
Figure 4-5 Regression line for each sensor	203
Figure 4-6 Temperature sensor calibration using hotplate and ice cubes..	204
Figure 4-7 Thermometer and sensor temperature during calibration	205
Figure 4-8 Location of sensors and source of water	206
Figure 4-9 Cross section of location of sensors and source of water.....	206
Figure 4-10 Reference image (before wetting the wall)	209
Figure 4-11 Image taken after wetting the wall with tap water	210
Figure 4-12 Relative humidity changes with time during before wetting, during wetting and drying process	211
Figure 4-13 Relative humidity sensors (RH1, RH2, RH3 & RH4), Temperature sensors (T1, T2, T3 & T4) and Temperature measured by Thermal camera before wetting	213
Figure 4-14 Relative humidity sensors (RH6), Temperature sensor (T6) and Temperature measured by the thermal camera	214

Figure 4-15 Relative humidity sensors (RH1, RH2, RH3 & RH4), temperature sensors (T1, T2, T3 & T4) and temperature measured by thermal camera during wetting.....	216
Figure 4-16 Relative humidity sensor (RH6), temperature sensor (T6) and temperature measured by the thermal camera during wetting	217
Figure 4-17 Relative humidity sensors (RH1, RH2, RH3 & RH4), temperature sensors (T1, T2, T3 & T4) and temperature measured by thermal camera during drying	219
Figure 4-18 Relative humidity sensor (RH6), temperature sensor (T6) and temperature measured by the thermal camera during drying	220
Figure 4-19 Front side of the test wall.....	224
Figure 4-20 Backside of the test wall	225
Figure 4-21 Moisture meter.....	225
Figure 4-22 Schematic diagram of moisture measurements on the wall....	226
Figure 4-23 Visual image @ 9.25 am.....	228
Figure 4-24 Thermography image @ 9.25 am	228
Figure 4-25 Visual image @ 9.50 am.....	229
Figure 4-26 Thermography image @ 9.50 am	229
Figure 4-27 Visual image @ 10:15 am.....	230
Figure 4-28 Thermography image @ 10:15 am	230
Figure 4-29 Visual image @ 12:00 pm.....	231
Figure 4-30 Thermography image @ 12:00 pm	231
Figure 4-31 Visual image @ 13:00pm.....	232
Figure 4-32 Thermography image @ 13:00 pm	232
Figure 4-33 Moisture measurements @ X, 1, 4,7,10 locations	233
Figure 4-34 Moisture measurements @ X, 2, 5,11,8 locations	233
Figure 4-35 Moisture measurements @ X, 3, 6,9,12 locations	234
Figure 4-36 Maximum moisture content @ each location	234
Figure 4-37 Variation of moisture content at different brick locations over surface temperature differences.	236
Figure 4-38 Variation of moisture content at different mortar locations over surface temperature differences	237
Figure 4-39 Moisture Content of the test wall at 9.25am.....	238
Figure 4-40 Moisture Content of the test wall at 9.50 am.....	239

Figure 4-41 Moisture Content of the test wall at 10.15 am.....	240
Figure 4-42 Moisture Content of the test wall at 12.00 pm.....	241
Figure 4-43 Moisture Content of the test wall at 13.00 pm.....	242
Figure 4-44 Metal frame with Thermal, Laser cameras and infrared red lights on a flat wagon.....	246
Figure 4-45 TL58 drip tray and water seepage location (between 127m and 128m) between Paddington and Edgware Road station	249
Figure 4-46 TL58 drip tray, cable and water seepage between Paddington and Edgware Road stations at chainage 127-128m	250
Figure 4-47 TL58 temperature of different objects between Paddington and Edgware road-stations between chainage 127-128m	251
Figure 4-48 TL58 Moisture content vs. the number of pixels between chainage 127m and 128	253
Figure 4-49 TL 41 drip trays between 90m and 93m Eastbound laser scanner 2015 inspection.....	254
Figure 4-50 TL41 thermogram panorama view between chainage 90m and 93m (Eastbound)	255
Figure 4-51 TL41 temperature measurements of thermograms on different objects between chainage 90m and 93m (East bound)	256
Figure 4-52 TL41 Moisture content vs the number of pixels between chainage 90m and 93m	258
Figure 4-53 TL7 drip trays and water seepage locations between chainages 16m-20m (between Liverpool Street and Aldgate stations -Eastbound) - 2015 Laser Inspection.....	259
Figure 4-54 TL77 thermogram panoramic view between chainage 16m and 20m (southbound).....	260
Figure 4-55 TL77 temperature measurements of thermograms on different objects between chainage 16m and 20m (southbound).....	261
Figure 4-56 TL77 Moisture content vs the number of pixels between chainage 16m and 20m	262
Figure 5-1 Multiview of Abutment and Wing wall	272
Figure 5-2 Diagonal crack to the northeast wing wall adjacent to the east abutment (LUL, principal inspection report 2013)	273

Figure 5-3 Total Station on fixed location for deformation monitoring (image from Geodata).....	276
Figure 5-4 Examples of prism (top) and retroreflective targets (bottom) used with total stations (Soni, 2016)	276
Figure 5-5 Local reference framework	278
Figure 5-6 Total Station - Leica FlexLine TS06.....	279
Figure 5-7 Measurements of targets using Total Station Radiation method	279
Figure 5-8 Static Laser Scanner (Mazzanti, 2016).....	282
Figure 5-9 Kinematic Laser Scanner (Mazzanti, 2016)	282
Figure 5-10 Overview of scanner types and applications.....	283
Figure 5-11 The principle of laser range measurement: (a) Triangulation measurements (Boehler and Marbs (2002) (b) Pulse distance measurements, after Boehler and Marbs (2002) and (c) Phase difference distance measurements, after Van Ree (2006).....	284
Figure 5-12 Comparison between Time of Flight and Phase Shift scanners (Mazzanti, 2016)	286
Figure 5-13 P20 and P40 3D Laser Scanning Product Specification Comparison	289
Figure 5-14 Target T101 fixed on the door –other side of the road.....	291
Figure 5-15 Target T103 fixed on the Lower part of CCTV	291
Figure 5-16 Target T104 top left of the Wing wall	291
Figure 5-17 Constraint list after registering	294
Figure -5-18 Optimize cloud alignment results.....	294
Figure 5-19 Nikon D700 Digital Camera	298
Figure 5-20 Silver Retro Target.....	299
Figure 5-21 point cloud obtained from the CRP and locations of the nine monitoring targets (red circles).....	300
Figure 5-22 Photo capturing method for 3D point cloud construction	301
Figure 5-23 Automated camera calibration parameters generated by Agi-Soft	303
Figure 5-24 Segmented point cloud for plane fitting.....	309
Figure 5-25 Colour surface displacement and histogram output from distance comparison in Cloud Compare.....	310

Figure 5-26 Comparison between TLS, CRP and TS of measuring deviation/deformation at Target points 1,2,3 and 4	312
Figure 5-27 Comparison between TLS, CRP and TS of measuring deviation/deformation at Target points 6,7,8 and 9	313
Figure 5-28 Non-suitable scanner position to scan the area of interest	315
Figure 5-29 Deformation displacement map of the whole wall between Feb16 TLS and March-15 TLS (deflection in metres)	317
Figure 5-30 Deformation displacement map of the whole wall between Feb16 TLS and June-15 TLS (deflection in metres)	318
Figure 5-31 Deformation displacement map of the whole wall between Feb16 TLS and Sep-15 TLS (deflection in metres)	319
Figure 5-32 Deformation displacement map of the whole wall between Feb16 TLS and March-16 TLS (deflection in metres)	320
Figure 5-33 Deformation displacement map of the whole wall between Feb16 TLS and April-16 TLS (deflection in metres)	321
Figure 5-34 Deformation displacement map of the whole wall between Feb16 TLS and Dec-15 CRP (deflection in metres)	323
Figure 5-35 Deformation displacement map of the whole wall between Feb16 TLS and Jan -16 CRP (deflection in metres).....	324
Figure 5-36 Deformation displacement map of the whole wall between Feb16 TLS and Feb-16 CRP (deflection in metres)	325
Figure 5-37 Deformation displacement map of the whole wall between Feb16 TLS and March-16 CRP (deflection in metres)	326
Figure 5-38 Deformation displacement map of the whole wall between Feb16 TLS and April-16 CRP (deflection in metres)	327
Figure 5-39 Deformation displacement map of the whole wall between Feb16 TLS and May-16 CRP (deflection in metres)	328
Figure 5-40 Deformation displacement map of the whole wall between Feb16 TLS and June-16 CRP (deflection in metres)	329
Figure 5-41 Location of the top, middle and bottom strips on the studied wall	331
Figure 5-42 Determining the rotation angle.....	332
Figure 5-43 Comparison between top, middle and bottom strips for June 2016 (last epoch of Photogrammetry)	334

Figure 5-44 Abutment at the back of the wall.....	334
Figure 5-45 Comparison of the middle strip from laser scanner and photogrammetry.....	336
Figure 5-46 Comparison between the first and the last epochs of Laser scanner and photogrammetry: a) Top strip; b) Middle strip and c) Bottom strip	338

List of Tables

Table 2-1 Definitions of asset management.....	11
Table 2-2 Typical decisions throughout the life cycle (WLV, 2016).....	19
Table 3-1 Defect Classification (S1055, 2012).....	46
Table 3-2 Types of defects detected by the new technologies	59
Table 3-3 Extent and severity category of the defect	70
Table 3-4 Inspection Report Summary	71
Table 3-5 Classification of Extent (Euroconsult, 2016)	71
Table 3-6 Classification of Severity (Euroconsult, 2016).....	72
Table 3-7 Defect chart for Tunnel 17 - Laser Inspection 2014	74
Table 3-8 TL 26 Visual Inspection-Defect Descriptions (LUL, 2013).....	76
Table 3-9 TL 26 Visual Inspection-Inspection report summary (LUL, 2013)	77
Table 3-10 TL 26 Visual Inspection- Substructure inspection report summary (LUL, 2013)	79
Table 3-11 Severity Colour coding system	82
Table 3-12 TL-26 Laser Scanner- Side walls inspection report summary	83
Table 3-13 TL 26 - Laser scanner- Substructure inspection report summary (LUL, 2014)	84
Table 3-14 Visual Inspection - Condition score of an asset- CW15 (LUL, 2011)	91
Table 3-15 Laser survey report CW 15 (LUL, 2014)	92
Table 3-16 Laser Inspection Report Summary CW 15 (LUL, 2014).....	93
Table 3-17 Visual Inspection- Condition score of an asset- TL17 (LUL, 2011)	98
Table 3-18 Laser Survey Report TL17 (LUL, 2014)	99
Table 3-19 Visual Inspection- Condition score of an asset- TL56 (LUL, 2014)	104
Table 3-20 Laser Survey Report TL 56 (LUL, 2014)	105
Table 3-21 Visual Inspection- Condition score of an asset- TL60 (LUL, 2011)	108
Table 3-22 Laser Survey Report TL60 (LUL, 2014)	108
Table 3-23 Visual Inspection- Condition score of an asset- CW61(LUL, 2011)	110

Table 3-24 Laser Survey Report CW 61(LUL, 2014)	111
Table 3-25 Visual Inspection- Condition score of an asset- TL53 (LUL, 2013)	113
Table 3-26 Laser Survey Report TL 53 (LUL, 2014)	114
Table 3-27 Tunnel sections and their inspection scores for further analysis	136
Table 3-28 TL6- Comparison of laser inspection scores between 2014 and 2015.....	137
Table 3-29 TL6 Comparison of Lining face loss (2014 and 2015 Laser inspection)	138
Table 3-30 TL6 comparison of mortar loss in joints at chainage 4 (2014 and 2015 Laser Inspection)	139
Table 3-31 TL17 Comparison of laser inspection scores between 2014 and 2015.....	141
Table 3-32 Comparison of damp patches between chainage 96 and 112 2014 and 2015 laser inspection	145
Table 3-33 Comparison of damp patches between chainage 125 and 170 2014 and 2015 laser inspection	146
Table 3-34 Comparison of damp patches between chainage 87 and 91 2014 and 2015 laser inspection	147
Table 3-35 Comparison of cracking between chainage 100 and 195 2014 and 2015 Laser inspection.....	148
Table 3-36 Comparison of lining face loss between chainage 86 and 111 2014 and 2015 Laser inspection	150
Table 3-37 TL53 Comparison of laser inspection scores between 2014 and 2015.....	154
Table 3-38 TL53 width and depth of scattering mortar loss at chainage 220	161
Table 3-39 TL56 Comparison of laser inspection scores between 2014 and 2015.....	165
Table 3-40 TL56 Mortar loss in joints between chainage 98 and 100	167
Table 3-41 TL72 Comparison of laser inspection scores between 2014 and 2015.....	169

Table 3-42 Inspections (laser vs visual) performance against requirements	171
Table 4-1 Emissivity Values of Materials	193
Table 4-2 Sensor performance Relative Humidity.....	199
Table 4-3 Relative humidity above saturated salt solutions at various temperatures (http://www.robertharrison.org/icarus).....	200
Table 4-4 Humidity Sensor Calibration measured and interpolated values	202
Table 4-5 Temperature Sensor, Thermal Camera and Relative Humidity measurements during drying.....	221
Table 4-6 Moisture measurement locations on the wall	227
Table 5-1 Comparison between embedded and non-embedded monitoring system	268
Table 5-2 Technology for monitoring infrastructure (Mazzanti, 2016)	269
Table 5-3 Data collection for the different epochs.....	274
Table 5-4 Comparison of Scanners parameters	289
Table 5-5 3D Displacement of targets computed by TS measurements	308

List of Acronyms

AM	Asset Management
AMP	Asset Management Plan
ACS	Asset Condition Assessment
AMS	Asset Management Strategy
ATR	Automatic Target Recognition
CRP	Close-Range Photogrammetry
EDM	Electromagnetic Distance Measurement
EPSRC	Engineering and Physical Sciences Research Council
FT	Flash Thermography
IAM	Institute of Asset Management
IRT	Infrared Thermography
ICP	Iterative Closest Point
LUL	London Underground Limited
NDE	Non- Destructive Evaluation
NR	Network Rail
PAS	Publicly Available Specification
RMS	Root-mean square
SfM	Structure from Motion
TLS	Terrestrial Laser Scanning
TS	Total Stations
SHM	Structural Health Monitoring
VWSG	Vibrating Wire Strain Gauges
WLC	whole life cost
WLAM	Whole Life Asset Management

Chapter 1. INTRODUCTION

The programme of research intends to evaluate new technologies that will assist in the understanding of the behaviour and insidious decline of physical civil engineering assets, in particular those related to London Underground Limited (LUL). This research work has collaboration between London Underground Limited (LUL) and University College London (UCL). It was research funded by LUL and Engineering and Physical Sciences Research Council (EPSRC), which has been hosted by the UCL doctoral training in Urban Sustainability and Resilience.

Underground railway systems are a popular solution to the increasing need for fast and efficient transport in urban environments. Many of these have been in existence for a considerable time and their maintenance and upgrade poses significant financial issues to operators. The consequences of tunnel failures would be catastrophic. There is, therefore, a need for improved methods of determining the condition of below ground structures that provide the required data and can be obtained speedily, with little or no disruption to service.

The Underground Railway system is the backbone of the London economy and connects people who live in different geographical locations. The London Underground is the world's first underground railway that opened on January 10th, 1863 with the construction of the Metropolitan line (Christian, 2004). This was followed by the District line (1868); the East London line(1869); the Circle line(1870); the Waterloo and City line(1898); the Central line(1900); the Bakerloo line(1906); the Piccadilly line(1906) and the Northern line (1907) (Christian, 2004). Sixty years had passed before any new underground lines were constructed, i.e., the Victoria line (1971); the Jubilee line (1979) and the Jubilee line extension (1999) (Christian, 2004). Given the substantial amount of early underground construction, it is important that maintenance of that work is an ongoing issue. Since 1863 London Underground Limited (LUL) has changed through evolving technology and striving for better, more efficient ways of working and dealing with its phenomenal growth.

The long-term maintenance and upgrade of civil engineering assets on metros, through the application of asset management, requires knowledge of the condition of the assets. Most of the assets suffer from a decline in condition and are affected adversely by adjacent new works. Without precise knowledge and indication of the assets condition and decline, the whole life costing and allocation of resources for the sustainability of the assets may become insufficient (Delatte *et al.* 2002).

There is a risk that assets can collapse and hence a possibility of injury to the public and service interruption. Condition assessments of tunnels and underground infrastructure are a considerable challenge for tunnel operators and managers due to the increasing age of the structures as well as the regular use in adverse (noise, vibrations) conditions (Delatte *et al.* 2002). Proper maintenance and management are necessary to prevent catastrophic failure of assets.

Severe environmental and man-made activities cause deterioration to tunnel linings. Activities such as new construction work, deep excavation (piling) and demolition of the existing structures (changing loads) affect nearby existing tunnels due to changes in earth pressures (Delatte *et al.* 2002). The continuous movement of trains causes vibration in the track and adjacent tunnel walls. Water ingress leads to corrosion of the reinforcing steel in concrete and erosion of soil behind the tunnel lining. Concrete spalling occurs due to corrosion in steel reinforcement. All these activities cause propagation of cracks in tunnel linings (Delatte *et al.* 2002). Furthermore, the mechanism of deterioration depends on soil quality, soil permeability, groundwater condition, chemical pollution and construction method (soft versus hard and cut and fill tunneling) (Delatte *et al.* 2002).

A reliable Structural Health Monitoring System (SHMS) would be able to measure deformations, strains, stresses, propagation of cracks and corrosion. These parameters provide a good indication of structural degradation and stability.

The rapid emergence of new technology/sensors and capabilities to analyse data and machine learning opportunities is driving a fundamental shift in the rail industry. The rail sector has embraced such technology over the last decade but its dominated by advances in technology and sensors on Rolling Stock. The next growth in the rail area is the adoption of smart infrastructure and IoT (Internet of Things) for rail (Lamas *et al*, 2017). Within rail infrastructure owners there is an increasing desire to implement new technology to reduce operating costs, improve reliability, performance and an awareness of how data and a digitally enhanced railway will enable the industry to meet the challenges of cost, capacity and performance (Fourie and Zhuwaki, 2017).

There are a number of benefits to using new technologies to monitor the condition of assets such as (Parmar *et al.*, 2010).

- Problems highlighted earlier allowing quicker intervention, thereby reducing the potential for performance/safety that can lead to failures.
- Reduces resource requirements providing lower operating costs.
- Improved condition data supports better decision making and improves the robustness of the long-term business plan.
- Enables a move to predictive maintenance.
- Reduced track access time.
- Digital condition data enhance the capability of LUL to more effectively and efficiently manage ageing civils assets by enabling Predictive Maintenance (PM) techniques to be implemented.
- Automation of visual inspection to make condition monitoring become digital, enabling reporting to become more reliable, accessible, consistent and analysable.
- Reduces risk of missed, delayed or incorrect maintenance.
- Reduces the number of resources and type of resources required to undertake inspections and examination and how frequently they have to be undertaken so reducing Opex (Operational expenditure) costs thus allowing resources to be freed up to perform other value-adding activity and or reduction in labour (direct and indirect).

1.1 Project Background

LUL is committed to providing a safe and efficient railway. A prerequisite for effective asset management strategies is meaningful, quality and timely asset management information; however, the lifecycle cost of this information is a considerable expense (Parmar *et al.*, 2010).

The Civils assets account for 56% of LUL's entire asset base. They encompass a wide variety of asset types and have been divided into four asset groups which consist of Bridge & Structures (B&S), Deep Tube Tunnels (DTT), Earth Structures and Pumps & Drainage (P&D). Each group is reported separately in their own Asset Condition and Certificate (ACAC) scores (Parmar *et al.*, 2010).

B&S assets comprise of 49 different asset types. These include various types of bridges, platforms, girderings, retaining walls, ranging from the lowest value assets type such as lighting to most valuable; brick tunnels because replacing these tunnels will cost significantly more than other assets. This asset group is constructed from mostly brick, concrete or steel. A large proportion of these assets are more than 100 years old.

DTT assets are comprised of 14 asset types formed by mining techniques consisting mostly of segmental linings and include running tunnels, shaft linings and cross passages. There are around 144km of tunnels on the Bakerloo, Central Victoria (BCV), Jubilee, Northern, Piccadilly (JNP) and Waterloo & City lines.

Earth Structure assets comprise two asset types; cuttings and embankments. There is more than 156km of Earth Structure (ES) on BCV and Sub Surface Line (SSL), which are on average each 200m in length.

Pumps & Drainage assets comprise of drainage at stations and along the track. There is more than 325km of track drainage and a further 365 pumps including all the control systems. There are in the order of 20,000 individual assets for Pumps and Drainage (P&D) (Parmar *et al.*, 2010).

Condition assessment of tunnels and underground infrastructure is a considerable challenge for tunnel operators and managers, due to the increasing age of the structures (Fourie and Zhuwaki, 2017). London Underground's assets are beyond their design life, with other assets having no design life specified. Over time, the assets deteriorate at different rates, depending on their age, a form of materials used and quality of construction (Fourie and Zhuwaki, 2017). Deterioration also occurs due to third-party impacts such as the construction of new buildings, utilities and other structures in proximity.

The deterioration and deformation are currently monitored by regular inspections, special inspections of vulnerable assets and special instrumentation schemes. Current techniques tend to rely on manual inspections, supported by some form of measurement. The major problem with this kind of inspection is the quality of the data, as this depends on the ability of the inspector to assess and interprets assets accurately. Furthermore, data collection is very time-consuming and costly when the whole of the metro network needs to be regularly inspected and there are limited periods when access is available.

The special inspections and special instrumentation schemes are demand on resources and are often dependent on getting access to the assets during engineering hours (between 01:00 am and 5.00 am) when no trains are running on the network. Gaining sufficient access to tunnels and to retaining walls in the deep subsurface cuttings is a particular problem. To determine the condition of metro assets, monitoring the changes in their condition is key to any further evaluation.

The problems associated with access to the infrastructure are becoming magnified by the implementation of night tube and will increase as the night tube is extended over the next 5 to 10 years.

Therefore, a need for improved methods of determining the condition of infrastructure (e.g., tunnels, bridges, and structures) is required in order that

the required data need to be obtained and interpreted, speedily, with little or no disruption to metro services.

LUL is looking for more efficient methods and techniques to improve on the Whole Life Asset Management (WLAM) of its civil assets. This can be achieved through improving the range, quality and availability of the information. However, collecting, maintaining and distributing information are a resource-intensive and costly process for LUL.

1.2 Research Objectives

Assessment and comparison of a range of monitoring and measurement techniques such as Infrared Thermography, Static/Kinematic Laser Scanner and Close-Range Photogrammetry will be performed, for the assessment of civil engineering assets. A reason for the selection of these techniques could be found in section 3.5.

Development of a standard approach to implementing technology to automate or semi-automate visual inspections and examinations will be considered. Leveraging advances in monitoring equipment and sensors to more efficiently perform these activities and enable the capture of reliable and detailed condition data and defects. This will reduce the amount of time taken to perform these activities so reducing track access time required and removes and/or reduces the resources required enabling cost reduction to be achieved. Further benefits will be exploited using new technology as the organisation will be able to utilise data not previously available and/or to a higher level of accuracy and this will be a key enabler to move to predictive maintenance regimes.

In some instances, the utilisation of the new technology and methods may highlight a need to intervene more quickly and/or frequently given this new insight into asset condition and degradation. This insight can allow the organisation to plan the intervention and reduce the likelihood of an unplanned intervention being required which are invariably expensive and usually involve an impact on operational performance.

1.3 Research Methodology

In order to initiate this research, case studies were selected to get an understanding of the current approach LUL is taking to the management of their assets. Given the vast number of civil assets, asset group (e.g. HC3 under bridge north-east wing wall) and line (e.g., sub-surface line brick tunnels) were selected as the case studies.

Following a review of the asset register, a statistical sample of inspection reports (e.g., principal inspection reports of SSL and wing wall) were reviewed and tracked to see how the information from the reports is transferred to a database (e.g. Ellipse). A number of the sample inspection reports were reviewed to determine the repeatability of the quality of inspections.

With asset condition being one of the key aspects of asset management, the new technologies that were investigated under this research project, aim to improve the understanding of asset decay and move towards further preventive maintenance rather than reactive maintenance.

A significant part of the research required the testing and comparison of a number of non-invasive technologies that recently became affordable and widely used in many different areas of monitoring and inspection. The techniques used in this research are Kinematic/Static Laser Scanner, Close-Range Photogrammetry, Thermography and Total Station Survey.

The areas were considered during the period of research include, but are not limited to, the following;

- What is being measured and why.
- What techniques are currently used to determine the state (condition) of the assets; how is this information converted into a format that enables cost-effective decisions to be made.
- What evolving technologies are available and suitable for use on metro systems (benefits are: enabling a move to predictive rather than reactive

and or time-bound interventions, therefore, reducing operating costs and improving asset performance.)

The research was carried out in three phases:

1. In the first phase, a case study was performed to compare and contrast the use of a high definition laser survey against a Principal Inspection report to determine the level of consistency in predicting the asset condition for a whole life cycle asset management. The assessments were performed on brick Tunnels (TL) and Covered Ways (CW) on the District line. The comparison of defects was performed between visual inspection and Euroconsult's laser scanner inspection.
2. In the second phase, two laboratory tests that were performed to calibrate the application of thermography, using relative humidity and temperature sensors to detect water seepage inside of the wall, and a handheld relative humidity, moisture sensor and temperature to test the surface of the materials. Based on the laboratory test, site trial was performed using thermography to detect water ingress in a Sub Surface Line. This site trial was to identify active water seepage in the brick tunnels as well as test the system in a configuration that would allow the survey was done using an engineering train, at the survey speed of 12km/h.
3. In the third phase, the case study was tested the Static Laser Scanner, Close-Range Photogrammetry and Total Station as a measuring tool to identify the wall movement/deformed shape, displacement values (between different epochs) and defect (cracks) on the HC3 Underbridge North East Wing wall.

1.4 Thesis Outline

This thesis consists of six chapters and three appendixes.

Chapter 1 introduces the project background and research objectives.

Chapter 2 discusses Infrastructure asset management and its functionality. This chapter also describes LUL asset management, maintenance regime and their inspection methodology. It also analyses the probable gaps in the current and desired level of inspection of LUL civil engineering infrastructure asset management.

In chapter 3, a literature review shows different tunnel inspection methods, currently taking place for tunnel monitoring and inspection around the world. Their applications, limitations, and performance are highlighted. Also, this chapter discusses a case study, performed to analyse and interpret Euroconsult's high definition laser scanner for condition monitoring of LUL's brick tunnel on a sub-surface line. Comparing the laser scanner data and the visual inspections, the performance, and the limitation of both systems has been analysed and interpreted.

In chapter 4, a literature review shows the fundamentals of thermography and different thermography techniques such as active and passive thermography to detect different types of defects. The first half of the chapter describes three lab tests which were performed to validate the application of thermography, relative humidity sensors, moisture sensors and temperature sensors to detect water seepage, relative humidity, moisture and temperature of the test walls. This chapter also describes the site trial which was performed on a Sub Surface Lines (SSL) tunnel to detect water seepage, using a thermal camera.

In chapter 5, a Terrestrial Laser Scanner and Close-Range Photogrammetry were used to measure the movement and deformation of a wing wall, which is known to be deforming. The data collection methods and different processing techniques are also discussed and proposed in order to understand the behaviour of these structures over time.

The final chapter 6 provides a summary and detailed conclusion from this work and the future direction this research could take.

Chapter 2. INFRASTRUCTURE ASSET MANAGEMENT AND GAP ANALYSIS

2.1 Introduction

This chapter describes major components of general asset management and the LUL asset management plan and their application to manage assets effectively and efficiently. A brief description of LUL's current inspection and maintenance strategies are also described. Furthermore, a gap analysis was performed to identify possible gaps in the current and desirable levels of LUL's inspection of civil assets. The gap analysis focuses on identifying the crucial tasks and making sure that they are given priority by considering affordability and benefit.

There are many definitions of asset management being used in different sectors. Some of the definitions are given in Table 2-1.

Table 2-1 Definitions of asset management

Definition	Source and Reference
<i>'Asset management is simply the way assets (such as trains, signals, stations and tunnels) are managed throughout their life to achieve the right balance of cost, performance and risk for the organisation'</i>	<i>The London Underground</i> <i>Moore and Parry 2010</i>
<i>'The systematic and coordinated activities and practices through which an organisation optimally and sustainably manages its assets and asset systems, their associated performance, risks and expenditures over their life cycles for the purpose of achieving its organisational strategic plan'</i>	<i>BSI PAS 55 (BSI, 2008)</i> <i>Edwards et al[ed] .2010:3</i>

Definition	Source and Reference
<i>'A strategic approach that identifies the optimal allocation of resources for the management, operation, preservation and enhancement of the highway infrastructure to meet the needs of current and future customers'</i>	<i>The highway asset management</i> <i>CSS 2004</i>

There are many other definitions of asset management around the world, but, essentially, asset management allows an asset-intensive business to use limited resources and maintain a level of services to achieve their stated business objectives in the most cost-effective way (Edwards *et al* [ed] 2010).

Whole life cycle asset management encompasses design, build, maintenance, repair, replacement, renewal and upgrades to an asset. To minimise service loss all these activities should be planned effectively and efficiently and timely executed. The benefits of implementing proper asset management plans are the increase of asset availability, higher productivity, improved asset safety, life-cycle cost reduction and further reduction of the possibility of a catastrophic system failure. When preparing an asset management plan, assets and interface assets in the network should be considered together to allow the management of the combined performance, reliability and safety (Prescott and Andrews, 2011).

2.2 Asset Management Policy, Strategy & Objectives

An organisational Asset management policy and strategy play an important role in achieving an asset management objective (Prescott and Andrews, 2011).

2.3 Asset Management Policy

Top-level management in organisations sets out rules and regulations of asset management policy to carry out the asset management objectives in a

coordinated and structured way. The organisation's board of members review and update each policy regularly endorsed by the organisation's senior management. An Asset Management Policy should satisfy legal obligations such as health and safety in the workplace (Hooper *et al* 2009: p12).

London underground is part of the Transport for London (TfL) business. TfL principal asset management policy statement is:

'TfL shall use effective, efficient and sustainable asset management practices for its physical assets to support the achievement of customer, Mayoral and organisational goals and outcomes. Asset management shall be holistic, co-ordinated, consider the whole lifecycle of the assets, and deliver optimum whole-life value through informed decision making that takes account of safety, risks, performance, the environment and costs' (Moore and Parry, 2010).

2.4 Asset Management Strategy (AMS)

Asset Management Strategy should be reviewed from time to time to meet the organisation's vision and goals. With the engagement of people from all parts of the business, the asset management strategy is developed by a nominated team. The senior management of the organisation should endorse the asset management strategy and make sure that this strategy is understood throughout the organisation (Hooper *et al* 2009: p13).

A long-term strategy view is essential for infrastructure assets due to its longer service life span. The strategy needs to accommodate variations such as a variation of government policy and an operational asset environment. According to U.K Health and Safety regulations, the asset management strategy should be a risk-based approach.

2.4.1 Asset Management Objectives

The organization should establish asset management objectives for relevant functions and levels. The organisation should consider stakeholders' requirements and other functionality such as technical, financial, legal and regulatory requirements when they establish asset management objectives.

Asset management objectives include clear and well-defined goals. For example, a financial manager needs the market value of an asset while an operational manager requires asset condition to monitor operational performance. The current service levels need to be measured and compared with stakeholders' demand to develop a service level objective (Roberts and Hollier, 2007).

2.5 Asset Management Information System

The establishment of good quality, timely Asset Management Information is essential for the effective and efficient long-term management of the assets. Asset Management Information requirement details a framework, based on good practice approaches to Asset Management, which will enable asset information to be delivered in a cost-effective and timely manner. The collection of asset data for any organisation is a resource-intensive exercise requiring a coordinated and structured approach to be successful. Data collection requirements must specifically consider how the collected information is going to be used at the various asset management decision-making levels (Roberts and Hollier, 2007).

2.5.1 Asset Information Requirements

The term asset information covers a range of information and data types. The level of detail and depth needed for the collection data vary according to the hierarchical level of the decision to be made.

The Asset Management Information must be linked to business outputs in order to allow proper business decisions. It should be recognised that organisations need to satisfy the following points (Gerardo and Bryant, 2006):

- Legislative commitment, e.g. asset accounting
- Legal compliance, e.g. building regulation
- Government reporting
- Improved investment planning
- Better Management of Safety Risk

- Improved operational performance

2.6 Asset Data Collection

Several variables will determine which methodology or combination of methodologies (e.g. manual, semi-automated or automated) will produce the data collection objective. The variables that need to be considered include;

- a. Asset category (e.g. tunnels, bridges, stations, vents, buildings and road)
- b. Asset location (e.g. over ground or underground)
- c. Asset value
- d. Asset criticality (e.g. bridges and tunnels)
- e. Asset geometry (e.g. point, linear and area)
- f. Available resources, both labour and budget
- g. Essential data to be collected
- h. Accuracy and relevance of legacy data

The data can be obtained from many sources and there are a number of methods to collect and collate this information:

- Legacy systems – including inspection and maintenance systems, existing asset registers/catalogue.
- Field or site data – which involves physically locating and recording the asset information/condition.
- External service providers – it includes maintenance contractors and suppliers' databases.
- Capital works – asset information will be collected as part of capital works.

Data collection method can be classified into three major categories. Proper data collection method leads to an effective and efficient way of interpreting the data for informed decision making.

- Manual data collection or field record book
- Digital data recorder
- Automatic data acquisition system (e.g. monitoring sensors)

The following information must also be collected for better decision making and effective management of assets.

- A record of a physical asset and the unique identification of that asset (e.g. Location Code System (LCS)).
- Attributes about the asset (e.g. make, model, serial number, age, capacity)
- Asset performance, structural condition, functional condition and serviceability information.
- Past, present and future costs associated with the asset.
- Documents, drawings and records of assets and systems.
- Spatial information detailing the location, boundaries and extent of assets.
- Statutory requirements (e.g. health and safety, fire safety, environmental)
- Configuration and systems engineering information.
- Operation and maintenance instructions and other documents.
- Relationship between assets (e.g. assets and interface assets)
- Life Cycle Cost (LCC)
- Value (capital value of each asset)/current value/replacement value.
- A history of the asset and the work undertaken on it.
- Photographs, video and multimedia representations of the asset.

2.7 Asset Failure Mode

For maintenance and strategic decision making, the failure mode of assets and how it may interfere with or cause the failure of other assets must be understood. An organisation must determine how an asset might fail to deliver the required level of service, especially if the failure is critical to the organisation.

Having identified the failure modes, risk costs, and treatment options for key assets, the appropriate option will be included in the asset management plan. The range of failure modes include:

- **Structural:** Measurements of deterioration shows the physical condition of the asset and their remaining life.
- **Capacity/utilisation:** To understand the level of under- or over capacity against the required level of service.
- **Level of service failures:** Performance targets are not achieved e.g. reliability
- **Obsolescence:** Lack of replacement parts or technological change that can render assets uneconomic to operate or maintain.
- **Cost or economic impact:** Where the cost to maintain and operate an asset is likely to exceed the economic return expected, or the customer's willingness to pay, to retain an asset.

Each of these modes has distinct attributes that require focussed evaluation to allow an organisation to understand the effect on the asset(s) and the service. Condition assessment is a typical failure mode assessment activity that is usually built into maintenance as an inspection task.

To identify critical failure modes for an asset, it is significant to refine and target maintenance plans, investigate activities, capital expenditure and to address that failure. Condition assessment can be focused on the critical mode of failure of an asset or its components (IIMM, 2002).

The stepped process for using failure mode information is (IIMM, 2002):

1. Understand the critical failure mode of the asset
2. Monitor the asset performance with respect to the failure mode, e.g. condition assessment
3. Develop deterioration curves and predict failure timing
4. Develop strategies covering maintenance and capital expenditure
5. Continue to monitor the performance of the asset

2.7.1 Failure Treatment Strategies

Failure treatment strategies must be prepared to avoid or react to the failure when an asset has failed or is expected to fail in the future. If the failure mode of an asset is critical to the organisation, failure avoidance is likely to be more effective than reactive activities. Depending on the failure mode, the strategies can include changed maintenance activities, rehabilitation works, replacement works or abandonment of the asset.

These strategies will require evaluation of:

- The cause of failure
- The failure mode and its criticality
- The current actions to manage the asset for that failure mode, e.g. maintenance plan, rehabilitation plan, augmentation plan etc.
- The suitability and economics of those actions to ensure reduced business risk.

Failure Modes, Effects and Criticality Analysis (FMECA) are generally undertaken to determine critical maintenance or renewal required for any asset. Also, it can be used to determine the critical failure mode and the consequences of failure for an organisation's assets.

2.8 Whole life value

Whole life value is the combination of all costs, risks and benefits over the remaining life of an asset. This is easier to understand when broken down (WLV, 2016):

- **Costs:** - This refers to cash flows and includes income
- **Risks:** - Risk = probability of an event occurring × negative impact on objectives if the event occurs
- **Benefits:** - This refers to the satisfaction of stakeholders' needs which encompass safety, service, environmental improvements and other opportunities.

Remaining life: - For decisions about an existing asset, contract or outsourcing arrangements, this could be the life cycle of the service to be supported – from the identification of need for the service to decommissioning, disposal and any residual liabilities. Only current and future costs, risks and benefits should be assessed when making decisions based on whole life value.

Whole life value should be assessed whenever a decision needs to be made. The greatest opportunity to influence the whole life value is at the start of the life cycle but big improvements can still be made later. Table 2-2 lists typical decisions that are made throughout the life cycle.

Table 2-2 Typical decisions throughout the life cycle (WLV, 2016)

Stage of the life cycle	Decision examples
Identify needs	<ul style="list-style-type: none"> • What is the strategic vision for the services the organisation provides? • What portfolio of projects and activities in the various stages of the life cycle best delivers the strategic vision? • What changes in the organisation should go ahead?
Acquire or create	<ul style="list-style-type: none"> • What new assets or services do we need? • How are we going to procure or build new assets or services? • Should we invest in innovative or familiar technology?
Use and maintain	<ul style="list-style-type: none"> • What performance improvements are necessary this year? • Can we simplify the support for technology services and introduce a more self-service capability? • Should we change our inspections regime? • Is the current organisational structure still appropriate?
Modify renew or improve	<ul style="list-style-type: none"> • Should we refurbish, renew or enhance our assets? When?

Stage of the life cycle	Decision examples
	<ul style="list-style-type: none"> What data improvements would significantly impact our decisions?
Decommission or dispose	<ul style="list-style-type: none"> What assets or services, if any, are no longer required? Should we mothball or dispose of our redundant assets? When?
Residual liabilities	<ul style="list-style-type: none"> Decisions are not made during this stage. Instead, plans are developed during the earlier stages of the life cycle.

2.9 London Underground Asset Management

London Underground use co-ordinated asset management activities to select, inspect, maintain, renew, improve and dispose of their assets in order to maximise customer satisfaction, maintain high levels of safety, manage risks, minimise whole life costs and enable the delivery of their outcomes and priorities (P020, 2014).

2.9.1 LUL Vision

The LU vision is to improve the range, quality and availability of information that is required to manage optimally the whole life of its assets (Parmar *et al*, 2010).

2.9.2 LUL Civils Assets Strategy

The strategy is to improve the condition of these assets, where it is economic and efficient to do so. This means that renewal works are generally limited to high-risk non-compliant assets and / or assets with excessive maintenance costs. A robust prioritisation process is required to ensure projects deliver maximum value for the available budget (Moore and Parry, 2010).

2.10 LUL Asset Life Cycle

Figure 2-1 illustrates major components of LUL's asset life cycle. All these activities must be performed at the right time in order to make effective asset

management decisions. LU's Asset Management has a whole life value approach and risk-based decision-making. In order to provide effective and efficient asset management, the whole organisation, such as Procurement, Strategic Planners, Capital Projects, Supply Chain, Finance, Operations and Maintenance, have to work together. All these sectors are led by top management and communicate a common understanding of Asset Management (Moore, 2014).

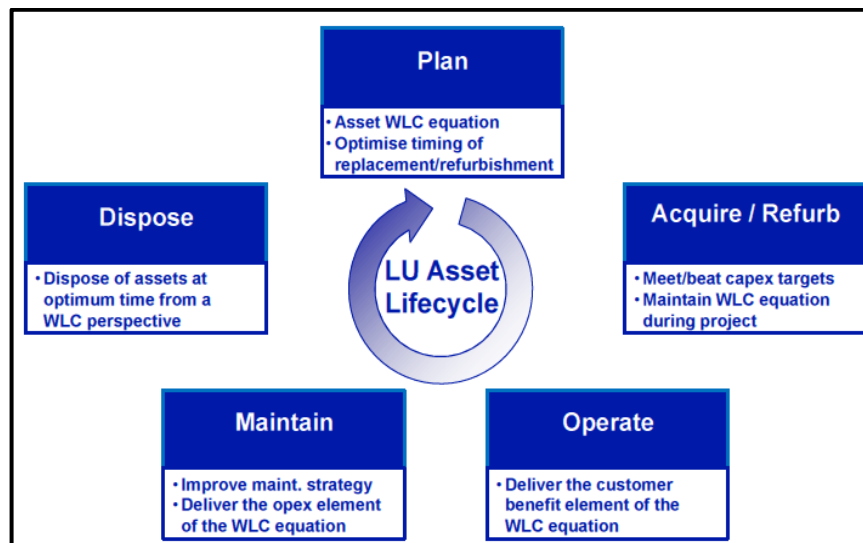


Figure 2-1 Decision required throughout asset lifecycle (Woodhouse et al., 2013)

2.11 LUL Asset Maintenance Regimes

The overall objective of maintenance is to ensure that the assets continue to meet their service and performance requirements including safety, environmental and output parameters. Selection of the appropriate maintenance and inspection regimes are important to identify the functional and physical condition of the assets.

Maintenance tasks can be divided into three groups (IAM, 2014):

- **Inspection and Monitoring** - non-intrusive checks to confirm the safety and integrity of assets and to provide information for determining maintenance and renewal needs, this may include the use of remote monitoring systems.

- **Preventative Maintenance** - planned maintenance undertaken to prevent or reduce the risk of faults and failures or excessive deterioration from occurring. The criteria for initiating preventative maintenance may be time-based, condition-based or usage-based but should always take account of risk.
- **Corrective Maintenance** - activities performed to repair defects, damage, a shortfall in performance and where work is necessary to bring the asset up to standard and keep it operational.

2.12 LUL Inspection

During the basic inspection (visual inspection) task, an inspector confirms the safety of the operational railway, records condition and identifies defects. This knowledge is then used to plan and manage maintenance in the medium term.

An effective inspection requires an understanding of the assets, how they work, their possible weaknesses, knowledge of the tell-tale signs of problems, and often where to look for them. In addition, effective inspection gathers detailed, accurate, well-presented and objective information, that permit other members of staff not directly involved in the inspection to understand the problems, draw conclusions, and take action when necessary. Even when no action is taken after the inspection is completed, an objective record of what was found is essential to permit the next inspection to measure or assess any deterioration during the intervening period (G1055, 2012: p18).

The following methodologies are used by London Underground's Inspectors for an inspection of the assets (S1055, 2012).

- Use of an inspection hammer to test for brickwork and concrete defects. Test for loose material and to, ensure measurements of crack dimensions, areas of dampness and spalling are taken.
- Use scrapers, wire brush or cold chisel to remove corrosion and to facilitate metal thickness measurement.
- Cast iron must not be hammer tested, tools such as wire brushes or scrapers are permissible for exposing cracks for accurate measurement

- During the inspection, appropriate photographs of the inspection site, including any significant defects identified must be taken.

The following tools are required for use in visual inspections (S1055, 2012):

- Inspection hammers
- Cold chisel
- Wire brush
- Measuring tape
- String line
- Access equipment
- Camera
- CCTV/Borescope
- Hand-held field data manager device
- Electric Digital Calliper
- Handlamp or torch
- Rubbish bags

Prior to, and during, the formal inspection and assessment work being undertaken, a detailed desktop study must be done prior, to review all available asset data. This will include the following (Chew, 2004):

- Asset plans and detail drawings
- Ordnance Survey plans
- Walkover survey of the surrounding site and initial visit to the site
- Historic inspection records with the emphasis on the defect logs
- Existing survey information
- Historic maintenance records
- Existing assessment reports
- Design and construction information of assets
- Information on adjacent structures including foundations and subsurface structures
- Geotechnical and Geological data
- Groundwater information

Inspectors need to identify the type of inspection required- either a principal or special inspection. These will be explained in more detail below.

2.12.1 Principal Inspection

These are a close inspection of all inspectable parts of the asset, carried out to give detailed visual confirmation of the condition necessary for the management of the assets. Where necessary inspection should be facilitated by cleaning surfaces or removing non-structural finishes (G1055, 2012).

Principal inspections are carried out for civil assets based on the engineering standard S1060 Bridges and Structures and the S1055 Deep Tube Tunnels and Shafts. The overall element rating reported for an inspected asset will be used to determine the asset condition for assessment classification.

2.12.2 Special Inspection

A special inspection is a close inspection of a particular area or a defect causing concern. The inspection should cover the following areas.

- Special Inspections should be close inspections of an asset, or particular areas of the asset and may include intrusive investigations.
- Sufficient information should be collected to enable the safety of the asset to be assessed and for the full reporting of any incident.
- The frequency of Special Inspections shall be dependent on the assessed risks' (S1055, 2012).

2.12.3 Inspections for Analytical Assessment

An inspection for Analytical Assessment should provide the physical information about an asset necessary for the assessment.

Information collected during an inspection for assessment is likely to include:

- i. the form of construction
- ii. the construction materials
- iii. dimensions
- iv. structural condition, including deformation

- v. any other changes that have resulted in different conditions from those applied at the time of any previous inspection (S1055, 2012).

Features which are commonly of particular relevance to the assessment include tunnel circularity, deformation at openings, longitudinal discontinuities and seepages.

Examples of LUL's asset degradation are given below Figure 2-2 to Figure 2-8 (Bowers, 2014). Detailed description of defect classification (e.g. A1) can be found in Table 3-1 in Chapter 3.



Figure 2-2 Water Ingress; harmless drip (A1)



Figure 2-3 Water ingress; Rail Corrosion, Signalling fault (A4)



Figure 2-4 Water ingress; short circuit – earth fault or Burning (A2)



Figure 2-5 Acidic soil (B4)



Figure 2-6 Soil ingress (C4)

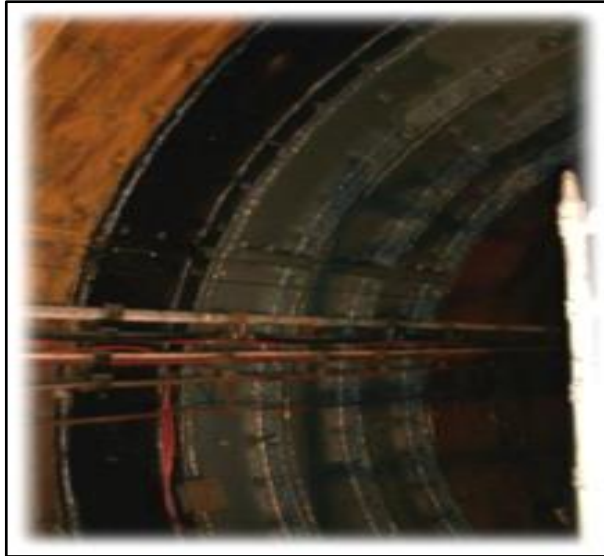


Figure 2-7 Corrosion (B3)



Figure 2-8 Overstress (B2)

2.13 Planned Preventive and Corrective Maintenance

The maintenance regimes, which currently exist within London Underground, are predominantly planned preventive, corrective repair following inspection or casualty maintenance upon failure. The implementation of a planned preventative maintenance regime which minimises degradation, minimise future corrective maintenance costs and minimise service disturbance. The planned preventive and corrective approach is ineffective in identifying problems that develop between scheduled interventions and means maintenance is often carried out on assets that are in good health, incurring a cost and the risk of introducing further failures. Faults that could become

service affecting failures will not be found earlier until failure happened (Caffull and Sims, 2014). Extend Planned Preventative Maintenance (PPM) is used to control major causes of asset degradation such as water ingress and vegetation/tree growth. Control of seepage through tunnels, in particular, will contribute to reliability by reducing the number of signal failures. Reactive maintenance can be used to address high priority water ingress affecting performance-critical assets i.e. rails or signals (Bowers, 2014).

2.14 Predictive and Preventive Maintenance

Predictive maintenance enables a failure to be identified early, so appropriate mitigation can be undertaken in a timely manner to reduce the risk of the failure occurring in service. This capability also allows the ability to optimise and minimise the frequency of the maintenance regime: only maintain those assets for which the maintenance activity is required.

Predictive and Preventive Maintenance will be achieved through a greater understanding of degradation rates, identification of optimum conditions for intervention (by balancing risk, performance and cost) and the introduction of new technologies, such as automated condition monitoring and laser survey techniques.

Automated condition monitoring can detect and identify deterioration in the infrastructure before the deterioration causes a failure. In simple condition monitoring, sensors show the changes in the condition of a structure. If the sensor readings reach a predetermined limit or fault condition, then an alarm is activated before they escalate, and improving safety and reliability (Victoria *et al*, 2014).

Asset information can be used to determine the condition of an asset, allowing a prediction of when a maintenance activity is required, in advance of the asset losing performance. Thus, the long-term asset maintenance regimes can be optimised, scheduling maintenance for the point in time when it is most cost-effective. The current time-based maintenance is ineffective in identifying problems that develop between scheduled inspections and is not cost-effective.

A predictive regime can be applied to legacy assets (an asset that has been in operation for a long period), but those assets may need additional hardware such as sensors if automated condition monitoring is to be performed. The earlier the asset is in the project life cycle, the cheaper it will be to install any additional hardware that is required for automated condition monitoring. For new assets and projects, predictive approaches should be considered from the outset when designing the asset.

The main benefits of a predictive maintenance strategy over a planned preventative strategy are reliability-based. Faults which could become service affecting failures will be found earlier and invasive interventions will only happen when warranted by the condition of the asset, reducing the likelihood of introducing failure through the work (Caffull and Sims, 2014).

2.15 Gap Analysis: LUL Civil Infrastructure Asset Management

2.15.1 Introduction

This section describes the analyses of possible gaps between the current and desired level of factors, including the level of service, in the inspection and maintenance of London Underground civil engineering infrastructure asset management. A gap analysis compares the current practice to the desired practice and quantifies the activities required to change current practice to that of the desired practice. Gap analyses are an important element of asset management, to identify the best practice, prompt innovation (new technologies), and understand the performance and limitations of an existing methodology. The gap should be determined to manage an asset across its whole life cycle, including; strategies and plans, asset inventory and location, maintenance records, capital and operational costing, asset condition, performance and risks.

2.15.2 Current Conditions of the LUL's Assets

The 'LUL network consists of 11 lines with 270 stations and a total route length of 402 kilometres. The network provides a high-frequency metro as well as an extensive suburban railway service. 56% of the network is at the surface; 10%

are in shallow cut and cover tunnels, and 34% are in deep, narrow-bore tube tunnels' (TfL, 2012).

Parts of LUL's assets were built more than 100 years ago using different materials (e.g. cast iron, bricks & mortar, and precast concrete) and construction methods (hand-built, cut & cover and TBM). LUL also has different types of tunnel linings such as brick lining, cast iron, bolted concrete sections, flexible iron and flexible concrete lining.

London Underground has a risk-based asset management strategy. The deterioration and deformation are currently monitored by principal inspections, special inspections of vulnerable assets and special instrumentation schemes. Principal inspections are carried out within touching distance of the asset. Furthermore, LUL performs Asset Condition Reports (ACR) and prepares Asset Safety Management Certificates together in order to identify an asset's residual safety and performance risks and their associated mitigations determined according to the S1042.

The relationship between condition and performance shows that poor condition has an impact on the level of service by increasing service disruption, higher maintenance costs and the imposition of slow speed zones, and other service quality measures (TAMP, 2010).

Due to ageing, third party impacts and adverse operational conditions, assets deteriorate in different ways, consequently showing different types of defects, such as seepage (water ingress), mortar loss in the joints, lining face loss (in brick tunnels), cracking, concrete delamination, chemical or biological deterioration of the lining, reducing structural capacity, corrosion or damage to bolts(in cast iron tunnel) and variation in tunnel geometry. For example, Parlikad (2014), worked on LUL research said: 'One issue with ageing tunnels is water seepage through minor cracks and joints. The risk of major structural failure has to be considered but is a relatively insignificant risk. Water seepage could affect the performance of the tunnel through various means including corrosion of rails and damaging signalling systems, disrupting the service and

affecting passenger safety. Seepage on a platform affects aesthetics, potentially damaging London's brand image'.

Asset condition can provide a good indication of the amount of investment required to maintain or improve these conditions, and how variations in funding will impact LU's ability to address investment needs over time.

The LUL maintenance strategy is to carry out Planned Preventative Maintenance (PPM) on assets, in order to reduce the need for Corrective Maintenance (CM) and hence reduce overall maintenance costs (Caffull and Sims, 2014).

2.15.3 Gap Identification

LUL currently relies on manual/visual inspection, supported by local measurements performed by the inspectors during the routine inspections. A visual inspection is performed on all tangible area of the asset and inspection surfaces need to be prepared (removing debris, corrosion, etc.) before the visual inspection takes place. Unseen parts of an asset are tapped using an inspection hammer to identify any defects. Using ringing sounds (low and high pitch) the material below the surface of an asset can be differentiated and defects identified (S1055, 2012).

Visual Inspection is time-consuming and costly particularly since the whole of the metro network needs to be regularly inspected, and there are limited periods when access is available.

The quality of the inspections depends solely on the ability of the inspector to interpret the data. Using this methodology, large parts of the assets cannot be inspected within a limited period. Cost-effectiveness, speed and reliability, are further limiting factors using manual/visual inspection. The maintenance of civil infrastructure requires low-cost and effective inspection techniques. In addition, these traditional inspection procedures require significant investment in both time and labour costs.

The following factors support the necessity of more reliable, objective and efficient infrastructure inspection methods:

- The limited kinematic envelop of tunnels (clearance between train and tunnel lining is very limited) due to this, conventional instruments take time to deploy.
- A visual inspection performed during limited engineering hours. Access to the infrastructure has become further limited by the implementation of the Night Tube.
- Adverse (e.g. vibration, noise and dark) operational conditions.
- Increasing demand

The gaps between current and desired levels of inspection are:

LUL currently relies on semi-automated /manual/visual inspection approach that is not compatible with predictive maintenance, only with reactive maintenance.

- Asset condition scores (severity and extent) are manually assigned, and scores can vary with the ability of the inspector to interpret the data.
- Large volume and variety of data (e.g., inspection reports, condition survey, monitoring ground movements, geology and hydrology) are processed and analyzed manually. Generally, paper driven reporting and record keeping. This process is time-consuming and can delay the asset-related decision-making process.
- Time base inspection/planned preventive maintenance with the use of risk and or condition-based parameters to determine intervention frequencies.

Therefore, there is a need for improved methods of determining the condition of structures and tunnels in order that the required data can be obtained and interpreted, speedily, with little or no disruption to metro services.

2.15.4 Factors Responsible for the GAP

London Underground has a significantly aged asset base, combined with increased demand for services, increased service expectations, and ever-increasing scrutiny from regulators and the public. Furthermore, LUL has a limited budget to perform their maintenance activities with minimum disturbance of services.

2.15.5 The Future State

In the future, LUL wants to minimize the service disturbance and speed up inspections in the form of automatic data capture and processing. LUL is looking for methods and or techniques that allow speedier decision-making when large quantities of data are collected, from measurements of particular aspects of an asset.

Efficient methods of maintaining the infrastructure through an automatic way of carrying out an inspection and automatic data processing would reduce the maintenance activities at night.

The following targets have been set up by LUL in order to provide better service to customers.

- Decrease maintenance cost with various efficiency initiatives (e.g. predict and preventive programs)
- Reduce maintenance frequency which leads to lower maintenance cost
- Improving operational safety and reliability
- Reduce Lost of Customers Hours (LCH) through the rail defect reduction program
- Optimized asset management interventions regimes
- More effective use of resources to drive asset performance
- Less reactive and more predictive works
- Reduced maintenance renewal costs
- Data analytics to support optimised maintenance strategies

2.15.6 Remedies, Actions and Proposals

Providing a safe, reliable and efficient transport system requires knowledge of the condition of the assets. LU must identify the condition of their assets and have a broad knowledge about the assets to enable economic life cycle management. A systematic way of inspection is required to establish the internal and external condition (physical and functional condition) of the assets for the foreseeable future.

London Underground must approach the inspections, with a plan to move towards a more automated based approach determining the type of inspection carried out, to optimize resource requirements and costs.

The effectiveness and efficiency of the inspection will be improved mainly by using new technologies. New technologies can be used to measure structural parameters (e.g. strain, and deformation), defects of the assets (e.g. concrete delamination, cracks, and seepage) and ground movements (e.g. due to new construction or demolition).

The data has to be processed into information, determining what is most useful and how it should be stored, accessed and integrated into business as usual task. This has a cross-over with digital engineering such as GIS, Ellipse/Maximo (asset database/register), Heartbeat (information reporting system) and BIM (Building Information Modelling).

The data needs to be analysed, and information extracted to understand patterns of asset behaviour and identify vulnerabilities. Identify patterns that run counter to expectation, improve coverage and speed of monitoring regime. Assessment needs to be performed to assess current and new inspection methods (see Chapters 3, 4 and 5) and including an assessment of costs, risks, benefits and impacts on other asset groups.

This Gap analysis has been used to identify appropriate new technologies to perform the inspection automatically to obtain asset condition rapidly.

Chapter 3. CASE STUDY - BRICK TUNNELS - DEFECTS COMPARISON AND CHANGE DETECTION

3.1 INTRODUCTION

The brick tunnels of the London Underground were constructed in the 1860s by the 'cut and cover' method (Euroconsult, 2014). As a part of this research project in the use of a non-destructive assessment method, some intimal assessments of these tunnels were made using high-resolution laser surveying for tunnel lining inspection. The work was performed between June-July 2014 and December 2015 by 'Euroconsult' with the 'Tunnelling' system at the request of LUL (Euroconsult, 2016).

The idea of automatic inspections already existed within the LUL brick tunnel inspection team. LUL used a Spanish specialist contractor called "Euroconsult" to carry out the laser scanning of the tunnels. The contractor provided the skilled team of data capture technicians, the analytics and the equipment to carry out the inspection. They analysed the raw data and provided it to LUL for review by the engineering team. Once all the data had been processed and digitalised, the data were analysed offline by the author using a 3D viewing software called "Tunnel Viewer". From the software and the input data, the author measured defects to the tunnel lining and collated all the data in graphs and screenshots to evaluate the performance and limitations of the laser scanner system against the traditional visual inspection.

The case study was performed to compare and contrast the use of a high definition laser survey against a Principal Inspection report to determine the level of consistency in predicting the asset condition for the whole life cycle asset management. This chapter aims to show the benefits of the automation of tunnel inspections to identify defects using the Euroconsult's laser scanner inspection system. It describes the fundamental parts of the technology and its applications. The comparison of defects was made of visual inspections performed in 2011 and Euroconsult's laser scans performed in July 2014 (first) and in December 2015 (second).

The first assessment (2014) was performed on brick tunnels (TL) and covered ways (CW) on the SSL (Sub Surface Lines), for the Circle, Hammersmith & City and District lines. The visual inspection scores of 112 assets on the SSL were compared to the 2014 first laser survey inspection scores. A detailed description of the laser survey inspections and the visual inspections (asset I.D and scores) can be found in Appendices A and B. In addition, four major defect types i.e. mortar loss in joints, cracking, lining face loss and dampness identified by the 2014 laser survey were compared with the same defects identified by the visual inspection. For these comparisons, reports of assets Covered Way-15 (D104/CW15), Tunnel-17 (D104/TL17), Tunnel-56 (D124/TL56), Tunnel-60 (D122/TL60) and Covered Way-61(M144/CW61) were used. Performance and limitations of both the systems were analysed and interpreted.

Tunnel sections 6, 17, 53, 56 and 82 (TL6, TL17, TL53, TL56 and TL82) were selected and defects such as mortar loss in joints, lining face loss, cracking and damp patches were compared to the 2015 second laser inspection. The objective of the 2015 inspection was to survey any deterioration of these tunnels from the previous inspection in July 2014. Since 2014 (first scan/reference scan) LUL have used Euroconsult's laser scanner inspection system to inspect their brick tunnels every year.

After comparing the laser inspection in 2014 with the previous visual inspection in 2011, the author suggested improvements in the laser scanning system's software. Compared to the first scanning; the second scanning system has an additional feature in the software (Tunnel viewer software) and hardware. The tunnel viewer software has been improved such that it can perform a comparison between two scans and is able to view changes in defect dimensions (e.g. length, width, and area). The 'Tunnel Viewer' software used the same algorithm for 2014 and 2015 inspections to identify defects from raw data. The updated version of the Euroconsult's "Tunnel viewer" software offers the capability of changing the threshold values of the defects' sizes. This gives the user the option to select different sizes e.g. length/depth of the crack, area of damp patches of the defect, and the corresponding overall percentage score of the tunnel section being analysed. The Tunnel Viewer software also has

tools to perform statistical analyses to diagnose defects on tunnel sections. Furthermore, this software has the facility to compare defects captured on different inspection dates (e.g., 2014 and 2015 inspection) to evaluate the tunnel performance and degradation rates.

On the hardware side, an Infrared camera and a LIDAR scanner were added to the system and also used in the 2015 inspections in order to improve the high spatial and high radiometric resolutions. High spatial resolution was used to detect small defects clearly, whilst the high radiometric resolution was used to differentiate defects in different materials by changes in the brightness levels of an image as different materials have different radiometric properties (Euroconsult, 2014).

3.2 Literature Review

Infrastructure owners and managers are currently facing challenges in the inspection, assessment, maintenance and safe operation of the existing aging civil assets. The factors that affect the structural integrity can be aging, adverse weather conditions, loading, usage changes as well as inadequate maintenance or deferred repairs (Fackler, 2012). All the above needs are more than apparent in underground transportation tunnels, including many tunnels operating for more than a century which already presents large evidence of deterioration. Several incidents related to tunnel collapse have occurred such as the 'Big Dig ceiling collapse' in 2006 in Boston. The collapse of the ceiling structure began with the simultaneous creep type failure of several anchors embedded in epoxy in the tunnel's roof slab. Each of the panel's intersecting connection points consists of several individual bolts anchored into the roof slab concrete. The failure of a group of anchors set off a chain reaction which caused other adjacent connection groups to creep then fail, dropping 26 short tons (24,000 kg) of concrete to the roadway below (National Transportation Safety Board, 2006). The Sasago Tunnel collapse, in 2012, in Tokyo, was due to the aging of the bolts or the concrete slabs (Fackler, 2012).

Visual inspection, visual checking and hammering tests are used by an inspector to inspect infrastructure and it is subjective and potentially inaccurate. A visual inspection is performed on all tangible areas of the asset. Inspection surfaces need to be prepared (e.g. removing debris and corrosion) before the visual inspection. Using ringing sounds (low and high pitch) good materials or defective materials, below the surface of an asset, can be differentiated (HRTT Inspection Manual, 2005). Using a hammering test, hidden defects (e.g., drumminess) no deeper than a few millimetres can be detected without any sophisticated inspection equipment. The data and diagnosis obtained by a hammering test are subjective and strongly dependent on the inspector's skill; a significant disadvantage because only skilled inspectors can differentiate defective and non-defective material using the hammering noise. Furthermore, only the visible part of the asset can be inspected and defects such as separation between rings of a brick arch lining could be difficult or impossible to identify from a visual inspection (Mckibbins et al, 2009).

Current advances in Laser Scanning, Photogrammetry, computer vision and other sensor technologies (e.g. fibre optics and thermography) are now such that they are able to provide automated combined solutions to inspect the aging civil infrastructure. Besides reducing the errors during an inspection, it also reduces the preparatory work of an inspection significantly, avoiding, for example, the marking of inspection sectors and cleaning the inspection surface (Balaguer et al., 2014).

The advantages of applying new inspection technologies include (Balaguer et al., 2014).:

- Overcoming human subjectivity.
- Providing objective digital records for historical inspection data comparisons.
- Improving efficiencies in civil asset inspection resource application.
- Identifying areas of civil assets to be targeted for closer inspection.

However, someone still has to interpret the huge amount of digital data to effective and efficient decision making. This is the major disadvantage of using new technologies. However, decision-making algorithms can be developed to deal with large data sets.

A laser inspection provides a systematic record of all defects present at the time of inspection and facilitates all subsequent inspections. This, therefore, provides the possibility of reducing the number of inspectors needed in future to perform the inspections. With the knowledge of the previous digital records, the inspector's work becomes more qualitative. However, Euroconsult's laser scanning method has limitations as well. The system could not be used on parts of the tunnels like portals and headwalls where surfaces are not visible in the kinematic scan. Similarly, Euroconsult's scanning system (kinematic laser scanner) could not be used in "covered ways" with the same camera configuration, or with a "one single pass" (e.g. scanning tunnels and covered way at the same time), due to the variation in distance between the camera and the object. The 2014 laser inspection trial was performed to capture defects on covered ways as well. Due to the variation in distance between the camera and the object, most of the defects were not captured. Therefore, only the static laser scanner method could be used for 'Covered Way'.

Improvements through the usage of laser scanning in the process of tunnel inspection and maintenance projects have been shown to be important because of the surface information that can be obtained. Therefore, LUL has decided to carry out Euroconsult's laser survey of the Sub-Surface Line (SSL) brick tunnels every year. The associated software (Tunnel Viewer Software) allows analysis and filtering of the data where the inspector can review and visualize significant defects.

The processed scan data will serve as a background to create the inspection report which shows the defects such as cracking, mortar loss in joints, damp patches and face loss. The actual state of a tunnel can be identified using mapping of defects. Scan data which shows defects and digital inspection reports are made available to inspectors on a tablet computer for further clarification and verification of defects (Balaguer et al., 2014). Euroconsult's

“Tunnel Viewer software” can be used to analyse defects data, both qualitatively and quantitatively. Based on this analysis result, a “works order” can be created; remedial works can be monitored (e.g. re-pointing work and control seepage) and the works orders can be closed after completing remedial works successfully (Euroconsult, 2016).

3.2.1 Tunnel Inspection Methods

The purpose of an inspection is to make sure tunnels, which are functioning in harsh environmental conditions (e.g. vibration or frequently used), over a long period, are still safe or not. A desirable way to perform the inspection is to use non-destructive testing (NDT) rather than a destructive method. As the name suggests, the destructive methods can cause damage to the tunnel surface or cause a problem in terms of structural geometry/integrity (Balaguer et al., 2014). Currently, most of the tunnels are being constructed using spray concrete lining (SCL) and steel reinforcement. However, in the past, tunnels were constructed with other materials as well, such as cast-iron segments (e.g. LUL’s Bakerloo, Central, Northern and Piccadilly lines) and bricks (e.g. LUL’s District, Circle and Metropolitan lines). Defects in tunnels can be varied as they are based upon the construction materials. Therefore, the selection of tunnel inspection methods depends upon the type of defect that needs to be detected. The following inspection methods are commonly used for tunnel inspections all over the world.

3.2.1.1 Visual Method

The visual method is one of the most valuable non-destructive testing (NDT) methods widely used by LUL inspectors. Well-trained inspectors can gather valuable defect information. Various signs of distress to tunnel linings can be identified during the inspection, and that gives the preliminary condition of an asset (Balaguer *et al.*, 2014).

3.2.1.2 Endoscopy Methods

The endoscopy method consists of rigid or flexible tubes that can be inserted into predrilled boreholes, where under surface investigation is needed to examine its condition. An external light source can be provided using glass

fibres, and viewing is provided through reflective prisms. A charge-coupled device (CCD) is used in the latest devices to improve image quality. Some surface material may need to be destructed for its proper use (Balaguer *et al.*, 2014). Carino (2001) and Sansalone and Carino (1989) showed that the endoscopy method can be used to identify subsurface defects in concrete slabs.

3.2.1.3 Sonic and Ultrasonic Methods

In the sonic method, when the inspection hammer impacts the surface, impulses are created. Several pick up places in the wall collect the time of travel of these sonic pulses. Figure 3-1 shows the inspection hammer and picks up places. The time of travel of the sonic pulses is related to the module of elasticity and strength of the material of the inspection surface. Carino (2001) showed that the impact echo method can detect delamination on the concrete surface.

In the ultrasonic method, devices are normally used to measure the velocity in the material of a pulse generated by a piezoelectric transducer. The measured pulse velocity depends on the structural material and its elastic properties (Blitz and Simpson, 1996).

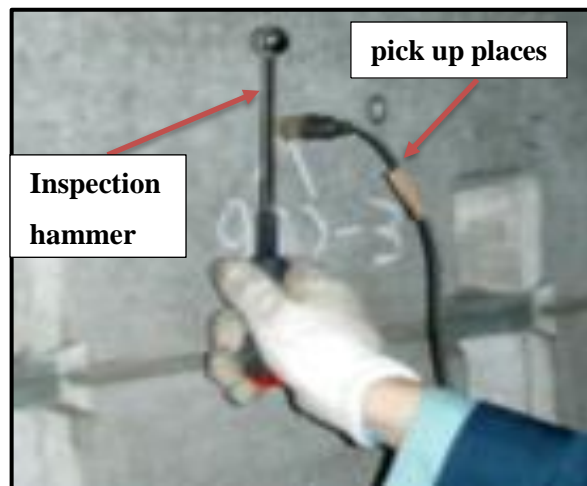


**Figure 3-1 Inspection using an impact hammer
(Balaguer *et al.*, 2014)**

3.2.1.4 ROBO-SPECT project

Using Robotic systems, inspections can be performed effectively and efficiently achieving objective results (Balaguer, 2010). Robotic methods can be used in dangerous environments (e.g. high-voltage cable tunnels and chemical wastage sewage tunnels) so that an inspector is not needed. Therefore, manual/visual inspection could be replaced by robotic systems which consist of a camera, a sonar, an echo sounder and a laser (Yu, 2007).

'ROBO-SPECT' is a project co-funded by the European Commission, under its 7th Framework Program (FP7). The ROBO-SPECT programme started in October 2013 and will finalize software and hardware components by the end of 2018. The purpose of this project is to create an automatic robotic system capable of performing an inspection in one pass' (Amdidtis et.al, 2016). Figure 3-2 shows ROBO-SPECT system concept.

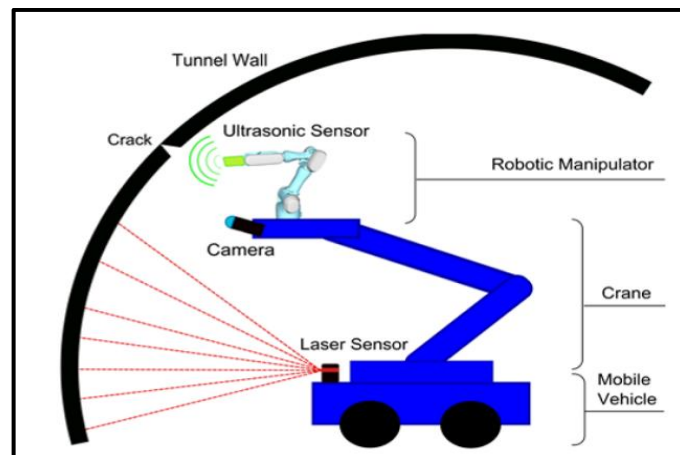


**Figure 3-2 ROBO-SPECT System - Concept
(Amdidtis et.al, 2016)**

The ROBO-SPECT system uses the ROBO vehicle, which can be operated in both Road and Rail environments to perform inspections. The vehicle is electrically powered and provides power to all onboard sensors and autonomous operation of its movement. The robotic system consists of three subsystems: the mobile robot, an automated crane arm (boom) and an industrial-quality robot manipulator. This system is under construction and various sensors will be used such as:

- laser, infrared and ultrasound proximity and distance sensors – 1 D
- vision camera and LIDAR sensors - 2D
- Laser and video camera -3D

Through the computer vision system (which will be attached on the Robotic Manipulator) the ROBO-SPECT system can detect structural anomalies such as spalling, staining, cracking, exposed-enforcement, white deposits and seepage. The Ultrasonic sensor is currently being developed in order to detect cracks' width and depth. A 3D laser scanner will be used to perform 3D scanning of the tunnel intrados at the point of interest (Amdidtis *et.al*, 2016).

3.3 Requirements of a Brick Tunnel Inspection

London Underground has an inspection system where the extent and severity of the condition of the lining are scored using prescribed inspection templates to provide an overall condition rating for the structure. Recommended actions and priorities are also indicated for each identified defect in the bridges and structures (S1060, 2014) inspection standard.

The overall requirements of a brick tunnel inspection should satisfy the requirements mentioned for the standard inspection of Bridges and Structures (S1060) and work instructions W2822 and W2909. These requirements are essential to identify individual characters, behaviour and maintenance needs for assets. To manage assets effectively and efficiently, the asset owner/manager has to know their functional and physical condition.

For more detailed information, the LUL engineering standard S1060 and work instructions W2822 and W2909 is referred to. These requirements should be used as specifications for any new inspection method (e.g. Euroconsult's high-definition laser scanner) of assets. However, in some instances, they will need to be updated in the light of new methods.

3.3.1 The standard for the Inspection of Bridges and Structures- S1060

The S1060 describes the types and frequencies of the visual inspections, the various forms to be used for reporting the data resulting from the inspections and the manner in which the forms are to be completed, together with inspection advice on the various assets. The requirements of S1060 are:

1. To provide all the necessary physical information on assets to meet the requirements for the Asset Condition Assessment and Certification (ACAC) and Asset Condition Reporting (ACR) process.
2. To identify defects, the causes and effects of damage and deterioration and Vulnerable Structures.
3. No Inspection shall commence unless the Inspector or inspection method has reviewed previous inspection reports and asset files to establish as far as possible information about the asset and likely hazards.
4. Identify deterioration in condition or visible development of defects.
5. List any significant defects that have occurred or worsened or changes which have occurred since the last inspection.
6. Record the extent and severity of any defects found.
7. Need to observe factors that may affect the safety of the asset.
8. Has to make recommendations for maintenance or strengthening and renewal works.
9. The report shall be written on the appropriate Pro-forma.
10. All inspectors must be Technician Members of the Institution of Civil Engineers or equivalent with suitable bridge and structure inspection experience.
11. Defects noted during the inspection shall be matched to the standard severity photographs in Clause 3.6 of the Standard S1060 in order to deduce the severity score that is to be entered in the Inspection Report.
12. Defects have to be classified according to the defect classification Table 3-1.

13. Where the condition of an element is anything less than B2 or an item score less than 6, the inspector shall describe the defects in a written narrative on a continuation sheet.
14. All reports shall contain at least a general photograph of the structure and a photograph of each item with a score indicating a worse condition than B2. Locations of the defects should be clearly indicated on the pictures.
15. The Condition Score is the lowest element rating contained in the structure and is derived from the scoring system mentioned in the standard S1060
16. Severity scores that are to be included in the inspection reports shall be based on comparisons with standard severity photographs mentioned in the standard S1060.
17. The standard graphical defect notation which must be used when showing defects on sketches or overlaying existing drawings (S1060, 2014).

Table 3-1 shows how to determine the defect classification according, using 2 categories: extent and severity, whilst the bottom part of the table shows the action to be taken and the priority.

Table 3-1 Defect Classification (S1055, 2012)

1	Extent	2	Severity
A-	Less than 5%	1-	No "significant defect"
B-	Between 5% and 10%	2-	"Minor"- defects of a non-urgent nature
C	-Between 10% and 20%	3-	"Heavy"- defects of an unacceptable nature
D	-Greater than 20%	4-	"Severe"-defects where action is needed(these shall be reported immediately to the supervisor)
3 Recommended action		4. Priority	
C-	Replace	I-	Immediate
P-	Paint	H-	High (within 12 months)
R-	Repair	M-	Medium (within 2 years)
M-	Monitor	L-	Low (before next Principal Inspection)
I-	Inspect	R-	Review (at next Principal Inspection)

3.3.2 The Management System Work Instructions Inspecting Brick Tunnels W2822

Work Instructions Inspecting Brick tunnels (W2822) shows how to conduct a principal, general and special inspection of a brick tunnel. Furthermore, it shows preliminary works have to follow before the inspection.

1. Type and location of inspection should be identified before starting any inspection.
2. Inspection history should be reviewed before starting any inspection especially when looking for recorded defects, access information, specific requirements, known specific hazards, environmental information and open work orders.
3. Risks associated with the inspection and appropriate mitigation controls.
4. Assets should be cleaned and free from debris before inspection in order to identify defects clearly.
5. Check for any deformation of tunnel portals and parapets such as bowing or leaning, or vehicle impact damage.
6. Check tunnel brickwork for damage due to efflorescence or frost on exposed elements.
7. Defects have to be checked at the interface between different structures such as pipe crossings and some girders.
8. Producing inspection reports using supporting materials such as photographs and locations of defects and tunnel chart.

3.3.3 Completion of Brick Tunnel Inspection Charts

At each brick tunnel inspection location, significant defects are manually recorded using two inspection charts: Forms F2353 and F2354.

1. Form F2353 shows the longitudinal section through the tunnel comprising a 0.5 m grid system depicting sidewalls haunch and crown areas. This chart comprises a maximum 50 m length zone per sheet page.

2. Form F2354 shows the end elevation(s) or headwall (or end wall) of the tunnel, again comprising a 0.5 m grid system.

According to the Engineering standard S1060, both forms should be merged in the office into the brick tunnel inspection spreadsheet.

Information relating to the following attributes should be included in the spreadsheet as follows:

- defect type
- specific location within the tunnel (alphanumeric identification assigned)
- specific depth of the specific location (where applicable)
- length (mm) of a specific location
- width (mm) of a specific location
- square metres totals of specific locations
- Asset entirety commutative totals.

The completed brick tunnel chart will form part of the principal inspection report.

3.3.4 The Management System Work Instructions- W2909- Producing A Brick Tunnel Inspection Chart.

- i. Brick tunnel information should be recorded on the hand-held device and headwall inspection charts template.
- ii. The defect types used are the standard notations provided in S1060, the inspection of bridges and structures.

These are:

- active water seepage
- bulging
- drummy
- efflorescence
- erosion, depth of erosion (millimetres)
- fractures and cracks
- hairline or dimension (millimetres)
- joint loss

- leached deposits
- missing brickwork
- repairs
- spalling and depth (millimetres)
- surface deposits
- vegetation
- wet or damp areas

Defects mentioned in the list above cause different rates of deterioration in assets. Therefore, the identification of a defect and its probable cause plays a crucial role in selecting the most appropriate new technologies.

3.4 Changes in Condition of an Asset

Transport infrastructure (e.g. tunnels, bridges and structures) are continuously under severe man-made and environmental conditions causing deterioration in construction materials. Some of the typical types of structural damage that may benefit significantly from monitoring are described below (Technical user manual, 2009 and Delatte *et.al*, 2009).

3.4.1 Water Seepage / Ingress

Water leaks in tunnels are a major cause of damage to tunnel walls and linings. Leakage of water through cracks causes corrosion in reinforced concrete, erosion of soil behind tunnel walls and propagation of cracks. This occurs when groundwater runs through the tunnel lining. Generally, if the tunnel is constructed below the water table, water seepage occurs more frequently than when the tunnel is constructed above the water table.

Figure 3-3 shows active seepage in brick tunnel lining. Mortar degradation resulting in the mortar 'washing out' from joints regularly leads to the subsequent saturation of the brickwork/masonry over time due to the consistent passage of water across its surface (Delatte *et.al*, 2009). Exposed areas of saturated masonry/brickwork are often subjected to successive freeze-thaw cycles, resulting in spalling. The combined effects of these actions can alter stresses and their distribution in the affected areas, instigating additional cracking. This generally exacerbates the problem of water ingress

leading to further loss of serviceability and ultimately failure of the structure element (Delatte *et.al*, 2009).

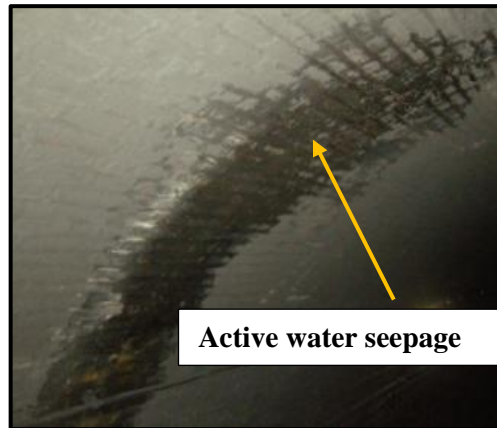


Figure 3-3 Active water seepage (TL 14, LUL 2011)

3.4.2 Bulging

Where parts of walls or arches are out of true, bulges or other irregularities can be seen and it can, therefore, be difficult to ascertain whether these are original features or deformations in response to stress in the lining. Also, deformation can be longstanding or recent and possibly continuing. Judgement is reliant on appearance (there may be associated deterioration) and quality of past inspections and records. Distortions can result in the local reduction of lining capacity (Mckibbins *et.al*, 2009).

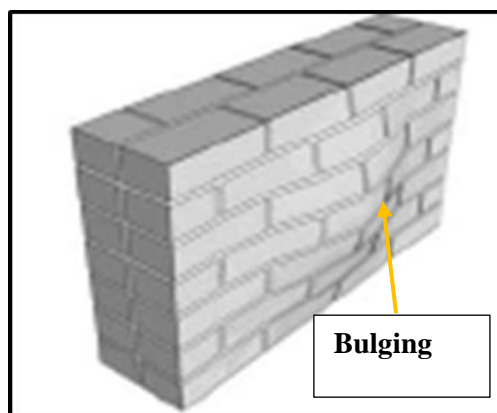


Figure 3-4 Bulging (Mckibbins *et.al*, 2009)

Bulging can often be found in tunnels (see Figure 3-4), either at a joint in construction or in more serious cases where water is present. Other irregular profiles and bulges may be the result of intrusive vegetation or forces acting on the structural elements such as lateral loading (Mckibbins et.al, 2009).

Bulging can be monitored using a laser scanner and then by comparison of different scans, identifying changes in the geometry of the tunnel lining.

3.4.3 Drummy/Hollow Brickwork

When sounding the brickwork with a tapping hammer it should resonate with a bright "bell" sound. It is generally accepted that this indicates the brickwork is well bonded and not distressed. A dull, flat tone often described as "drummy", is an indication of potentially hollow brickwork. This could either be attributed to ring separation or spalled brickwork (Mckibbins et.al, 2009).

The drumminess can be observed and calculated by using a hammering test during the visual inspection. At present, there is no direct technology/sensor to monitor drumminess of brickwork. However, thermography can be used to detect subsurface information (e.g. loosen brickworks) up to a depth of 10cm if the surface is heated for short periods (e.g. 1 minute) using a minimum of 500W infrared heat lamp and observing a cooling down process. A recorded thermogram needs to be processed in a signal reconstruction method to identify any drumminess or loosened bricks work (Sham, 2009). However, this defect did not identify during this research due to an authorisation problem to use the heating equipment in the running tunnel.

3.4.4 Efflorescence

Efflorescence is when a powdery white residue (see Figure 3-5) is formed when dissolved sulphates crystallize on the surface of brickwork (Technical user manual, 2009). Although this has no detrimental effect on the structure, in ideal conditions crystallisation can occur within the brick pores just beneath the brick surface resulting in spalling of the brickwork. This is known as sub florescence (W2822, 2014).

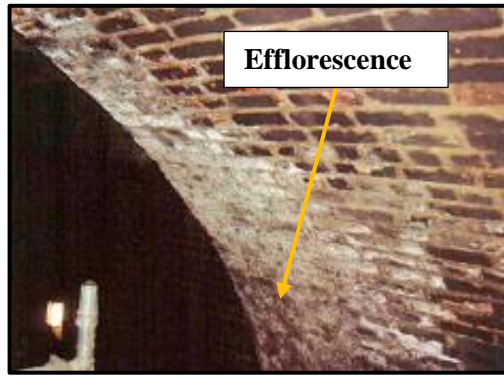


**Figure 3-5 Efflorescence to a brick tunnel
(TL27, 2011)**

According to the Engineering standard S1060, Efflorescence is not a scorable (no need to assign extent and severity) defect.

3.4.5 Fractures and Cracks

Fractures (see Figure 3-6) and cracks are created by rotational movement or local bending stresses in the tunnel lining (Technical user manual, 2009). They are of serious concern as they can indicate lining failure and are often associated with ring separation. Many longitudinal cracks are a result of the gradual movement of the lining over time. This could be due to settlement of the sidewalls, outward movement of the sidewalls due to lack of confinement or inward movement of the sidewalls due to lack of invert (Technical user manual, 2009).

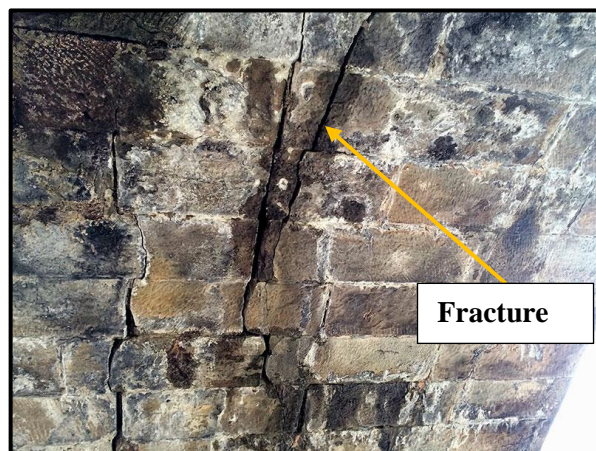


**Figure 3-6 Fractures and Cracks
(www.inspectapedia.com)**

3.4.6 Hairline and Dimension

Hairline cracks (see Figure 3-7) may be caused by overloading of the lining, differential settlement, localised poor construction or possibly a joint in the lining. The cause of the crack is crucial to finding an appropriate solution. Many hairline cracks will exist in tunnels without significant effect on the load-carrying effect of the lining (Technical user manual, 2009).

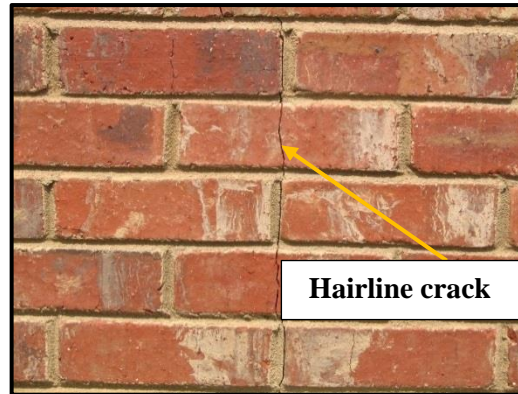


Figure 3-7 Hairline crack (Technical user manual, 2009)

3.4.7 Joint Loss

Where there is movement in the structure, possibly as a result of works being undertaken in the vicinity, the mortar may become lost through abrasion. Continuous wash out will result in joint loss and ultimately a breakdown of the bonding agent can occur causing local areas to become unstable. In some cases, this can occur to such an extent that bricks become loose and even fall out (W2822, 2014).



Figure 3-8 Joint loss (TL60, 2012)

Joint loss (see Figure 3-8) can be detected using static/kinematic laser scanner and close-range photogrammetry.

3.4.8 Leached Deposits and Surface Deposits

Leached deposits on tunnel structures (see Figure 3-9) often inhibit close inspection of the brickwork in a similar fashion to calcite formations and they can also contribute to chemical reactions in mortars.

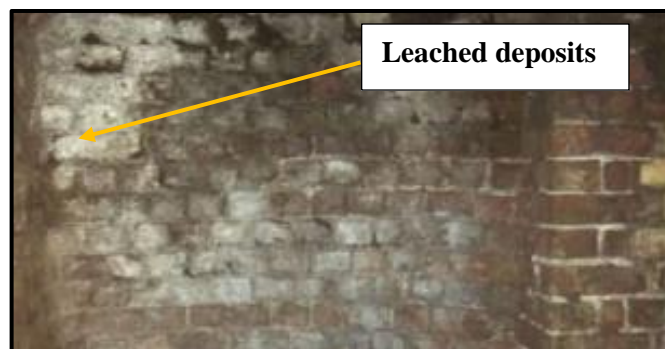


Figure 3-9 Leached deposits (TL56, LUL 2013)

Ochre is a brown/orange deposit, resembling greasy mud that leeches through joints and fissures, staining the brick surface. It may be organic in nature and is particularly prevalent in tunnels. Ochre breaks down the bonding properties of mortar resulting in the surrounding brickwork becoming loose and in extreme cases falling away (Technical user manual, 2009).

3.4.9 Spalling and Missing Brick Works

Spalling arises when bricks are subjected to constant water saturation (Figure 3-10). During freezing and thawing in winter they will become frost damaged and friable (W2822, 2014).

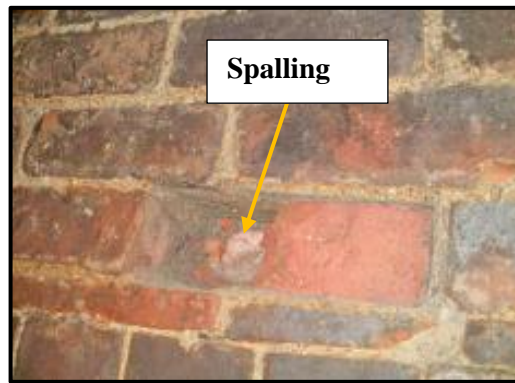


Figure 3-10 Spalling and missing brick works (W2822, 2014)

3.4.10 Repairs

Various types of repairs may have taken place during the life of the infrastructures (Technical user manual, 2009). The repaired areas (see Figure 3-11) are not scorable items, however; their locations should be clearly identified during the inspection in order to verify whether remedial works have been carried out properly.

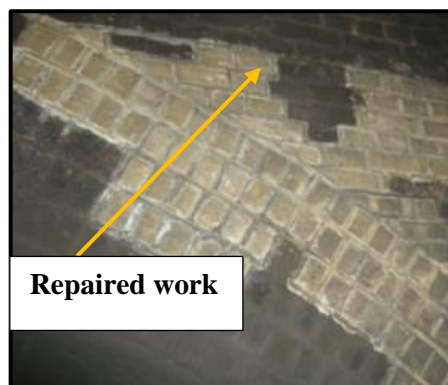


Figure 3-11 Repaired work (TL14, LUL 2011)

A laser scanner and close-range photogrammetry can be used to identify repaired work.

3.4.11 Intrusive Vegetation

The task of maintaining structures free from vegetation is important, which, if left unattended, can seriously destabilise a structure (see Figure 3-12).

Vegetation can take root in the most unexpected places including vertical faces such as face rings, spandrels and wing walls (Technical user manual, 2009).



Figure 3-12 Intrusive vegetation (TL10, LUL 2011)

An ideal environment for propagation often occurs where the distressed activity is already evident in a structure. Every type of plant from grasses to full-sized trees will if given the opportunity, take root. The most prolific and destructive is Buddleia (a semi-evergreen shrub), which has an affinity for lime and will rapidly invade and split lime mortar joints (Technical user manual, 2009).

3.4.12 Wet or Damp Areas

In tunnels, wet patches (see Figure 3-13) generally occur as a result of water-bearing features in the surrounding ground. This may cause the appearance of irregular profiling or bulging. Evidence of water percolation can also be seen in shafts where the existing drainage provision has become blocked by mineral deposits or is inadequate (Technical user manual, 2009).

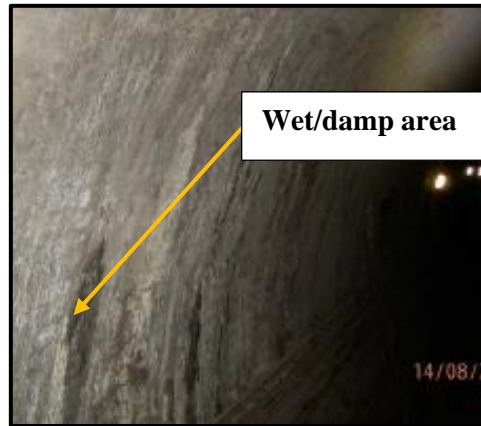


Figure 3-13 Wet or damp area (TL14, 2011)

Running water can cause mortar washout and serious effects on signaling equipment. Damp or wet patches also exposed to significant temperature changes can lead to spalled brickwork, which might typically be expected near portals and shafts.

Wet patches may indicate the more serious problem of an adjacent burst water main. Where the latter occurs in close proximity to a tunnel, the structure should be closely monitored for signs of distress (Technical user manual, 2009).

3.5 Selection of Appropriate Technologies

During the Master of Research (MRes) dissertation (first year of Eng.D programme), the author performed a detailed literature review of techniques mentioned in Table 3-2. Then, issues and problems in tunnels' and structures' maintenance were reviewed through the literature in order to select appropriate new technologies. The visual inspection reports of assets were reviewed which identified different types of defects in assets (tunnels, bridges and retaining walls).

This research mainly focused on automatically identifying defects on LUL brick tunnel inspections. Water seepage (dampness), mortar loss in joints, Cracks (fracture and hairline) and lining face loss (spalling) occurred most frequently on brick tunnels compared to other defects. These defects are surface defects that appear on a larger area rather than a point. Therefore, laser Scanner

(static and kinematic), close-range photogrammetry and thermography were selected in this research to monitor the condition of the tunnel. Other techniques mentioned in Table 3-2 provide discrete information rather than surface information.

From the asset management point of view, the rate of deterioration of assets is an important parameter in understanding the change in the condition of assets. Selections of different technologies are depended on the nature of the structure (e.g. bridges, headwalls, retaining walls and tunnels), construction method, access and space restriction.

New technologies would assist LUL in detecting different defects like water ingress, seepage, cracks, corrosion, voids, cavities and spalls as mentioned in section 3.3.4. New technologies can be used to assess and monitor the condition of assets and improve the efficiency of inspection, repair, and rehabilitation efforts. Monitoring how damage or deterioration changes over time will provide LUL with additional information used to prioritise their critical maintenance and repair activities. The objective of using new technologies is to observe infrastructure conditions, assess in-service performance, detect deterioration, and estimate remaining service life.

The use of new technologies, mentioned in Table 3-2, are potential methods to address the challenges (see Chapter 2 and section 2.6.3) currently faced by LUL, providing both qualitative and quantitative measures of an asset's condition. The selected technologies such as Thermography, Laser scanner and Close-Range Photogrammetry can be used for any LUL's assets, even though deep tube tunnels are smaller in diameter (3.1m) than Sub Surface Line (SSL).

Table 3-2 Types of defects detected by the new technologies

Defects	Laser Scanner	Thermography	Close Range Photogrammetry	Automatic Optical Survey	Digital Image Correlation	Fibre Optic Sensor	Wireless Sensor Network	Ground Penetration Radar
Bulging	✓		✓		✓			✓
Drummy		✓						✓
Efflorescence	✓		✓					
Joint loss	✓		✓					
Leached deposits			✓					
Erosion, depth of erosion	✓		✓					
Missing brickwork	✓		✓					
Repairs	✓							
Spalling and depth	✓	✓						
Surface deposits	✓	✓	✓					
Vegetation	✓							
Wet or damp areas	✓	✓	✓					
Active water seepage		✓						
Fractures and cracks	✓	✓	✓		✓		✓	
Hairline or dimension					✓		✓	
Strain					✓	✓	✓	
Deformation			✓	✓	✓	✓	✓	

The selection and performance of new technologies are based on the following criteria, mentioned by Gucunski, *et al.* (2010).

- i) Accuracy
- ii) Repeatability
- iii) Ease of data collection, analysis, and interpretation
- iv) Speed of data collection and analysis
- v) Cost of data collection and analysis

3.6 Scanning System Description

The '*Tunnelling*' system, developed by Euroconsult (Euroconsult, Tunnelling system, 2014), is a high-performance inspection system that enables tunnel evaluation to be carried out by analysing different defects in tunnel linings with a 1mm resolution at survey speeds up to 30km/h. The provision of 3D information enables the identification of relative displacements between assembled segments, in both the longitudinal and transverse directions. The system allows for the inspection of 12m long arc sections at survey speeds up to 30km/h, with a depth accuracy of 0.5mm. The system provides 1mm accuracy in the longitudinal and transverse directions. If the tunnel diameter is more than 12m, the entire perimeter of the tunnel can be covered in two opposite scan directions in order to scan the whole area at survey speeds of 30km/h.

The scanning was performed using a locomotive and a flat wagon. The metal frame was assembled on the flat wagon, and all the necessary systems were installed to survey half the section of the tunnel on each run. Figure 3-14 shows a Schematic diagram of the cameras mounted on the flat trolley.

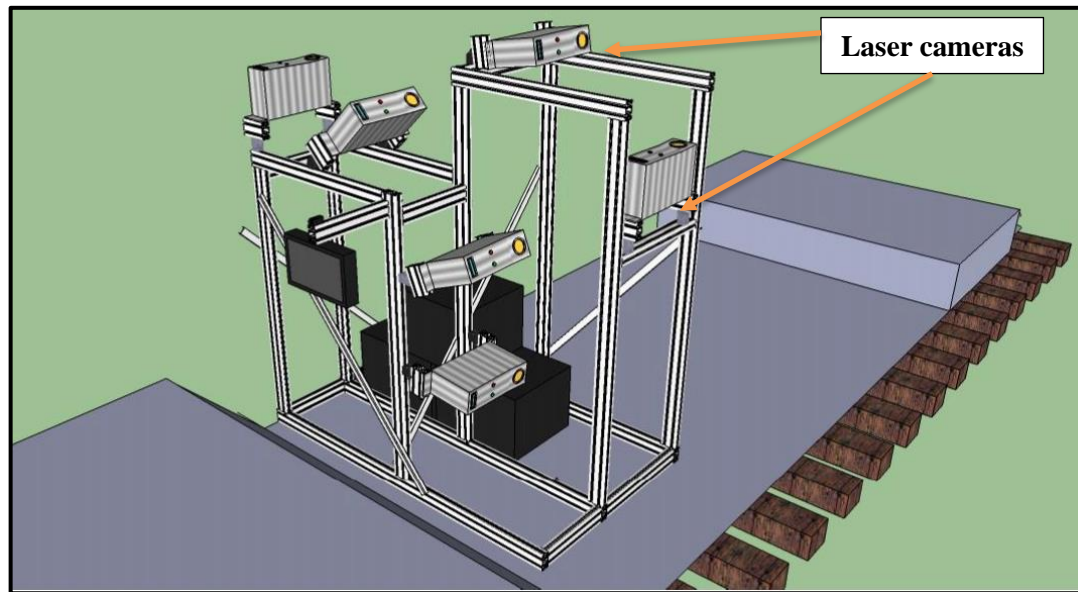


Figure 3-14 Schematic diagram of the cameras mounted on the flat trolley (Euroconsult, 2014)

In addition, its computer vision-based software for the automatic evaluation of the tunnel condition offers the following advantages:

- **Tunnel linings:** detection of cracks (brick lining) and areas with missing or chipped lining (in cast iron linings), dampness and running water (brick lining). Identification of poorly assembled segments, protruding edges and poor workmanship.
- **Railway evaluation:** includes the assessment of the transverse section by means of 3D geometry and rail flaws detection such as; lack of fixing elements, corrosion, cracks in sleepers or slab tracks.
- **Structure evaluation:** 3D reconstruction and clearance analysis (Euroconsult- Tunnelling system, 2014).

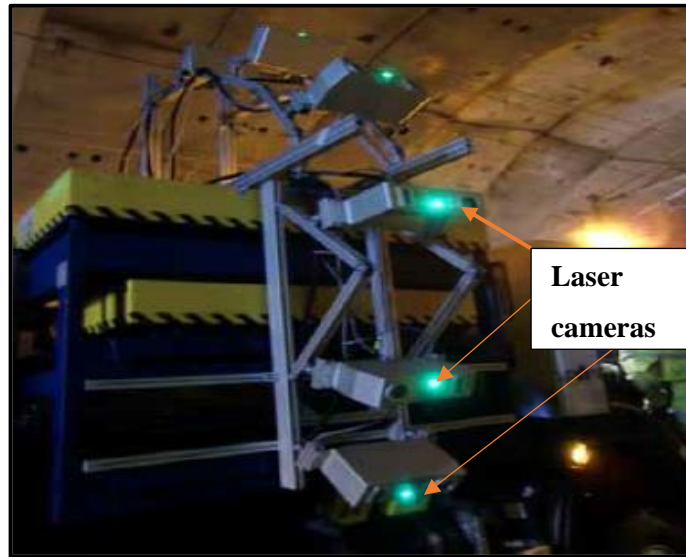


Figure 3-15 View of the side sensors that inspect the sidewalls (Euroconsult, 2014)

The second inspection (2015) scanning system consisted of a 3D laser and video camera, LIDAR and the panoramic cameras with infrared light. Each unit was independent of each other. However, they were synchronized to an odometer system to obtain a common geo-reference system. Detail description of each system is given below.

1. **3D laser camera:** camera providing digital mapping. The system allows for the reporting of superficial defects of the tunnel, such as cracks, water ingress, mortar loss in joints and face loss.
2. **LIDAR:** (Light Detection And Ranging) that measures distance by illuminating a target with a laser and analysing the reflected light. The LIDAR allows for acquiring an accurate geometry representation of tunnels.
3. **Visible-infrared camera:** These are used to take a high-resolution panoramic image to see the characteristics of the lining and facilities (e.g. cables and brackets) in detail. Three high-resolution cameras with visible-infrared illuminators were installed to allow for the synchronization of the images and the reconstruction of the tunnel in an illuminated panoramic view (Euroconsult, 2016).

3.7 Tunnelling System Description

The Tunnelling system uses high-speed cameras, custom optics, and laser line projectors to acquire both 2D images and high-resolution 3D profiles of the surveyed tunnel. It can be operated under all types of lighting conditions, providing high-quality data in both illuminated and shaded areas. The Tunnelling system allows for the acquisition of both 3D and 2D image data with 1mm transversal resolution over a 12-meter length of tunnel section, at survey speeds up to 30km/h, depending on the longitudinal resolution selected (Laurent, 2014).

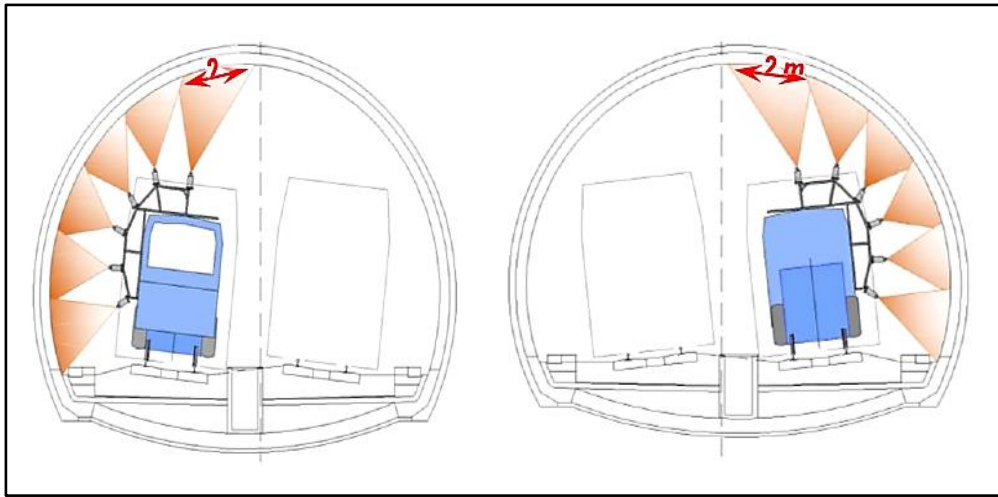


Figure 3-16 Tunnel scanning sensor Deployment (Laurent, 2014)

Figure 3-16 shows the scanning sensor deployment and each scanner cover the only 2m of swath width when they acquire data. Therefore, 6 sensors are required to scan the 12m of tunnel lining. The acquired high-resolution images lighted by laser emitters make it possible to conduct an assisted analysis to detect and analyse flaws, such as cracks, face loss, mortar loss and moisture. The provision of 3D information facilitates the evaluation when the damage is found in the tunnel's surface and allows for deformations and relative displacement, to be located and assessed (Laurent, 2014).

The system includes the following main components:

1. **Laser-camera units** (laser line projector and digital scanning camera).
- Depth accuracy: 0.5mm.
 - Sampling rate: max. 2800 profiles/second
 - Longitudinal resolution (profile spacing): 1mm (adjustable)
 - Transversal resolution: 2048 points/profile. The suggested trade-off between transversal accuracy and transversal field of view is 1 mm – 2 m.



Figure 3-17 Laser-camera units/laser line projector and digital scanning camera (Euroconsult, 2016)

The System installed for this second inspection included six cameras (see Figure 3-17) so 12 m of the lining can be inspected with a continuous single run (Euroconsult, 2016).

2. Odometer

A distance measurement indicator (DMI), also known as an odometer, is installed on the vehicle used for surveying purposes (Figure 3-18).



**Figure 3-18 The odometer
(Euroconsult, 2016)**

The odometer is of high precision (20.000 pulses per revolution, approx. 0.1mm.) and it is used to ensure that the speed of the vehicle does not exceed the pre-established conditions to guarantee the integrity of the data collection (i.e. data out of range).

3.7.1 Principles of the survey system (3D-camera-laser units)

The Tunnelling system extracts the 3D information using the principle of triangulation as displayed in Figure 3-19. A pattern of known lighting, a line, in this case, is projected from the laser onto the object to be inspected. The line is recorded by a digital camera positioned at a fixed distance away at an oblique angle relative to the projected light. The intersection between the pattern of emitted light and the field of view of the digital camera defines the range of operation of the 3-D sensor. The positions of the lighted points on the surface of the object are displayed in the image obtained by the camera and the distance between these points and the camera can be calculated using trigonometry. This technique enables high-quality digital images and superimposed 3D information to be obtained in a single capture (Euroconsult, 2016).

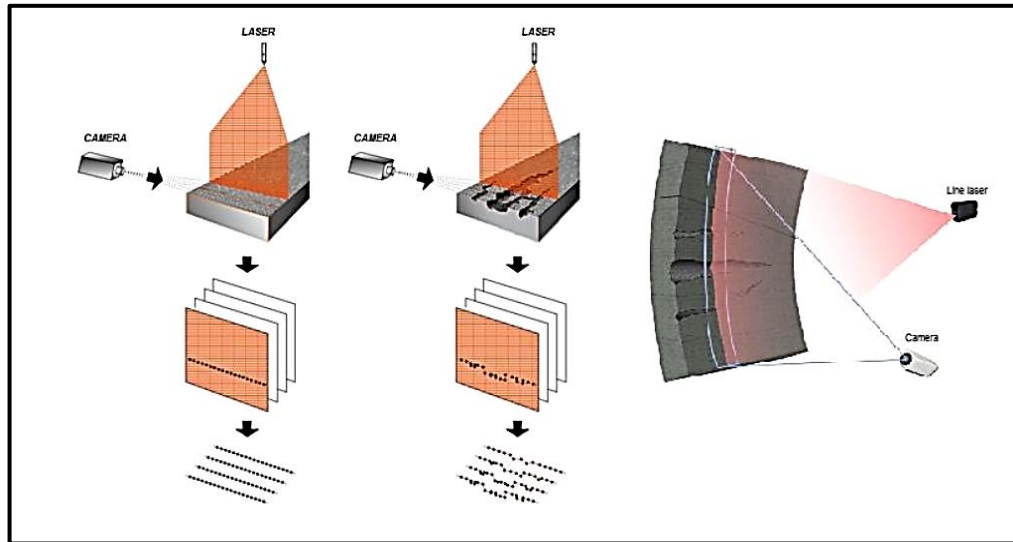


Figure 3-19 Principles of the survey system (3D-camera-laser units)

3.7.2 Acquisition and synchronization software

The Tunnelling system acquisition software performs control and synchronization tasks during the survey. An industrial computer is used to ensure the synchronization of the laser camera's units. The acquisition spacing can be set by the system operator to obtain the most acceptable trade-off between speed and resolution. The signal received from the odometer is used to trigger all the sensors at the right time (Euroconsult, 2016).

3.7.3 Data provided by the Tunnelling System

The data provided by the Tunnelling system comprises of 3D images, which contain information in a radial direction relative to the direction of the condition survey, combined with 2D images, with greyscale intensity information. The following types of results can be extracted from the survey:

High-quality digital images of the tunnel lining with a resolution of 1 mm were captured at a travelling speed of 20Km/h. However, data acquisition can be performed at speeds up to 100Km/h with less resolution (1cm). Figure 3-20 shows various inspection speed and achievable resolution (Laurent, 2014).

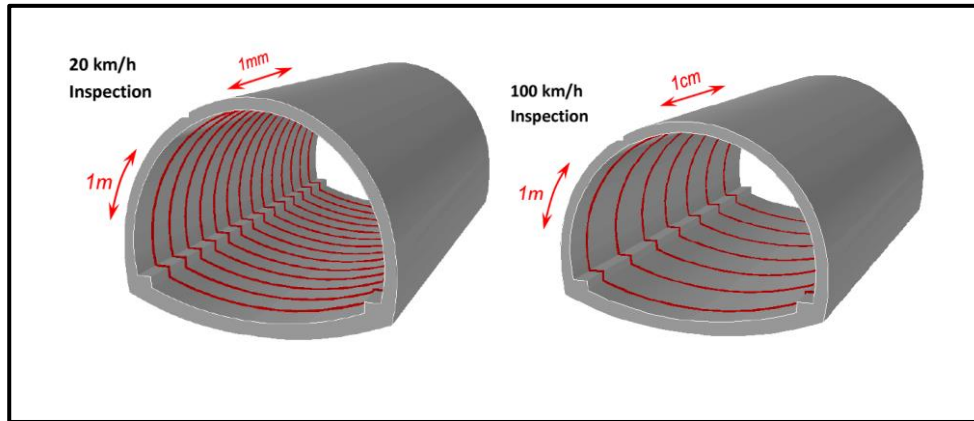


Figure 3-20 Resolution Vs Inspection speed (Laurent, 2014)

Transverse sections of the lining were obtained from the 3-D data information available. High-quality digital images and a 3D reconstruction of the inspected area can be obtained from the captured data. Examples of the 3D segment reconstruction and distinctness of mortar loss on the lining are shown in Figure 3-21.

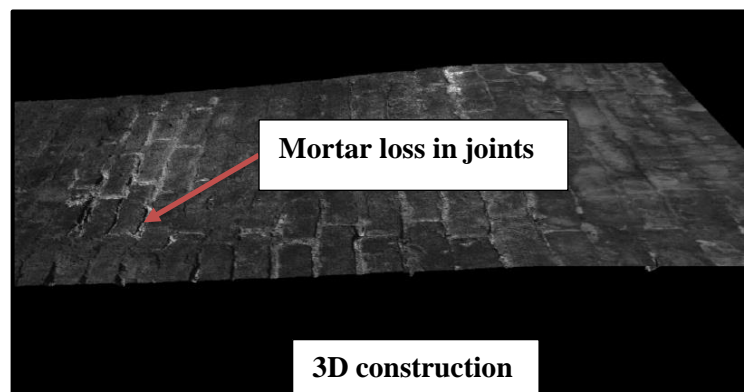


Figure 3-21 Mortar loss in joints- 3D segment re-construction

3.7.4 LIDAR System Description

Two LIDAR scanners have been installed on the system in order to obtain a point cloud of the tunnel and to take as many geometrical measurements as necessary.

The setup for each LIDAR was:

- Angular resolution 1° to 0.167° (adjustable)
- Scanning frequency, 100 Hz
- Scanning angle Max. 190°

- Max. range 80 m

Data from the LIDAR will be used for clearances and geometric information of the tunnels. Figure 3-22 shows an example of point cloud data created by the LIDAR system of a covered way (Euroconsult, 2016).

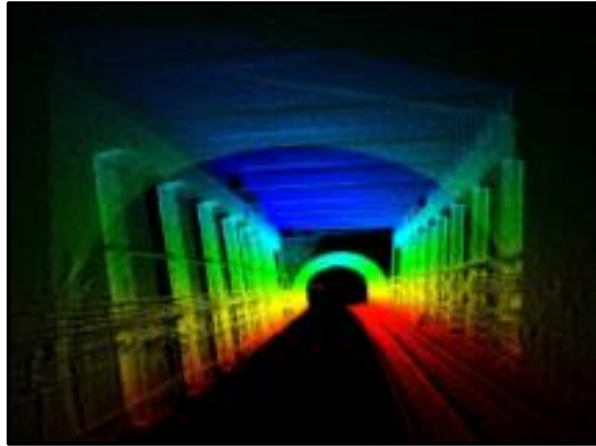


**Figure 3-22 Point cloud of the underground tunnel
(Euroconsult, 2016)**

3.7.5 Visible infrared cameras

This type of camera can be used to acquire images in unlit environments from which a global vision of the route is required. Figure 3-23 shows the equipment which includes a set of illuminators and infrared cameras able to acquire high-resolution images in completely dark environments.



**Figure 3-23 Set of illuminators and Infrared Cameras
(Euroconsult, 2016)**

The cameras have a CMOS sensor which features good quality and sensitivity at the near-infrared region of the light spectrum. In addition, these cameras also include a global shutter that allows for accurate moving snapshots and reproduction of sharp contrasts.

Main characteristics:

- Interface GigE
- Sensor: 1/1.8" CMOS
- Optics: 8mm.
- Resolution: 1280 x 1024
- Colour intensity: 10/12bit
- Global shutter
- Max. Speed: 50 fps

Figure 3-24 shows an example of the acquisition of a tunnel in complete darkness.



Figure 3-24 Data acquired in complete darkness

3.8 Raw Data Analysis

Automatic algorithms were developed by Euroconsult to analyse each raw data stream in order to extract different data elements; for example, the presence of dark moist areas were detected from intensity images and the presence of cracking was detected from 3D range data. The Laser Tunnel Scanning System (LTSS) acquires 3D range data by measuring the distance from the sensor to the surface for every sampled point. The range data were converted to a greyscale image using an image processing algorithm and a

wide variety of tunnel defects such as mortar loss, joint loss, damp patch and face loss were identified.

Results from data processing were stored using the open XML data format, and Range, Intensity and Merged 3D images were output as standard JPEG images to facilitate sharing and viewing (Laurent *et al.*, 2014).

3.8.1 Evaluation of tunnels conditions using laser survey

- **Overall tunnel rating**

Overall, the tunnel rating is computed by Euroconsult's tunnel evaluation method using an arithmetic average of the item scores of all the types of defects evaluated in a particular tunnel section.

- **Item (defect) score**

The item score is obtained for each defect through Table 3-3 according to the extent and severity category of the defect. Further information about Table 3-3 can be found in engineering standard S1060.

For each type of defect, the extent and severity levels were determined, then Table 3-3 was used to calculate the item score of each defect. Table 3-4 shows the inspection summary report and overall element rating of tunnel TL29.

Table 3-3 Extent and severity category of the defect

EXTENT/SEVERITY RATING	A1	A2	A3	A4	B1	B2	B3	B4	C1	C2	C3	C4	D1	D2	D3	D4
ITEM SCORE	8	7	5	4	7	6	4	3	6	5	3	2	5	4	2	1

Table 3-4 Inspection Report Summary

INSPECTION REPORT SUMMARY							
Structure No / Location: D084/TL29			Inspector's Name:				
Date of Inspection 06/07/2014			Weather/Temp:				
SUBSTRUCTURE DETAILS							
ITEM REF	SIDE WALLS **	COMMENT AND PRINCIPAL CONSTRUCTION MATERIAL	DEFECTS				ITEM SCORE
			E	S	X	P	
	Side Wall 1: (State)						
1	Location and Description						
2	Foundations Invert						
3	Material						
* 4	Condition (General Surface)		A	1			8
* 5	Joint Condition/Width/Depth		A	3			5
* 6	Alignment						
* 7	Arch Springing						
8	Drainage						
9	Other Comments						
			TOTAL ITEM SCORE (X)				13
			No. of ITEMS SCORED (Y)				2
			OVERALL ELEMENT RATING $(X \div Y) \times 12.5 =$				81.2 %

- **Extent category (A to D)**

The extent category is assigned depending on the extent value of the defect expressed as a percentage. Table 3-5 shows a classification of Extent and is categorised between A and D.

Table 3-5 Classification of Extent (Euroconsult, 2016)

Extent (E)	Category
A	Less than 5%
B	Between 5% and 10%
C	Between 10% and 20%
D	Greater than 20%

- **Severity category (1 to 4)**

Severity category is assigned depending on an average severity value of the defect in millimetres. The Severity and Extent thresholds are set out in Table

3-5 and Table 3-6; this is in line with the LUL Engineering Standard S1060 for Extent and Severity calculation. Equations (3.1) to (3.10) were developed by Euroconsult to calculate defects using laser scanner data.

Table 3-6 Classification of Severity (Euroconsult, 2016)

Severity	Cracking width (mm)	Joint loss depth (mm)	Face loss depth (mm)
1	less than 1	less than 15	less than 10
2	between 1 and 5	between 15 and 25	between 10 and 30
3	between 5 and 10	between 25 and 30	between 30 and 40
4	greater than 10	greater than 30	greater than 40

- **Extent value (%) computation method for cracking**

The total length with cracking is computed as the summation of the length of all the cracking defects

$$TL_{Defects}(mm) = \sum_{All\ defects} Length_{Defect} \quad (3.1)$$

$$\text{Total length tunnel: } TL_{Tunnel}(mm) \quad (3.2)$$

$$\text{Extent (\%)} = 100 \times \frac{TL_{Defects}}{TL_{Tunnel}} \quad (3.3)$$

- **Extent value (%) computation for face loss, mortar loss and damp areas**

The total area is computed as the summation of the area of the defects of the type evaluated,

$$TA_{Defects}(mm^2) = \sum_{All\ defects} Area_{Defect} \quad (3.4)$$

For total area tunnel, computed as the total length of the tunnel by length of the transversal section

$$TA_{Tunnel}(mm^2) \quad (3.5)$$

$$\text{Extent (\%)} = 100 \times \frac{TA_{Defects}}{TA_{Tunnel}} \quad (3.6)$$

- Area of mortar loss is estimated from its length and

- Area of face loss = 1/8 x length face loss
- **Severity value (mm) Computation**
 - **for cracking**

$Width_{Defect}$, the width of each crack is computed by the Euroconsult's computer vision software.

$$Width_{Average} = \frac{1}{\sum_{All\ defects} Length_{Defect}} \times \sum_{All\ defects} Width_{Defect} \times Length_{Defect} \quad (3.7)$$

$$Severity\ (mm) = Width_{Average} \quad (3.8)$$

- **for face loss and mortar loss**

$Depth_{Defect}$, the depth of each face loss or mortar loss is computed by the computer vision software developed by Euroconsult.

$$Depth_{Average} = \frac{1}{\sum_{All\ defects} Area_{Defect}} \times \sum_{All\ defects} Depth_{Defect} \times Area_{Defect} \quad (3.9)$$

$$Severity\ (mm) = Depth_{Average} \quad (3.10)$$

- **for damp patches (areas)**

Computation for damp patches is not performed by Euroconsult and is always considered to be severity 1.

All Severity 4 defects are reviewed and checked on site by inspectors to verify and confirm the defects. This will be mentioned in the principal inspection report.

Table 3-7 shows defect charts that show the average quantification of each defect. For cracking it is the sum of the length of cracking per metre length of the tunnel, similarly, the average of other defects scores is also calculated.

Table 3-7 Defect chart for Tunnel 17 - Laser Inspection 2014

TL17_14		TL17		LENGTH TUNNEL (m)		196											
INCIDENT	LENGTH (m)	AREA (m2)	EXTENT (%)	CATEGORY	AVERAGED MEASURE	S	ITEM SCORE										
CRACKING	2.52		1.29	A	27	4	4										
JOINT LOSS	15.63	0.63	0.02	A	30.92	4	4										
FACE LOSS		0.44	0.01	A	77.4	4	4										
DAMPNESS		9.92	0.33	A		1	8										
					TOTAL SCORE		62.5 %										
INCIDENT	COMMENTS																
CRACKING																	
JOINT LOSS																	
FACE LOSS																	
DAMPNESS																	
SECTION	INTERVAL																
TL17	From 0 m to 196 m																

database (asset register). The visual inspection report contains the following sections (S1060, 2014):

1. Referral Sheet
2. Bridge & Structure General Reference Sheet
3. Inspection & Maintenance Summary
4. Defect Description
5. Inspection Details
6. Inspection Report Summary

Defects are already described *via* the number of ‘concerns’ that form part of the system in ACAC engineering standards for structure and bridges (in these cases tunnels and covered ways) in order to obtain unique ACAC scores from different inspectors when they perform inspections. However, these scores can be varied depending on the ability of the inspector to interpret the data. An example of a visual inspection defect description is given Table 3-8 for an asset TL26.

Table 3-8 describes part of the tunnel (TL 26) assets (e.g South side wall, North side wall and brick arch) inspected and a description of the corresponding defects (e.g: drumminess, joint loss, corrosion on pipe and cracking). Furthermore, this table shows severity/extent scores (e.g. A3, B1 and B2) and recommendation (e.g. trace/stop, remove and review at next inspection) to rectify or control defects.

Where: -

E- Extent

S-Severity

R- Recommended Action

P-Priority

Table 3-8 TL 26 Visual Inspection-Defect Descriptions (LUL, 2013)

DEFECT DESCRIPTION					A0c
LCS/Structure No: D086 / TL26			Number of ID Plates present: 2		
Name of Inspector: GANALON REGINO			Inspection Date: 14 & 15 /08/2013		
Location: MANSION HOUSE/BLACKFRIARS					
Item			Defects		Recommendation & Approx Quantity
Scoring Sheet	Ref	Description	Type	Description (please state if defects are above 2m height)	
				Slight increase in drumminess, wetness and leaching on comparison to the last PI dated 17 th April 2011. See tunnel chart(Defects update are in red colour) Those defects identified on last PI dated 17 th April 2011 shows no significant change on comparison to the attached tunnel charts & photos.	
A16A	4	<u>SOUTH SIDE WALL:</u> CONDITION(GENERAL SURFACE)	A3	Some new drumminess and wetness identified in isolated areas. Photo 2 and tunnel charts.	Trace/stop or control seepage.
A16A	5	JOINT CONDITION/WIDTH/DEPTH	B1	Minor old standing isolated joint loss to side wall. Photos 2 & 3.	Review at next inspection.
A16A	9	OTHER COMMENTS	A3	Seepage/leaching to wall. Also causing corrosion damage to the attached electrical lighting pipe. 3Nos attached timber materials to the wall, appears partly rotten due to seepage. Photos 8 & 9.	Check the corroded pipe; Removed the timber materials.
		<u>NORTH SIDE WALL:</u>			
A16A	4	CONDITION(GENERAL SURFACE)	A3	New isolated wetness identified between chainage 285m to 300m. Photo 22	Trace/stop or control seepage.
A16A	5	JOINT CONDITION/WIDTH/DEPTH	B1	All the joint loss already been identified on last PI. No new joint loss has been identified. See attached tunnel charts.	Review at next inspection.
		<u>BRICK ARCH:</u>			
A16A	12	PROFILE CONDITION/ DEFORMATION	B2	Previously identified isolated slight bulging from 10mm to 20mm to brick arch haunching shows no significant change. Photo 18. Some isolated new drumminess identified. Photo 13 Previously identified drumminess remains the same at time of inspection.	Review at next inspection.
A16A	13	MATERIAL DESCRIPTION/ CONDITION	A3	There is slight increase in seepage and dampness to haunching. See attached channel charts. Previously reported spalling to old concrete patched repair remains the same since the last PI. Photo 15	Trace/stop or control seepage. Remove loose concrete and patch repair.
A16A	14	JOINT CONDITION/WIDTH/ DEPTH	B2	Old standing isolated joint loss to brick tunnel. No change since the last PI. Photo 12.	Review at next inspection.
A16A	15	CRACKING (LOCATE AND DESCRIBE)	A3	No significant change on the condition of the old standing fractures. Photo 10 I only inspected 50% part of the asset – The South side wall (adjacent to W/B tracks) and the brick arch tunnel over the W/B tracks. Bayo Bolaji carried out PI on the remaining 50% part of the asset - The North side wall(adjacent to E/B tracks) and the brick arch tunnel over the E/B tracks.	Review the fractures at next inspection for any signs of movement.

Table 3-9 gives brief comments of each asset and scoring of all mandatory fields denoted by (*). The score of the Arch Springing is not taken into account when calculating the overall element rating, because this is not the scorable item according to the inspection standard S1060. However, an inspector has to report the condition of the Arch Springing in the comment column.

Table 3-9 TL 26 Visual Inspection-Inspection report summary (LUL, 2013)

A16a (Form 1 of 2)

BRICK TUNNEL
INSPECTION REPORT SUMMARY

Structure No / Location: D086 / D086/TL26 Inspector's Name: GANALON REGINO

Date of Inspection: 14 & 15/08/2013 Weather / Temp: DRY / 19 deg C

SUBSTRUCTURE DETAILS

ITEM REF	SIDE WALLS **	COMMENT AND PRINCIPAL CONSTRUCTION MATERIAL	DEFECTS				ITEM SCORE
			E	S	R	P	
	Side Wall 1: (State)	Abutment					
1	Location and Description	South Side Wall, adjacent to Metropolitan Line W/B Tracks					
2	Foundations / Invert	N/V	-	-			
3	Material	Brickwork					
* 4	Condition (General Surface)	Spalling, drummy, seepage, leaching/	A	3	R	L	5
* 5	Joint Condition / Width / Depth	Isolated old standing joint Loss	B	1	I	R	7
* 6	Alignment	No obvious sign of misalignment	A	1	I	R	8
* 7	Arch Springing	Wetness, leaching, joint loss	A	2	I	R	0
8	Drainage	Drainage Hole to south side wall/Not active at time of inspection.	A	1	I	R	
9	Other Comments	Seepage/leaching causing corrosion to electrical pipe/ 3Nos timber materials attached to wall.	A	3	I	R	
TOTAL ITEM SCORE (X)							20
No. of ITEMS SCORED (Y)							3
OVERALL ELEMENT RATING $(X \div Y) \times 12.5 =$							83.33%

	Side Wall 2: (State)	Sidewall					
1	Location and Description	North Side Wall, adjacent to Metropolitan Line E/B Tracks					
2	Foundations / Invert	N/V	-	-			
3	Material	Brickwork					
* 4	Condition (General Surface)	Spalling, drummy, seepage, leaching	A	3	R	L	5
* 5	Joint Condition / Width / Depth	Isolated old standing joint loss	B	1	R	L	7
* 6	Alignment	No obvious signs of deformation	A	1	I	R	8
* 7	Arch Springing	Wetness, Leaching, joint loss	A	2	I	R	7
8	Drainage	N/A	-	-			
9	Other Comments	N/A	-	-			
TOTAL ITEM SCORE (X)							20
No. of ITEMS SCORED (Y)							3
OVERALL ELEMENT RATING $(X \div Y) \times 12.5 =$							83.33%

Indicate items not applicable (N/A) or not visible (N/V)
* Items to receive an 'Item Score' if item is applicable

Defects of Arch Springing can be provided only by visual inspection because Visual/Principal Inspection divides the tunnel into the following sections (see Figure 3-25);

- Sidewalls 1
- Haunch (the area between sidewall and Crown)
- Crown
- Sidewall 2

Condition scores of the Arch Springing come from the haunch area of the tunnel.

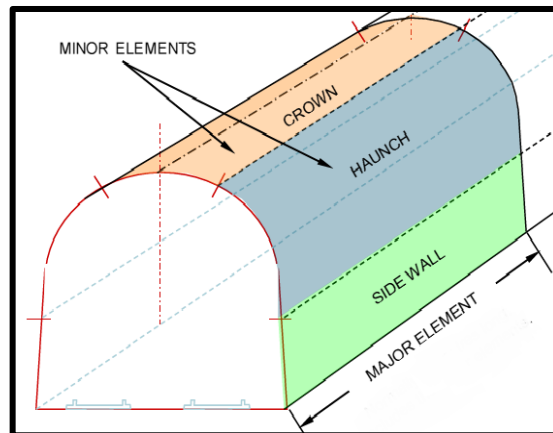


**Figure 3-25 Division of tunnels for visual inspection
(Network Rail, 2014)**

Using the requirements of Engineering Standard S1060, a score of 80.36% (see Table 3-10) has been obtained as the condition score of an asset. The Inspection Review Engineer uses this score along with the comments mentioned by the inspector to recommend suitable remedial work.

Table 3-10 TL 26 Visual Inspection- Substructure inspection report summary (LUL, 2013)

BRICK TUNNEL						A16a (Form 2 of 2)	
INSPECTION REPORT SUMMARY							
Structure No / Location: D086 / D086/TL26				Inspector's Name: GANALON REGINO			
Date of Inspection: 14 & 15/08/2013				Weather / Temp: DRY / 19 deg C			
SUBSTRUCTURE DETAILS							
ITEM REF	ARCH, HEADWALLS, PARAPETS, SURFACING AND DRAINAGE	COMMENT AND CONSTRUCTION MATERIALS	DEFECTS				ITEM SCORE
			E	S	R	P	
	Brick Arch:	District Line single span brick tunnel with side walls.					
10	No Rings (square/skew*)	7 rings(square)					
11	Arch Profile (known/assumed*)	Circular - Assumed					
* 12	Profile Condition/Deformation	Old standing 10mm to 20mm bulging, Drumminess	B	2	I	R	6
* 13	Material Description/Condition	Seepage,dampness, leaching, efflorescence, spalling	A	3	R	L	5
* 14	Joint Condition/Width/Depth	Joint loss of 10mm to 30mm depth	B	2	I	R	6
* 15	Cracking (Locate and describe)	Minor H/L cracks/No change on comparison to last PI	A	3	R	L	5
16	Other Comments	re-pointing works carried out	-	-			
	Headwalls:						
17	Arrangement	Bricks					
* 18	Alignment	No signs of deformation.	A	1	I	R	8
* 19	Joint Condition/Width/Depth	Minor joint loss	A	2	I	R	7
* 20	Cracking	No cracking noted	A	1	I	R	8
21	Other Comments		-	-			
	Parapets:	N/A					
22	Arrangement	N/A					
* 23	Alignment	N/A	-	-			0
* 24	Joint Condition/Width/Depth	N/A	-	-			0
* 25	Cracking	N/A	-	-			0
26	Other Comments	N/A	-	-			
	Surfacing:						
27	Carriageway	Queen Victoria Street	-	-			
28	Footway	Good	-	-			
29	Other Comments		-	-			
	Drainage:						
30	Arrangement/Support	N/A	-	-			
31	Condition/Effectiveness	N/A	-	-			
32	Other Comments		-	-			
Indicate items not applicable (N/A) or not visible (N/V)							
* Items to receive an 'Item Score' if item is applicable							
			TOTAL ITEM SCORE (X)				45
			No. of ITEMS SCORED (Y)				7
			OVERALL ELEMENT RATING (X ÷ Y) x 12.5 =				80.36%

3.10 Inspection Frequency

London Underground Inspection frequencies are risk-based, the risk being that of a structure developing a fault sufficient to interrupt the passenger service either by partial or complete station closure, speed restriction or line closure (S1060, 2014). Bridges and structures are subject to a 4 yearly (minimum requirement) Principal Inspection frequency as per the S1060 inspection standard.

When the rate of deterioration is unknown, it may be necessary to undertake a number of frequent special inspections to check and report on any change. The rate of deterioration can be found in historical information (previous defects information) of assets in the Ellipse database.

The frequency of inspection depends on the following factors:

- Age of the structure
- Value of the asset
- Operational condition
- Construction method/material of the asset
- Inspection/maintenance history
- Physical/ functional condition of the asset
- Organisation's policy, strategy, objective and goal in asset management

3.11 Euroconsult's Laser Scanner First Inspection 2014

3.11.1 Description of the Laser Survey

The laser survey was carried out during engineering hours (1.30 am to 5.00 am) over two weekend periods (Saturday 28th and Sunday 29th of June 2014 and Saturday 5th and Sunday 6th July 2014).

The inspection was carried out using a locomotive and flat wagon (see Figure 3-26). The metal frame was assembled on a flat wagon, and six laser-camera units were installed to survey half of the section for each run. Two types of tunnel sections were inspected: brick tunnels, known as TL sections and covered ways (CW). The inspection comprised 34 tunnel sets between contiguous stations, 27 of them within the Circle line and 7 of them within the Hammersmith & City line (Euroconsult, Tunnelling system 2014). A complete schedule of the tunnel laser surveyed with severity scores can be found in Appendix A.

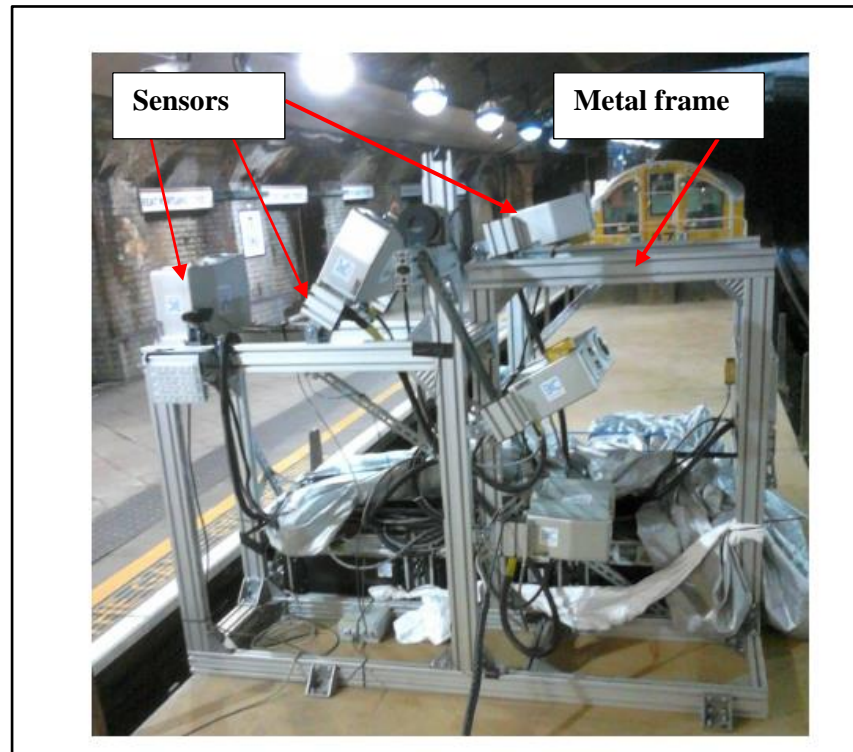


**Figure 3-26 Metal frame with six sensors on a flat wagon
(Euroconsult, 2014)**

3.11.2 Laser Scanning Inspection

The laser scanner inspection consisted of detecting any possible pathology that might affect the tunnel performance and its deterioration over time. Therefore, incidences analysed on the tunnel lining were grouped into the following categories (Euroconsult Tunnelling system, 2014):

1. Mortar loss in joints
2. Lining face loss
3. Cracking
4. Damp patches

A colour code system was used in the “Tunnel Viewer” software to identify the severity rating of the defects and it is shown in Table 3-11.

Table 3-11 Severity Colour coding system

Severity	Description	Colour
4	Severe	Red
3	Heavy	Orange
2	Minor	Brown
1	No 'significant defect.'	Green

To identify different defects in the tunnel chart, the following key was used in the software. Examples of defects on the tunnel chart can be found in Appendix D.

**Figure 3-27 Tunnel Defects Key**

In order to categorise the severity rating of the defects, users can change the desired threshold value for each defect and sort it in ascending or descending value. An example of Euroconsult's laser scanner report for the same asset (TL26) is given in Table 3-12.

**Table 3-12 TL-26 Laser Scanner- Side walls inspection report summary
(LUL, 2014)**

<u>BRICK TUNNEL</u>							A16a
<u>INSPECTION REPORT SUMMARY</u>							Sheet of
Structure No / Location: D086/TL26				Inspector's Name			
Date of Inspection 06/07/2014				Weather/Temp.....			
<u>SUBSTRUCTURE DETAILS</u>							
ITEM REF	SIDE WALLS **	COMMENT AND PRINCIPAL CONSTRUCTION MATERIAL	DEFECTS				ITEM SCORE
			E	S	R	P	
	Side Wall 1: (State)						
1	Location and Description						
2	Foundations/Invert						
3	Material						
*4	Condition (General Surface)		A	1			8
*5	Joint Condition/Width/Depth		A	2			7
*6	Alignment						
*7	Arch Springing						
8	Drainage						
9	Other Comments						
			TOTAL ITEM SCORE (X)				15
			No. of ITEMS SCORED (Y)				2
			OVERALL ELEMENT RATING $(X \div Y) \times 12.5 =$				93.8 %
	Side Wall 2: (State)						
1	Location and Description						
2	Foundations/Invert						
3	Material						
*4	Condition (General Surface)		A	3			5
*5	Joint Condition/Width/Depth		A	2			7
*6	Alignment						
*7	Arch Springing						
8	Drainage						
9	Other Comments						
			TOTAL ITEM SCORE (X)				12
			No. of ITEMS SCORED (Y)				2
			OVERALL ELEMENT RATING $(X \div Y) \times 12.5 =$				75 %

Indicate items not applicable (N/A) or not visible (N/V)
* Items to receive an 'Item Score' if item is applicable

Compared to the visual inspection, only major defects were captured during the laser inspection giving quite different degrees of accuracy and overall element rating (see Table 3-12 and Table 3-13).

The scores for the Alignment of the sidewalls, as can be seen in Table 3-13, were not provide by the Euroconsult laser survey. Therefore, the Euroconsult survey only does the average between two defects, whilst the visual inspection compares 3 defects for sidewalls. The non-availability of scores for alignment will be reflected in the overall element rating of asset scores when compared

to the principal inspection. The scanning system also does not provide any comments, on the General Comments column, for each defect.

Table 3-13 TL 26 - Laser scanner- Substructure inspection report summary (LUL, 2014)

BRICK TUNNEL							Sheet of
INSPECTION REPORT SUMMARY							
Structure No / Location: D086/TL26			Inspector's Name				
Date of Inspection 06/07/2014			Weather/Temp.....				
SUBSTRUCTURE DETAILS							
ITEM	ARCH, HEADWALLS, PARAPETS,	COMMENT AND PRINCIPAL CONSTRUCTION MATERIALS	DEFECTS				ITEM
REF	SURFACING AND DRAINAGE		E	S	R	P	SCORE
	Brick Arch:						
10	No Rings (square/skew*)						
11	Arch Profile (known/assumed*)						
* 12	Profile Condition/Deformation						
* 13	Material Description/Condition		A	3			5
* 14	Joint Condition/Width/Depth		A	2			7
* 15	Cracking (Locate and describe)		A	4			4
16	Other Comments						
	Headwalls:						
17	Arrangement						
* 18	Alignment						
* 19	Joint Condition/Width/Depth						
* 20	Cracking						
21	Other Comments						
	Parapets:						
22	Arrangement						
* 23	Alignment						
* 24	Joint Condition/Width/Depth						
* 25	Cracking						
26	Other Comments						
	Surfacing:						
27	Carriageway						
28	Footway						
29	Other Comments						
	Drainage:						
30	Arrangement/Support						
31	Condition/Effectiveness						
32	Other Comments						

Indicate items not applicable (N/A) or not visible (N/V)

* Items to receive an 'Item Score' if item is applicable

TOTAL ITEM SCORE (X)	16
No. of ITEMS SCORED (Y)	3
OVERALL ELEMENT RATING $(X \div Y) \times 12.5 =$	66.7 %

The scanning system divides the tunnel into three major parts: **side wall 1** (right side of the tunnel scans direction/ 0° to 45°), **Crown** (45° to 135°) and **sidewall 2** (135° to 180°) for defect scoring purposes, unfortunately, this is different than the model followed by LUL and Network Rail (see Figure 3-25). Therefore, the system can provide scores only for the following sections of the inspection report summary:

- Condition (general surface) - average of all the defects mentioned above
- Joint condition/width/depth - average of mortar loss and lining face loss
- Cracking – average of all types of cracking (hairline, fractures and partial/full opened)

The laser scan takes the average of all the defects' scores (average of mortar loss in joint, cracking, lining face loss and dampness) to calculate the condition score of an asset.

The combination of the laser scanner inspection and the visual inspection are currently being used to produce the Principal Inspection report. Assets that have severity scores of 3 and 4 need further investigation. In some cases, night inspectors need to be asked to perform visual inspections of particular locations (Severity 3 or 4) in order to further clarify the asset's condition.

A sample of the Euroconsult output, with all the incidents identified by the laser survey for tunnel 26 (TL26), is found in Appendix D.

3.11.3 Data Analysis

The overall condition rating of 112 assets (brick tunnels and covered ways on the SSL) provided by Euroconsult were initially compared to visual inspection scores. The summary of scores of both systems can be found in Appendices A and B. The visual inspections were performed in different years between 2009 and 2014. However, high-resolution laser survey was performed during June and July 2014. Most of the assets' scores, using the different methods, were not comparable. In fact, for some assets, significant differences were identified, as can be seen in Figure 3-29.

Figure 3-29 shows the comparison of scores obtained by both methods. The laser survey only captured and scored the defects mentioned in section 3.11.2. The difference in inspection scores between both systems varies throughout the assets. Compared to the visual inspection, the laser survey does not capture all defects mentioned in the Engineering Standard S1060. This might be one of the reasons for variation in inspection scores.

In order to identify the number of assets and the corresponding percentage range difference, a bar chart was generated (Figure 3-28). Figure 3-29 shows that 35 assets out of 112 had only less than 5% difference between Euroconsult rating and visual inspection and twenty-seven assets less than 10% and 19 assets less than 15% difference.

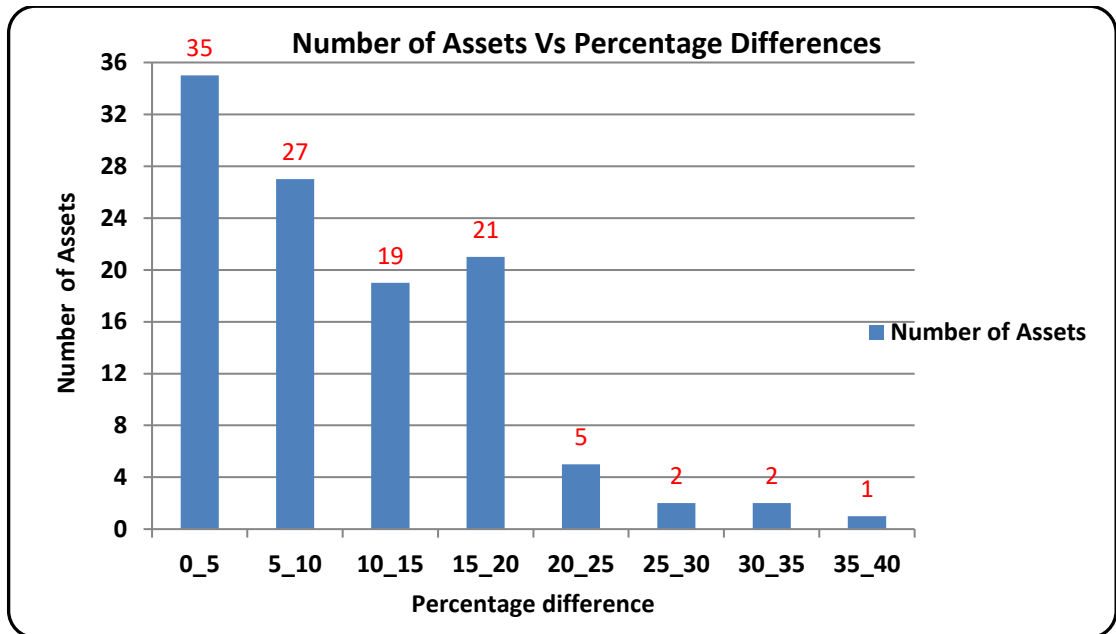


Figure 3-28 Number of Assets Vs percentage difference

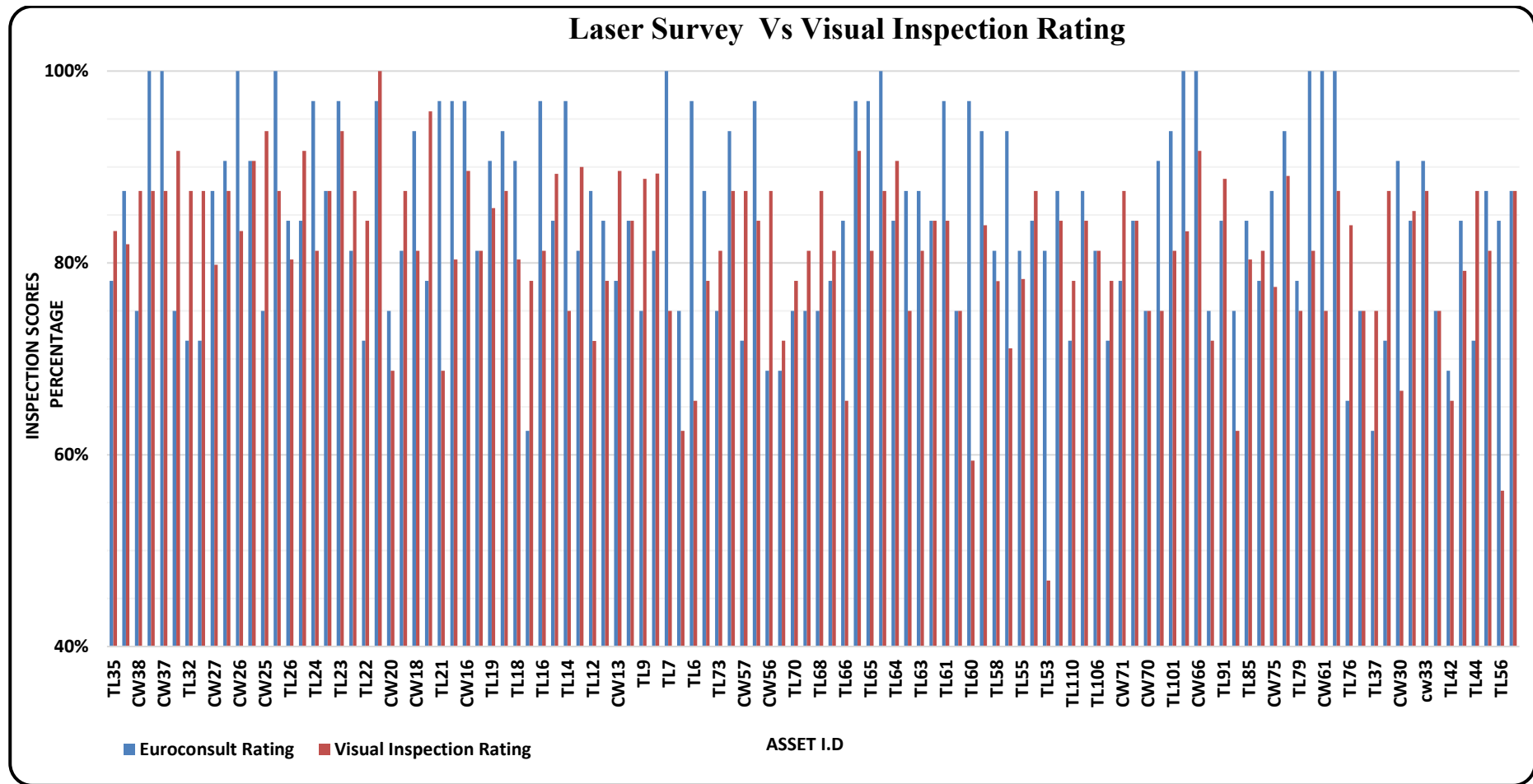


Figure 3-29 Laser Survey Vs Visual Inspection Rating of 112 assets in the SSL

Figure 3-29 shows that direct comparison of laser scanning against visual inspection of assets is inappropriate because the laser scanner does not capture all the defects mentioned in the Engineering Standard, S1060. Partial data from the laser scanner were compared directly with visual inspection data that contained more defect information. This is one of the main reasons for variation in both inspection scores shown in Figure 3-29.

Scoring methods for visual inspection and Euroconsult's laser inspection are not the same. The overall tunnel rating is computed using the arithmetic average of the item scores of all the defect types, evaluated on a particular tunnel section. Afterwards, equations (3.1) to (3.10) are used to calculate the extent and severity scores of each defect. Finally, equation (3.11) is used to calculate the inspection score of an asset (overall element rating). During a visual inspection, the inspector assigns extent and severity scores for each part of an asset, using a tunnel chart (field note). Equation (3.11) is then used to calculate the inspection scores for each part of an asset. Assigning a score to defect (severity and extent) solely depends on the ability of an inspector to interpret the data. This method has drawbacks because of the inconsistencies between the scores of different inspectors, given the subjectivity of the method. Using the requirements of Engineering Standard S1060, the lowest score of an asset has been obtained as the condition score. Due to two different types of scoring methods, this means it is not reasonable to compare inspection scores. Therefore, further analyses were performed to focus only on defects captured by the laser inspection and compared to the visual inspection. Sometimes it is necessary to change an inspection standard (S1060) to identify defects in a more reliable way. LUL has already appointed a committee to determine which method is more suitable to identify defects in a less subjective and more repetitive manner.

3.11.4 Comparison of Visual Inspection and Laser Scanner Inspection of Assets

To understand the difference between scores, the visual inspections and the laser scanner inspection reports of the following assets were further analysed:

- Covered Way 15
- Tunnel 17
- Tunnel 56
- Tunnel 60
- Covered Way 61

Unfortunately, some of the pictures taken from the LUL visual inspection reports do not show clearly the defect mentioned and this is a problem seen in many reports, however, the pictures were still used as they also offered a means to localise the defect within the Euroconsult software.

3.11.4.1 Covered Way 15

Covered way 15 is a 48m in length, located between St James's Park and Victoria stations above the District and Circle lines. The asset carries Vandon Street, Caxton Street and Buckingham Gate.

Euroconsult developed the "Tunnel Viewer" software to view defects in tunnels and covered ways captured using their laser survey system. The location of defects in a covered way is referenced to the mileage system. However, during visual inspections, the inspectors referenced all defects in covered ways with respect to adjacent girder numbers (13 and 14 in this case). Two different referencing methods were in use, therefore, a direct comparison of the defects was only possible after converting the adjacent girder number to mileage. Figure 3-30 shows a general view of the covered way 15.



**Figure 3-30 General view of the covered way 15
(LUL, 2011)**

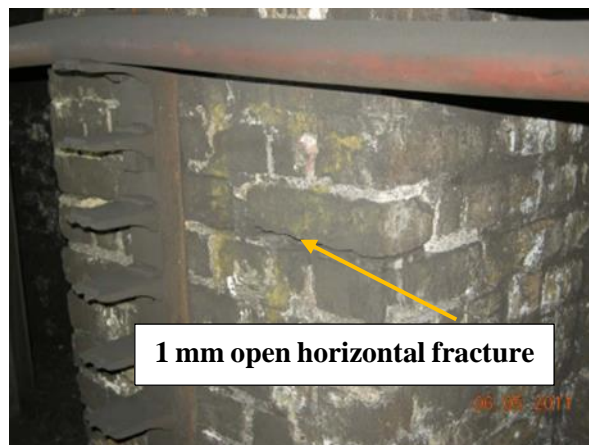


**Figure 3-31 North abutment 1mm open horizontal fracture
(LUL, 2011)**

Figure 3-31 shows the north abutment, with a minor 1mm open horizontal fracture between girders 13 and 14. This defect was not identified by the laser survey due to it being out of line of sight between the laser and the object. Furthermore, other defects mentioned in the visual inspection report for this asset could not be compared with the laser inspection because of the two different referencing systems mentioned above.

Due to areas of surface corrosion and loss of cast iron, the lower score of A3 (item score 5 /extent A and severity3) was given by the inspector (see Table 3-14). Using the requirements of Engineering Standard S1060, the lowest score of 81.25% (score of superstructure) was obtained as the condition score of the asset for this inspection.

The laser inspection system does not pick up painted areas; however, works for painting and remedial work for active seepage were completed before the laser inspection.

Table 3-14 Visual Inspection - Condition score of an asset- CW15 (LUL, 2011)

COVERED WAY INSPECTION REPORT							
Structure No / Location: D104 / CW15			Inspector's Name: BOWER MATTHEW				
Date of Inspection: 06/05/2011			Weather / Temp: DRY / 15 deg C				
SUPERSTRUCTURE DETAILS							
ITEM REF	SPANNING MEMBERS / DECK	COMMENT AND CONSTRUCTION MATERIALS	DEFECTS				ITEM SCORE
			E	S	R	P	
Spanning Members:							
9	Type and No.	girders 18 no					
10	Location and Description	cast iron girders only bottom flange visible					
* 11	Top Face (Flange)	not visible	-	-			0
* 12	Bottom Face (Flange and Deck Soffit)	numerous areas of surface corrosion, holed area 35mm wide and depth of 35mm loss of the cast iron	A	3	R	H	5
* 13	Sides (Web)	not visible	-	-			0
* 14	Edges at End	as built	A	1	I	R	8
15	Other Comments						
Surfacing:							
16	Carriageway	Caxton street & Buckingham Gate, Vandon street	A	1	I	R	
17	Footway	Footpath	A	1	I	R	
18	Other Comments						
Drainage:							
19	Arrangement / Support						
20	Condition / Effectiveness		-	-			
21	Other Comments						
Indicate items not applicable (N/A) or not visible (N/V)							
* Items to receive an 'Item Score' if item is applicable							
TOTAL ITEM SCORE (X)						13	
No. of ITEMS SCORED (Y)						2	
OVERALL ELEMENT RATING $(X \div Y) \times 12.5 =$						81.25%	

The laser survey did identify cracking and assigned the score of A4 (see Table 3-15). This clearly indicated that both scores cannot be compared because of different inspection periods (visual 2011 and laser inspection 2015) and only partial parameters were captured by the laser inspection.

Scoring methods for both systems were not the same, the laser survey calculated each defect using equations (3.1) to (3.10) then using this average extent (A, B, C, D) and severity scores (1, 2, 3, 4) for each defect were assigned.

According to the inspection standard, S1060 both systems have used the following formula to calculate the final score of an asset.

Total Item Score (X)

$$\text{Overall Element Rating} = (X / Y) * 12.5 \quad (3.11)$$

Visual inspection assigns an extent and severity score for each part of an asset using a tunnel chart (field note). Then the overall element rating equation (3.11) is applied to calculate the inspection scores for each part of an asset. Assigning a score to defect (severity and extent) solely depends on the ability of an inspector to interpret the data. Using the requirements of Engineering Standard S1060, the lowest score has been obtained as the condition score of the asset.

Table 3-15 Laser survey report CW 15 (LUL, 2014)

TUNNEL		D104/CW15			LENGTH TUNNEL (m)		51	
		St Jame's Park - Victoria			AREA TUNNEL (m2)		825,231	
INCIDENT	LENGTH (m)	AREA (m2)	EXTENT (%)	CATEGORY	AVERAGED MEASURE	S	ITEM SCORE	
CRACKING	0,55	8,96	1,09	A	24,29	4	4	
DAMPNESS		0	0	A		1	8	
JOINT LOSS	6,18	0,25	0,03	A	22,02	2	7	
FACE LOSS		0,02	0	A	17,16	2	7	
					TOTAL SCORE		81,25%	
INCIDENT	COMMENTS							
CRACKING								
DAMPNESS								
JOINT LOSS								
FACE LOSS								
SECTION	INTERVAL	<div><div><div>1. EXTENT (E)</div><div>A Less than 5% B Between 5% and 10% C Between 10% and 20% D Greater than 20%</div></div><div><div>2. SEVERITY (S)</div><div>1 No 'significant defect' 2 'Minor' - defects of a non-urgent nature 3 'Minor' - defects of a non-acceptable nature which shall be included for attention within the next two annual maintenance programmes 4 'Severe' - defects where action is needed (these shall be reported immediately to the supervisor). These defects shall require action within the next financial year.</div></div></div>						
CW15	From 0 m to 51 m							
TL19	From 54 m to 84 m							
CW14	From 87 m to 219 m							
TL18	From 231 m to 297 m							
TL17	From 351 m to 507 m	<div><div><div>3. RECOMMENDED ACTION (R)</div><div>C Replace P Paint R Repair M Monitor I Inspect</div></div><div><div>4. PRIORITY (P)</div><div>- Immediate H - High (within 12 months) M - Medium (within 2 years) L - Low (before next principal inspection) R - Review (for assessment at next principal inspection)</div></div></div>						

Table 3-16 Laser Inspection Report Summary CW 15 (LUL, 2014)

INSPECTION REPORT SUMMARY																			
Structure No / Location: D104/CW15										Inspector's Name									
Date of Inspection 06/07/2014										Weather/Temp.....									
SUBSTRUCTURE DETAILS																			
ITEM	SIDE WALLS **	COMMENT AND PRINCIPAL CONSTRUCTION MATERIAL	DEFECTS				ITEM												
REF							SCORE												
			E	S	R	P													
	Side Wall 1: (State)																		
1	Location and Description																		
2	Foundations/Invert																		
3	Material																		
* 4	Condition (General Surface)		A	2			7												
* 5	Joint Condition/Width/Depth		A	2			7												
* 6	Alignment																		
* 7	Arch Springing																		
8	Drainage																		
9	Other Comments																		
			TOTAL ITEM SCORE (X)				14												
			No. of ITEMS SCORED (Y)				2												
			OVERALL ELEMENT RATING (X ÷ Y) x 12.5 =				87.5 %												
	Side Wall 2: (State)																		
1	Location and Description																		
2	Foundations/Invert																		
3	Material																		
* 4	Condition (General Surface)		A	1			8												
* 5	Joint Condition/Width/Depth		A	3			5												
* 6	Alignment																		
* 7	Arch Springing																		
8	Drainage																		
9	Other Comments																		
Indicate items not applicable (N/A) or not visible (N/V)																			
* Items to receive an 'Item Score' if the item is applicable			TOTAL ITEM SCORE (X)				13												
			No. of ITEMS SCORED (Y)				2												
			OVERALL ELEMENT RATING (X ÷ Y) x 12.5 =				81.2 %												

3.11.4.2 Tunnel 17 (TL77)

TL17 is located between Victoria and St James Park stations; the tunnel is 196m in length. Active water seepage at chainage 60 from the arch springer to track the level on the left side wall (see Figure 3-34) was identified during the visual inspection. However, this water seepage was not identified by the laser inspection and was not seen in the “Tunnel Viewer” software (see Figure 3-33). This seepage may have been inactive during the laser inspection.



Figure 3-32 General view of tunnel 17 (LUL, 2011)

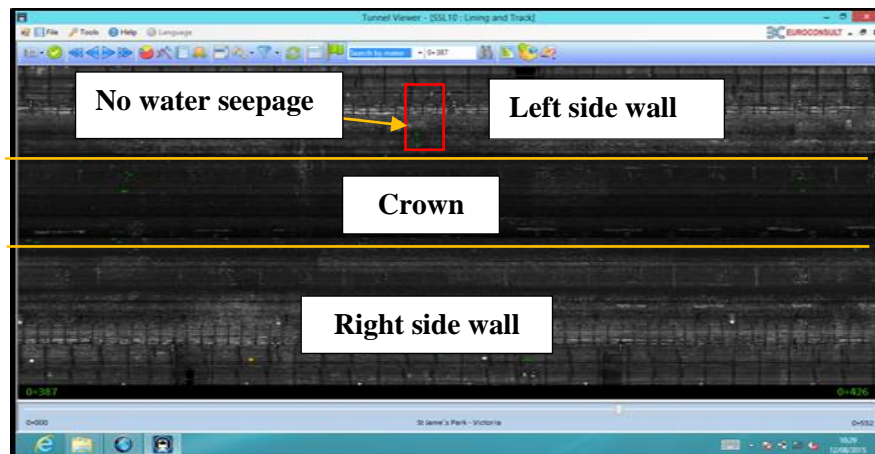


Figure 3-33 Laser inspection water seepage -TL17

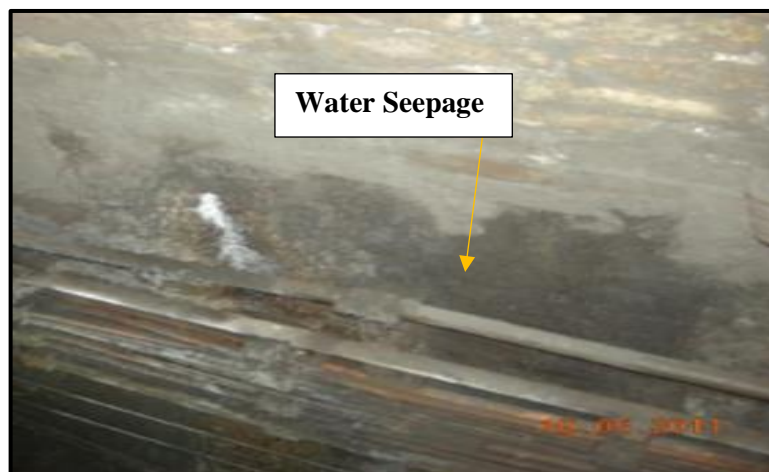


Figure 3-34 Visual inspection water seepage – TL17 (LUL, 2011)

The view of typical spalling and mortar loss in joints in the arch soffit at chainage 65 of tunnel 17 (left side) is shown in Figure 3-35 and Figure 3-36 and was identified by both inspection methods.

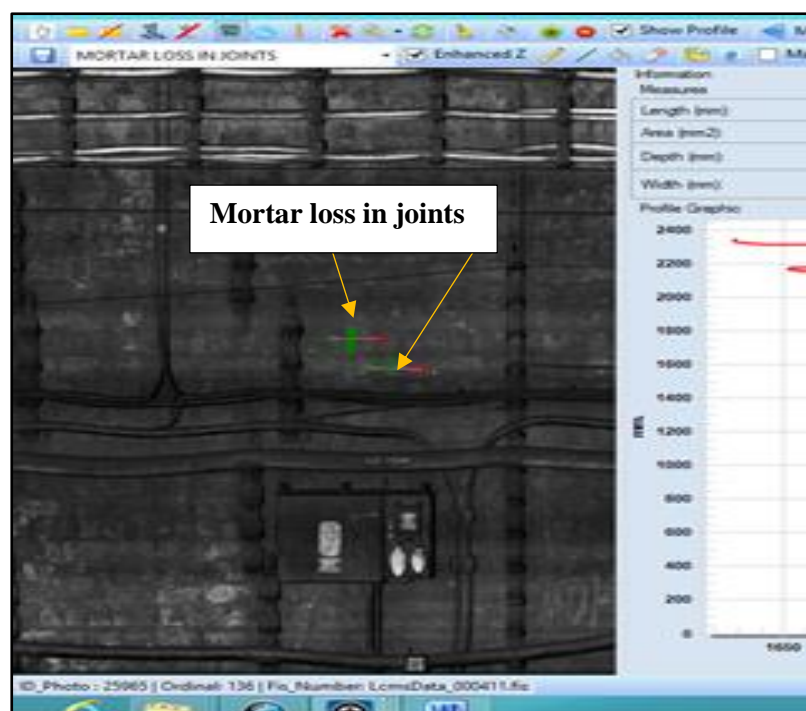


Figure 3-35 Laser inspection Mortar loss in joints- TL17 (LUL, 2011)

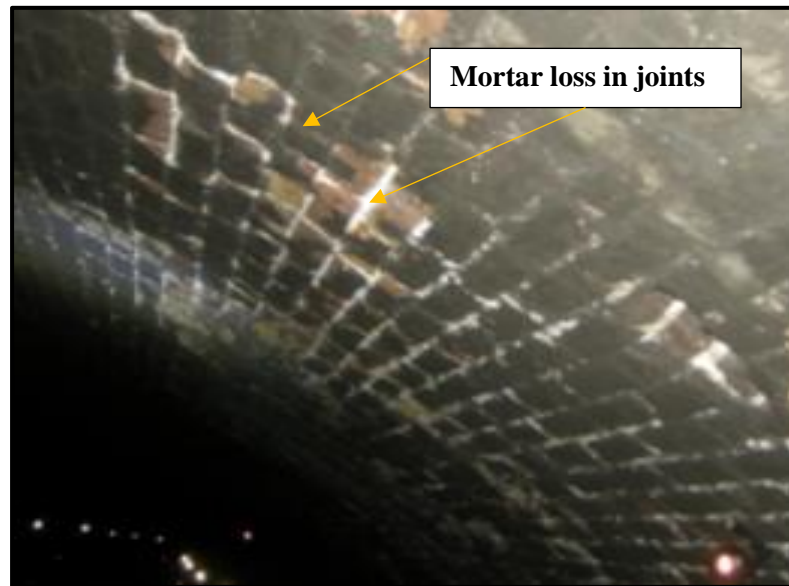


Figure 3-36 Visual inspection Mortar loss in joints – TL17, LUL 2013

The active water seepages between chainage 80 and 100 were identified as damp patches in the laser survey shown as a blue rectangle in Figure 3-37. The visual inspection tunnel chart (see Figure 3-38) shows this defect using standard defect notification “w” (wet and damp area) at the left sidewall.

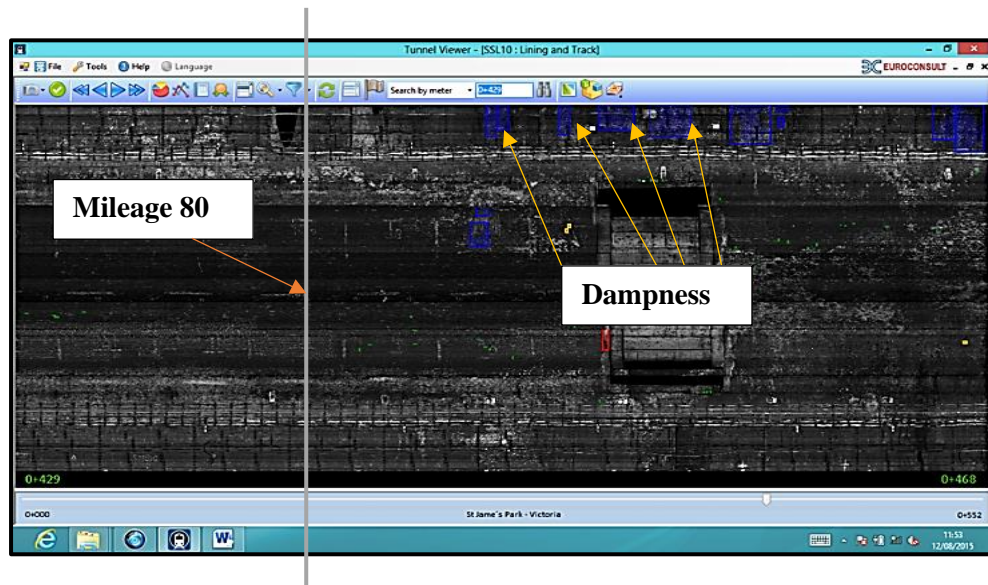


Figure 3-37 Laser inspection Dampness TL-17

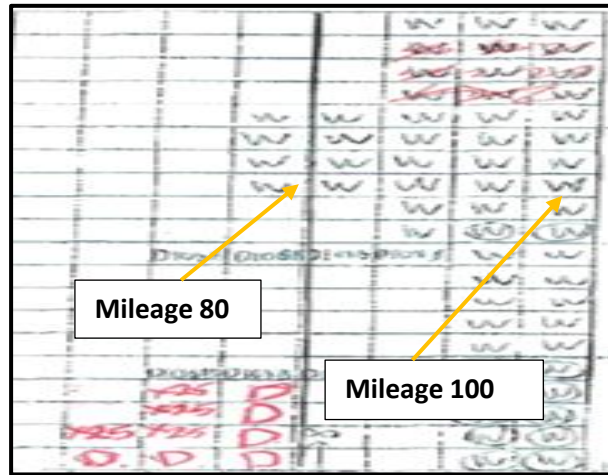


Figure 3-38 Visual inspection water seepage tunnel chart TL-17 (LUL, 2011)

Figure 3-39 shows face loss in brick arch soffit area (scattered green dots). However, this defect was not identified by the visual inspection because it may have appeared after the visual inspection (there was a 3-year gap between the two inspections).

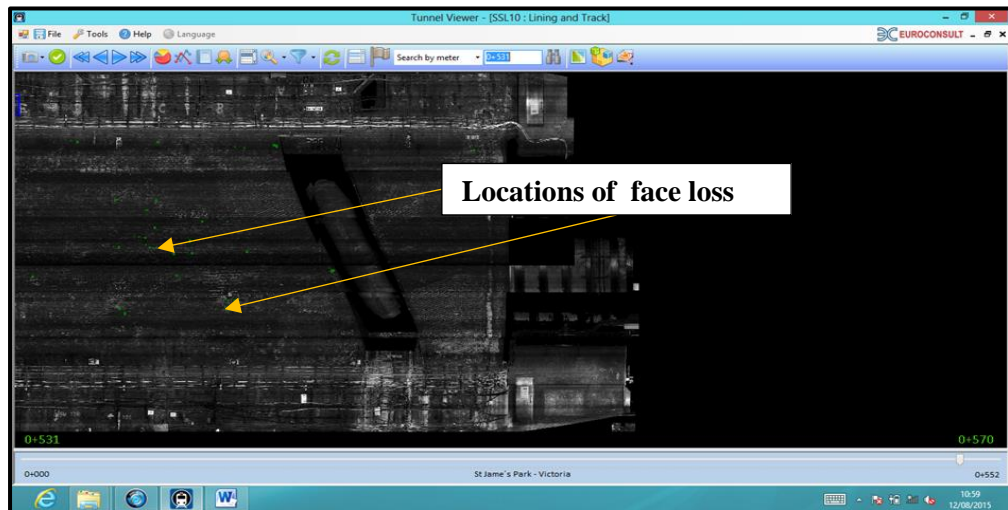


Figure 3-39 Face loss in the arch soffit-TL17

The lowest score of 78.13% (see Table 3-17) was obtained as the condition score of this asset. Leaching, wet area and drumminess influenced the lower score of B3 (extent B and severity 3). Leaching and drumminess were not identified by the laser survey. These are the reasons for differences in the scores.

Table 3-17 Visual Inspection- Condition score of an asset- TL17 (LUL, 2011)

BRICK TUNNEL							Sheet of
INSPECTION REPORT SUMMARY							
LCS/Structure No: ..D104-TL17.....			Inspector's Name ..Matthew Bower.....				
Date of Inspection.....9-11/05/2011.....			Weather/Temp.....dry /10c.....				
SUBSTRUCTURE DETAILS							
ITEM REF	SIDE WALLS **	COMMENT AND PRINCIPAL CONSTRUCTION MATERIAL	DEFECTS				ITEM SCORE
	Side Wall 1: (State)	North side					
1	Location and Description	beside east bound track					
2	Foundations/Invert	n/v					
3	Material	brick					
*4	Condition (General Surface)	leaching, wet areas, drummy	B	3	R	M	4
*5	Joint Condition/Width/Depth	minor loss	A	2	I	R	7
*6	Alignment	AS BUILT	A	1	I	R	8
*7	Arch Springing	drummy brickwork, leaching, min joint loss	B	2	M	M	6
8	Drainage	n/v					
9	Other Comments	none					
			TOTAL ITEM SCORE (X)				25
			No. of ITEMS SCORED (Y)				4
			OVERALL ELEMENT RATING $(X \div Y) \times 12.5 =$				78.13%
	Side Wall 2: (State)	South side					
1	Location and Description	beside west bound track					
2	Foundations/Invert	n/v					
3	Material	brick					
*4	Condition (General Surface)	leaching, wet areas drummy	B	3	R	H	4
*5	Joint Condition/Width/Depth	minor joint loss	A	2	I	R	7
*6	Alignment	AS BUILT	A	1	I	R	8
*7	Arch Springing	drummy brickwork, leaching, min joint loss	B	2	M	M	6
8	Drainage	n/v					
9	Other Comments	none					
			TOTAL ITEM SCORE (X)				25
			No. of ITEMS SCORED (Y)				4
			OVERALL ELEMENT RATING $(X \div Y) \times 12.5 =$				78.13%

Indicate items not applicable (N/A) or not visible (N/V)
 * Items to receive an 'Item Score' if item is applicable

The laser survey identified cracking, joint loss and face loss and assigned a lower score of A4 for these defects (see Table 3-18). These defects influenced the overall inspection score of 62.50 %. This score was lower than the visual inspection scores and would have been expected to be higher than the visual inspection as it does not take into account defects such as leaching and

drumminess. However, the visual inspection was performed in 2011 and the laser inspection was performed three years after that. During these 3 years, cracking, joint loss and face loss could have exacerbated the damage on the tunnel surface; achieving the lower score of A4.

Table 3-18 Laser Survey Report TL17 (LUL, 2014)

TUNNEL		D104/TL17			LENGTH TUNNEL (m)		156			
		St Jame's Park - Victoria			AREA TUNNEL (m2)		2414,256			
INCIDENT	LENGTH (m)	AREA (m2)	EXTENT (%)	CATEGORY	AVERAGED MEASURE	S	ITEM SCORE			
CRACKING	2,52	39,03	1,62	A	27	4	4			
DAMPNESS		9,56	0,4	A		1	8			
JOINT LOSS	15,52	0,62	0,03	A	31,05	4	4			
FACE LOSS		0,44	0,02	A	77,4	4	4			
TOTAL SCORE						62,50%				
INCIDENT	COMMENTS									
CRACKING										
DAMPNESS										
JOINT LOSS										
FACE LOSS										
SECTION	INTERVAL		1. EXTENT (E)		2. SEVERITY (S)		3. RECOMMENDED ACTION (R)		4. PRIORITY (P)	
CW15	From 0 m to 51 m		A Less than 5%		1 No 'significant defect'		I Replace		- Immediate	
TL19	From 54 m to 84 m		B Between 5% and 10%		2 'Minor' - defects of a non-urgent nature		H Paint		- High (within 12 months)	
CW14	From 87 m to 219 m		C Between 10% and 20%		3 'Heavy' - defects of an unacceptable nature which shall be included for attention within the next two annual maintenance programmes		M Repair		- Medium (within 2 years)	
TL18	From 231 m to 297 m		D Greater than 20%		4 'Severe' - defects where action is needed (these shall be reported immediately to the supervisor). These defects shall require action within the next financial year.		L Monitor		- Low (before next principal inspection)	
TL17	From 351 m to 507 m						I Inspect		- Review (for assessment at next principal inspection)	
			</							

Figure 3-41 shows that the left side wall was wet due to seepage between chainage 0 and 5. This wet area was identified by the laser inspection and is shown as the blue rectangle in Figure 3-41. The visual inspection also identified this defect as a wet area.

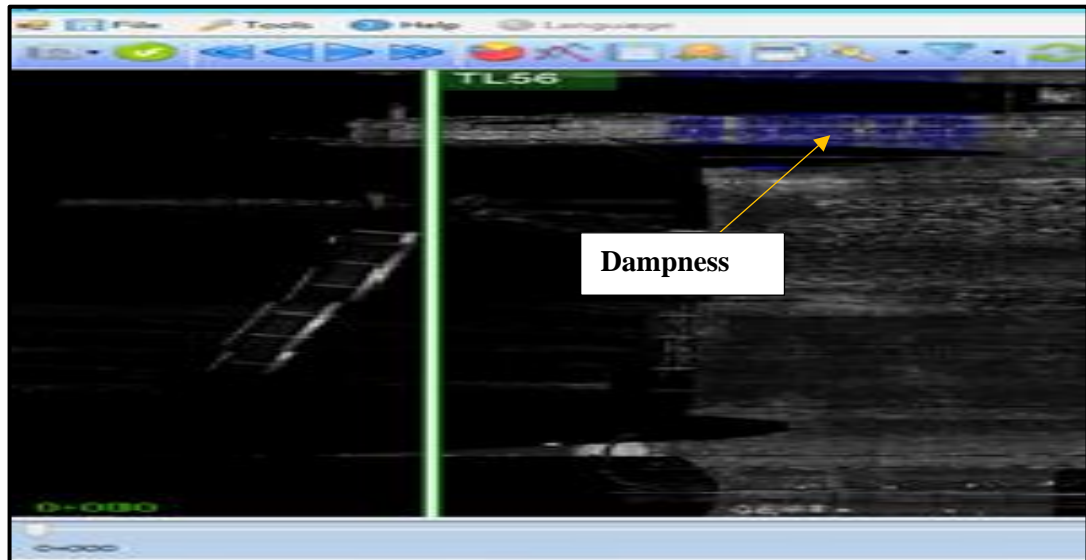


Figure 3-41 Laser Inspection Dampness- TL56

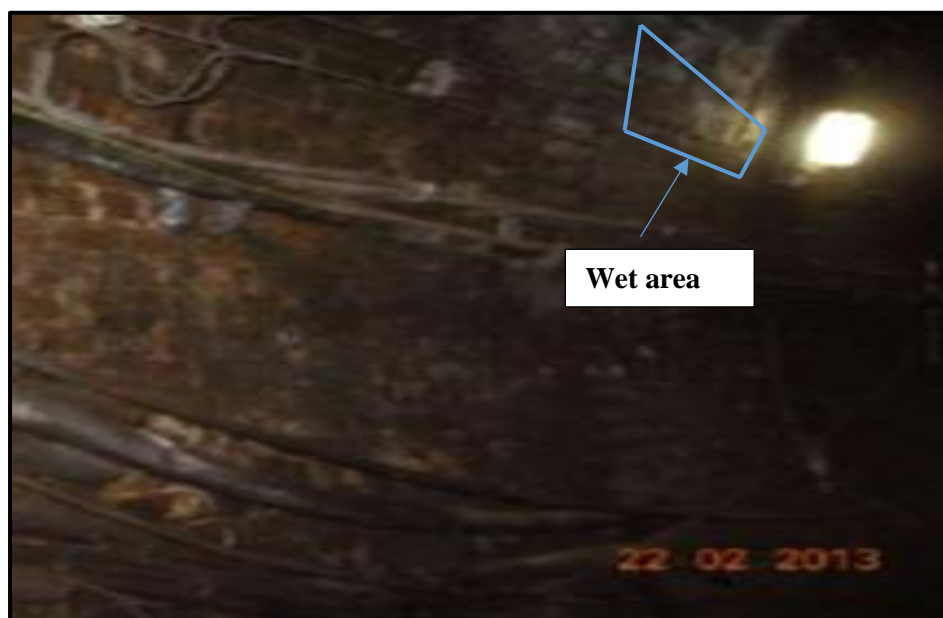


Figure 3-42 Visual Inspection Wet area TL56 (LUL, 2011)

Figure 3-43 shows face loss and joint loss of the south side wall of TL56 at chainage 100 identified by the laser inspection. At the same time, Figure 3-44 shows joint loss and spalling (visual inspection called face loss as spalling). According to the inspector's comment, drumminess was also identified by the inspector in this area. The laser survey cannot identify drumminess and this seems to be one of the major limitations of this method.

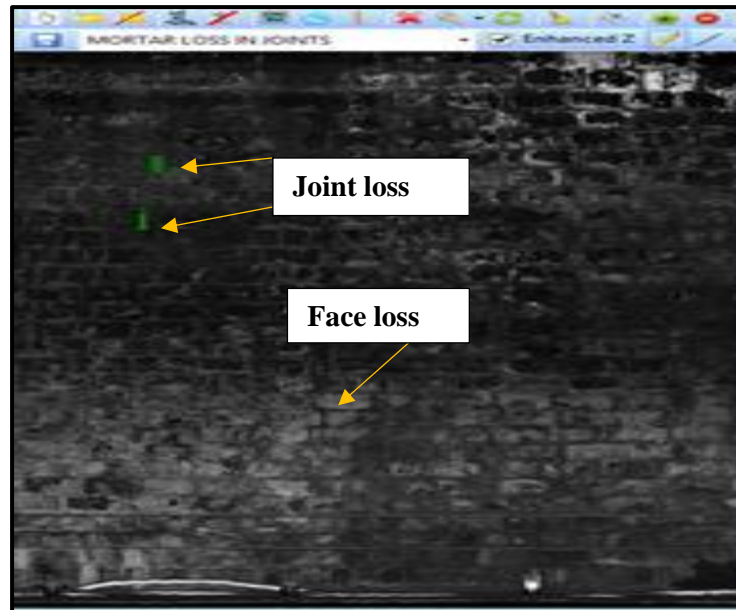


Figure 3-43 Laser Inspection Face and Joint loss- TL56

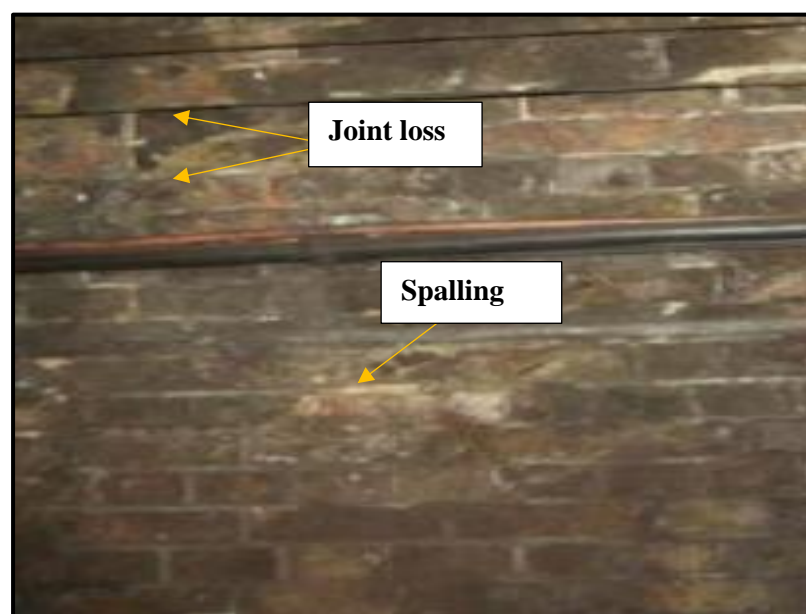


Figure 3-44 Visual Inspection Face and Joint loss- TL56 (LUL, 2011)

Figure 3-45 shows the repaired area of the Northside haunching at chainage 38 which was clearly captured by the laser survey. According to the visual inspector's comment, the area suffered a 50mm depth spalling of the brickwork and was repaired (see Figure 3-46). According to the Engineering standard S1060, repaired areas and re-pointing works should be clearly shown in the photographs with a clear description of previous defects.

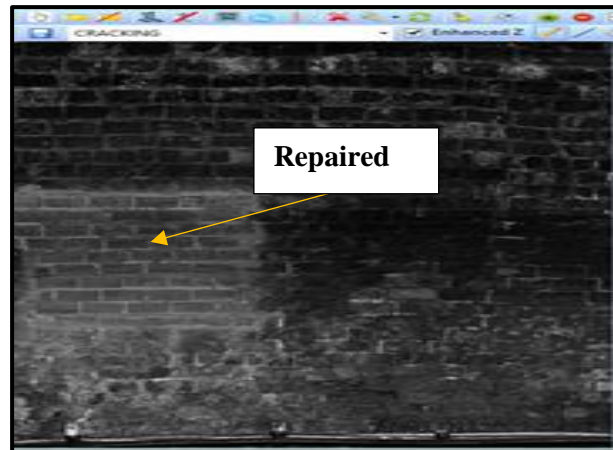


Figure 3-45 Laser inspection Repaired area-TL56



Figure 3-46 Visual Inspection Repaired area - TL56 (LUL, 2011)

Figure 3-47 shows re-pointing work at the Northsides haunching (between chainage 55 and 60) which was captured by the laser survey using the radiometric property of the laser. This work was noted by the visual inspection as well (see Figure 3-48).



Figure 3-47 Laser Inspection Re-pointing work - TL56

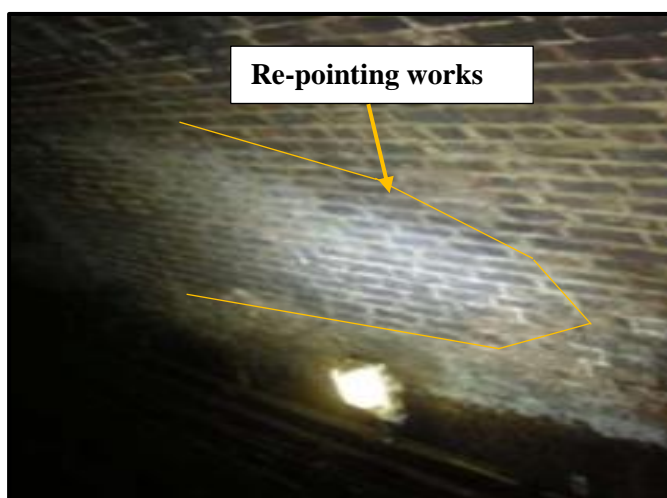


Figure 3-48 Visual Inspection Re-pointing work- TL56 (LU, 2011)

The lowest score of 56.25% (see Table 3-19) was obtained as the condition score of an asset. Joint loss, spalling and seepage influenced the lower score of C3 (extent C and severity 3).

Table 3-19 Visual Inspection- Condition score of an asset- TL56 (LUL, 2014)

BRICK TUNNEL INSPECTION REPORT SUMMARY							
Structure No / Location: D124 / TL56				Inspector's Name: GANALON REGINO			
Date of Inspection: 19 to 22 Feb 2013 & 5 March 2013				Weather / Temp: DRY / 7 deg C			
SUBSTRUCTURE DETAILS							
ITEM REF	SIDE WALLS **	COMMENT AND PRINCIPAL CONSTRUCTION MATERIAL	DEFECTS				ITEM SCORE
			E	S	R	P	
	Side Wall 1: (State)	South Sidewall					
1	Location and Description	Brick adjacent to E/B track					
2	Foundations / Invert	N/V	-	-			
3	Material	Brick					
* 4	Condition (General Surface)	Heavy spalling, seepage/ Brickwork patched repairs carried out.	D	3	R	H	2
* 5	Joint Condition / Width / Depth	Joint loss max 30mm/ Isolated reporting works carried out.	C	2	R	H	5
* 6	Alignment	No obvious signs of deformation/ Survey monitoring target points attached to tunnel crown	A	1	I	R	8
* 7	Arch Springing	Joint loss, seepage	C	3	R	M	3
8	Drainage	N/V but isolated seepage visible to sidewall	-	-			
9	Other Comments	Isolated re-pointing works has been carried out	-	-			
TOTAL ITEM SCORE (X)							18
No. of ITEMS SCORED (Y)							4
OVERALL ELEMENT RATING (X + Y) x 12.5 =							56.25%
	Side Wall 2: (State)	North Sidewall					
1	Location and Description	brick adjacent to W/B track					
2	Foundations / Invert	N/V	-	-			
3	Material	Brick					
* 4	Condition (General Surface)	Heavy spalling, seepage/ Brickwork patched repairs carried out.	D	3	R	H	2
* 5	Joint Condition / Width / Depth	Joint loss of max 30mm/ Isolated reporting works carried out.	C	2	R	H	5
* 6	Alignment	No obvious signs of deformation	A	1	I	R	8
* 7	Arch Springing	Joint loss, seepage	C	3	R	M	3
8	Drainage	Some drainage pipes inserted to western section of north sidewall/Some are now blocked with silt.	B	2	R	M	
9	Other Comments	Isolated re-pointing works has been carried out.					
TOTAL ITEM SCORE (X)							18
No. of ITEMS SCORED (Y)							4
OVERALL ELEMENT RATING (X + Y) x 12.5 =							56.25%

Indicate items not applicable (N/A) or not visible (N/V)

* Items to receive an 'Item Score' if item is applicable

Table 3-20 shows that the laser survey identified spalling as a face loss, assigning a score of A4, however, a score of A1 was assigned for dampness. Therefore, the determination of seepage played an important role in the differences seen in the inspection scores.

Table 3-20 Laser Survey Report TL 56 (LUL, 2014)

TUNNEL		D124/TL56			LENGTH TUNNEL (m)		435									
		Paddington - Edward Road			AREA TUNNEL (m2)		7304,085									
INCIDENT	LENGTH (m)	AREA (m2)	EXTENT (%)	CATEGORY	AVERAGED MEASURE	S	ITEM SCORE									
CRACKING		0	0	A		1	8									
DAMPNESS		38,1	0,52	A		1	8									
JOINT LOSS	60,92	2,44	0,03	A	23,52	2	7									
FACE LOSS		0,09	0	A	55,66	4	4									
					TOTAL SCORE	84,38%										
INCIDENT	COMMENTS															
CRACKING																
DAMPNESS																
JOINT LOSS																
FACE LOSS																
SECTION	INTERVAL		1. EXTENT (E)		2. SEVERITY (S)											
TL56	From 6 m to 441 m		A Less than 5% B Between 5% and 10% C Between 10% and 20% D Greater than 20%		1 No 'significant defect' 2 'Minor' - defects of a non-urgent nature 3 'Heavy' - defects of an unacceptable nature which shall be included for attention within the next two annual maintenance programmes 4 'Severe' - defects where action is needed (these shall be reported immediately to the supervisor). These defects shall require action within the next financial year.											
CW29	From 75 m to 117 m															



Figure 3-50 Laser Inspection Joint loss - TL60

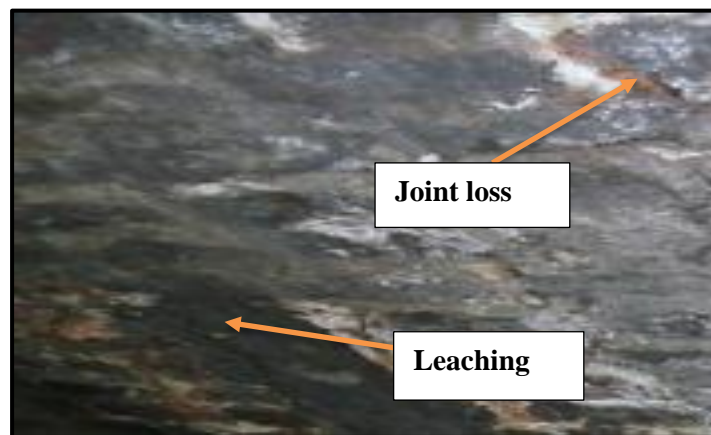


Figure 3-51 Visual Inspection Joint loss- TL60 (LUL, 2011)

Figure 3-52 shows dampness at chainage 3m on the right side of tunnel 60. This defect was identified by the visual inspection as active water seepage (see Figure 3-53).



Figure 3-52 Laser inspection Dampness- TL60

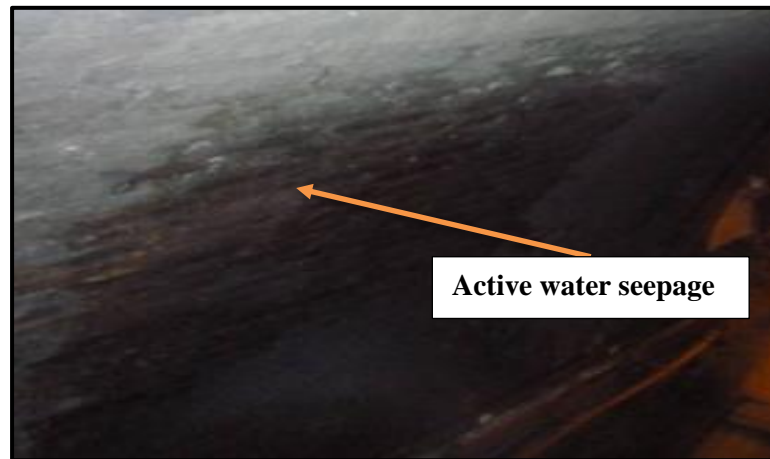


Figure 3-53 Visual inspection Water Seepage -TL60 (LUL, 2011)

The lowest score of 59.38% (see Table 3-21) from the sidewall was obtained as the condition score of this asset. Active water seepage at various locations and different areas of drummy brickwork influenced the lower score.

According to the engineer's comments on the inspection review: "The asset has suffered seepage for some time and remedial works subject to work order 50315349". This work order was completed before the laser survey and seepage were controlled. Therefore, the laser survey assigned a higher score for seepage (dampness A1) than the visual inspection (Table 3-22). Again, seepage played an important role in the difference between the scores.

Table 3-21 Visual Inspection- Condition score of an asset- TL60 (LUL, 2011)

BRICK TUNNEL						
INSPECTION REPORT SUMMARY						
Structure No / Location: D122/TL60, Paddington tube station			Inspector's Name Oscar Chew			
Date of Inspection: 10/05/2011			Weather/Temp Fair/10C			
Side Wall 2: (State)						
1 Location and Description	North sidewall, next to east bound line to Paddington tube station.					
2 Foundations/Invert	Not visible					
3 Material	Brick lined, metal ribs Ch 85m, 159m					
* 4 Condition (General Surface)	Generally covered with leaching and efflorescence height 0-2m. Moderate spalling and erosion 5-20mm, active water seepage at various locations, heavy at metal ribs. Various areas of drummy brickwork.	D	2	I	R	4
* 5 Joint Condition/Width/Depth	Joint loss 5-30mm, with isolated missing bricks. Cracked recess arch masonry Ch 18m.	D	2	R	L	4
* 6 Alignment	10mm crack running down the side of wall recess arch next to curved footing brick profile, Ch 18m.	A	3	M	L	5
* 7 Arch Springing	Patches of active water seepage at various chainages, with leaching deposits, see tunnel charts.	B	2	R	L	6
8 Drainage	Cess drain Ch 6-90m					
9 Other Comments						
Indicate items not applicable (N/A) or not visible (N/V)						
* Items to receive an Item Score if item is applicable						
TOTAL ITEM SCORE (X)						19
No. of ITEMS SCORED (Y)						4
OVERALL ELEMENT RATING $(X \div Y) \times 12.5 =$						59.38%

Table 3-22 Laser Survey Report TL60 (LUL, 2014)

TUNNEL		D122/TL60			LENGTH TUNNEL (m)		189												
		Bayswater - Paddington			AREA TUNNEL (m2)		3060,099												
INCIDENT	LENGTH (m)	AREA (m2)	EXTENT (%)	CATEGORY	AVERAGED MEASURE	S	ITEM SCORE												
CRACKING		0	0	A		1	8												
DAMPNESS		38,67	1,26	A		1	8												
JOINT LOSS	18,53	0,74	0,02	A	21,71	2	7												
FACE LOSS		0,02	0	A	5,21	1	8												
					TOTAL SCORE	96,88%													
INCIDENT	COMMENTS																		
CRACKING																			
DAMPNESS																			
JOINT LOSS																			
FACE LOSS																			
SECTION	INTERVAL																		
CW55	From 0 m to 21 m		<div><div><div>1. EXTENT (E)</div><div>A Less than 5% B Between 5% and 10% C Between 10% and 20% D Greater than 20%</div><div>2. SEVERITY (S)</div><div>1 No "significant defect" 2 "Minor" - defects of a non-urgent nature 3 "Heavy" - defects of an unacceptable nature which shall be included for attention within the next two annual maintenance programmes 4 "Severe" - defects where action is needed (these shall be reported immediately to the supervisor). These defects shall require action within the next financial year.</div></div><div><div>3. RECOMMENDED ACTION (R)</div><div>C Replace P Paint R Repair M Monitor I Inspect</div><div>4. PRIORITY (P)</div><div>- Immediate H - High (within 12 months) M - Medium (within 2 years) L - Low (before next principal inspection) R - Review (for assessment at next principal inspection)</div></div></div>																
TL65	From 24 m to 33 m																		
CW54	From 36 m to 42 m																		
TL64	From 45 m to 78 m																		
CW53	From 81 m to 96 m																		
TL63	From 99 m to 243 m																		
TL62	From 291 m to 447 m																		
TL61	From 459 m to 522 m																		
CW52	From 525 m to 708 m																		
TL60	From 711 m to 900 m																		
EXTENT/SEVERITY RATING			A1	A2	A3	A4	B1	B2	B3	B4	C1	C2	C3	C4	D1	D2	D3	D4	
ITEM SCORE			8	7	5	4	7	6	4	3	6	5	3	2	5	4	2	1	

3.11.4.5 Covered Way 61

Covered way 61 is located between Aldgate junction and Aldgate East junction.



Figure 3-54 General View of CW61 (LUL, 2011)

Table 3-23 shows the lowest score of 75% (from superstructure) which was obtained as the condition score of this asset. Surface corrosion influenced the lower score of B2 (Extent B, Severity2 and item score 6).

Table 3-23 Visual Inspection- Condition score of an asset- CW61 (LUL, 2011)

COVERED WAY INSPECTION REPORT							
Structure No / Location: M144 / M144/CW61				Inspector's Name: LOUCHI MALEK			
Date of Inspection: 01/07/2011				Weather / Temp: DRY / 15 deg C			
SUPERSTRUCTURE DETAILS							
ITEM REF	SPANNING MEMBERS / DECK	COMMENT AND CONSTRUCTION MATERIALS	DEFECTS				ITEM SCORE
			E	S	R	P	
Spanning Members:							
9	Type and No.	OLD CAST IRON BEAMS PLUS ADDITIONAL RE-STRENGTHENING STEELWORK: EIGHT CAST IRON GIRDERS, ONE PLATED GIRDER AND NINE RESTRENGTHENING GIRDERS 8					
10	Location and Description	SPANNING BOTH TRACKS					
* 11	Top Face (Flange)	N/V					
* 12	Bottom Face (Flange and Deck Soffit)	WIDE CAST IRON BOTTOM FLANGES- SURFACE COROSION	B	2	P	L	6
* 13	Sides (Web)	N/V					
* 14	Edges at End	SURFACE CORROSION TO EDGES	B	2	P	L	6
15	Other Comments						
Surfacing:							
16	Carriageway						
17	Footway						
18	Other Comments						
Drainage:							
19	Arrangement / Support						
20	Condition / Effectiveness						
21	Other Comments						
Indicate items not applicable (N/A) or not visible (N/V)							
* Items to receive an 'Item Score' if item is applicable							
			TOTAL ITEM SCORE (X)				14
			No. of ITEMS SCORED (Y)				2
			OVERALL ELEMENT RATING $(X \div Y) \times 12.5 =$				75%

Table 3-24 shows the laser survey did not pick up any defect during its inspection and assigned the highest score of 100%. This clearly indicated that surface corrosion, and seepage did not appear during the laser inspection. Furthermore, covered way 61 did not have any other defects such as cracking, joint loss, dampness and face loss during the laser inspection.

Table 3-24 Laser Survey Report CW 61(LUL, 2014)

TUNNEL		M144/CW61			LENGTH TUNNEL (m)		75											
		Liverpool Street - Aldgate			AREA TUNNEL (m2)		1168,575											
INCIDENT	LENGTH (m)	AREA (m2)	EXTENT (%)	CATEGORY	AVERAGED MEASURE	S	ITEM SCORE											
CRACKING		0	0	A		1	8											
DAMPNESS		0	0	A		1	8											
JOINT LOSS		0	0	A		1	8											
FACE LOSS		0	0	A		1	8											
TOTAL SCORE						100,00%												
INCIDENT	COMMENTS																	
CRACKING																		
DAMPNESS																		
JOINT LOSS																		
FACE LOSS																		
SECTION	INTERVAL	1. EXTENT (E) 2. SEVERITY (S)																
TL77	From 3 m to 300 m	A Less than 5% 1 No 'significant defect'																
CW61	From 303 m to 378 m	B Between 5% and 10% 2 'Minor' - defects of a non-urgent nature																
CW60	From 381 m to 423 m	C Between 10% and 20% 3 'Heavy' - defects of an unacceptable nature which shall be included for attention within the next two annual maintenance programmes																
		D Greater than 20% 4 'Severe' - defects where action is needed (these shall be reported immediately to the supervisor). These defects shall require action within the next financial year.																
		3. RECOMMENDED ACTION (R) 4. PRIORITY (P)																
		C Replace I Immediate																
		P Paint H High (within 12 months)																
		R Repair M Medium (within 2 years)																
		M Monitor L Low (before next principal inspection)																
		I Inspect R Review (for assessment at next principal inspection)																
		EXTENT/SEVERITY RATING																
		A1	A2	A3	A4	B1	B2	B3	B4	C1	C2	C3	C4	D1	D2	D3	D4	
		ITEM SCORE																
		8	7	5	4	7	6	4	3	6	5	3	2	5	4	2	1	

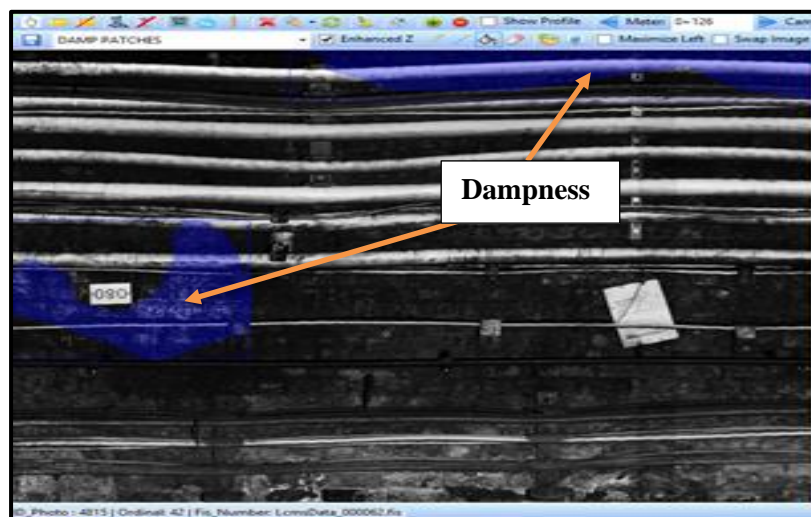


Figure 3-56 Laser Inspection Dampness- TL53

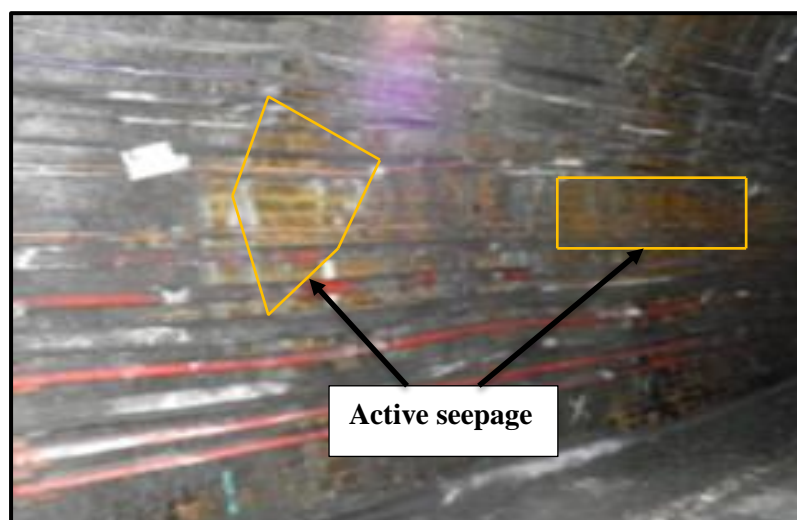


Figure 3-57 Visual Inspection Active Seepage- TL53 (LUL, 2011)

Table 3-25 shows the lowest score of 46.88% (from superstructure), obtained as the condition score of this asset. Heavy spalling, fracture, active seepages and leaching reduced the general surface score to D3 (Extent D, Severity 3 and item score 2).

Table 3-25 Visual Inspection- Condition score of an asset- TL53 (LUL, 2013)

BRICK TUNNEL							A16a
INSPECTION REPORT SUMMARY							
Structure No / Location: ...M168/TL53..				Inspector's Name ...Jigar Desai.....			
Date of Inspection.....18/21/03/13				Weather/Temp.....Rain/5c			
SUBSTRUCTURE DETAILS							
ITEM REF	SIDE WALLS **	COMMENT AND PRINCIPAL CONSTRUCTION MATERIAL	DEFECTS				ITEM SCORE
			E	S	R	P	
	Side Wall 1: (State)	North abutment					
1	Location and Description	Adj to e/b track vertical side wall					
2	Foundations/Invert	N/V					
3	Material	brick work					
* 4	Condition (General Surface)	Heavy spalling, fractures, active seepages, leaching	D	3	R	M	2
* 5	Joint Condition/Width/Depth	Joint losses up to 30mm noted	C	2	R	M	5
* 6	Alignment	Old standing bulging and drummy section - strapped	B	2	R	M	6
* 7	Arch Springing	Defects as above	D	3	R	M	2
8	Drainage	N/V - seepages throughout					
9	Other Comments						
			TOTAL ITEM SCORE (X)				15
			No. of ITEMS SCORED (Y)				4
			OVERALL ELEMENT RATING $(X \div Y) \times 12.5 =$				46.88%

Table 3-26 shows, the laser survey assigned higher scores for dampness and face loss compared to the visual inspection. The laser survey did not pick up some of the defects mentioned in the visual inspection report. This is one of the main reasons for the significant difference between the scores that were stated above.

Table 3-26 Laser Survey Report TL 53 (LUL, 2014)

TUNNEL		M168/TL53			LENGTH TUNNEL (m)		594										
		Eduard Road - Baker Street			AREA TUNNEL (m2)		8981,874										
INCIDENT	LENGTH (m)	AREA (m2)	EXTENT (%)	CATEGORY	AVERAGED MEASURE	S	ITEM SCORE										
CRACKING	8,72	131,93	1,47	A	15,71	4	4										
DAMPNESS		136,77	1,52	A		1	8										
JOINT LOSS	60,31	2,41	0,03	A	23,36	2	7										
FACE LOSS		0,12	0	A	10,88	2	7										
					TOTAL SCORE		81,25%										
INCIDENT	COMMENTS																
CRACKING																	
DAMPNESS																	
JOINT LOSS																	
FACE LOSS																	
SECTION	INTERVAL	1. EXTENT (E) A Less than 5% B Between 5% and 10% C Between 10% and 20% D Greater than 20% 3. RECOMMENDED ACTION (R) C Replace P Paint R Repair M Monitor I Inspect 2. SEVERITY (S) 1 No 'significant defect' 2 'Minor' - defects of a non-urgent nature 3 'Heavy' - defects of an unacceptable nature which shall be included for attention within the next two annual maintenance programmes 4 'Severe' - defects where action is needed (these shall be reported immediately to the supervisor). These defects shall require action within the next financial year. 4. PRIORITY (P) I - Immediate H - High (within 12 months) M - Medium (within 2 years) L - Low (before next principal inspection) R - Review (for assessment at next principal inspection)															
TL53	From 42 m to 636 m																
CW19	From 444 m to 549 m																
		</															

shows all the defects which need to be added to the chart if they are identified on the inspection.

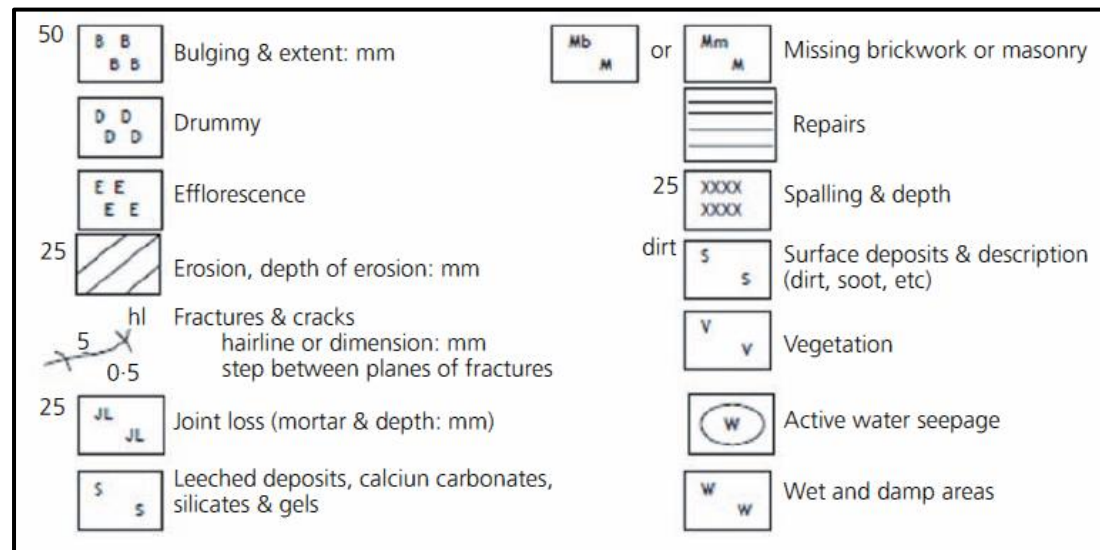


Figure 3-58 Standard defect notation masonry structures and structural components (S1060, 2011)

Figure 3-59 shows an example of a brick tunnel inspection chart which is added to every tunnel principal inspection report for the visual inspection process. The chart divides the tunnel in two halves of approximately 8m in length. At the central portion of the chart is located the ballast whilst at the left and right edges the crown is located. Therefore, by joining the crown lines a cylinder, in the shape of a tunnel is formed, allowing the defect location to be easily visualised. On the vertical axis is the chainage of the tunnel, running at intervals of 1m.

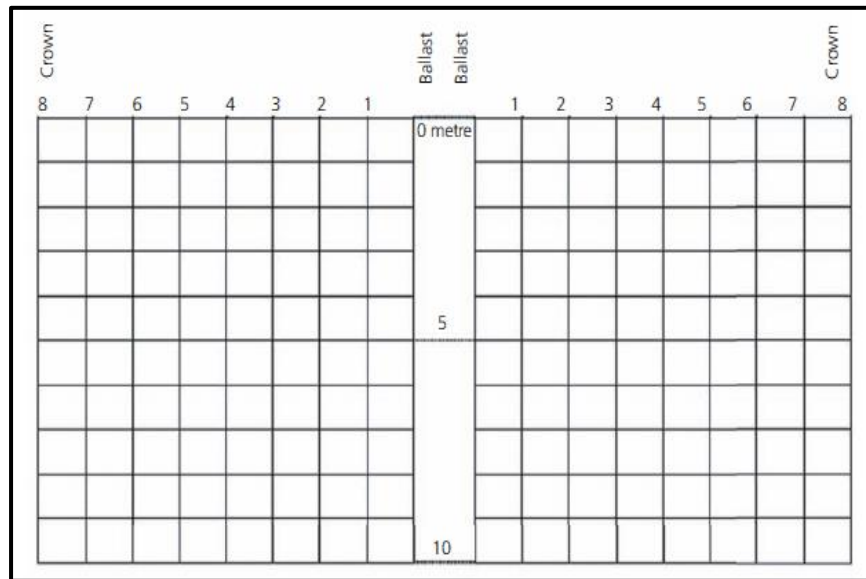


Figure 3-59 London Underground Inspection Tunnel Chart

Currently, the visual inspection of the crown area is carried out using a Rotamag scaffold tower fitted onto a track trolley (Figure 3-60) and pushed through the tunnel on foot.



Figure 3-60 Rotamag tower set-up used for visual inspection (Permaquip, 2016)

The inspector will then create tunnel charts which are hand-drawn and scanned into the computer; this usually reduces their quality and makes them difficult to read. This tunnel chart then continues for the total length of the asset depending on the extent of the tunnel. Each square on the tunnel chart (Figure 3-59) represents a 1 m² section of the brick tunnel. Finally, all the defects on

the tunnel chart are tabulated and included in the principal inspection report to show the total quantities of each defect, which are also compared to the previous principal inspection results. Subsequently, comparisons can be made on any deteriorations to the asset as there is a trend of either an increase in the area of defect, no change in the area of defect or a decrease in the area of defect. A decrease in the defect area occurs when there has been maintenance work carried out to the asset at some point within the years between the principal inspections to remove a section of the defects noted. The next inspection of the tunnel is subsequently conducted 4 years later where an inspector will need to be able to read the charts clearly to see if any further defects have occurred.

3.12.2 Defects Identified by Euroconsult high definition laser scanning system

The computer software (Tunnel Viewer) used to process the data captured with the laser tunnel inspection enables zooming into a particular defect to carry out further analysis and evaluations. A measuring tool within the program enables the geometry, including the surface width and depth of individual defects, to be computed. The measuring tool can be used to calculate joint loss, fractures, spalled areas and the amount of seepage to a specific area. This tool will measure not only one affected area but also the whole asset, thereby providing the inspector with a better insight into a particular defect that may be a cause of concern. This feature of the software is particularly good as these types of defects would have had to be measured on-site, whereas they can all be carried out off-site with a higher degree of accuracy.

3.12.3 Comparison of defects

Defects identified by visual inspection were computed from Tunnel 17 (D104 / TL17); its inspection chart is shown in Figure 3-61. Each square denoted by “W” (water seepage) was added to the whole distance of the tunnel to calculate total defects of dampness identified by the inspector visually. Similarly, other defects were also calculated and plotted in Figure 3-64 to Figure 3-67.

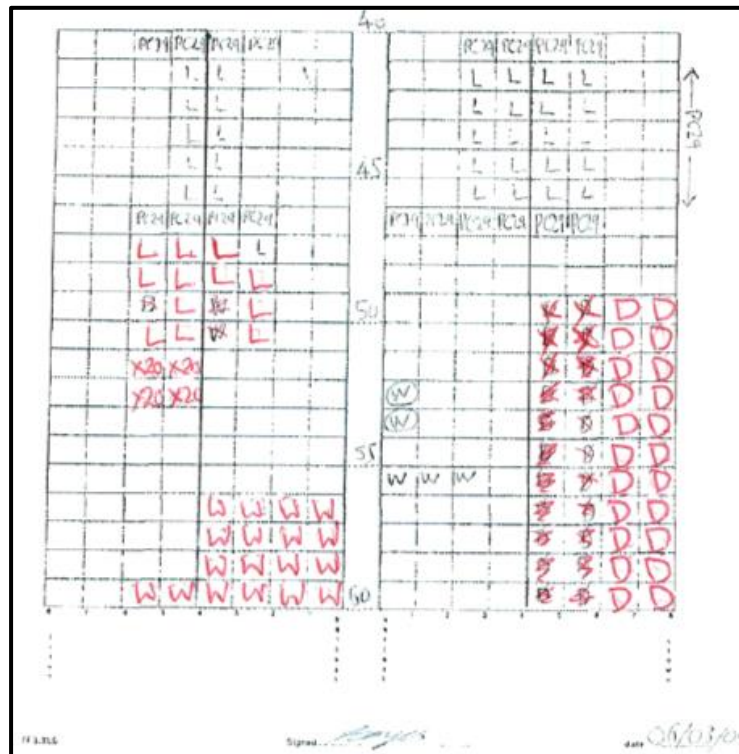


Figure 3-61 Tunnel 17 (D104 / TL17) visual inspection chart

For the 2014 laser inspection, the total number of defects were computed from the laser inspection report and the defects graph is shown in

Figure 3-62 for damp patches. Similarly, other defects were also collated from graphs mentioned in the Laser Inspection of the 2014 report and replotted in Figure 3-64 to Figure 3-67.

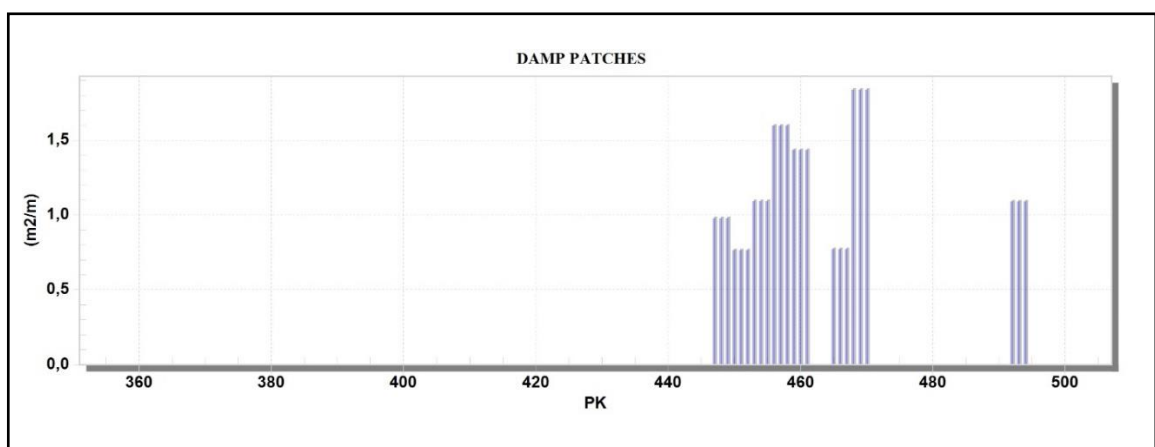
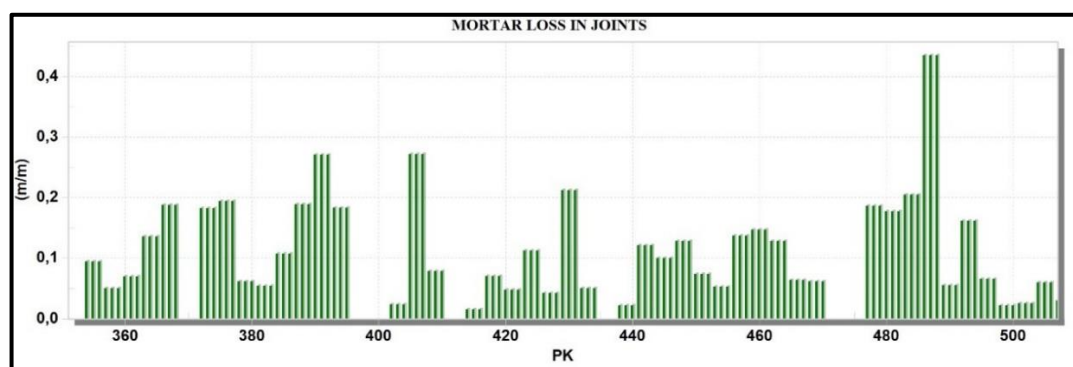


Figure 3-62 Dampness show in laser inspection 2014 (Euroconsult, 2016)

3.12.4 Joint loss

Joint loss occurs when there is mortar loss in the brick joints. This is a very common defect in old masonry, but it can also be caused by frost damage. If left unattended, it can result in weakened and loose bricks. The mortar can be easily replaced by a maintenance process called repointing, where the new mortar is added to the joints. It is a major concern having loose bricks within a tunnel carrying up to 33 trains per hour. LUL has a contract to repair any joint loss required for a year, but to do this, it must be identified correctly.

Joint loss, in the Inspection Tunnel Chart, is marked by the letters JL followed by the depth of the joint loss, measured on-site, in millimetres, for example, JL10, JL15 and JL20 were found in the inspection report, indicating joint loss depths of 10, 15 and 20mm respectively. In order to calculate the total joint loss for a particular meter of chainage, from the data in the Inspection Tunnel Chart, the different joint loss per metre of chainage were added and divided by 16 (the length of the circumference of the tunnel), therefore the variation would be between zero, or no joint loss, to 1, indicating that the whole wall on that particular chainage suffered from joint loss. In this method, the depth of the joint loss was not taken into account as it was not clear if the depth corresponded to the deepest value measured or an average. The total Joint loss identified by the Laser inspection in 2014 was directly extracted from the Euroconsult's report (Euroconsult, 2016) show in Figure 3-63 and the chainage mentioned in the X-axis as "PK" was converted into tunnel chainage, used by LUL and mentioned in all Inspection reports.



**Figure 3-63 Joint loss identified by the Laser Survey 2014
(Euroconsult, 2016)**

Figure 3-64 shows the joint loss comparison between the visual inspection (2011) and the laser inspection (2014). The laser inspection identified more locations of joint loss in tunnel 17 (TL17) compared to the visual inspection. Laser scanner systems are excellent at determining even very small mortar loss given that the measurements are made with an accuracy of 0.5mm, far better than the human eye, particularly in a tunnel environment where there are low levels of light. On the other hand, both inspections were performed in two different periods; the visual inspection in 2011 and the laser inspection in 2014, therefore, it is possible that part of the discrepancy could be due to the appearance of new joint losses. To understand this discrepancy, a visual inspection must be performed in a small length of tunnel, immediately after the laser scanner so a visual check of the mortar loss can then be performed.

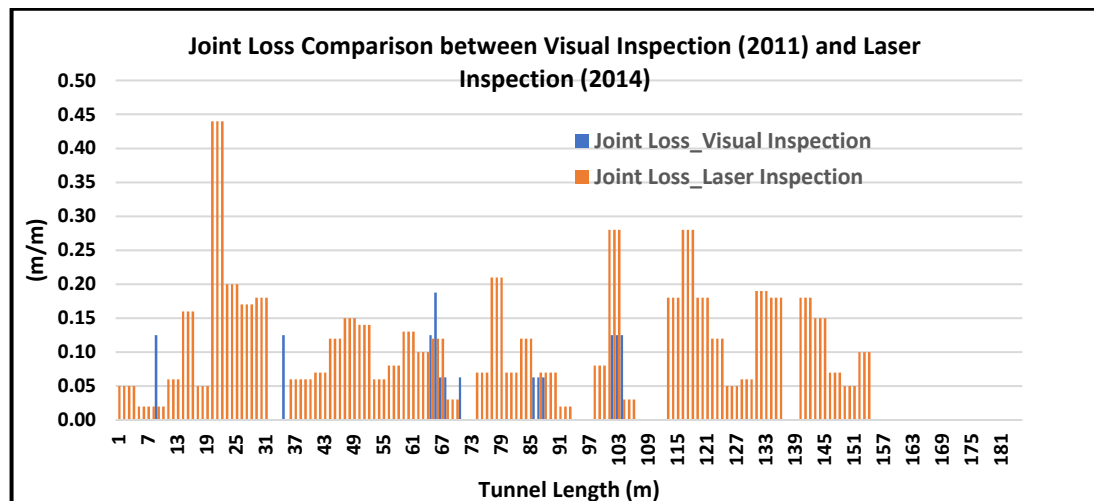


Figure 3-64 Joint Loss comparison between visual inspection and Laser Inspection

3.12.5 Dampness/water ingress

Water ingress is a common defect within the ageing tunnels of the LUL. Water ingress can be caused by groundwater penetration through the tunnel lining and into the tunnel, but the more common ingress is from pipe leaks from the third-party Thames Water, often under mains pressure. The laser identifies water ingress by the slower response time of the laser beam to bounce back, making the wall look illuminated.

Figure 3-65 shows dampness/water ingress detected by the visual inspection in 2011, where the number of square meters of dampness corresponds to a

simple count of the squares marked with the seepage symbol. One major drawback of this calculation is that the area affected in each square is not known, therefore the whole area (1m^2) needs to be considered. This figure did not show any correlation between the two methods to identify dampness/water ingress. This may be due to the different inspection periods (visual inspection in 2011 and laser inspection in 2014), as the moisture areas identified by the laser scanner system were checked visually in the software.

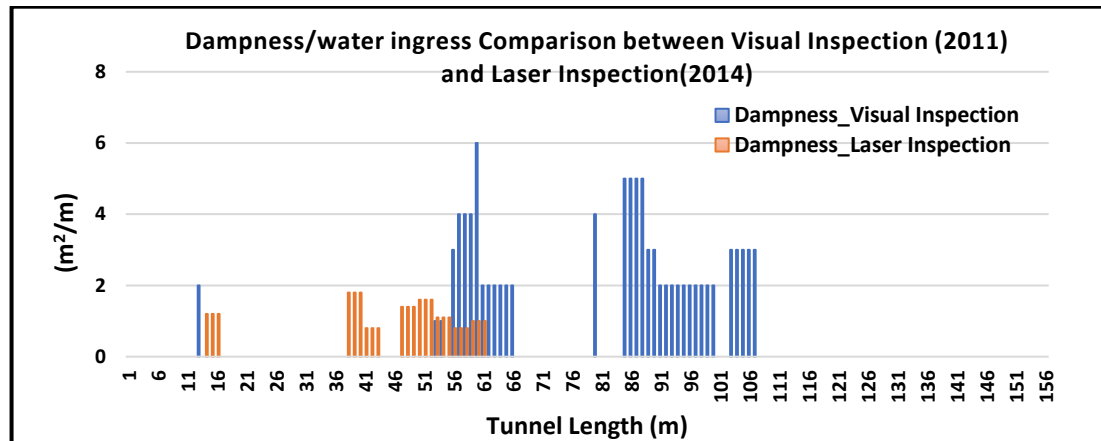


Figure 3-65 Dampness Comparison between Visual Inspection and Laser inspection

3.12.6 Lining face loss/Spalling

Face loss also occurs to old brickwork, in particular those exposed to weathering. This is when the face of the brickwork breaks away, often in large pieces in a large section of brickwork. It can also lead to a serious defect in a tunnel if left unattended, particularly in the crown above the train path. Repairs can be done by cutting out the bricks and replacing them where required; however, as before, these need to be identified.

Figure 3-66 shows a comparison of lining face loss between Visual Inspection (2011) and the Laser Inspection (2014). The sizes of lining face loss identified by the visual inspection (2011) were very small. To show the lining face loss/spalling values detected by both systems in the same graph, the lining face loss identified by the laser inspection was divided by ten. It is worth mentioning that the laser scanner system can detect these kinds of defects easily and the selection of appropriate thresholds is very important. Again, it is difficult to compare both epochs and values as the values identified by the

laser scanner are in different positions and it is not clear if the defects mentioned in the visual inspection were rectified or not.

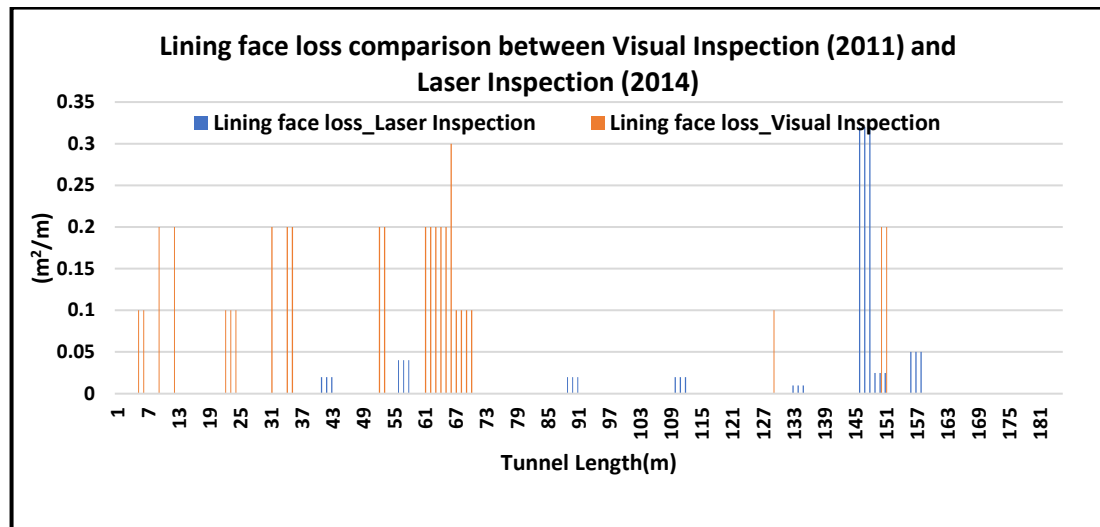


Figure 3-66 Lining face loss comparison between Visual Inspection and Laser Inspection

3.12.7 Cracks/Fractures

Cracks/Fractures can present enormous safety hazards within tunnels and have several causes, the most common being movements within the tunnel. There is often an underlying problem with the tunnel when cracks/fractures occur. Fractures can lead to loosened brickwork and equipment, which could result in the train service becoming affected. Traverse cracks/fractures present a more serious defect than longitudinal cracks/fractures as they indicate flattening of the arch and possible rotation of the tunnel. However, longitudinal fractures are more common and related to the lack of load distribution. Figure 3-67 show cracks identified by the laser inspection in 2014 and these are in a small area of the tunnel. However, cracks have not been identified by the inspector during the visual inspection in 2011.

Unfortunately, after this work, the chance to accurately compare the Euroconsult system with visual inspections was lost as a visual inspection of certain parts of the tunnel was not performed immediately after the laser inspection. This would be important in order to understand the accuracy of the system in detecting the individual defects highlighted above: mortar loss, seepage, brick loss and cracks/fractures.

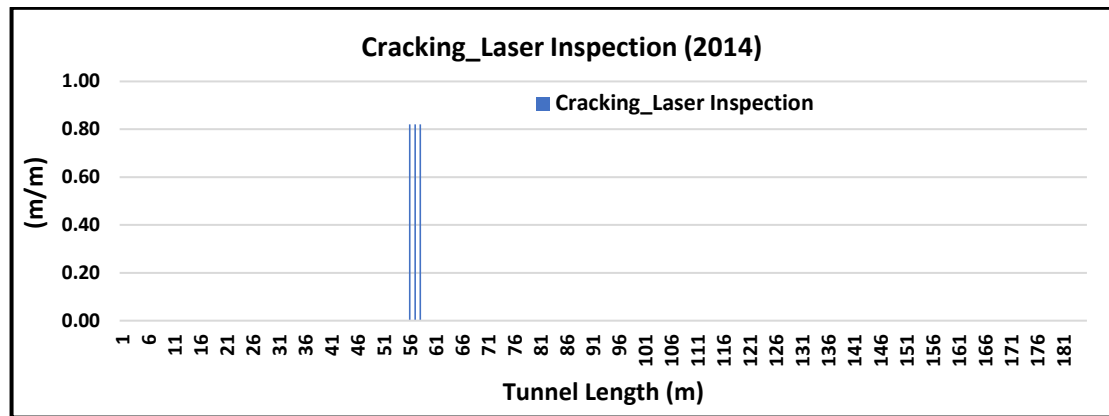


Figure 3-67 Cracking Laser Inspection

3.13 Description of Euroconsult's Laser Scanner Second Inspection 2015

The scanning was carried out on the Metropolitan Line and District Line on the 11th, 18th, and 19th December 2015.

The inspected sections on the District Lines are shown in Figure 3-68 and marked with red boxes.

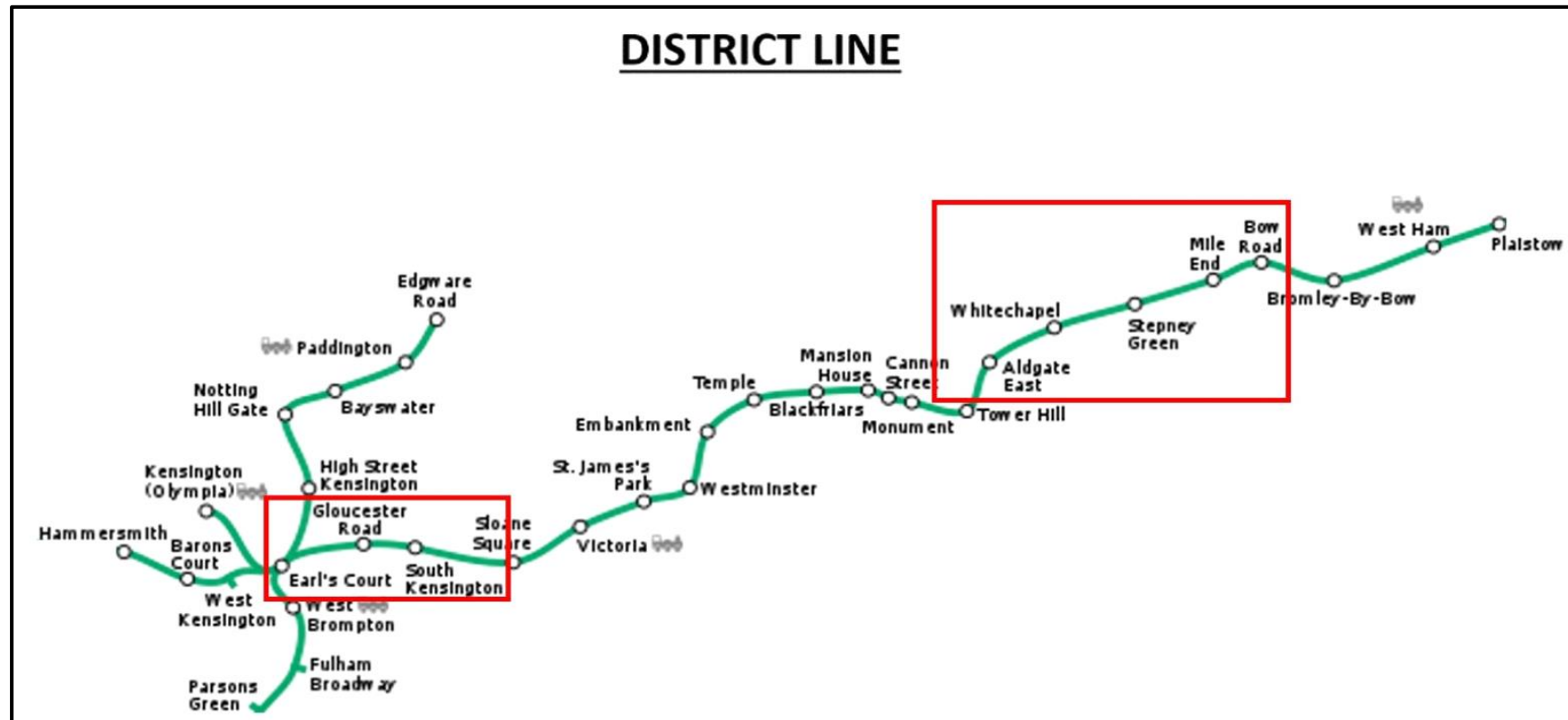


Figure 3-68 Laser scanning inspected section in the District Line

On the Metropolitan line, the whole line was inspected clockwise and counter-clockwise (see Figure 3-69).

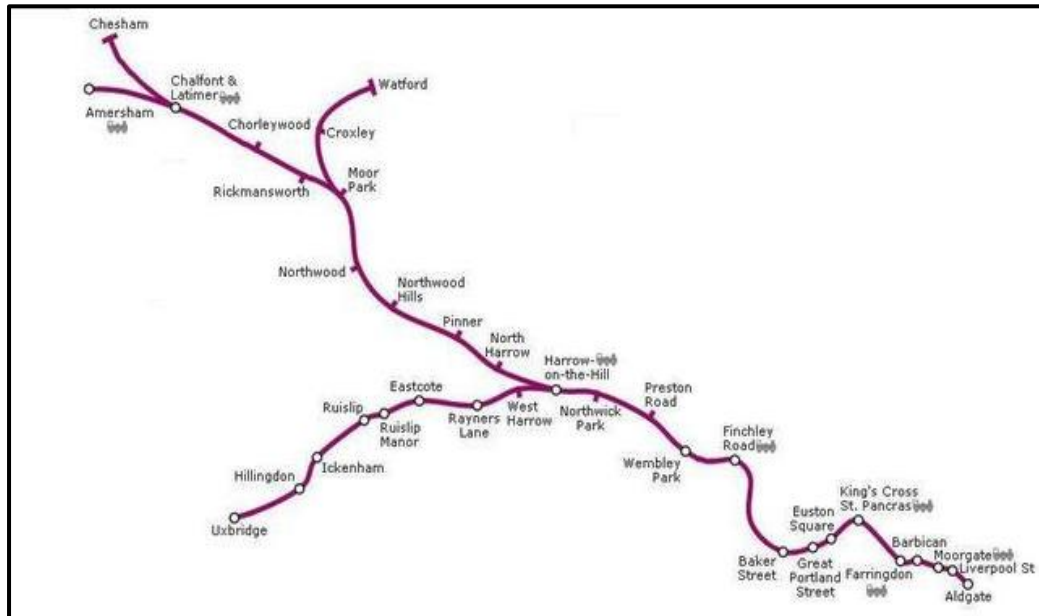


Figure 3-69 Laser scanning inspected section in the Metropolitan Line (Euroconsult, 2016)

3.14 Laser Survey Flow Chart

Figure 3-70 shows the work flow chart of the Euroconsult's Laser Scanner Inspection. It illustrates the whole procedure required prior to inspection, including the required approvals and the data analysis steps in a simple way.

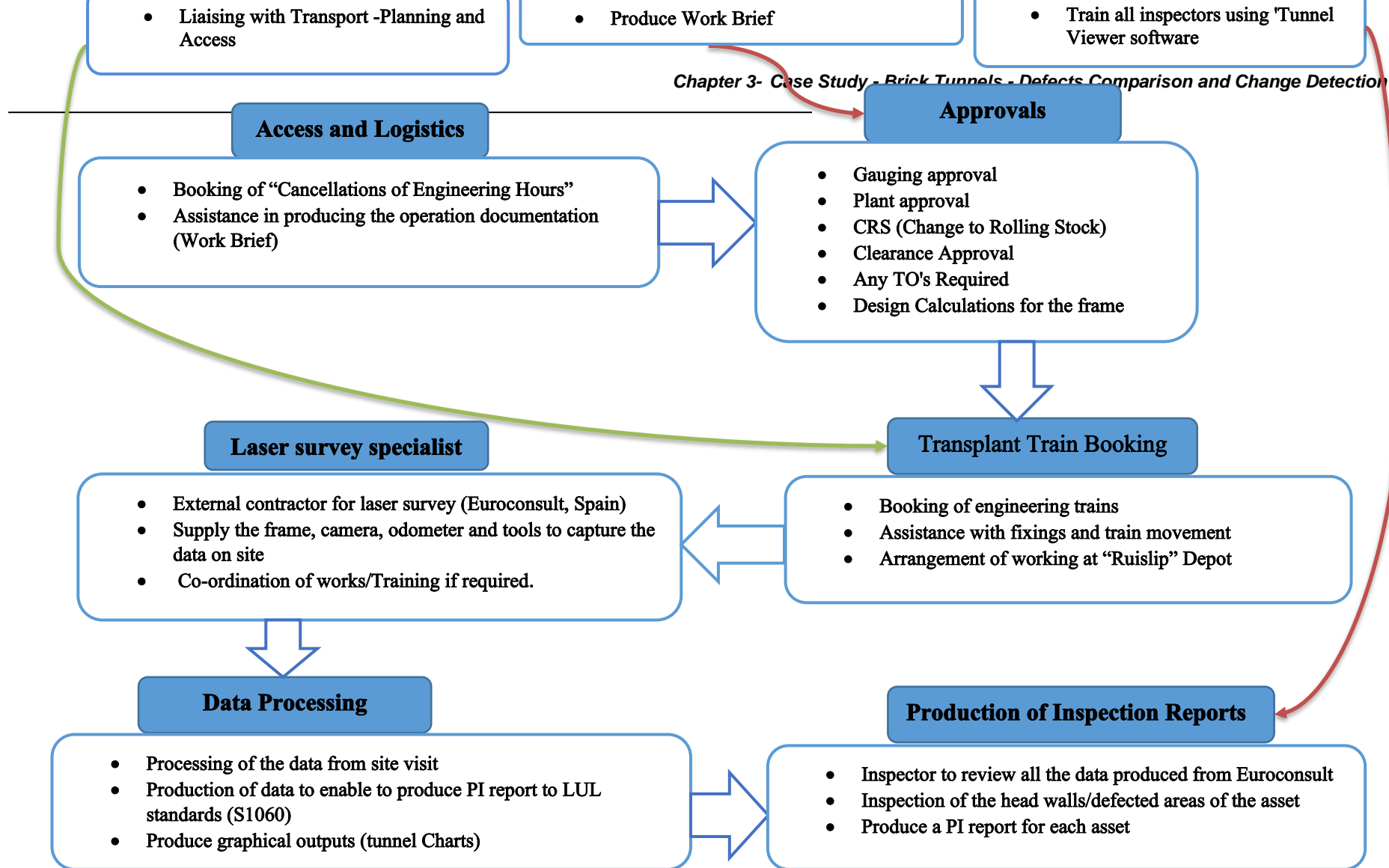


Figure 3-70 Euroconsult's Laser Scanner Workflow

3.15 Condition Survey

The objective of the December 2015 inspection was to determine the differences in the defects initially found by the previous survey, performed in July 2014. This comparison would provide an idea of deterioration of the brick tunnels between this period.

As in the previous inspection, the incidents (defects) considered were:

1. Mortar loss in joints
2. Lining face loss
3. Cracking
4. Damp patches

In this second inspection, the deflector plates of the tunnel were also captured, as requested by LUL. In addition to this, a customized Tunnel viewer software was developed by Euroconsult for bracket detection and location. The 2014 data were considered as a reference measurement, and changes of each defect were compared.

Thus, the final incidents presented by the new software are as follows:

1. Mortar loss in joints
2. Lining face loss
3. Cracking
4. Damp patches
5. Deflector plate (installed to divert water ingress)
6. Cable brackets

3.16 Laser scanning scores comparison between 2014 and 2015 inspection

The laser inspections performed in July 2014 and December 2015 were compared in this section in order to identify defects that had newly appeared, and also check whether works' orders had been completed for previously raised defects.

Figure 3-71 shows the comparison of the overall rating of 72 tunnel sections between the two inspections. Compared to the inspection of 2014, the overall scores of the 2015 inspection decreased in most of the tunnel sections (e.g., TL6, TL7, TL8, TL9, TL10, TL11, and TL12). However, in some places, both inspections achieved similar (e.g. TL17, TL22, TL38, TL51, TL54, TL61, TL62, TL69 and TL102) scores. To understand the factors, influencing this score variation throughout the tunnel sections, each defect type was analysed separately.

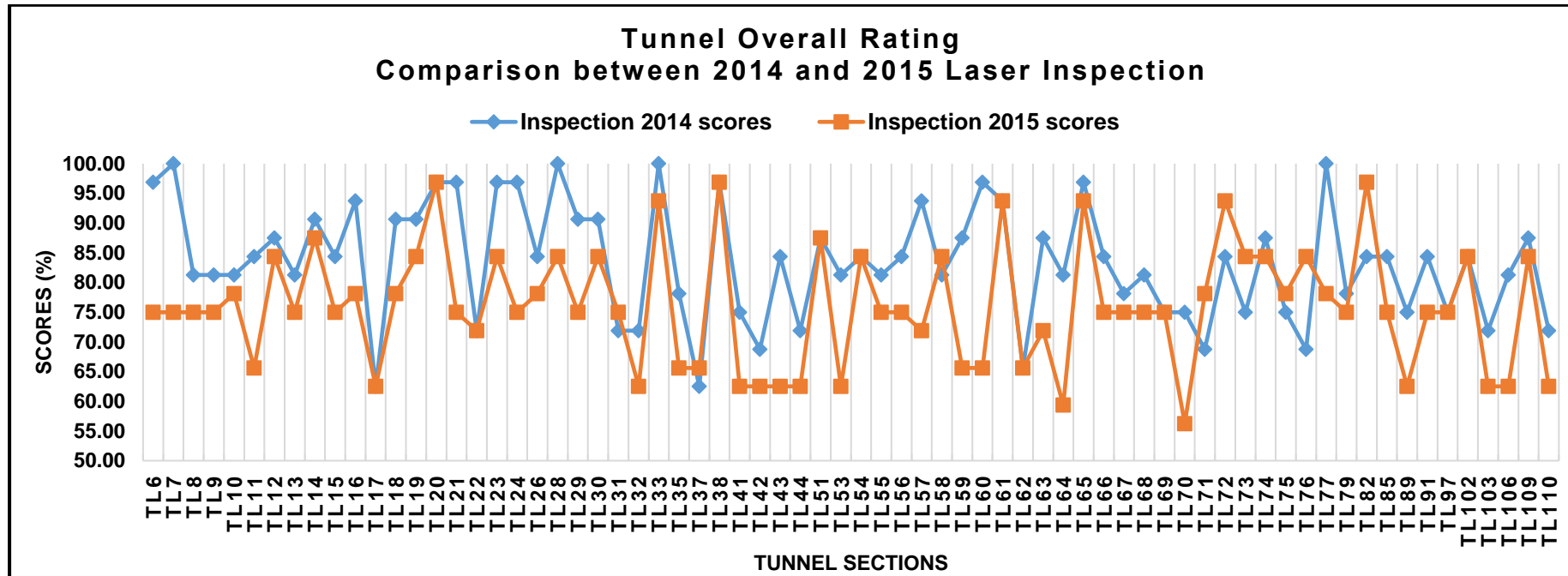


Figure 3-71 Comparison of tunnel scores between 2014 and 2015 Laser inspection

Figure 3-72 shows a comparison of cracking of 72 sections of tunnels between the 2014 and 2015 laser inspection. In most of the tunnels' sections, there were no changes in cracking between the two inspections. However, tunnel sections TLS' 10,13, 26, 31, 55, 58, 66, 68, 69, 71, 72, 73, 75, 79, 85, 91, 97 and 102 were significantly improved from score 4 in the 2014 inspection, to score 8 in the 2015 inspection. This indicates repairs for cracking were performed in between two inspections and this was confirmed with a completed works order. For tunnel sections TLS' 28, 59 and 60, the overall scores had decreased from 8 to 4 between the 2014 and 2015 inspections. This indicates that new cracks appeared between the 2014 and 2015 laser inspection and confirmed with the route inspector. The newly appeared cracks, therefore, reduced the overall scores.

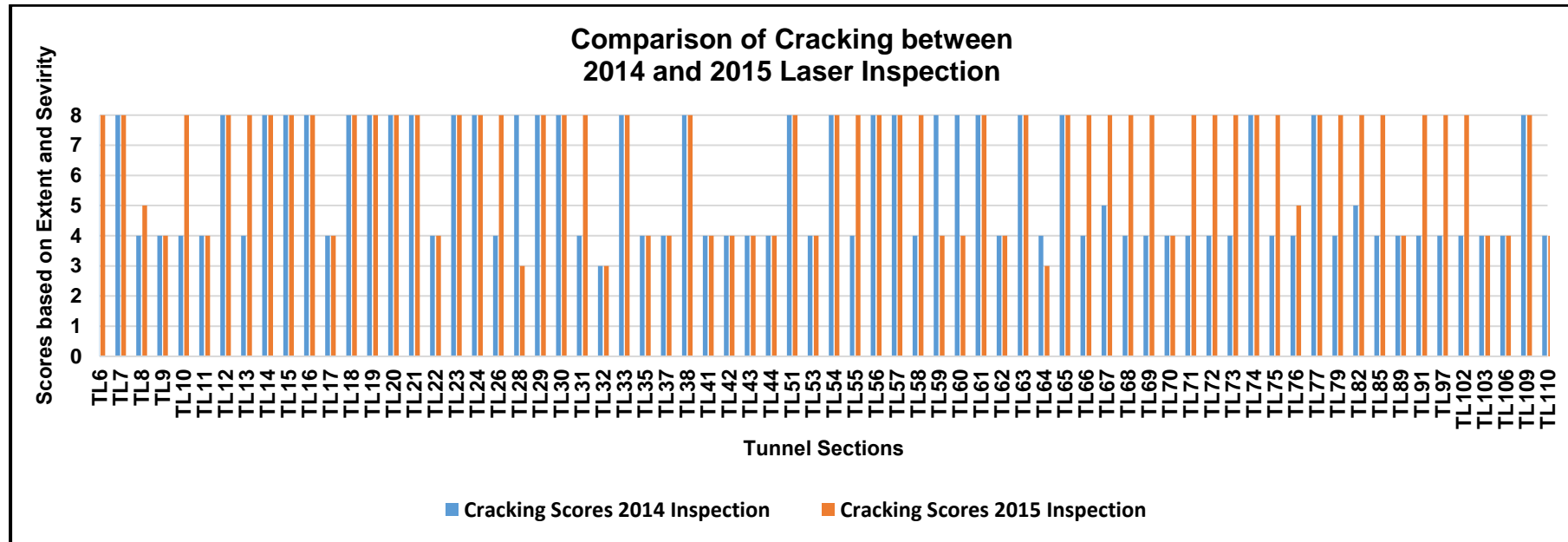


Figure 3-72 Comparison of cracking between 2014 and 2015 Laser inspection

Figure 3-73 shows a comparison of damp patches of 72 sections of tunnels between 2014 and 2015 laser inspection. In most of the tunnel's sections, there were no significant changes in damp patches between two inspections. Tunnel sections, TL23, TL57 and TL63 scores were slightly reduced from 8 to 7 between the 2014 and 2015 inspections. This indicates that water seepage/damp patches did not much influence the overall inspection scores between 2014 and 2015.

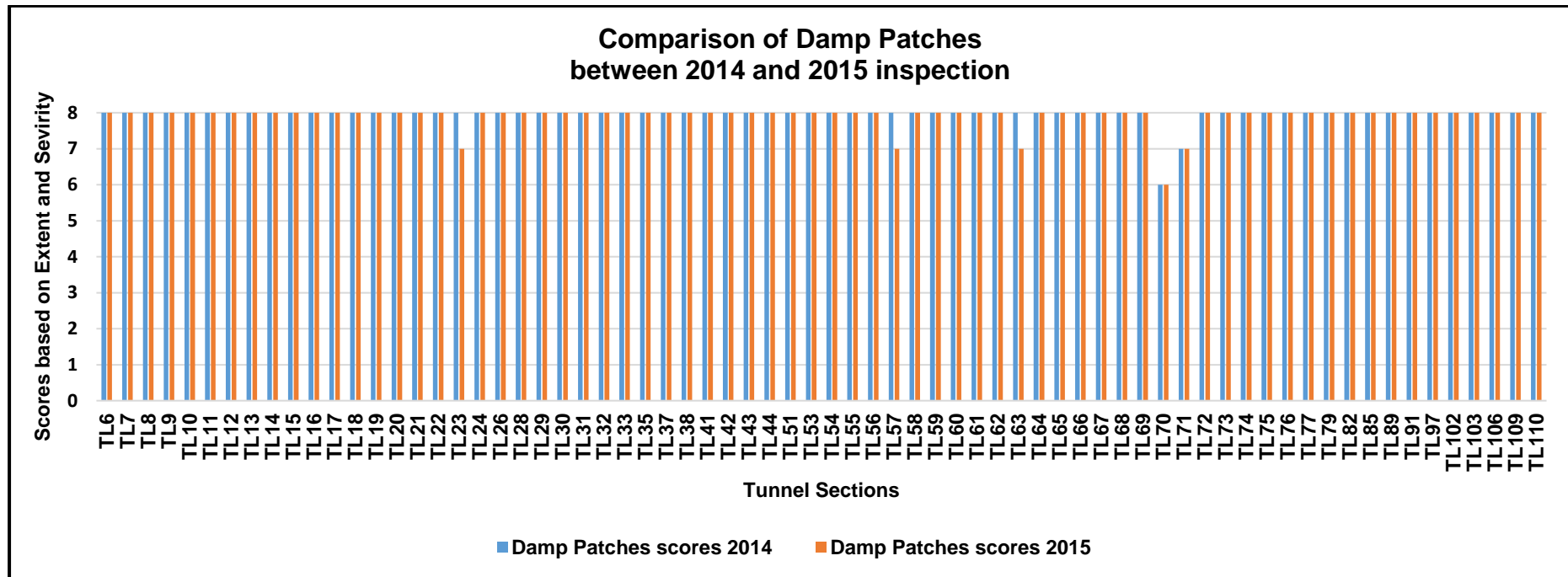


Figure 3-73 Comparison of damp patches between 2014 and 2015 Laser inspection

Figure 3-74 shows a comparison of joint loss for 72 sections of tunnels between the 2014 and 2015 laser inspections. In 29 tunnel sections, the overall score for joint loss was reduced from 7 to 4 between the 2014 and 2015 inspection. At the same time, TL20 and TL82 scores were increased from 7 to 8. Eight tunnel sections (e.g., TL11 and TL15) have the same score of 4 in both inspections. The joint loss score for tunnel section TL76 increased from 5 to 7, indicating that new joint losses appeared between the 2014 and 2015 inspections. Therefore, remedial (e.g., repointing) works should be carried out to improve the scores before the December 2016 inspection and also avoiding falling bricks from the tunnel.

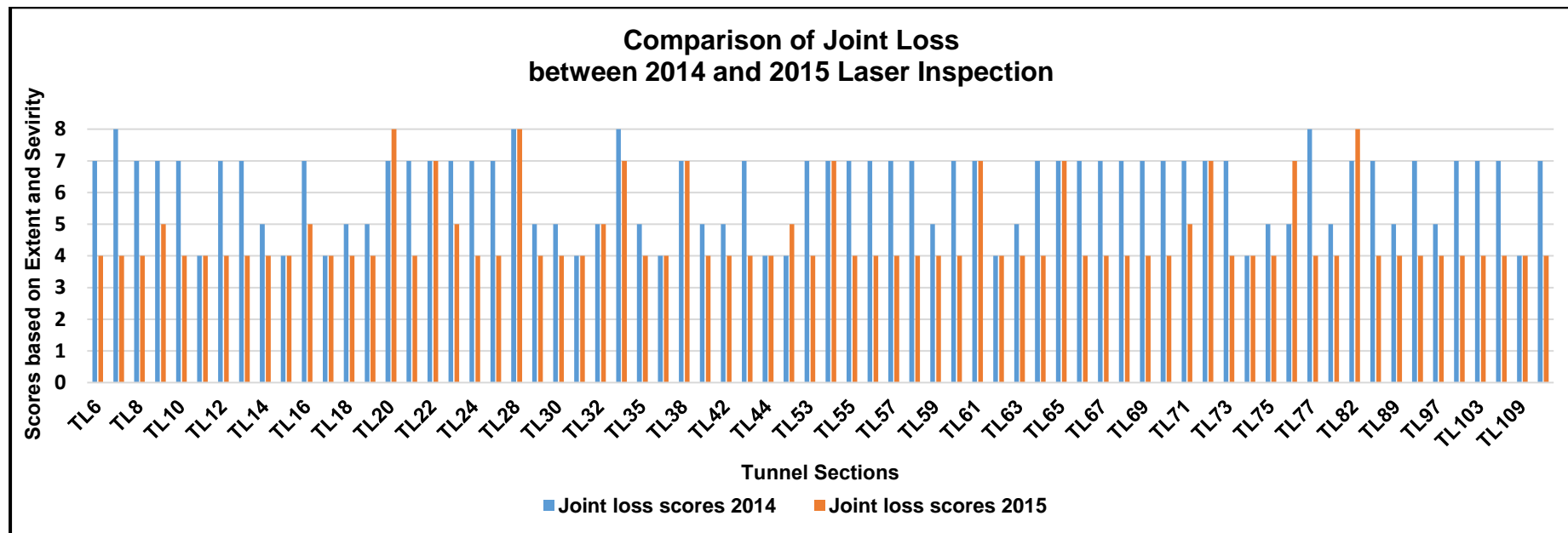


Figure 3-74 Comparison of Joint Loss between 2014 and 2015 Laser inspection

Figure 3-75 shows a comparison of face loss for 72 sections of tunnels between 2014 and 2015 laser inspections. Seven tunnel sections (e.g. TL54, TL56) have the same score of 4 in both inspections. Seventeen (e.g. TL13, TL15), seven (e.g. TL6, TL7) and three (e.g. TL42, TL67) tunnel sections decreased scores from 7 to 4, 8 to 4 and 5 to 4, respectively. At the same time, seven tunnel sections (e.g. TL54, TL56) and another three tunnel sections (e.g. TL58, TL61) have the same score of 4 and 7 respectively for both inspections. Tunnel sections TL12, TL76 and TL76 scores were increased from 5 to 7. These scores indicate remedial works (brickworks) have to be carried out before the next laser inspection to fix the defects and improve the face loss scores.

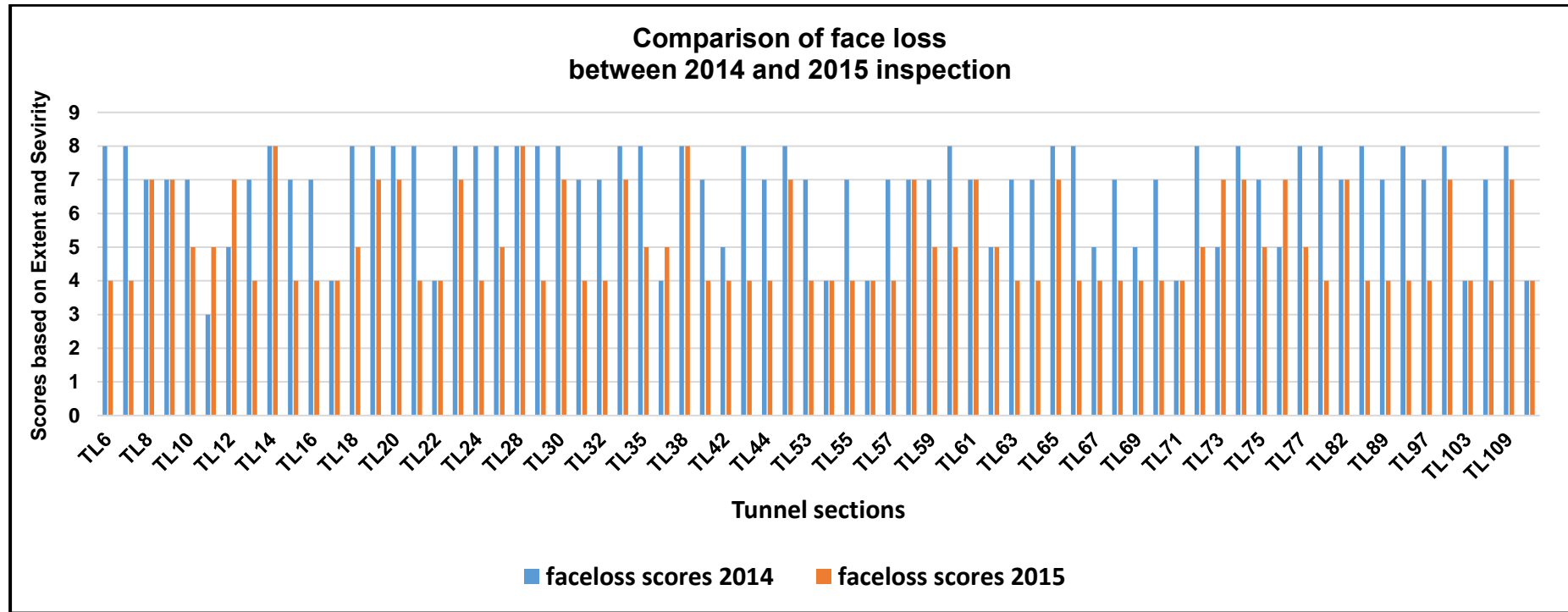


Figure 3-75 Comparison of face loss between 2014 and 2015 Laser inspection

Figure 3-74 and Figure 3-75 show that joint loss and face loss were significantly influenced (decrease) in overall rating measured by the 2015 laser inspection (see Figure 3-71).

Table 3-27 shows assets that have been selected for further analysis to distinguish score differences between the 2014 and 2015 laser inspections.

Table 3-27 Tunnel sections and their inspection scores for further analysis

Tunnel Sections	Overall rating 2014 Inspection (%)	Overall rating 2015 Inspection (%)
TL6	96.88	75.00
TL17	62.50	62.50
TL53	81.25	62.50
TL56	84.38	75.00
TL82	84.38	96.88

Cable brackets and deflector plate assets were only accounted for in the 2015 inspection at the request of LUL, and it only appeared on the 2015 inspection columns (see Table 3-28 Table 3-31 Table 3-37 and Table 3-39). In order to compare defects between the 2014 and the 2015 laser inspection, several screenshots were taken from Euroconsult's "Tunnel Viewer" software. Direct comparison of major defects (e.g. water ingress, face loss, joint loss and cracking), identified by the last visual inspection (2013) and the laser inspections (2014 and 2015) was not performed on all sections of the tunnel. This is due to a discrepancy with the chainage distances between the laser inspection and the visual inspection. Therefore, the comparison of defects between both systems are more difficult because the laser equipment traversed more than one asset during a single trip. The recorded chainages run consecutively from the trip start point in the direction of travel. For the second and subsequent assets, the chainages are not recorded as starting at zero like the visual inspection.

3.17 TUNNEL 6

Tunnel 6 (TL6) is located between Gloucester Road and High Street Kensington. Table 3-28 shows a comparison of laser inspection scores between the 2014 and 2015 inspections of tunnel section TL6.

Table 3-28 TL6- Comparison of laser inspection scores between 2014 and 2015

TUNNEL TL 06	2015 Inspection			2014 Inspection (Reference Scan)		
	Gloucester Road - HS Kensington					
	LENGTH TUNNEL (m)	96		LENGTH TUNNEL (m)	96	
INCIDENT	LENGTH (m)	AREA (m ²)	UNITS(u)	LENGTH (m)	AREA (m ²)	UNITS (u)
Cracking	0			0		
Dampness		0			0	
Joint Loss	26.72	1.07		3.13	0.13	
Face Loss		0.08			0	
Brackets			1,146			
Deflector Plates			8			
2015 INSPECTION SCORES	INCIDENT	EXTENT (%)	CATEGORY	AVERAGED MEASURE	S	ITEM SCORE
	Cracking	0	A		1	8
	Dampness	0	A		1	8
	Joint Loss	0.1	A	33.83	4	4
	Face Loss	0.01	A	42.73	4	4
				TOTAL SCORE		75.00%
2014 (Reference) INSPECTION SCORES	INCIDENT	EXTENT (%)	CATEGORY	AVERAGED MEASURE	S	ITEM SCORE
	Cracking	0	A		1	8
	Dampness	0	A		1	8
	Joint Loss	0.01	A	24.3	2	7
	Face Loss	0	A		1	8
				TOTAL SCORE		96.88%

Compared to the 2014 inspection, the 2015 inspection score was lower by 21.88%, due to the identification of new defects in joint loss and lining face loss. The total length of joint loss increased from 3.13m to 26.72m and the area also increased from 0.13m² to 1.07m² between the 2014 and the 2015 inspections. Due to these changes, the item scored for joint loss reduced from 7 to 4. In the 2015 inspection, face loss was identified at an area of 0.08m²

and no face loss was identified in the 2014 inspection. Therefore, the item score for face loss reduced from 8 to 4. Cracking and the damp patches did not appear on the tunnel lining in both inspections.

3.17.1 Lining Face Loss

Table 3-29 shows a comparison of lining face loss between 2014 and 2015 Laser inspection in whole TL6 tunnel section. The lining face loss did not appear in the 2014 laser inspection, however, lining face loss appeared at 17 new locations (newly formed defects) in the 2015 laser inspection.

**Table 3-29 TL6 Comparison of Lining face loss
(2014 and 2015 Laser inspection)**

Incidence comparative - TL06_15 - TL06_14													
Export to Word													
TL06_15 - TL06_14	Meter	Type	TL06_15 Measure	TL06_15 Width	TL06_15 Depth	TL06_15 CRACKING	TL06_14 Measure	TL06_14 Width	TL06_14 Depth	TL06_14 CRACKING	Measure Difference	Width Difference	Depth Difference
Show	3	LINING FACE LOSS	0.004	0	77.00						-0.004	0	77.00
Show	3	LINING FACE LOSS	0.002	0	77.00						-0.002	0	77.00
Show	10	LINING FACE LOSS	0.001	0	77.00						-0.001	0	77.00
Show	10	LINING FACE LOSS	0.001	0	77.00						-0.001	0	77.00
Show	19	LINING FACE LOSS	0.002	0	77.00						-0.002	0	77.00
Show	31	LINING FACE LOSS	0.005	0	38.00						-0.005	0	38.00
Show	37	LINING FACE LOSS	0.003	0	77.00						-0.003	0	77.00
Show	55	LINING FACE LOSS	0.009	0	38.00						-0.009	0	38.00
Show	56	LINING FACE LOSS	0.005	0	127.00						-0.005	0	127.00
Show	66	LINING FACE LOSS	0.011	0	23.00						-0.011	0	23.00
Show	66	LINING FACE LOSS	0.010	0	28.00						-0.01	0	28.00
Show	68	LINING FACE LOSS	0.018	0	25.00						-0.018	0	25.00
Show	68	LINING FACE LOSS	0.006	0	32.00						-0.006	0	32.00
Show	70	LINING FACE LOSS	0.001	0	77.00						-0.001	0	77.00
Show	71	LINING FACE LOSS	0.003	0	27.00						-0.003	0	27.00
Show	88	LINING FACE LOSS	0.001	0	31.00						-0.001	0	31.00
Show	88	LINING FACE LOSS	0.001	0	24.00						-0.001	0	24.00

Figure 3-76 shows that two locations of lining face loss were identified at chainage 3, by the laser inspection in 2015. However, this defect did not appear in the 2014 laser inspection, therefore it is a newly formed defect.

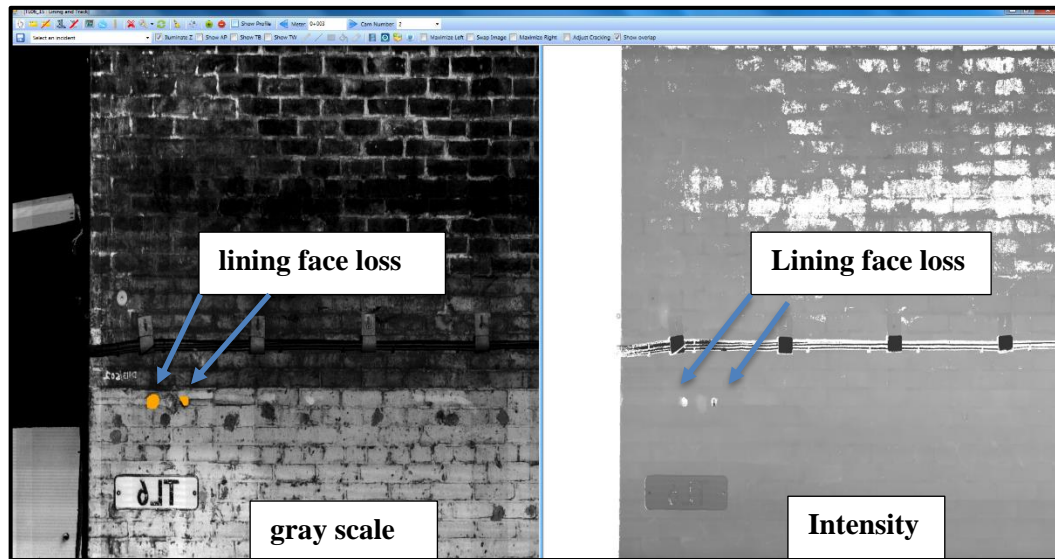


Figure 3-76 TL6 lining face loss at chainage 3- 2015 Laser inspection

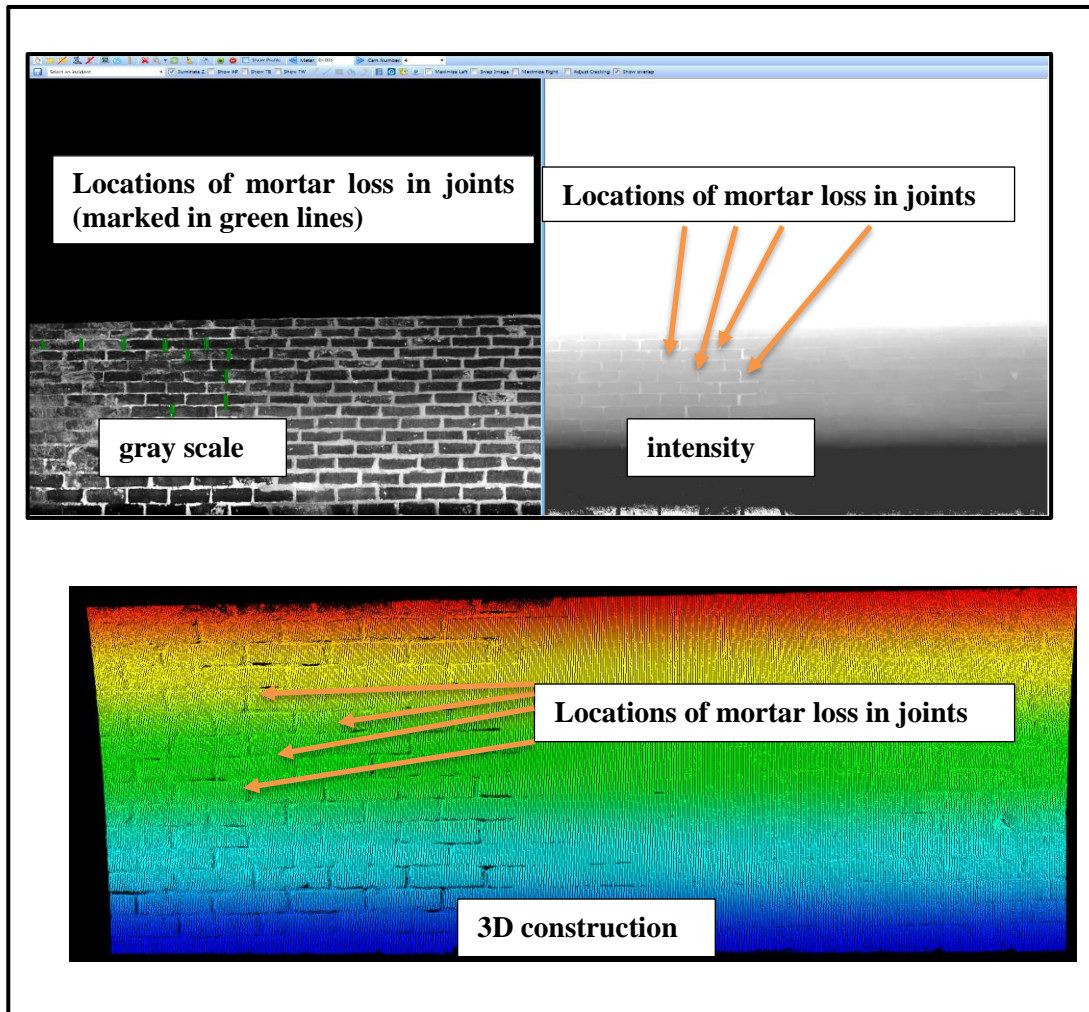
3.17.2 Mortar Loss in Joints

Table 3-30 shows dimensions (length, width and depth) of newly appeared mortar loss in joints at chainage 4 in the 2015 Laser inspection. However, these defects did not appear on the tunnel lining in the 2014 Laser inspection.

Table 3-30 TL6 comparison of mortar loss in joints at chainage 4 (2014 and 2015 Laser Inspection)

TL06_15 - TL06_14	Meter	Type	TL06_15 Measure	TL06_15 Width	TL06_15 Depth	TL06_15 CRACKING	TL06_14 Measure	TL06_14 Width	TL06_14 Depth	TL06_14 CRACKING	Measure Difference	Width Difference	Depth Difference
Show	3	MORTAR LOSS IN JOINTS	0.057	55.00	13.00						-0.057	55.00	13.00
Show	3	MORTAR LOSS IN JOINTS	0.046	17.00	18.00						-0.046	17.00	18.00
Show	3	LINING FACE LOSS	0.004	0	77.00						-0.004	0	77.00
Show	3	LINING FACE LOSS	0.002	0	77.00						-0.002	0	77.00
Show	4	MORTAR LOSS IN JOINTS	0.062	68.00	35.00						-0.062	68.00	35.00
Show	4	MORTAR LOSS IN JOINTS	0.061	23.00	32.00						-0.061	23.00	32.00
Show	4	MORTAR LOSS IN JOINTS	0.072	17.00	38.00						-0.072	17.00	38.00
Show	4	MORTAR LOSS IN JOINTS	0.083	27.00	32.00						-0.083	27.00	32.00
Show	4	MORTAR LOSS IN JOINTS	0.072	21.00	27.00						-0.072	21.00	27.00
Show	4	MORTAR LOSS IN JOINTS	0.067	26.00	25.00						-0.067	26.00	25.00
Show	4	MORTAR LOSS IN JOINTS	0.088	22.00	25.00						-0.088	22.00	25.00
Show	4	MORTAR LOSS IN JOINTS	0.066	22.00	33.00						-0.066	22.00	33.00
Show	4	MORTAR LOSS IN JOINTS	0.069	19.00	20.00						-0.069	19.00	20.00
Show	4	MORTAR LOSS IN JOINTS	0.074	44.00	24.00						-0.074	44.00	24.00

Figure 3-77 shows locations of mortar loss in joints (their dimensions are shown in Table 3-30) at chainage 4. This defect was identified by the laser inspection in the 2015 scan and did not appear in the 2014 scan.



**Figure 3-77 TL 6 Scattered mortar loss in joints at chainage 4
2015 Laser inspection**

3.18 TUNNEL 17

Tunnel 17 (TL17) is located between Victoria and St James Park station; the tunnel is 196m in length. Table 3-31 shows the comparison between laser inspection scores between the 2014 and 2015 inspections of tunnel section, TL17.

Table 3-31 shows TL17's, 2014 and 2015 inspection scores that obtained the same total score of 62.50%. Each defect scored different numerical values between the 2014 and 2015 inspections. However, the item score for each defect obtained the same value (e.g. cracking and dampness) between the

2014 and 2015 inspections. This is a result of the range values mentioned in Table 3-6.

Table 3-31 TL17 Comparison of laser inspection scores between 2014 and 2015

TUNNEL TL17	2015 Inspection			2014 Inspection (Reference Scan)		
	St James`s Park - Victoria					
	LENGTH TUNNEL (m)		219	LENGTH TUNNEL (m)		219
INCIDENT	LENGTH (m)	AREA (m2)	UNITS(u)	LENGTH (m)	AREA (m2)	UNITS(u)
Cracking	6.82			2.52		
Dampness		52.98			9.92	
Joint Loss	21.15	0.85		15.63	0.63	
Face Loss		0.57			0.44	
Brackets			8,044			
Deflector Plates			72			
2015 INSPECTION SCORES	INCIDENT	EXTENT (%)	CATEGORY	AVERAGED MEASURE	S	ITEM SCORE
	Cracking	3.11	A	45.96	4	4
	Dampness	1.6	A		1	8
	Joint Loss	0.03	A	40.37	4	4
	Face Loss	0.02	A	44.11	4	4
				TOTAL SCORE		62.50%
2014 (Reference) INSPECTION SCORES	INCIDENT	EXTENT (%)	CATEGORY	AVERAGED MEASURE	S	ITEM SCORE
	Cracking	1.56	A	27	4	4
	Dampness	0.4	A		1	8
	Joint Loss	0.03	A	30.92	4	4
	Face Loss	0.02	A	77.4	4	4
				TOTAL SCORE		62.50%

Due to a discrepancy with the chainage distances between the laser inspection and the visual inspection, the comparison of defects between both systems is difficult since the laser equipment traversed more than one asset during a single trip. The recorded chainages run consecutively from the trip start point in the direction of travel. For second and subsequent assets, the chainages are not recorded as starting at zero, similarly to the visual inspection.

3.18.1 Damp patch

Determining damp patches is important as water ingress in the tunnel, via small runoffs on the tunnel wall, can be detrimental not to the tunnel itself but the signalling and other electrical systems. Therefore, areas of the tunnel where water was detected are considered damp patches.

Figure 3-78 shows that active water seepage at chainage 77 from the arch springer to the track level. The darker areas seen on the ballast was caused by the seepage; this was identified by the visual inspection in 2013. Figure 3-79 indicates that the same defect was identified by the laser inspection in 2015. However, this defect was not determined by the laser inspection in 2014(see Figure 3-80). This indicates that water seepage at this location was not permanent and may due to seasonal variations.



Figure 3-78 TL17- active water seepage at chainage 77, from the arch springer to track level- visual inspection 2013

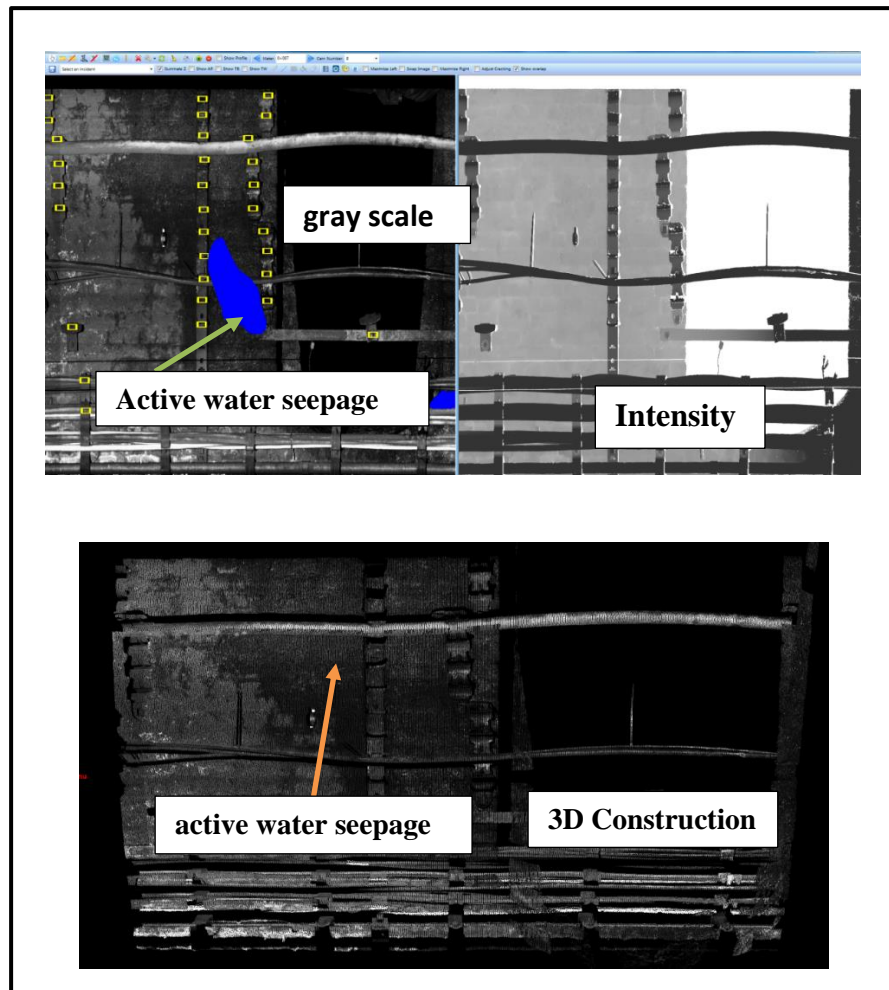


Figure 3-79 TL17 water seepage at chainage 77 -2015 Laser Inspection

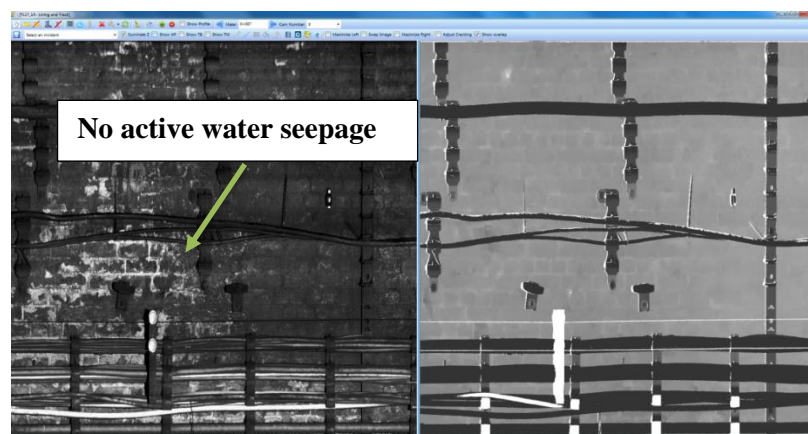


Figure 3-80 TL17 no water seepage at chainage 77-2014 Laser Inspection

Figure 3-81 shows a comparison of damp patches between 2014 and 2015 inspections at chainage 102. It clearly indicates that an area of damp patches (active seepage) has considerably increased in the 2015 inspection when compared to the images from the 2014 inspection. This indicates that remedial

works were not carried out between the two inspections and the severity of the defect increased, as can be seen by the larger water seepage area on the 2015 Laser inspection.

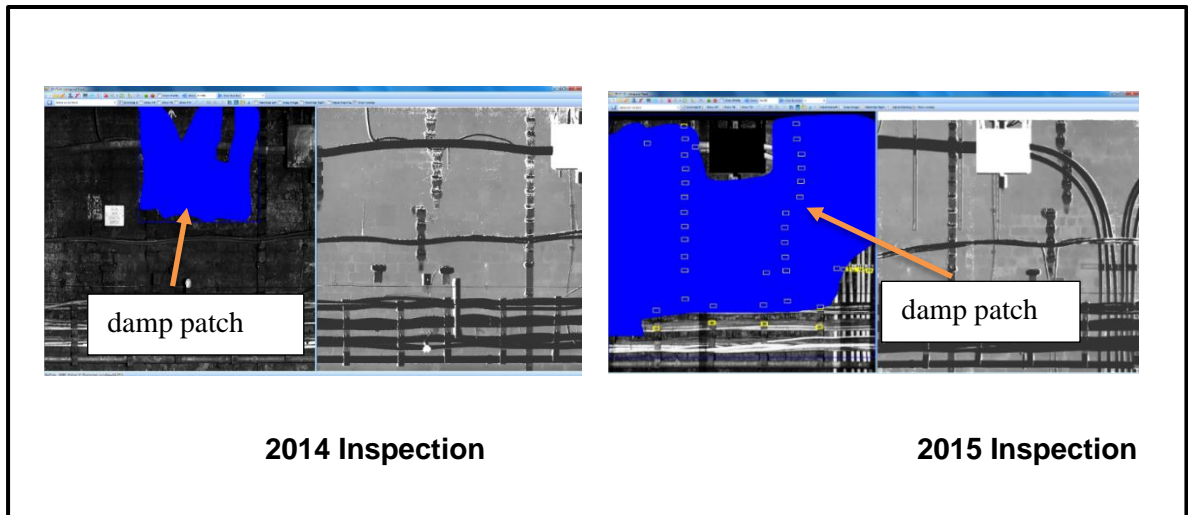


Figure 3-81 TL 17 area of damp patches at chainage 102 2014 and 2015 Laser Inspection

Table 3-32 shows a comparison of damp patches between the 2014 and 2015 inspections between chainages 96 and 112. Table 3-32 shows that the damp patches at chainage 102 occupied an area of 1.094m^2 . Since the 2014 inspection, these have significantly increased by 3.541m^2 , reaching the total area of 4.635m^2 .

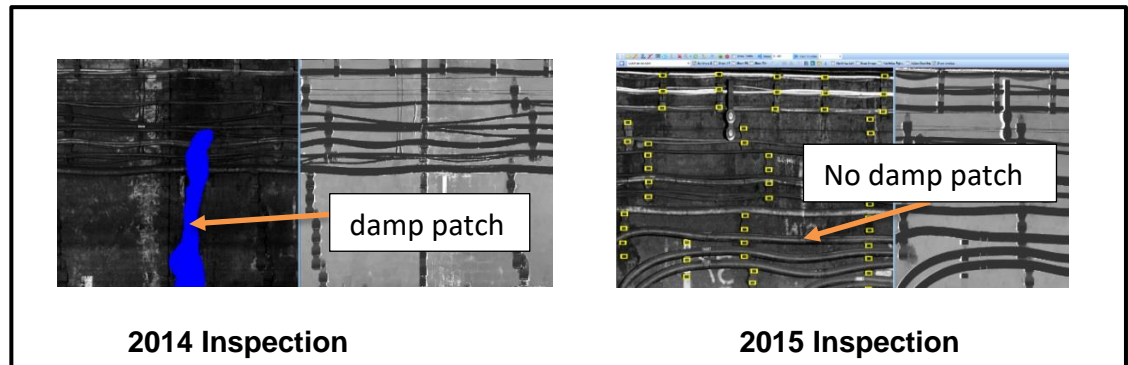
**Table 3-32 Comparison of damp patches between chainage 96 and 112
2014 and 2015 laser inspection**

Incidence comparative - TL17_15 - TL17_14												
Export to Word												
TL17_15 - TL17_14	Meter	Type	TL17_15 Measure	TL17_15 Width	TL17_15 Depth	TL17_15 CRACKING	TL17_14 Measure	TL17_14 Width	TL17_14 Depth	TL17_14 CRACKING	Measure Difference	Width Difference
Show	96	DAMP PATCHES					0.202	0	0		0.202	0
Show	96	DAMP PATCHES					0.000	0	0		0	0
Show	96	DAMP PATCHES					0.353	0	0		0.353	0
Show	97	DAMP PATCHES	0.000	0	0						0	0
Show	97	DAMP PATCHES	0.000	0	0						0	0
Show	97	DAMP PATCHES					0.423	0	0		0.423	0
Show	97	DAMP PATCHES					0.422	0	0		0.422	0
Show	97	DAMP PATCHES	0.160	0	0						-0.16	0
Show	98	DAMP PATCHES	3.841	0	0						-3.841	0
Show	98	DAMP PATCHES	0.998	0	0						-0.998	0
Show	99	DAMP PATCHES					0.341	0	0		0.341	0
Show	100	DAMP PATCHES	0.459	0	0						-0.459	0
Show	101	DAMP PATCHES	0.230	0	0						-0.23	0
Show	102	DAMP PATCHES	4.635	0	0		1.094	0	0		-3.541	0
Show	103	DAMP PATCHES	0.000	0	0						0	0
Show	104	DAMP PATCHES					1.596	0	0		1.596	0
Show	105	DAMP PATCHES	5.761	0	0						-5.761	0
Show	107	DAMP PATCHES	1.367	0	0		1.308	0	0		-0.058999...	0
Show	108	DAMP PATCHES					0.072	0	0		0.072	0
Show	108	DAMP PATCHES					0.051	0	0		0.051	0
Show	108	DAMP PATCHES	0.265	0	0						-0.265	0
Show	108	DAMP PATCHES	0.201	0	0						-0.201	0
Show	112	DAMP PATCHES	0.096	0	0						-0.096	0

Table 3-33 shows that a damp patch at chainage 164 appeared in the 2014 inspection with an area of 0.358m² and did not appear in the 2015 inspection. Figure 3-82 shows that in 2015, the damp patch did not appear, and any repair work also did not take place at that location. This indicates a temporary defect of water seepage at chainage 164 and this may be connected to a seasonal effect (a seepage that appears when a certain rainfall occurs).

**Table 3-33 Comparison of damp patches between chainage 125 and 170
2014 and 2015 laser inspection**

TL17_15- TL17_14	Meter	Type	TL17_15 Measure	TL17_15 Width	TL17_15 Depth	TL17_15 CRACKING	TL17_14 Measure	TL17_14 Width	TL17_14 Depth	TL17_14 CRACKING	Measure Difference	Width Difference	Depth Difference
Show	125	DAMP PATCHES	0.184	0	0						-0.184	0	0
Show	125	DAMP PATCHES	0.437	0	0						-0.437	0	0
Show	133	DAMP PATCHES	0.757	0	0						-0.757	0	0
Show	134	DAMP PATCHES	0.624	0	0						-0.624	0	0
Show	134	DAMP PATCHES	2.328	0	0						-2.328	0	0
Show	135	DAMP PATCHES	0.751	0	0						-0.751	0	0
Show	136	DAMP PATCHES	0.409	0	0						-0.409	0	0
Show	140	DAMP PATCHES	0.546	0	0						-0.546	0	0
Show	140	DAMP PATCHES	1.757	0	0						-1.757	0	0
Show	141	DAMP PATCHES	0.183	0	0						-0.183	0	0
Show	141	DAMP PATCHES	0.101	0	0						-0.101	0	0
Show	142	DAMP PATCHES					0.159	0	0		0.159	0	0
Show	142	DAMP PATCHES					0.713	0	0		0.713	0	0
Show	142	DAMP PATCHES					0.215	0	0		0.215	0	0
Show	149	DAMP PATCHES	0.027	0	0						-0.027	0	0
Show	161	DAMP PATCHES	0.000	0	0						0	0	0
Show	161	DAMP PATCHES	0.000	0	0						0	0	0
Show	161	DAMP PATCHES	0.160	0	0						-0.16	0	0
Show	164	DAMP PATCHES					0.358	0	0		0.358	0	0
Show	168	DAMP PATCHES	0.183	0	0						-0.183	0	0
Show	169	DAMP PATCHES	0.049	0	0						-0.049	0	0
Show	170	DAMP PATCHES	0.111	0	0						-0.111	0	0

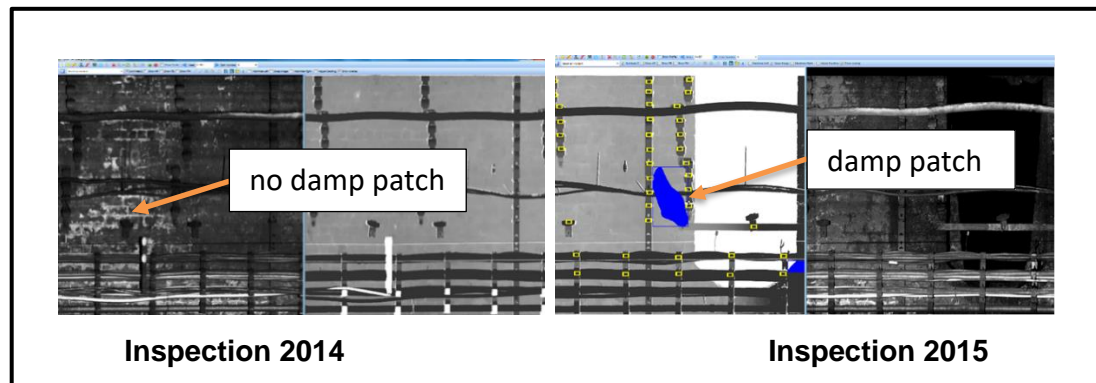


**Figure 3-82 TL 17 area of damp patch at chainage 164
2014 and 2015 Laser Inspection**

Table 3:35 shows that the damp patch at chainage 87 appeared in the 2015 inspection with an area of 0.130m² but it did not appear in the 2014 inspection.

**Table 3-34 Comparison of damp patches between chainage 87 and 91
2014 and 2015 laser inspection**

TL17_15 - TL17_14	Meter	Type	TL17_15 Measure	TL17_15 Width	TL17_15 Depth	TL17_15 CRACKING	TL17_14 Measure	TL17_14 Width	TL17_14 Depth	TL17_14 CRACKING	Measure Difference	Width Difference	Depth Difference
Show 87		DAMP PATCHES	0.130	0	0						-0.13	0	0
Show 88		DAMP PATCHES	0.016	0	0						-0.016	0	0
Show 88		DAMP PATCHES	0.078	0	0						-0.078	0	0
Show 91		DAMP PATCHES	2.260	0	0						-2.26	0	0
Show 91		DAMP PATCHES	0.339	0	0						-0.339	0	0

**Figure 3-83 TL 17 area of a damp patch at chainage 87
2014 and 2015 Laser Inspection**

3.18.2 Cracking

The crack previously marked was reviewed and compared to the new inspection. The tunnels have also been inspected for new cracks that could have appeared between the first (2014) and the second (2015) inspections. Table 3:36 shows a comparison of cracks in two inspections between chainage 100 and 195. Cracks were classified into transverse and diagonal. Cracks at chainage 101, in the 2014 inspection have disappeared in the 2015 inspection because remedial works have been completed and verified with a completed works order. However, new cracks appeared at chainage 195.

**Table 3-35 Comparison of cracking between chainage 100 and 195
2014 and 2015 Laser inspection**

Incidentes comparative - TL17_15 - TL17_14													
Export to Word													
TL17_15 - TL17_14	Meter	Type	TL17_15 Measure	TL17_15 Width	TL17_15 Depth	TL17_15 CRACKING	TL17_14 Measure	TL17_14 Width	TL17_14 Depth	TL17_14 CRACKING	Measure Difference	Width Difference	Depth Difference
Show	100	CRACKING	0.896	69.00	64.00	Transversal					-0.896	69.00	64.00
Show	101	CRACKING					0.560	19.02	11.35	Transversal	0.56	19.02	11.35
Show	101	CRACKING					0.354	19.12	21.93	Diagonal	0.354	19.12	21.93
Show	101	CRACKING					1.608	31.51	32.04	Transversal	1.608	31.51	32.04
Show	195	CRACKING	1.435	79.00	24.00	Transversal					-1.435	79.00	24.00
Show	195	CRACKING	2.057	57.00	134.00	Transversal					-2.057	57.00	134.00
Show	195	CRACKING	1.977	6.00	178.00	Transversal					-1.977	6.00	178.00
Show	195	CRACKING	0.452	20.00	25.00	Transversal					-0.452	20.00	25.00

Figure 3-84 shows transverse and diagonal cracks, on TL17, at chainage 101 in the 2014 inspection. The dimensions of these cracks can be seen in Table 3-35.

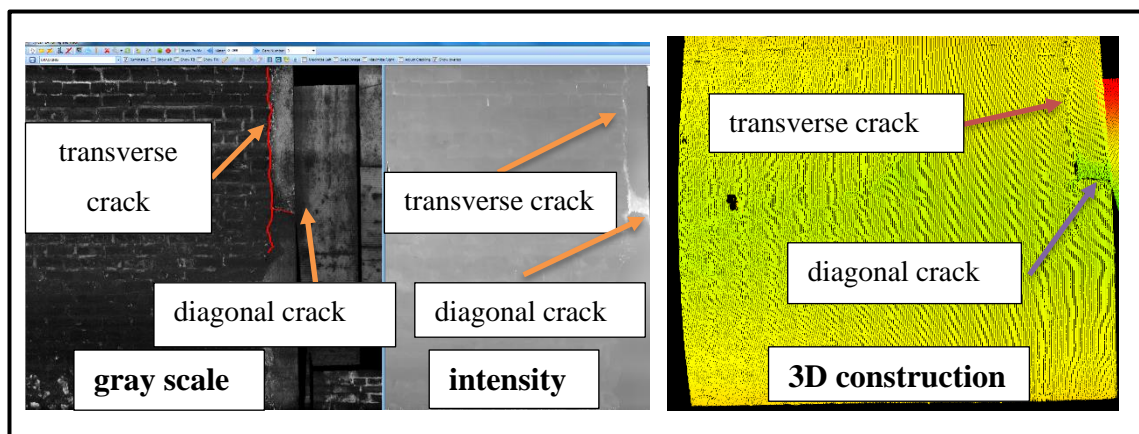


**Figure 3-84 TL17 transverse and diagonal cracks at chainage 101
2014 inspection**

3.18.3 Mortar loss in joints

This category presents the bricks' joints that were detected on the lining. Width and depth of mortar loss in the joints can be clearly assessed using Euroconsult's Tunnel Viewer software. Figure 3-85 shows mortar loss in a joint at chainage 100, as it is seen on the tunnel viewer software. In the 2014 inspection, this defect was identified in two locations (A & B) at chainage 100, however, in the 2015 inspection it was identified only at location B. The same length of the defect does not show at location A in the two inspections and this may be due to poor data quality and so there is difficulty in interpreting the defect length. Analysing the pictures, the reader can understand that this is likely not to be mortar loss but imperfections in the connection between the

brick tunnel and concrete. Imperfections that are likely to be linear will always show as mortar loss by this system.

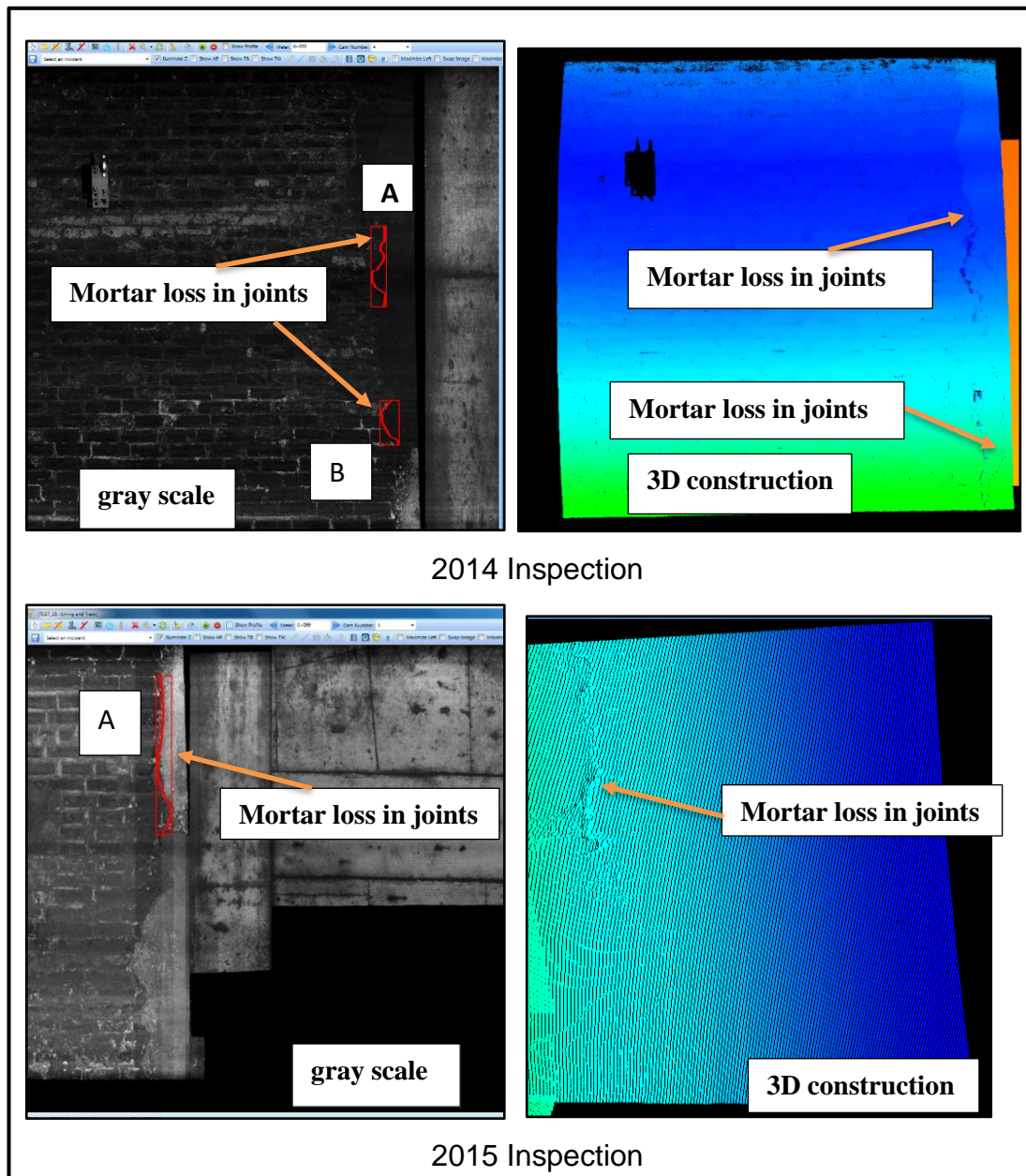


**Figure 3-85 TL17 mortar loss in joints at chinage 100
2014 and 2015 Laser Inspection**

3.18.4 Lining face loss

The areas on the bricks that show significant lining face breaking, missing parts and major material loss have been referred to as 'lining face loss'. These areas are detected by Euroconsult's computer vision 3D image software and have

been clearly marked on the surface by irregularities, distorting the profile of the tunnel.

Table 3-36 shows a comparison of lining face loss between chainage 86 and 111 of the 2014 and the 2015 laser inspection. In 2014, laser inspection lining face loss was identified at two locations with depths of 52.06mm and 39.43mm (see Figure 3-76). However, in the 2015 laser inspection, these defects had disappeared at those places, and another two-new lining face loss defects appeared with depths of 104mm and 42mm (see Figure 3-87). This may highlight the problem of the odometer not being able to identify the location of defects precisely in between two epochs of observation.

**Table 3-36 Comparison of lining face loss between chainage 86 and 111
2014 and 2015 Laser inspection**

TL17_15 - TL17_14	Meter	Type	TL17_15 Measure	TL17_15 Width	TL17_15 Depth	TL17_15 CRACKING	TL17_14 Measure	TL17_14 Width	TL17_14 Depth	TL17_14 CRACKING	Measure Difference	Width Difference	Depth Difference
Show	86	LINING FACE LOSS	0.004	0	12.00						-0.004	0	12.00
Show	87	LINING FACE LOSS	0.004	0	13.00						-0.004	0	13.00
Show	89	LINING FACE LOSS	0.011	0	17.00						-0.011	0	17.00
Show	92	LINING FACE LOSS	0.012	0	13.00						-0.012	0	13.00
Show	93	LINING FACE LOSS	0.005	0	19.00						-0.005	0	19.00
Show	99	LINING FACE LOSS	0.007	0	112.00						-0.007	0	112.00
Show	99	LINING FACE LOSS	0.010	0	66.00						-0.01	0	66.00
Show	99	LINING FACE LOSS	0.000	0	49.00						0	0	49.00
Show	99	LINING FACE LOSS	0.002	0	49.00						-0.002	0	49.00
Show	100	LINING FACE LOSS					0.009	0	52.06		0.009	0	52.06
Show	100	LINING FACE LOSS					0.012	0	39.43		0.012	0	39.43
Show	100	LINING FACE LOSS	0.002	0	104.00						-0.002	0	104.00
Show	100	LINING FACE LOSS	0.001	0	42.00						-0.001	0	42.00
Show	111	LINING FACE LOSS	0.001	0	75.00						-0.001	0	75.00

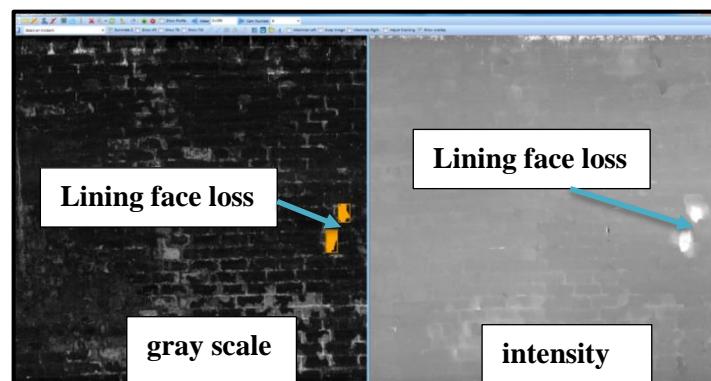


**Figure 3-86 TL17 lining face loss at chainage100
2014 Laser inspection**

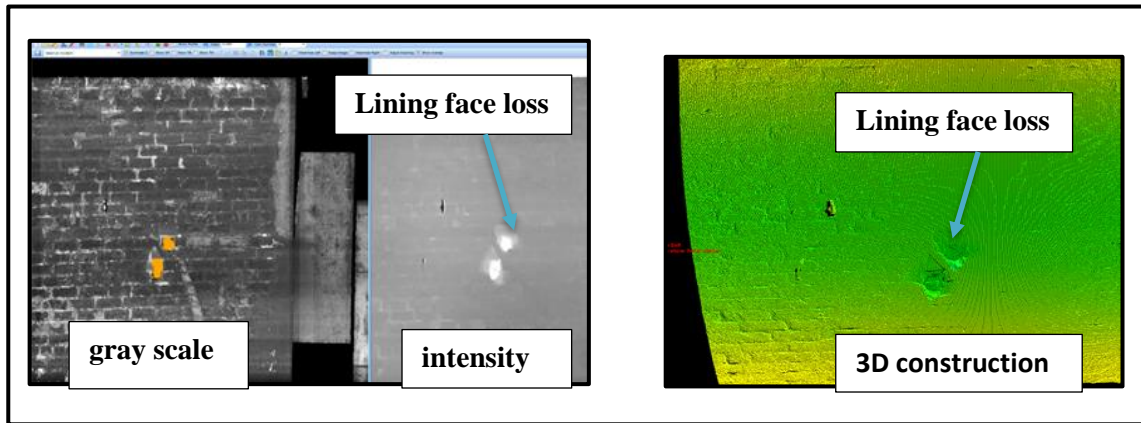


Figure 3-87 TL17 lining face loss at chainage100 -2015 Laser inspection

Figure 3-88 shows spalling of the brickwork around the recess area. This was identified by visual inspection at the North abutment 513m from the west. However, this defect was not identified in both laser inspections because remedial work was previously done. Figure 3-89 shows a screen shot of the laser scan software indicating that nothing was found.



**Figure 3-88 Spalling North abutment at chainage 513m from West
Visual Inspection-2013**

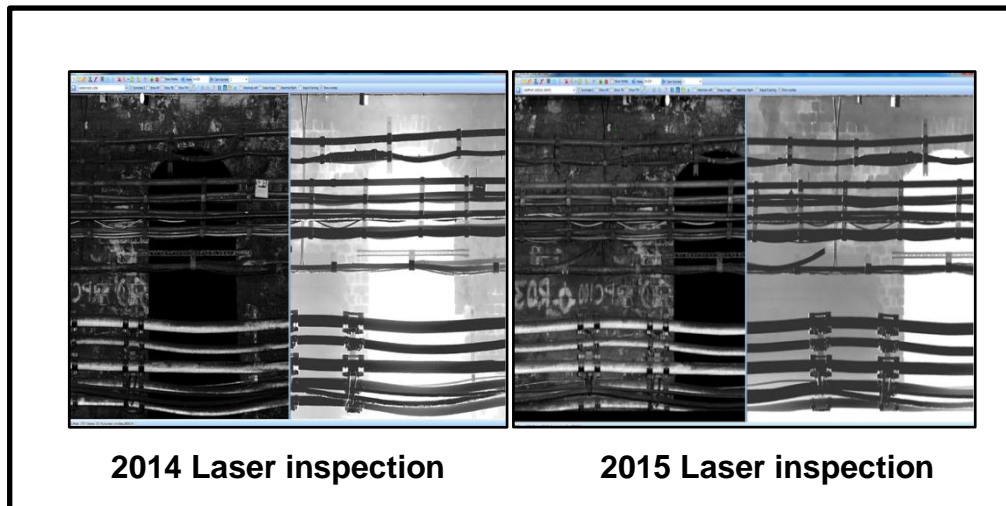


Figure 3-89 TL17 no spalling around recess area at chainage 513m

3.18.5 Brackets and Deflector plates

During the second inspection, deflector plates were detected. Deflector plates are metallic and can be any object fixed to the tunnel wall such as drip trays, naming plates and chainage markers. Deflector plates can be seen in Figure 3-90, according to the Tunnel Viewer software.

Deflector plates and Cable brackets are recorded and marked on the tunnel charts, but not scored. The Laser method records the location of the deflector plates that can be visualised on the greyscale images and on the 3D construction.

The defects behind the deflector plates cannot be seen by the laser method. Therefore, a separate inspection regime must be in place, and appropriate details are given as additional information or as part of the principal inspection report.

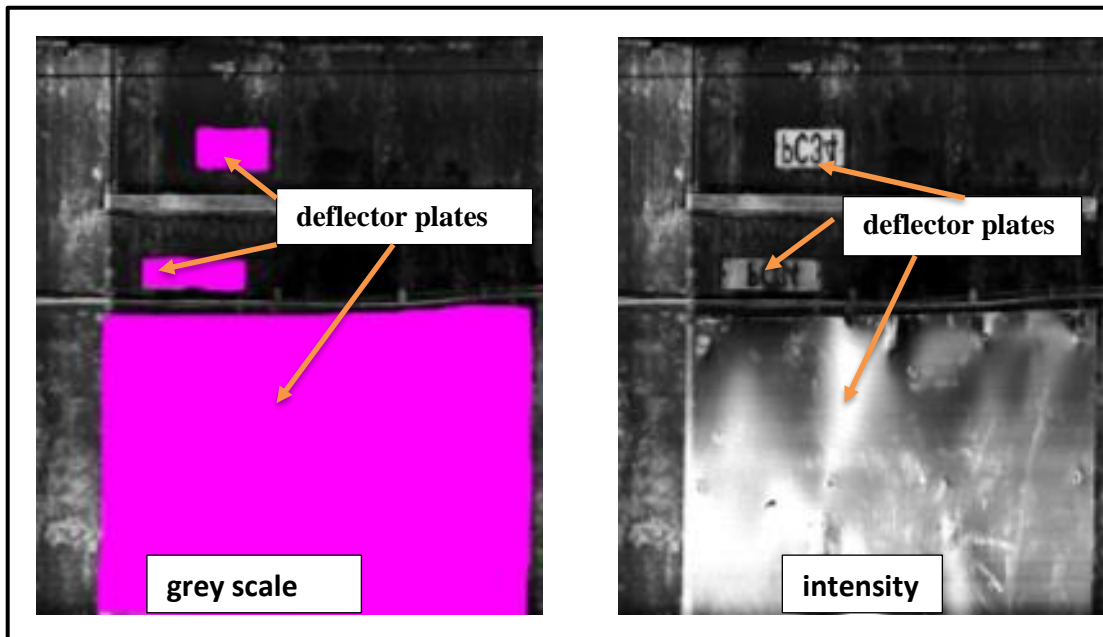


Figure 3-90 Deflector plates

Cable brackets (see Figure 3-91) used for securing cables were detected by Euroconsult's automatic algorithm to identify and locate these data and store them in the database. However, to confirm the algorithm has the capacity to detect automatically, part of this detection was manually conducted by Euroconsult.

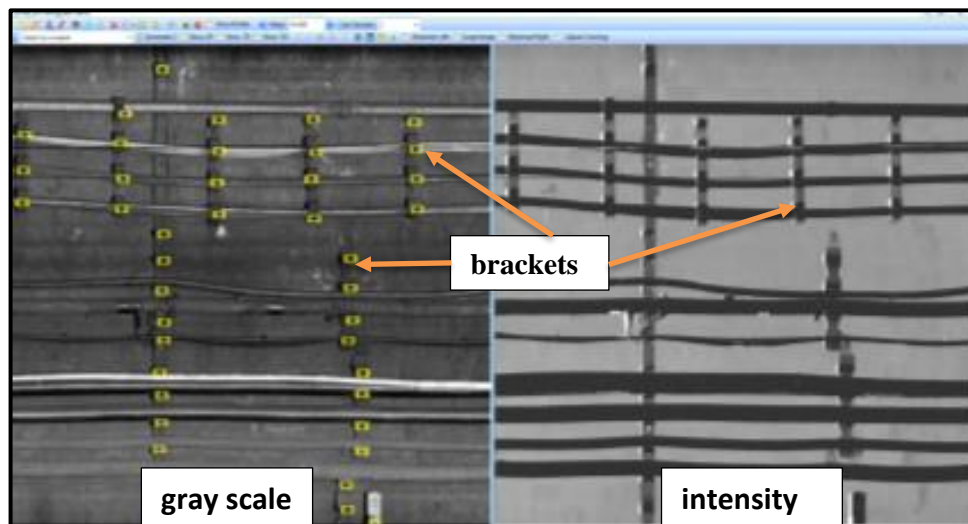


Figure 3-91 Cable brackets

3.19 TUNNEL 53

TL 53 is situated between Edgware Road station and Baker Street station and the tunnel is 615m in length.

Table 3-37 shows that the scores from the laser scanner inspection of TL 53 were reduced from 81.25% to 62.50% between 2014 and 2015. The average measure of joint loss increased from 23.22m to 36.17m and the average measure of face loss also increase from 10.88m to 60.69m between the 2014 and 2015 inspections. Due to this increment, both scores for joint loss and face loss reduced from 7 to 4. The drop in these scores significantly contributed to the difference between the total score of the 2014 and 2015 inspections.

Table 3-37 TL53 Comparison of laser inspection scores between 2014 and 2015

TUNNEL TL53	2015 Inspection			2014 Inspection (Reference Scan)		
	Edgware Road - Baker Street					
	LENGTH TUNNEL (m)		615	LENGTH TUNNEL (m)		615
INCIDENT	LENGTH (m)	AREA (m2)	UNITS(u)	LENGTH (m)	AREA (m2)	UNITS (u)
Cracking	16.83			8.72		
Dampness		80.62			137.3	
Joint Loss	26.31	1.05		60.31	2.41	
Face Loss		0.25			0.12	
Brackets			17,234			
Deflector Plates			311			
2015 INSPECTION SCORES	INCIDENT	EXTENT (%)	CATEGORY	AVERAGED MEASURE	S	ITEM SCORE
	Cracking	2.74	A	28.88	4	4
	Dampness	0.88	A		1	8
	Joint Loss	0.01	A	36.17	4	4
	Face Loss	0	A	60.69	4	4
				TOTAL SCORE		62.50%
2014 (Reference) INSPECTION SCORES	INCIDENT	EXTENT (%)	CATEGORY	AVERAGED MEASURE	S	ITEM SCORE
	Cracking	1.45	A	15.71	4	4
	Dampness	1.51	A		1	8
	Joint Loss	0.03	A	23.22	2	7
	Face Loss	0	A	10.88	2	7
				TOTAL SCORE		81.25%

3.19.1 Cracking

The vertical crack which was identified by the principal inspection on 18th of May 2013 was also identified by the laser inspections of 2014 and 2015. The location of the defect was identified by the visual inspection of the South abutment 581m from the West shown in Figure 3-92.

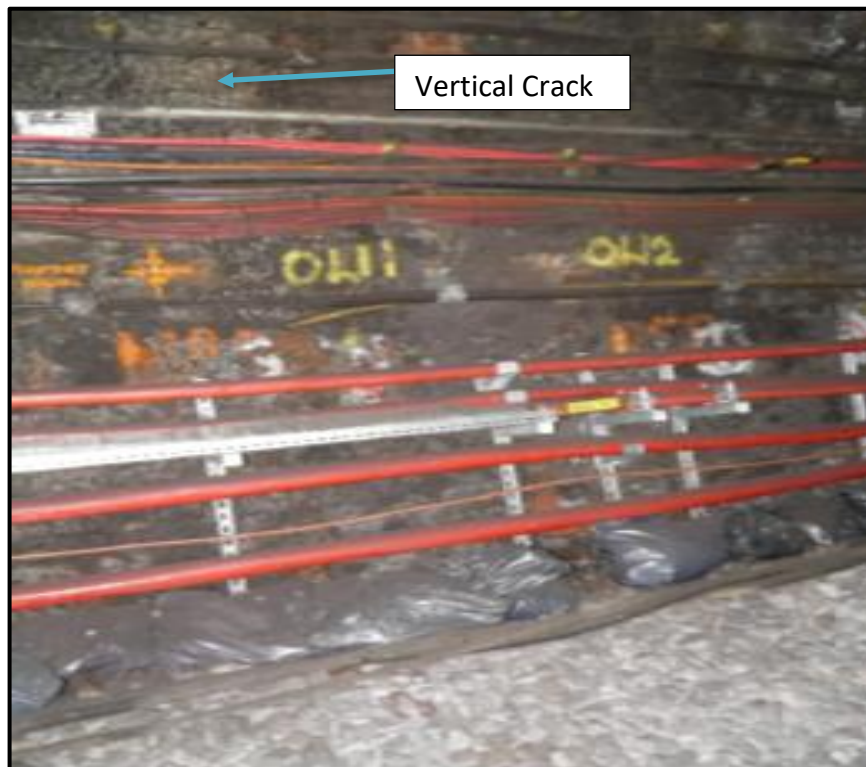


Figure 3-92 TL53 vertical crack at south abutment 581m from west visual inspection

Figure 3-93 and Figure 3-94 shows the same crack identified by the laser inspection in 2014 and 2015.

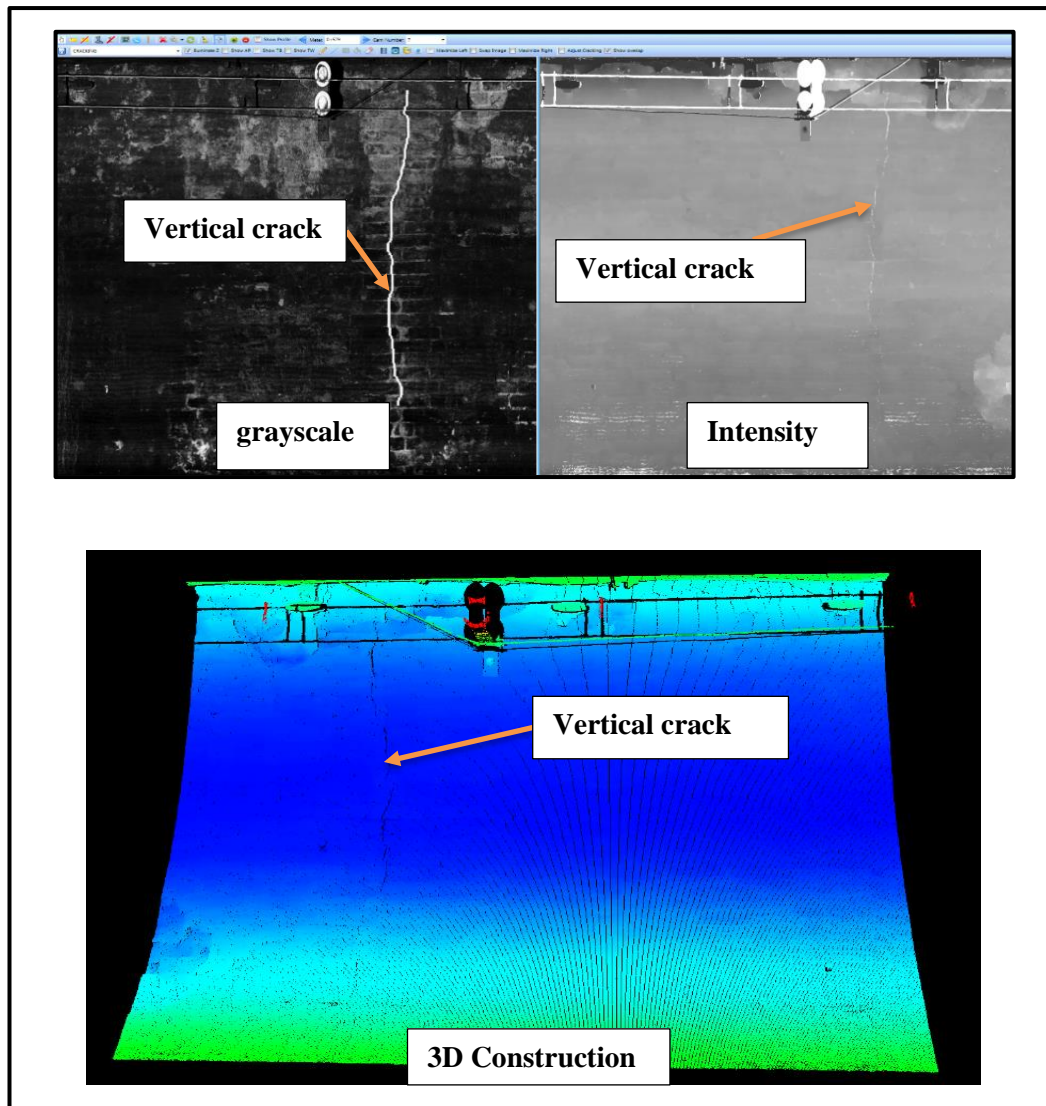


Figure 3-93 Vertical crack at South abutment 581m from West-2014
Laser inspection

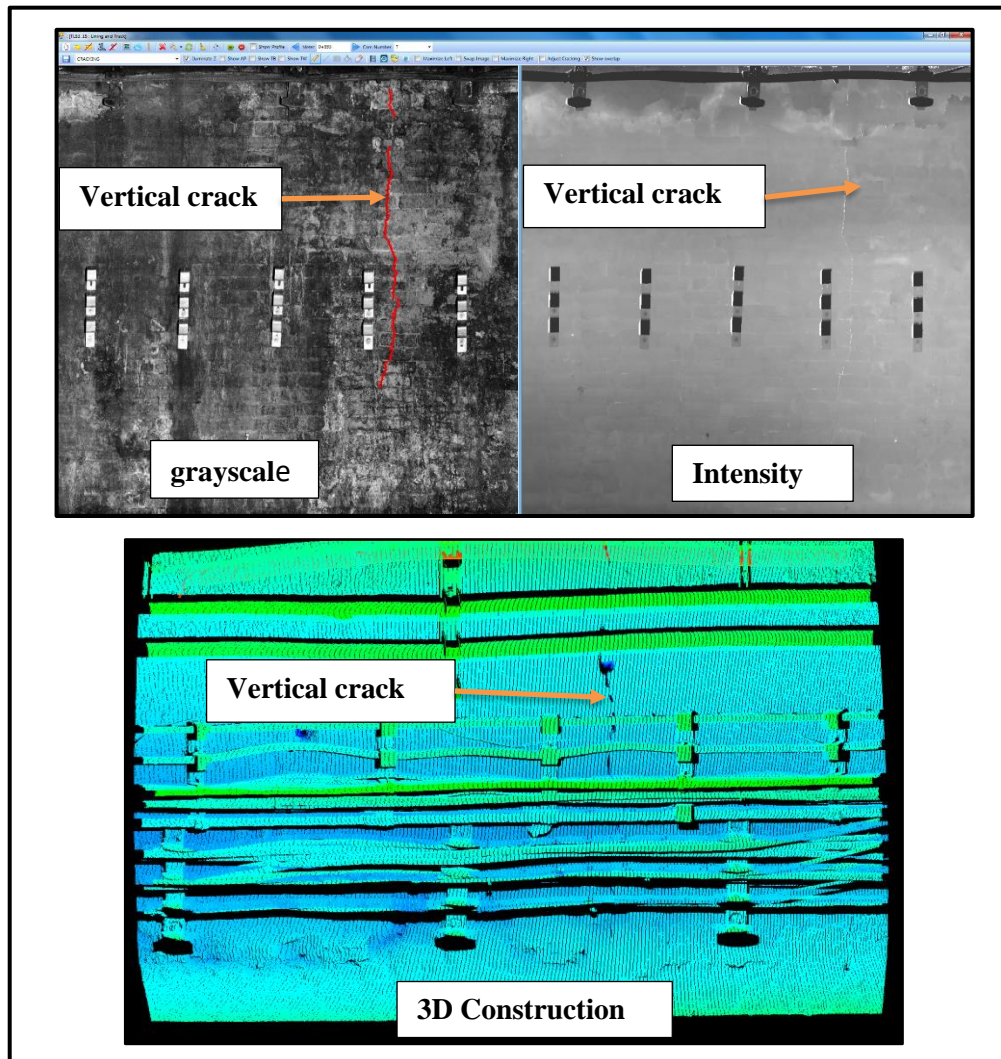


Figure 3-94 Vertical crack at South abutment 581m from West-2015 Laser inspection

3.19.2 Mortar loss in joints

Figure 3-95 shows screenshots of the Tunnel Viewer software. Starting on the left, a grayscale image of the tunnel is used to manually select points (highlighted in red). The second image shows a profile of the depth between the two points previously selected. This profile shows a lack of material in the joint and it could be measured to understand how deep the mortar loss is. The intensity image (third from the left), shows mortar loss identified as a bright white line. Finally, the last image is what the Tunnel Viewer software presents to the user mortar loss in the tunnel wall after analysing the laser scanner data, represented by the green lines.

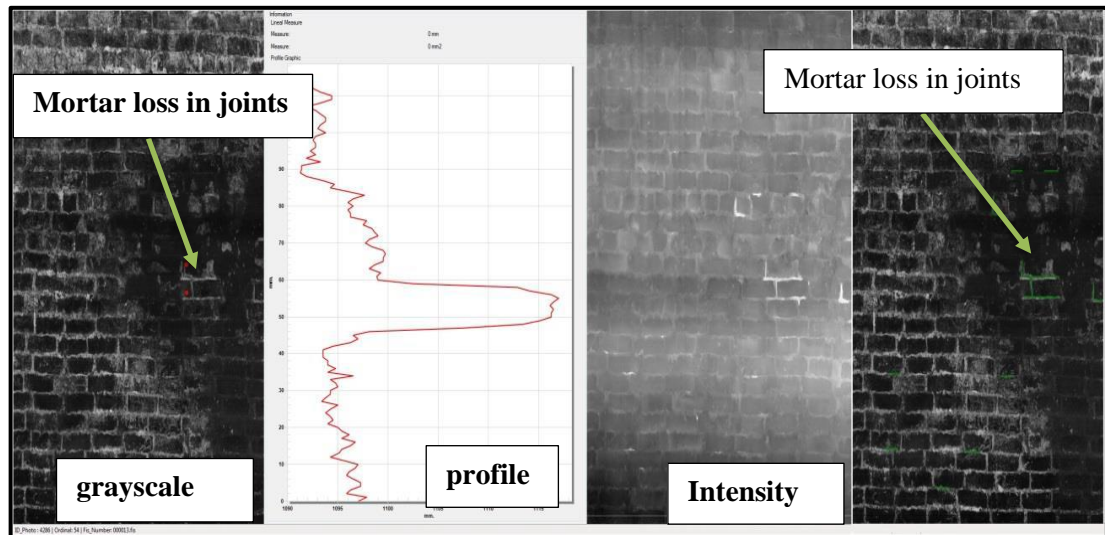


Figure 3-95 TL53 mortar loss in joints

To better analyse the results of mortar loss in brick joints, Figure 3-96 shows an enlarged image where the red points indicate the beginning and end of the evaluated profile. The brighter pixels on the depth image (right image) indicate the presence of the greater depth.

Figure 3-97 shows the profile from the points mentioned above. Here the mortar loss has a width of 5mm and a depth of 13mm.



Figure 3-96 Mortar loss in joints, (enlarged)

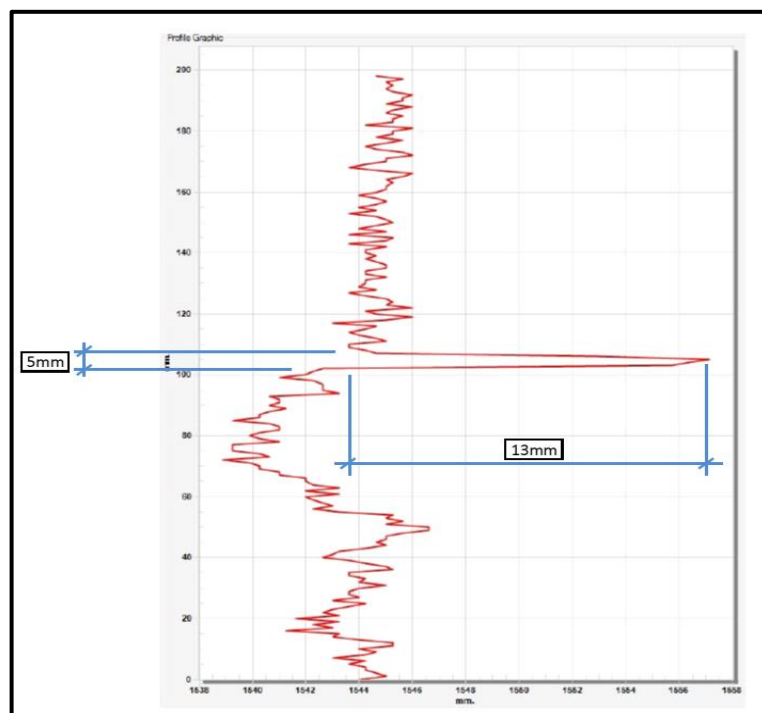
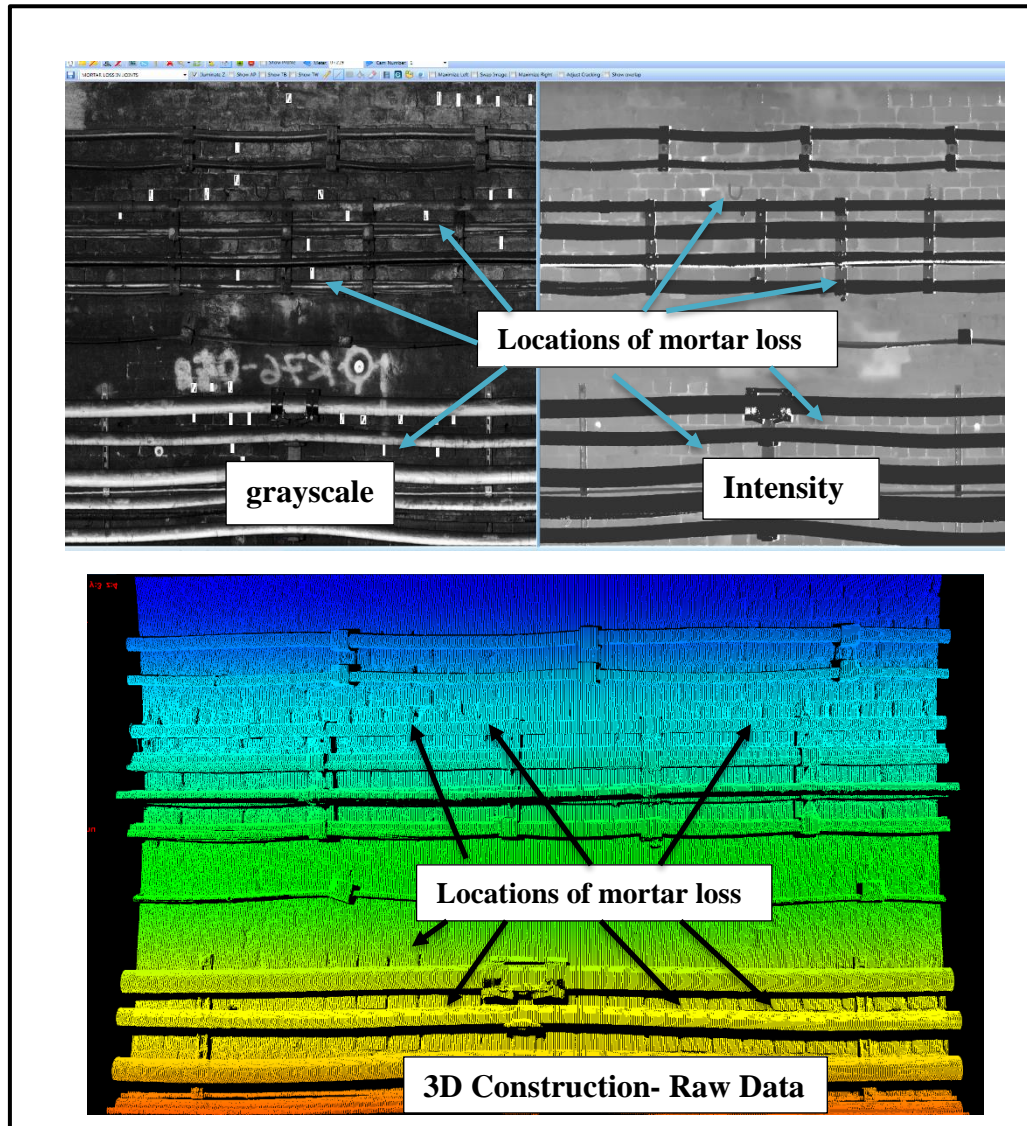


Figure 3-97 TL53 mortar loss in joints- profile

Figure 3-98 shows locations of mortar loss in joints at chainage 220 in the 2014 and the 2015 laser inspections. However, this defect did not appear in the Principal Inspection of 2013.



**Figure 3-98 TL 53 Locations of mortar loss in joints at chainage 220
2014 Laser inspection**

Table 3-38 shows the width and depth of mortar loss at chainage 220 in the 2015 laser inspection. Using different sizes of width and depth, trigger values could be assigned to mortar loss and optimise the remedial works for asset maintenance.

Table 3-38 TL53 width and depth of scattering mortar loss at chainage 220

List of Incidents - TL53_15							
	Section	Camera	Type of Incident	Width	Depth	Meter	CRACKING
Show	TL53	2	MORTAR LOSS IN JOINTS	41.00	34.00	220	
Show	TL53	2	MORTAR LOSS IN JOINTS	62.00	39.00	220	
Show	TL53	2	MORTAR LOSS IN JOINTS	25.00	34.00	220	
Show	TL53	2	MORTAR LOSS IN JOINTS	26.00	45.00	220	
Show	TL53	2	MORTAR LOSS IN JOINTS	66.00	38.00	220	
Show	TL53	2	MORTAR LOSS IN JOINTS	83.00	24.00	220	
Show	TL53	2	MORTAR LOSS IN JOINTS			220	
Show	TL53	2	MORTAR LOSS IN JOINTS	20.00	39.00	220	
Show	TL53	2	MORTAR LOSS IN JOINTS	46.00	21.00	220	
Show	TL53	2	MORTAR LOSS IN JOINTS	13.00	31.00	220	
Show	TL53	1	MORTAR LOSS IN JOINTS	47.00	49.00	220	
Show	TL53	1	MORTAR LOSS IN JOINTS	20.00	21.00	220	
Show	TL53	1	MORTAR LOSS IN JOINTS	41.00	41.00	220	
Show	TL53	1	MORTAR LOSS IN JOINTS	87.00	23.00	220	
Show	TL53	1	MORTAR LOSS IN JOINTS	17.00	26.00	220	
Show	TL53	1	MORTAR LOSS IN JOINTS	18.00	24.00	220	
Show	TL53	1	MORTAR LOSS IN JOINTS	35.00	47.00	220	
Show	TL53	8	MORTAR LOSS IN JOINTS	123.00	35.00	221	
Show	TL53	2	MORTAR LOSS IN JOINTS	17.00	27.00	221	

3.19.3 Face loss/ spalling

The laser survey identified spalling as a face loss. Figure 3-99 shows face loss at chainage 470 (south abutment from the West) which was identified by the laser survey in the 2015 inspection. This defect was not identified by the 2014 laser survey and last visual inspection.

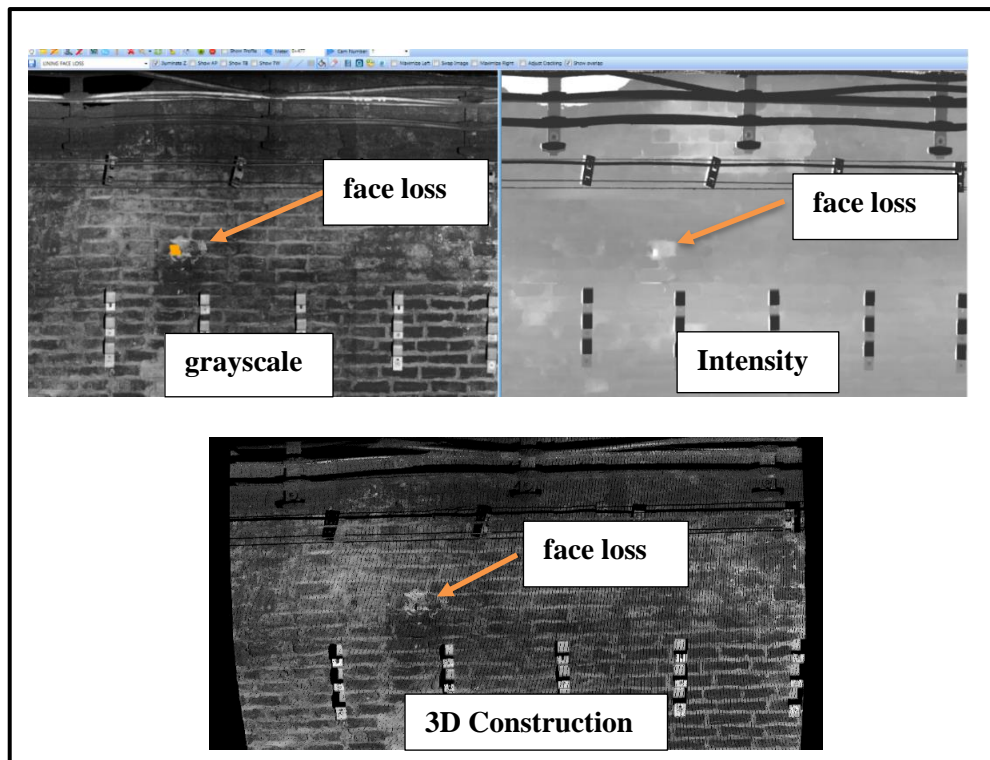
**Figure 3-99 TL53 face loss at chainage 470 2015 Laser survey**

Figure 3-100 shows same face loss was identified by the 2013 visual inspection as well.

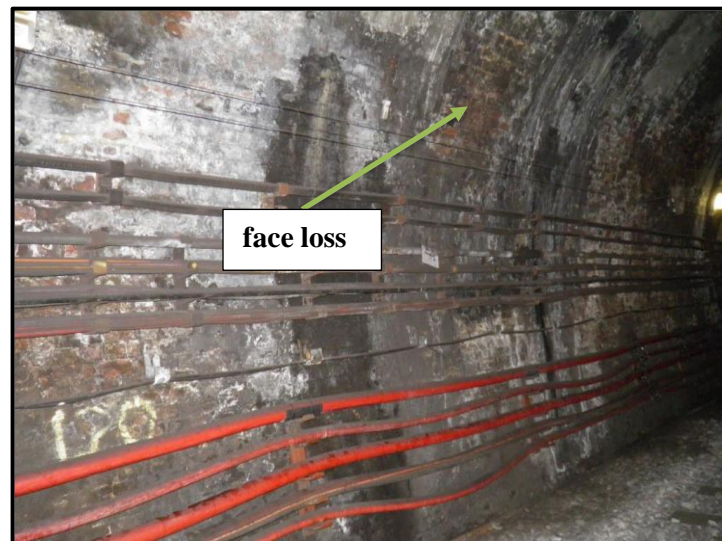


Figure 3-100 TL53 face loss at chainage 470 visual inspection

3.19.4 Damp patches

Figure 3-101 shows that the visual inspection identified an active water seepage, but this was difficult to locate in the picture apart from the water stain on the ballas and on the black pipe located where the tunnel wall meets the ballast. The seepage is located between chainage 95m and 100m in the west direction. Figure 3-102 shows that the laser inspection identified the same active water seepage as damp patches and in slightly different locations at the same chainage.



Figure 3-101 TL53 active water seepage at north abutment chainage between 95m and 100m West

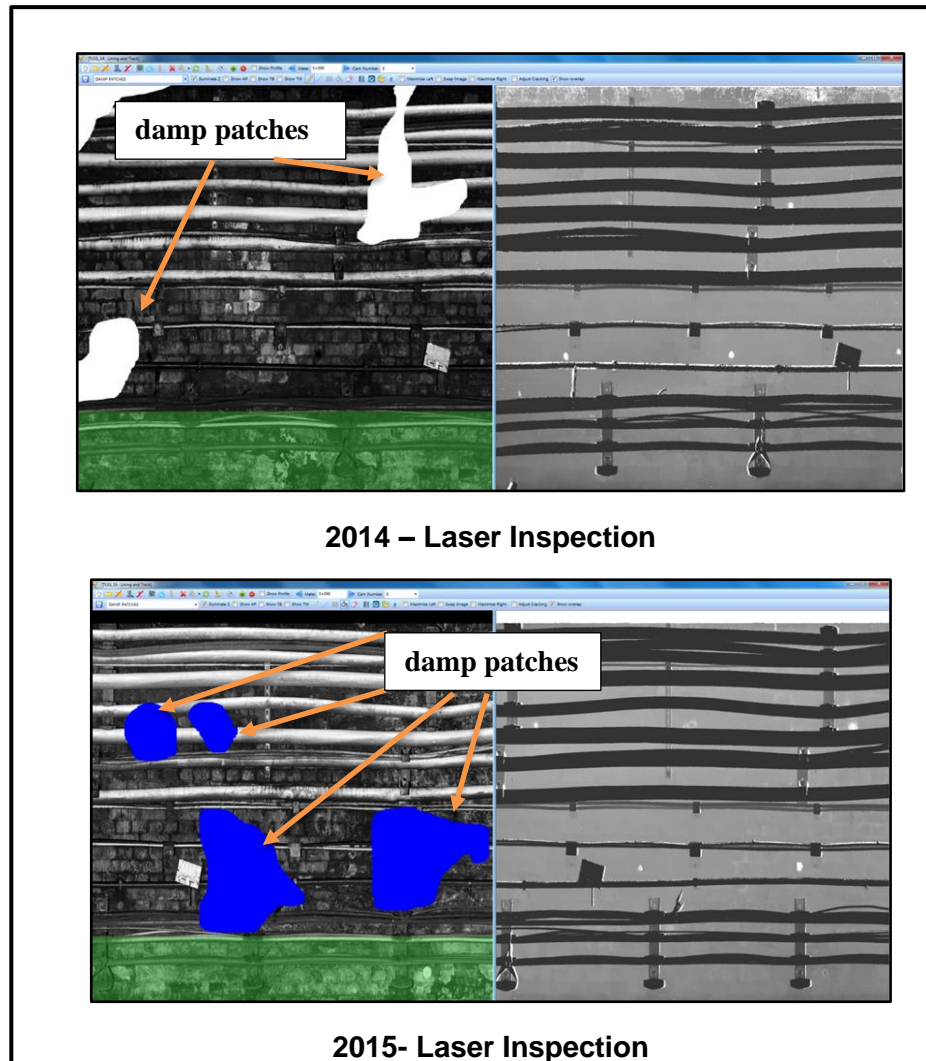


Figure 3-102 TL53 water seepage between chainage 95m and 100m

3.19.5 Repaired area

Repaired areas (see Figure 3-103) are regarded as areas which have undergone obvious repair work, either by replacing bricks or by applying a cement mortar layer. Although they have already been structurally taken care of, it could certainly be of interest to be able to compare this information with other maintenance data (e.g. time of repair, type of solution).

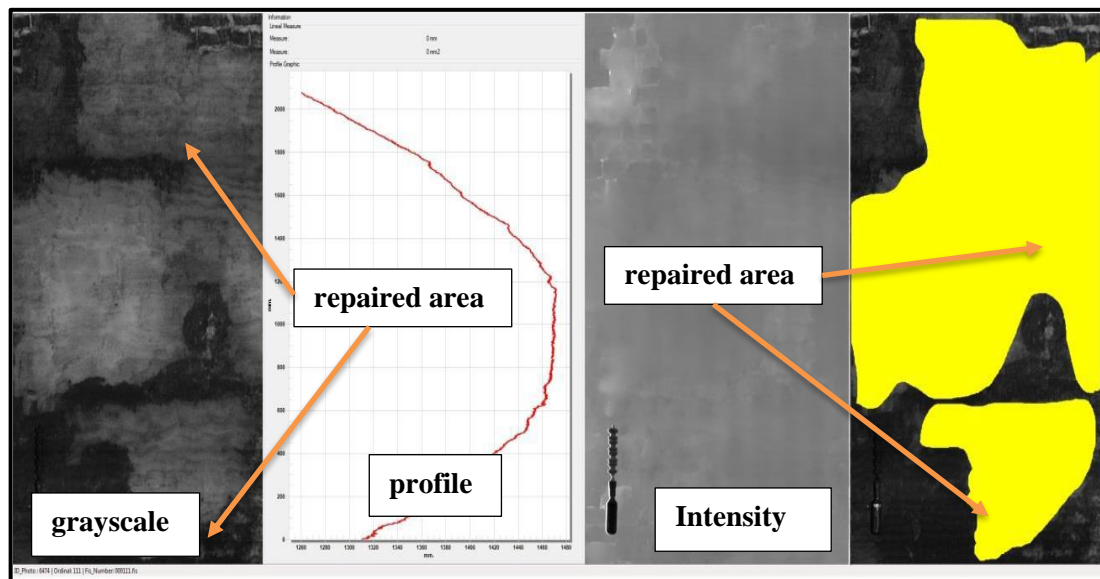


Figure 3-103 TL53 repaired area

3.20 TUNNEL 56

The 432m long tunnel TL56 consists of a brick arch of 6 rings. The tunnel is located between Edgware Road station and Paddington station and runs under the South Wharf Road.

Table 3-39 shows an overall comparison of the defects detected by the 2014 and 2015 laser inspections. The table shows that no cracking was found during the inspection interval and both inspection scores were A1. Joint loss has reduced from approximately 60.92m, occupying an area of 2.44m², to 40.09m within an area of 1.6m². This was confirmed by a completed works order, increasing the score from A4 to A2. The average face loss was reduced from 55.66% (2014) to 51.71% (2015), however, small incremental changes did not influence the extent and severity score of the face loss (A4). The total score of the tunnel section was improved from 75.00% to 84.38% due to the remedial works of the joint loss. The results of the number of brackets (4,181) and the number of deflector plates (50) are shown only for the 2015 inspection.

Table 3-39 TL56 Comparison of laser inspection scores between 2014 and 2015

TUNNEL TL56	2015 Inspection			2014 Inspection (Reference Scan)		
	Paddington - Edward Road					
	LENGTH TUNNEL (m)		435	LENGTH TUNNEL (m)		435
INCIDENT	LENGTH (m)	AREA (m2)	UNITS(u)	LENGTH (m)	AREA (m2)	UNITS(u)
Cracking	0			0		
Dampness		41.04			38.1	
Joint Loss	40.09	1.6		60.92	2.44	
Face Loss		0.58			0.09	
Brackets			4,181			
Deflector Plates			50			
2015 INSPECTION SCORES	INCIDENT	EXTENT (%)	CATEGORY	AVERAGED MEASURE	S	ITEM SCORE
	Cracking	0	A		1	8
	Dampness	0.57	A		1	8
	Joint Loss	0.02	A	34.4	4	4
	Face Loss	0.01	A	51.71	4	4
				TOTAL SCORE		75.00%
2014 (Reference) INSPECTION SCORES	INCIDENT	EXTENT (%)	CATEGORY	AVERAGED MEASURE	S	ITEM SCORE
	Cracking	0	A		1	8
	Dampness	0.51	A		1	8
	Joint Loss	0.03	A	23.52	2	7
	Face Loss	0	A	55.66	4	4
				TOTAL SCORE		84.38%

3.20.1 Seepage/ Damp patches

Figure 3-104 shows water seepage identified by the 2014 laser inspection. The same seepage was also identified on the visual inspection of 2011. However, seepage was identified in the 2015 laser inspection of the same area (see Figure 3-105). Furthermore, the 2015 inspection did not show any repaired areas in the same location. Therefore, this seepage may have been inactive during the 2015 scan, indicating that it may be weather-related.

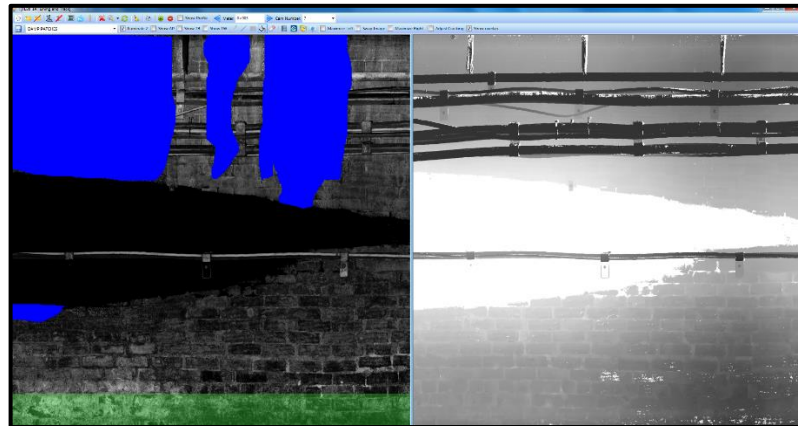


Figure 3-104 TL56 water seepage at 2014 scan

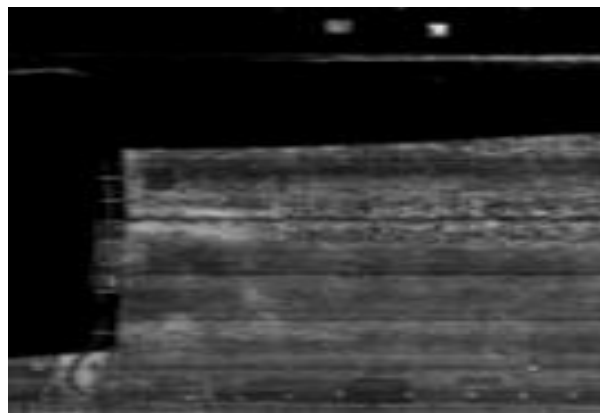


Figure 3-105 TL56 no water seepage at 2015 scan



Figure 3-106 TL56 visual inspection wet area
(LUL, 2011)

3.20.2 Mortar loss in Joint

Table 3-40 shows mortar loss in joints between chainage 98 and 100. Mortar loss in joints at chainage 100 were identified by the visual inspection also (see Figure 3-107, which was taken from the visual inspection report). However, in the 2015 inspection, this defect was not detected.

Table 3-40 TL56 Mortar loss in joints between chainage 98 and 100

TL56_15 - TL56_14	Meter	Type	TL56_15 Measure	TL56_15 Width	TL56_15 Depth	TL56_15 CRACKING	TL56_14 Measure	TL56_14 Width	TL56_14 Depth	TL56_14 CRACKING	Measure Difference	Width Difference	Depth Difference
Show	98	MORTAR LOSS IN JOINTS					0.053	9.69	17.85		0.053	9.69	17.85
Show	98	MORTAR LOSS IN JOINTS					0.081	16.83	26.11		0.081	16.83	26.11
Show	99	MORTAR LOSS IN JOINTS					0.054	15.84	23.26		0.054	15.84	23.26
Show	100	MORTAR LOSS IN JOINTS					0.066	18.20	9.50		0.066	18.20	9.50

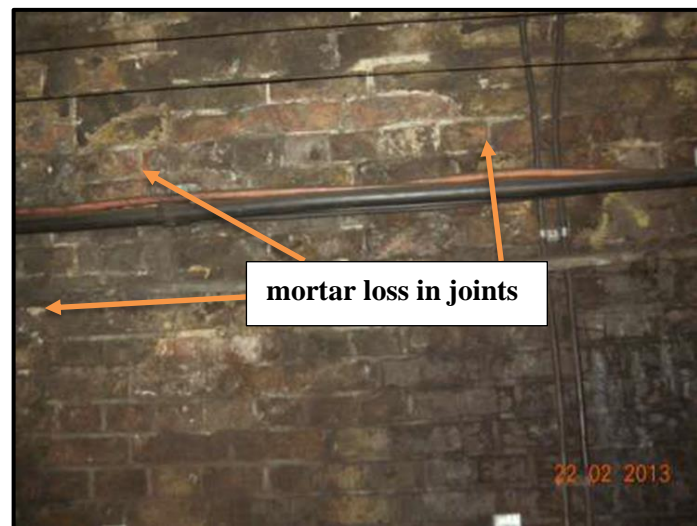


Figure 3-107 TL56 mortar loss in joints at chainage 100m south sidewall visual inspection, 2013

Figure 3-108 shows locations of mortar loss (shown by green dots) in joints at chainage 100 in the 2014 laser inspection.



**Figure 3-108 TL56 mortar loss in joints at chainage 100
2014 laser inspection**

3.21 Tunnel 72

Tunnel 72 is located between High Street Kensington and Notting hill stations. The 2014 laser inspection identified that 2.72m, corresponding to 4.72% of the tunnel, had cracks and this item scored 4. However, in the 2015 inspection, the system did not identify any cracking and the item score was raised from 4 to 8. Compared to the 2014 laser inspection, the 2015 laser inspection, decreased the face loss score by 1. The total score of the 2015 inspection is higher than the 2014 inspection due to the improvement seen in the tunnel (crack repair), whilst the other sub-scores were maintained (see Table 3-41).

Table 3-41 TL72 Comparison of laser inspection scores between 2014 and 2015

TUNNEL TL72	2015 Inspection			2014 Inspection (Reference Scan)		
	HS Kensington - Notting hill					
	LENGTH TUNNEL (m)	48		LENGTH TUNNEL (m)	48	
INCIDENT	LENGTH (m)	AREA (m2)	UNITS(u)	LENGTH (m)	AREA (m2)	UNITS(u)
Cracking	0			2.26		
Dampness		10.44			7.05	
Joint Loss	1.91	0.08		2.02	0.08	
Face Loss		0.11			0	
Brackets			1,045			
Deflector Plates			30			
2015 INSPECTION SCORES	INCIDENT	EXTENT (%)	CATEGORY	AVERAGED MEASURE	S	ITEM SCORE
	Cracking	0	A		1	8
	Dampness	1.32	A		1	8
	Joint Loss	0.01	A	22.15	2	7
	Face Loss	0.01	A	28.45	2	7
				TOTAL SCORE		93.75%
2014 (Reference) INSPECTION SCORES	INCIDENT	EXTENT (%)	CATEGORY	AVERAGED MEASURE	S	ITEM SCORE
	Cracking	4.72	A	19.25	4	4
	Dampness	0.95	A		1	8
	Joint Loss	0.01	A	16.18	2	7
	Face Loss	0	A		1	8
				TOTAL SCORE		84.38%

3.22 Ranges of Interpretative Variability for Each Inspection

Depth, width, area and location are the interpretative variables used to identify the defect's severity and extent. A laser survey can measure defect dimensions (width, depth and area) more accurately than a visual inspection because the "Laser Tunnel Scanning System" (LTTS) uses a laser profiler dimensions (laser footprint) of 428mm (h) x 265mm (l) x 139mm (w). Its laser point dimension can detect defects with a transversal resolution of 1mm and vertical accuracy of 0.5mm (Pavemetrics, 2014). Using this size of laser footprint can detect 1mm wide cracks. In a visual inspection, it is difficult to measure a 1mm defect size by using a tape measurement but it is even more difficult to detect them in a tunnel environment. Furthermore, a laser survey

can scan 5,000 transversal profiles per second and create a 3D model; by utilizing 3D models, defect locations can be detected more accurately than by the visual inspection.

3.23 Evaluation of Laser and Visual Inspection performance against requirements

Table 3-42 describes the requirements of a brick tunnel inspection (S1060) and evaluates each requirement against the laser inspection and the visual inspection performances.

Table 3-42 Inspections (laser vs visual) performance against requirements

Items	Requirements (S1060)	Laser Inspection		Visual Inspection	
		Satisfied (Y/N) N/A	Remarks N/A	Satisfied (Y/N) N/A	Remarks N/A
1	Physical information on assets to meet the requirements for ACAC & ACR	N	Computer vision algorithm that is currently used to identify defects automatically has to be developed further to report requirements of ACAC & ACR	Y	Information gathered by the inspector during his/her site visit
2	Review previous inspection reports/history and asset files before inspections	Y	Do not need to check reports by the inspector before the inspection because the system can be configured and can	Y	N/A

Items	Requirements (S1060)	Laser Inspection		Visual Inspection	
		Satisfied (Y/N) N/A	Remarks N/A	Satisfied (Y/N) N/A	Remarks N/A
			automatically check the previous condition of the tunnel		
3	Identify deterioration in the condition	Y	Compared to previous inspections and as-built information deterioration could be identified	Y	N/A
4	List any significant defects and compare with the last inspection	Y	Significant defects were listed. Does not detect all the defects listed in S1060	Y	N/A
5	Record the extent and severity of any defects	Y	The computer algorithm assigned values for the extent and severity. Insufficient data to validate with visual inspection. Must validate with visual inspection	Y	Inspector assigns extent and severity. Scores depend on ability of the inspector to interpret the data. Therefore, it is not repeatable

Items	Requirements (S1060)	Laser Inspection		Visual Inspection	
		Satisfied (Y/N) N/A	Remarks N/A	Satisfied (Y/N) N/A	Remarks N/A
6	Observe factors influencing the safety of the assets	Y	Decision-making algorithm has to be developed, to make sure the safety of the assets.	Y	N/A
7	Recommendations for maintenance or strengthening and renewal	Y	Using previous knowledge to develop the algorithm with trigger values.	Y	N/A
8	Reporting using appropriate Pro-forma	Y	Did not use the Pro-forma	Y	N/A
9	Qualification of the inspector	N/A	Based on LUL requirements Euroconsult's Computer engineers developed the software to identify defects automatically.	Y	N/A

Items	Requirements (S1060)	Laser Inspection		Visual Inspection	
		Satisfied (Y/N) N/A	Remarks N/A	Satisfied (Y/N) N/A	Remarks N/A
10	Defects noted shall be matched to standard severity photographs	N	Computer vision software has assigned severity scores based on trigger values and captured digital images.	Y	Photo taken by an inspector and match to standard severity photos, then assign severity scores for each defect.
11	Defect classification based on the standard defect classification table	Y	Computer vision software automatically identifies the defects, depends on what parameters are set as on a standard	Y	N/A
12	The scores less than B2 or an item score less than 6, defects in written narrative format	N	Laser survey did not mention any comments at the time. However, there is a potential for the "Tunnel Viewer" software to be changed to written narrative format	Y	N/A

Items	Requirements (S1060)	Laser Inspection		Visual Inspection	
		Satisfied (Y/N) N/A	Remarks N/A	Satisfied (Y/N) N/A	Remarks N/A
13	General photograph of the structure/ defects photographs	Y	Laser system captures whole structure of as digital images	Y	N/A
14	Condition score- a lowest element of the structure Scoring system follows standard S1060	N potential to be "Y"	Currently, applied average method. In the future would have to do according to the standard or more suitable way by changing the algorithm in the software. Currently, LUL appointed the committee to identify suitable scoring system	Y	N/A
15	Identify type and location of the defects before the inspection	Y	The system can be scanned the whole tunnel. Therefore, no need for previous information before the inspection	Y	N/A

Items	Requirements (S1060)	Laser Inspection		Visual Inspection	
		Satisfied (Y/N) N/A	Remarks N/A	Satisfied (Y/N) N/A	Remarks N/A
16	Perform risk assessment associated with inspection	N	Risk assessment has to be performed by the inspector and provide information to plant approval person.	Y	N/A
17	Identify defects to the superstructure and substructure brick tunnels/covered-way	Y		Y	
	• bulging	Y	Shape of the tunnel can be compared with as-built survey. A small deviation can be detected.	Y	N/A
	• drummy	N	Limitation of laser survey does not detect.	Y	N/A
	• efflorescence	N	Not a scorable defect in the inspection standard. However, using laser	Y	N/A

Items	Requirements (S1060)	Laser Inspection		Visual Inspection	
		Satisfied (Y/N) N/A	Remarks N/A	Satisfied (Y/N) N/A	Remarks N/A
			images, defect can be identified		
	• joint loss	Y	All dimensions measured width, length and depth	Y	N/A
	• leached deposits	N	Not a scorable defect in the inspection standard. However, using laser image, defect can be identified	Y	N/A
	• erosion, depth of erosion (millimetres)	N	Not a scoreable defect in the inspection standard. However, using laser image, defect can be identified	Y	N/A
	• missing brickwork	Y	Embedded on tunnel lining, given the sizes of bricks there is a potential to separate the missing brickwork	Y	N/A

Items	Requirements (S1060)	Laser Inspection		Visual Inspection	
		Satisfied (Y/N) N/A	Remarks N/A	Satisfied (Y/N) N/A	Remarks N/A
	• repairs	Y	Detects repairs in only certain categories such as mortar loss in joints and face loss/spalling	Y	N/A
	• spalling and depth (millimeters)	Y	Embedded on tunnel lining, given the sizes of bricks there is a potential to separate the spalling.	Y	N/A
	• surface deposits	N	Not a scoreable defect in the inspection standard. However, using laser images, a defect can be identified.	Y	N/A
	• vegetation	N	Not a scoreable defect in the inspection standard. However, using laser image, defect can be identified	Y	N/A

Items	Requirements (S1060)	Laser Inspection		Visual Inspection	
		Satisfied (Y/N) N/A	Remarks N/A	Satisfied (Y/N) N/A	Remarks N/A
	• wet or damp areas	Y	N/A	Y	N/A
	• active water seepage	Y	Has to be compared with a different epoch of scans in order to identify active water seepage.	Y	N/A
	• fractures and cracks:	Y	Only classified as crack. Can be further divided into the fractures. (based on width and depth)	Y	N/A
	• hairline or dimension	N	Only classified as a crack. Can be further divided into hairline (based on width and depth)	Y	N/A
	• deformation of tunnel portals and parapets	N	Can be inspected by using a static laser survey	Y	Using severity photos inspector can detect deformation

Items	Requirements (S1060)	Laser Inspection		Visual Inspection	
		Satisfied (Y/N) N/A	Remarks N/A	Satisfied (Y/N) N/A	Remarks N/A
19	Check defect interface between different structures (e.g., pipe crossings, girdering)	Y	Line of sight is important to identify defects	Y	N/A
20	Producing inspection report using the following supporting materials				N/A
	• defects' photographs	N	All defects related to change in geometry are quantified	Y	N/A
	• defects' locations	Y	N/A	Y	N/A
	• tunnel chart	Y	N/A	Y	N/A
21	Follow standards inspection chart,	N	The programme generates a tunnel chart in a slightly	Y	N/A

Items	Requirements (S1060)	Laser Inspection		Visual Inspection	
		Satisfied (Y/N) N/A	Remarks N/A	Satisfied (Y/N) N/A	Remarks N/A
	forms F2353 and F2354		different format than F2353 and F2354		

Euroconsult's laser scanning system has to include all the requirement's mentioned in the table for the next inspection.

3.24 Requirements for Replacing Existing Methodology

3.24.1 Organisational Change Processes

Data collection, analysis, and presentation are important elements in the process of change. In order to implement new technology, end-users (e.g. inspectors, night inspectors, inspection review engineers, inspection managers, maintenance managers, maintenance contractors, asset managers and head of professionals) who are involved in the programming have to understand and have confidence in its value. Changing the process involves project planning, implementing software and installing new computer networks; overall, the decisions and actions designed to help employees embrace new methodology, technology and ways of working.

3.24.2 Changes to Standards

London Underground has been performing visual/manual inspections since 1930 as a means of managing its aging infrastructure. The high-resolution laser survey that was conducted by Euroconsult is based on the inspection standard S1060. This standard was last reviewed by LUL in April 2014 and provides instructions and requirements (see section 3.3 for requirements) to perform visual/manual inspections of bridges and structures.

After reviewing the high-definition laser survey inspection report, the following revisions might be required to the existing standard S1060:

- The threshold value for severity rating of defects is important to rate a tunnel section and determine the overall condition of a tunnel. Currently, this value is not included in the standard.
- The inspection of some assets' categories mentioned in the standard could not be automated due to their location, construction methods and materials. Therefore, asset types for automated inspection have to be defined.
- Inspection frequency and associated reporting format must be redesigned if new inspection technologies are to be used.

- Amend or replace the examples of 'Standard severity photographs', used to categorise defects, because the laser survey with high-resolution cameras can capture pictures that can detect defects specified much earlier in the standard (1mm width of cracks can be shown in the photograph).
- Defined new scoring methods to assign condition scores to assets. Currently, the Condition Score is the lowest element rating contained in the structure and is derived from the scoring system mentioned in section 3.10.1.
- Set up the new accuracy levels to detect defects.

3.24.3 IM Support and Resources Needed

Euroconsult's data analysis software is currently available only on a few laptops due to access restrictions to the installation of the software on TfL's I.T network system. LUL's inspection/maintenance team requires high-performance I.T equipment to use high volumes of image data. In addition, inspectors/engineers need the training to use the software and create principal inspection reports using the laser survey report.

3.25 Advantage and Limitation of Technology

The following advantages and limitations were identified when using Euroconsult's high-definition laser scanner.

3.25.1 Advantages

The significant advantages in using this system are:

- Reduction in the amount of time inspectors spend on-site for inspection.
- Eliminates manual handling and working at heights in the tunnels, thereby reducing risks.
- Obtains defects to an accuracy of 1mm (e.g. crack width 1mm).

Using this technology, substantial parts of the asset can be inspected within a short period when compared to visual inspection. The system can be used for any size and any operating condition of the tunnel/covered way (small diameter, lengthy network and adverse operating conditions such as in dark and noisy environments). In addition, the system can be used rapidly and easily, it can be mounted on a flat wagon and pulled by a locomotive. With a proper configuration (switching off the scan at the station platform to avoid harmful laser effects to passengers), the scan can potentially be pulled by a commuter train without waiting for engineering hours.

All the analysed defect data are stored in a database that can be used for the prediction of asset conditions. Using software analysis, statistical data can be extracted and displayed for the inspected tunnel as a whole or in individual sections or assets. This can be subsequently used to draw conclusions about the overall condition of the tunnel. Results can be shown in a graphic form or as reports in various formats.

Figure 3-109 shows different defect types, such as lining face loss, mortar loss in joints, damp patches and cracking, along scan direction of the D086/TL26 tunnel. The X-axis is in m and the Y-axis the area and length of the defects.

The laser survey can significantly reduce the amount of time spent by inspectors to walk along the track to identify the defects on assets. Using a tunnel chart and grayscale images (that are produced by the software) an inspector can be directed to the area of interest for further clarification of defects. The defects reports can store all the data for future analysis and comparison of different scans to predict the rate of deterioration of the asset. Comparison of different scan data can facilitate the asset manager in forecasting resource requirements for inspection and remedial work regime and an asset's physical and functional condition can also be determined more frequently. Therefore, risk can be managed effectively and efficiently minimize service loss (loss of customer hours) and improve passenger safety, reliability

and performance. Falling bricks from the tunnel lining can be predicted using mortar/joint loss information which are collected by the laser survey.

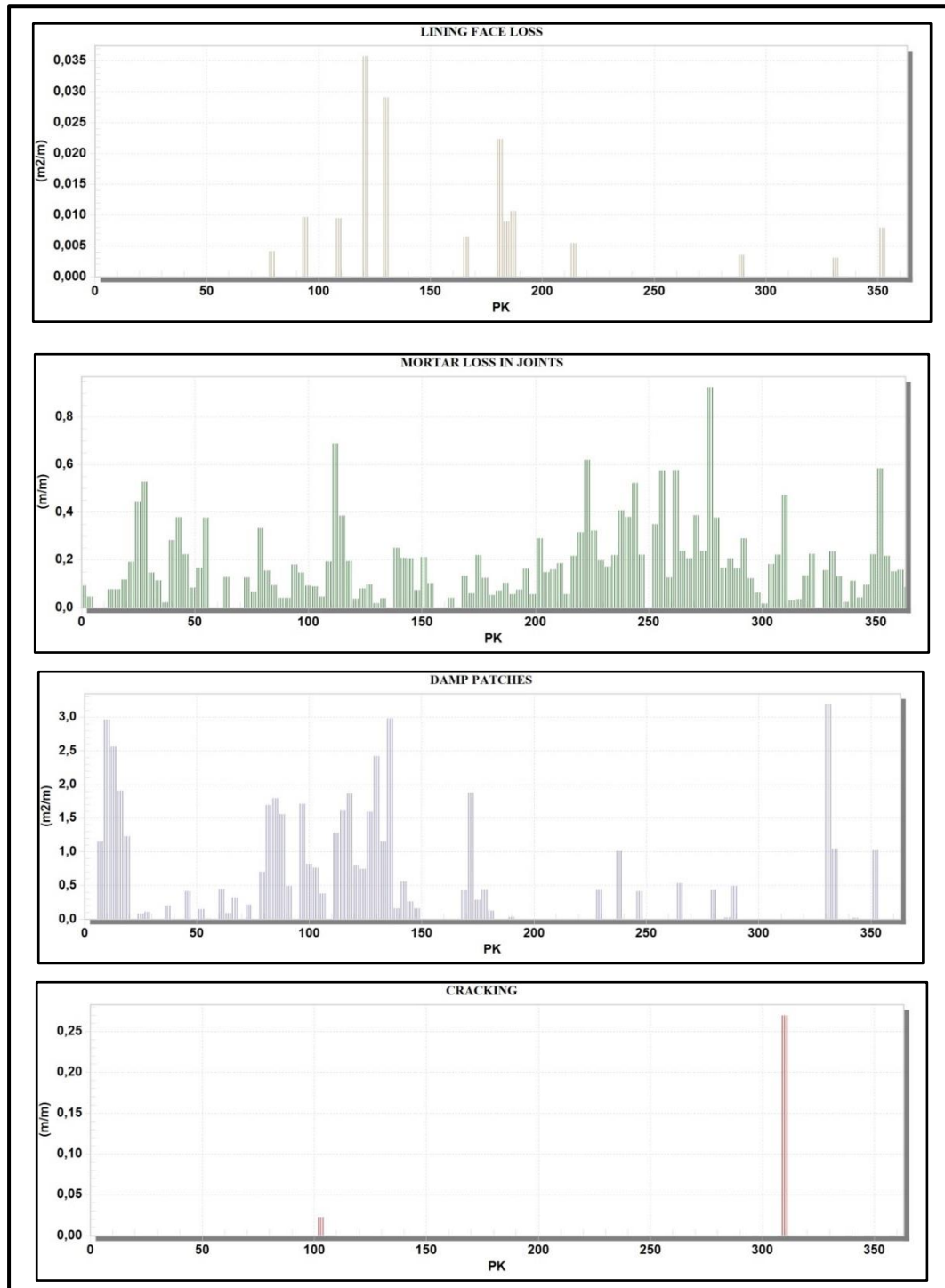


Figure 3-109 Defects along tunnel 26

3.25.2 Limitations

Compared to a visual inspection, the laser survey requires a significant amount of time to process the raw data (extract the defect information from the point cloud data) to produce an inspection report. The amount of time required processing raw data depends on the level of detail of the defect expected by the end-user, as well as the size of point clouds used. For data processing and producing inspection reports, LU relies on Euroconsult's engineers input because they use the in-house computer vision software.

The laser scanner system does not measure the drumminess (loose bricks in the subsurface) of the tunnel lining or drumminess of a covered way surface. The drumminess has to be determined by using a hammering test during the visual inspection.

In the laser scanner report, the reporting of the scores is based on the identification of the defects by the computer vision software algorithms. During the brick tunnel surveys, the software only identified major defects mentioned in Figure 3-27. Laser survey data were acquired in a kinematic mode and the laser was configured to point towards the tunnel surface, therefore the system does not report other problems that would be identified by an inspector, such as headwalls' details. Sometimes, this limitation will degrade the overall element rating score of a particular asset, because the number of the item score in equation (3-11) will be lower than the visual inspection.

The scan identifies and assigns severity and extent scores for cracks based on depth and width of the crack. However, the system does not further classify cracks into fractures and hairlines. If fractures and hairlines occur in joints, they have to be measured precisely (length, width and depth) to predict their consequences the structure and on the development of other defects, such as seepage.

The system can identify areas of dampness but is unable to determine whether it is inactive. Severity scores for damp patches are not provided on the 'list of incidents' (one of the outputs generated by the software) table, as this only

provides the extent (%) of the damp patches. However, a visual inspection can capture all the defects in detail, mentioned in the engineering standard S1060.

3.26 Integration of Different Technologies with Laser Survey

Integration of Thermography and laser surveys could significantly improve the identification of various defects (crack detection, water intrusions, moisture and warm anomalies) currently faced by LUL assets. Figure 3-110 shows the integration of thermography with the laser digital image (extracted from point cloud data) and can be used to identify the root cause (surface crack causing water ingress) of a seepage problem.

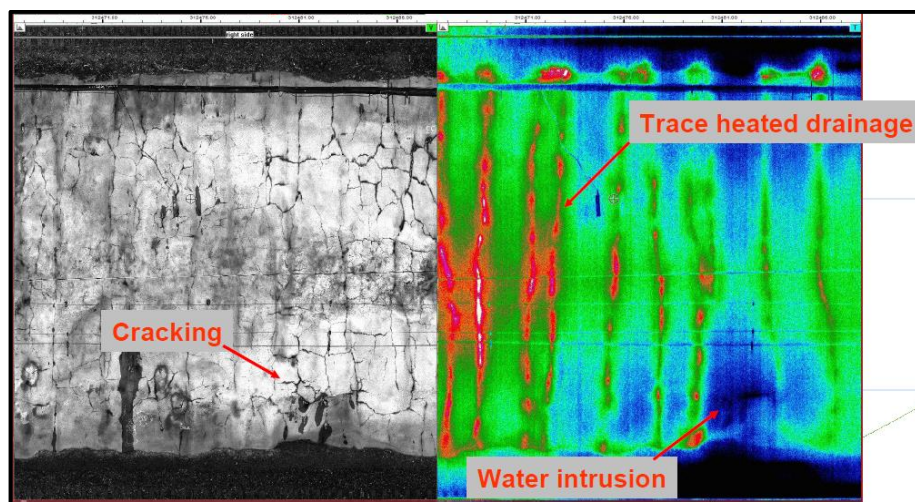


Figure 3-110 Visual Image and Thermal Image can be viewed in parallel (space tech)

To close the gap between the laser survey and visual inspection, laser surveys would have to be performed every year in brick tunnels (compared to cast iron tunnels, brick tunnels deteriorate faster) and compare the changes in assets with the previous scans. Tomography/ultrasound technology has the potential to be used in tunnel inspections to detect subsurface defects such as drumminess and voids. Therefore, this technology should be investigated in the future.

Each technology has some advantage over the others; therefore, the user requirements play a significant role in selecting the most suitable inspection system.

3.27 Conclusions

This chapter focused on Euroconsult's first and second laser inspections on the sub surface line tunnels. During this case study, laser surveys of brick tunnels and covered-ways (only in the first inspection), as well as Principal Inspection reports' scores were compared. Initial assessment of performance and limitations of both systems were compared against the case studies. Each method has some advantages over the other. For this reason, user requirements play a significant role in the selection of the right technique to perform an inspection.

- Figure 3-29 shows that the majority (102 out of 112) of the assets have less than 20% difference between the two inspection methods. However, this comparison is not ideal to assess the performance of both systems. Figure 3-29 shows that direct comparison of laser inspection against visual inspection of assets is inappropriate because the laser inspection does not capture all the parameters mentioned in the Engineering Standard S1060. Therefore, further analyses were performed to focus only on defects (mortar loss in joints, cracking, lining face loss and dampness) captured by the laser and visual inspection. The results showed that the Euroconsult system surpasses expectations at measuring mortar loss, cracking and lining face all defects based in geometrical changes.
- A comparison of the overall ratings between the 2014 and the 2015 Euroconsult's laser inspection on 72 tunnels sections showed that the majority of the overall scores of the 2015 inspection decreased in most of the tunnel sections. The analysis showed that water seepage/damp patches did not influence a decrease in overall scores in the 2015 inspection. However, Figure 3-74 and Figure 3-75 indicate that newly appeared joint loss and face-loss have significantly influenced the decrease in the overall rating of most of the tunnel sections in the 2015 laser inspection.

- Wet and damp areas can be identified using laser surveys of dampness, but they do not show the severity (e.g. active or inactive). Therefore, integration of thermography, moisture sensors (to be addressed in Chapter 4) and laser surveys could significantly improve the identification of active seepage and water path detection in brick tunnels.
- The laser survey system still requires manual intervention to complete the visual inspection report. Therefore, the laser inspection and the visual inspection methods are not mutually exclusive. The laser inspection system needs to be further developed to interpret/report the data automatically and satisfy all the requirements mentioned in the Engineering standard S1060.

Chapter 4. APPLICATION OF INFRARED THERMOGRAPHY

4.1 Introduction

This chapter describes the background information to thermography and its application to the detection of moisture on a brick tunnel surveyed during the execution of research work.

The first half of this chapter describes two laboratory tests that were performed to calibrate the application of thermography, using relative humidity and temperature sensors to detect water seepage inside of the wall, and a handheld relative humidity, moisture sensor and temperature to test the surface of the materials.

The second half describes the site trial that was performed on the Sub-Surface Lines of London Underground tunnels to detect water seepage using the thermal camera. This section considers the application of thermography in an underground tunnelling environment to identify seepage in a larger area effectively and efficiently with, minimum resources.

4.2 Literature Review

4.2.1 Fundamentals of Infrared Thermography

Infrared thermography is a method which detects infrared energy emitted from object converts it to temperature and displays image of temperature distribution. It has been applied to diagnose defects in buildings in the early 20th century and in the beginning, video recording was used for storing the infrared images and for visual analysis (Sham, 2008). Towards the end of the 20th century (mid-1950), with the rapid improvements in technology, infrared signals were digitised and stored on a computer for future analysis. A major achievement has been the development of an infrared camera with higher sensitivity and higher capturing frequency, where a small deviation of the temperature field of an object can be recorded and analysed (Sham, 2008).

Due to its non-destructive nature, using IR thermography to detect the presence of excessive moisture can be valuable.

Infrared energy is part of the electromagnetic spectrum and behaves similarly to visible light (Barreira *et al.*, 2012). It travels through space at the speed of light and can be reflected, refracted, absorbed, and emitted. The wavelength (λ) of infrared energy is about an order of magnitude longer than visible light, between 0.7 and 1000 μm as can be seen on Figure 4-1 (Barreira *et al.*, 2012).

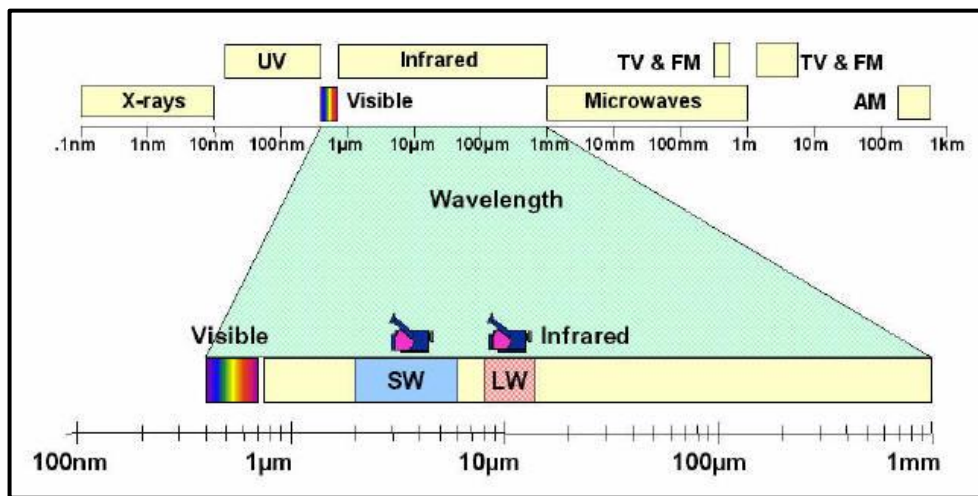


Figure 4-1 Electromagnetic Spectrum (Barreira *et al.* 2012)

The infrared part of the electromagnetic spectrum covers the range from roughly 0.75 μm to 1000 μm . It can be divided into three parts: far-infrared, from 1000 μm to 20 μm , mid-infrared, from 20 μm to 1.5 μm and near-infrared, from 1.5 μm to 0.75 μm (Barreira *et al.*, 2012).

Radiation is a function of an object's surface temperature, which makes it possible for the camera to calculate and display the temperature. The radiation measured by the camera does not depend only on the object's surface temperature but is also a function of the constant emissivity. Emissivity is a measure of the efficiency of a surface to act as a radiator (Barreira *et al.*, 2012). In general, concrete has a relatively high emissivity, between 0.9 and 1.0 and, it is a good emitter relative to other materials such as metals (Barreira *et al.*, 2012). **Error! Reference source not found.** shows emissivity value for different materials.

Table 4-1 Emissivity Values of Materials
<http://www.infrared-thermography.com/material>

Material	Wavelength (μm)	Emissivity
Aluminium: anodized		0.77
Aluminium: anodized sheet, chromic acid process		0.55
Aluminium: disk, roughened	3	0.275
Aluminium: foil	3	0.09
Aluminium: heavily weathered	2-5.6	0.83-0.94
Brick: alumina	2-5.6	0.68
Brick: common	2-5.6	0.81-0.86
Brick: common, red		0.93
Brick: facing, red	2-5.9	0.92
Brick: facing, yellow	2-5.6	0.72
Brick: fireclay		0.85
Brick: fireclay		0.75
Brick: fireclay		0.59
Brick: masonry	5	0.94
Brick: red		0.90
Brick: waterproof	2- 5.6	0.87
Chromium: polished	8-14	0.1
Concrete		0.92
Concrete: dry	5	0.95
Concrete: rough	2- 5.6	0.92- 0.97
Cement	8-14	0.54
Mortar	2-5.6	0.87
Mortar: dry	5	0.94
Iron, cast, casting	8-14	0.81
Iron, cast, casing	8-14	0.81
Iron: cast, oxidized		0.64
Iron: hot rolled	8-14	0.77
Iron: oxidized	8-14	0.74
Iron: sheet, galvanized, burnished	8-14	0.23
Iron: sheet, galvanized, oxidized	8-14	0.28
Iron: sheet, heavily rusted		0.69

The equation for the radiation of an object is expressed according to the Stefan–Boltzmann law, as given below (Washer *et al*, 2009).;

$$E = \epsilon \sigma T^4 \quad (4.1)$$

where E is the radiation (W/m^2)

ϵ is the emissivity

σ is the Stefan–Boltzmann constant ($5.67 \times 10^{-8} \text{ W/m}^2 \text{ K}^4$)

T is the temperature (K)

As shown in this equation, the radiant energy, emitted from a material, is proportional to emissivity and the fourth power of its temperature, such that small variations in temperature will result in large changes in the radiant energy (Washer *et al*, 2009).

Potential problems can occur when the object reflects radiation originating from the surroundings. Atmospheric absorption of radiation will also affect the measured temperature (Washer *et al*, 2009).

There are three methods of heat transfer conduction, convection and radiation. An infrared camera is able to record the amount of radiated, reflected and emitted heat from an object. The rate of heat transfer through an object, which is dominated by convection and conduction depends on the object's material, determines how much energy can be radiated at the surface. One of the most important factors of each material, when talking about heat transfer, is the heat capacity of the material (Clark, 2003).

4.2.2 Active and Passive Thermography

According to Sham 2008, infrared thermography can be divided into two categories: active and passive. The active technique uses an external heat source to excite the object to be analysed and the analysis is concentrated on the loss or gain of heat by the object. The passive technique measures the

energy radiated by a mass without interfering with the stored energy (Sham, 2008).

4.2.2.1 Active Thermography (AT)

According to Sham (2009), active thermography can be classified into simple and complex active thermography. The simple one applies heat and only identifies temperature differences on the tested object for detection of anomalies. Complex active thermography includes the considerations of time, intensities and sequential recordings of temperature change. Complex active thermography enables further processing and hence additional information such as the depth of defects can be determined (Sham, 2009).

Traditionally, there are two basic methods of complex AT. They are Lock-in Thermography (LT) and Pulsed Thermography (PuIT) (Sham, 2008). PuIT with longer pulse lengths (\approx minutes to hours) are called step thermography (ST) and shorter duration of the heat pulse (\approx 2.5ms) is called flash thermography (FT). It is a qualitative IR technique and heat is measured in its transient state. It can provide the quickest and the most repeatable data in testing.

The other type of complex AT is lock-in thermography (LT) (Sham, 2009). Different from pulsed thermography, it employs sinusoidal heat stress to the test object and additional information such as depth and type of defects can be determined by carrying out further analysis on the thermal data. Heat is measured at its steady state in this complex AT (Sham, 2009). Besides the above-introduced heat source, there are a wide range of stimuli available for stressing the test object, such as sonic, pressure, microwaves, induction heating, current and laser. Different kinds of stressors should be selected depending on the thermal properties of the tested objects (Sham, 2009).

4.2.2.2 Passive Thermography

Passive thermography is the most commonly applied technique for investigation of building envelopes, such as walls and roofs (Titman, 2001). It is a valuable tool for inspecting building elements and detection of energy leakage on building envelopes.

Performance of building installations such as heating, ventilating and air conditioning can be assessed by passive thermography (Sham, 2009).

Passive thermography has become a commonly applied technique for water seepage analysis in building structures. It has been introduced and widely used for water seepage detection on building structures as presented in previous research by Avdelidis, Moropoulou and Theoulakis (2003); Ljungberg (1995); Chields, Courville and Chields (1983); Busher, Wild and Wiggenghauser (1999) and Grinzato and Mazzoldi (1991). It has also been applied in moisture measurements of roof structures (Jenkinns, Knab and Mathey 1982). Passive thermography is based on the principle of temperature differences arising between wet and dry surfaces on the inspected sample. The moist concrete will have a lower temperature than dry concrete due to its higher latent heat (Ludwig and Rosina 1997).

4.2.3 Detection of Moisture by Infrared Thermography

In the building and construction sector, infrared (IR) thermography is one of the non-destructive examination (NDE) techniques that is used to detect thermal irregularities and air infiltration problems of a building's envelope, moisture and delamination problems (Balaras and Argiriou, 2002).

Infrared thermal imaging is a more versatile tool (it can be used to scan larger areas in a short time) for *in-situ* moisture detection. It can be used to scan a surface to determine irregular thermal patterns and thermal anomalies (Kominsky *et al*, 2010).

Areas of high-moisture content appear either warmer or colder than the surrounding infrastructure. The difference in temperature can be imaged and

measured using an infrared camera; the recorded visual image is a thermogram or a thermal scan.

In the detection of moisture within a system, there are generally two different driving forces that create observable surface temperature differences, which are:

- (i) evaporative cooling
- (ii) higher thermal inertia of water versus the building materials' thermal behaviour (Rosina and Ludwig, 1999), in other words, increased heat capacity of moist material.

Evaporation depends on the relative humidity and temperature of air near the object's surface, water content, physical characteristics of the object, and soluble salt content. Surface cooling occurs in moist areas due to the endothermic nature of evaporation (Rosina and Ludwig, 1999; Barreira and de Freitas, 2007). When soluble salts are present in the material, the evaporation rate decreases and therefore the decrease in surface temperature and the temperature difference between moist and dry zones becomes less significant (Matias *et al.*, 2008; Rosina & Ludwig, 1999). High relative humidity of the air, e.g. more than 80%, also prevents evaporation and temperature differences between moist and dry areas due to surface cooling and becomes less significant (Rosina *et al.*, 1998).

The cause of moisture penetration, in most cases, can be found in the construction components that are in contact with the ground, where moisture is absorbed and distributed over the entire masonry by capillary action. Here, the moisture is the catalyst for most building damage whether the processes are biological, chemical or physical (Frossel, 2006).

The passive thermography technique was used in experiment #1 and 2 to identify moisture on test walls and water seepage on the tunnel lining.

4.3 Laboratory Testing

Thermography lab tests were performed before the site trial on an LUL sub-surface line to establish the relationship between moisture and temperature measurements. Furthermore, these tests evaluated the performance and reliability of the camera to identify water ingress in the control environment. In addition, the lab test was used to establish data acquisition and data processing methodology for the site trial. Then, the thermal camera was used on the site in an uncontrolled environment.

The objectives of these experiments include using infrared thermography and humidity/temperature sensors to locate areas of probable moisture anomalies in the test wall. A wall, made of mortar and old bricks (taken from old structures), initially prepared and used in research on the effects of moisture in old structures was made available for testing. The wall was 1m in height and 0.5m in width.

4.3.1 Sensors Calibration

The sensors used in this experiment were known as the Chipcap 2 low-cost humidity and temperature sensor. According to Chipcap2 manufacturer's recommendation "within the normal range, ChipCap 2 performs in a stable manner. Prolonged exposures to conditions outside the normal range, especially at humidity over 90% RH, may temporarily offset the RH signal by up to $\pm 3\%$ RH. When conditions return to the normal range, the sensor will gradually recover back to the calibration state".

Applying the calibration equation increases the absolute accuracy of the humidity and temperature measurements, therefore sensors were calibrated using different salt solutions to represent different %RH values. Table 4-2 shows the performance of Chipcap 2 to relative humidity.

Table 4-2 Sensor performance Relative Humidity (RH %)
(Chipcap 2 application guide)

Resolution	14 bit (0.01%RH)
Accuracy	±2.0%RH (20~80%RH) (Accuracies measured at 25°C, 5.0V) (Custom accuracy tolerance available.)
Repeatability	±0.2%RH
Hysteresis	±2.0%RH
Linearity	<2.0%RH
Response Time	7.0 sec (τ 63%) (Measured at 25°C, 1 m/sec airflow for achieving 63% of step from 33%RH to 90%RH)
Temperature Coefficient	Max 0.13%RH/°C (at 10~60°C, 10~90%RH)
Operating Range	0 ~ 100%RH (Non-Condensing)
Long Term Drift	<0.5%RH/yr (Normal condition)

4.3.2 Humidity Sensor Calibration

The humidity sensors were first calibrated in the laboratory, by measuring the response time and the sensor response to various humidity conditions. To reduce a potential difference in the relative calibration between the six sensors, all six sensors were calibrated together at the same time and in the same environment.

Humidity sensors (H1, H2, H3, H4, H5 and H6) were calibrated using different saturated salt solutions such as sodium chloride, sodium bromide and potassium sulphate prior to the wall experiment. These salts provide different humidity values for different temperature ranges and were recommended by the sensor manufacturer for calibration.

All six sensors were inserted into a jar which was made airtight with a split rubber bung. These sensors were connected to the data logger and Triax data recording software. Sensors were left overnight to reach a stable reading (equilibrium).

Humidity and temperature were recorded separately for each saturated salt solution for each sensor. Using Table 4-3 the humidity for each salt solution was interpolated between the temperature 20 °C and 25 °C because these are the measured temperature ranges. Compared to potassium sulphate and

sodium chloride, sodium bromide gave a larger variation of relative humidity (2.5%) between the temperatures of 20 °C and 25 °C.

Table 4-3 Relative humidity above saturated salt solutions at various temperatures (<http://www.robertharrison.org/icarus>)

Salt/Temperature (C)	5.0	10.0	15.0	20.0	25.0
Sodium bromide	63.5	62.2	60.7	59.1	57.6
Sodium chloride	75.7	75.7	75.6	75.7	75.3
Potassium sulphate	98.5	98.2	97.9	97.6	97.3

Figure 4-2 shows humidity changes created by a potassium Sulphate salt solution measured by humidity sensors over a period of 4 hours and 52 minutes. With the exception of sensor H5, the other readings were close to each other and reached stability after 3 to 4 hours. Figure 4-2 shows a malfunction of sensor H5, therefore the readings drifted compared to the other readings. Relative humidity values between these ranges were used to calculate the average relative humidity of each sensor to create calibration equations.

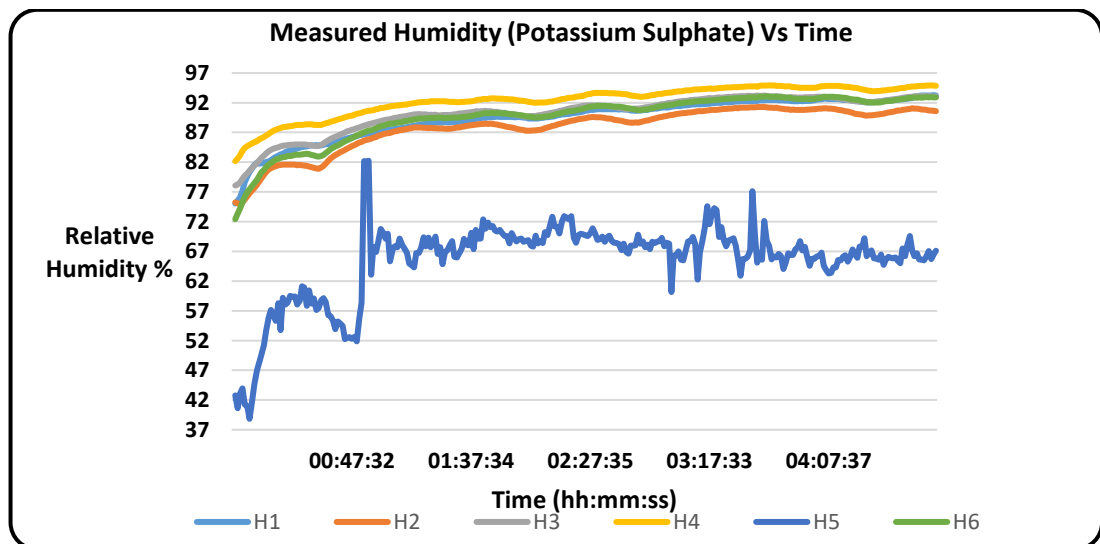


Figure 4-2 Calibration using Potassium Sulphate

Figure 4-3 shows humidity changes created by sodium bromide measured by the humidity sensors over a period of more than 17 hours. Except for sensor

H5, the other readings were close to each other and reached stability between 6 and 8 hours. Relative humidity values between these ranges were used to calculate the average of the relative humidity of each sensor to create calibration equations.

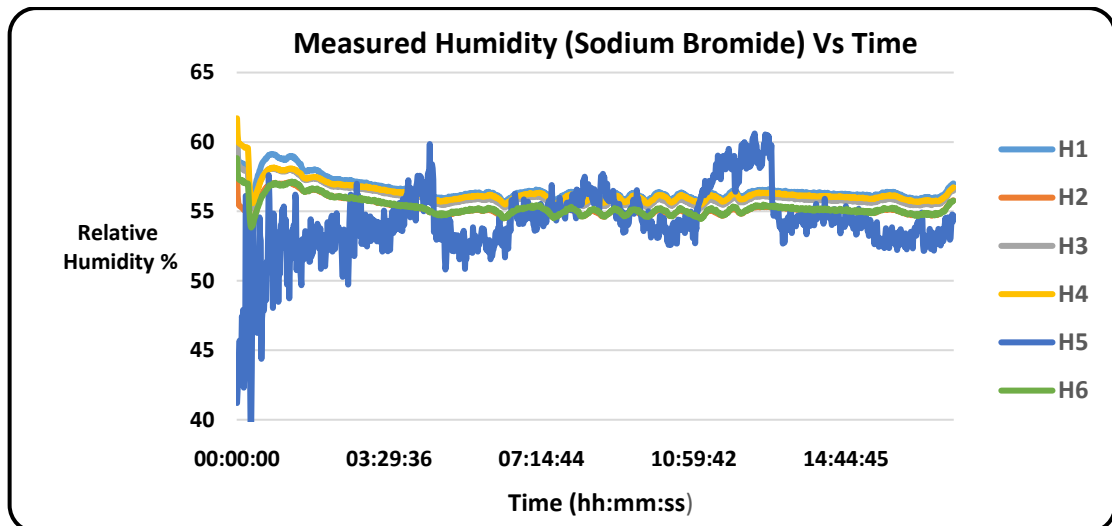


Figure 4-3 Calibration using Sodium Bromide

Figure 4-4 shows humidity changes created by sodium chloride measured by humidity sensors over a period of 19 hours and 09 minutes. Except for sensor H5, the other readings follow the same pattern. Stable readings between 10 and 13 and a half hours were used to calculate the relative humidity for each sensor to create the calibration equations.

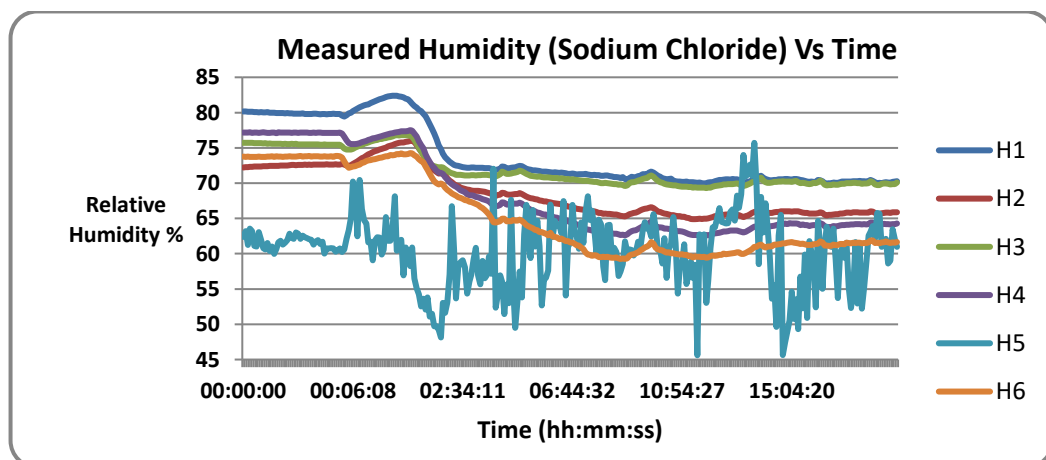


Figure 4-4 Calibration using Sodium Chloride

Figure 4-2, Figure 4-3 and Figure 4-4 show that during the calibration process using potassium sulphate, sodium bromide and sodium chloride sensor H5 did not work well and the humidity measured by H5 was very different from the other sensors' readings. Therefore, sensor H5 was not used in this experiment. The other sensors consistently measured RH values lower than those given in Table 4-3. For the case of potassium sulphate, the listed RH values can only be conducted at constant room temperature. Nevertheless, the values measured for the potassium sulphate and sodium bromide were 3% lower than the table values. The sodium chloride results had a large variation and, since this was the first test and commercial table salt was used, the results were not considered as it was not pure sodium chloride but mixed with Sodium Ferrocyanide.

Regression lines (see Figure 4-5) for each sensor were drawn using values from Table 4-4. The calibration equations are shown in figure 5-6 for each sensor that was used to calibrate each of the humidity sensors.

Table 4-4 Humidity Sensor Calibration measured and interpolated values

Chemical	Interpol	H1 (mea)	H2 (mea)	H3 (mea)	H4 (mea)	H5 (mea)	H6 (mea)
Sodium Bromide	58.600	56.314	55.098	55.860	56.114	54.455	55.155
Sodium Chloride	75.540	74.624	72.009	72.994	56.298	61.878	59.902
Potassium Sulphate	97.558	92.136	90.892	92.889	94.547	67.837	92.637

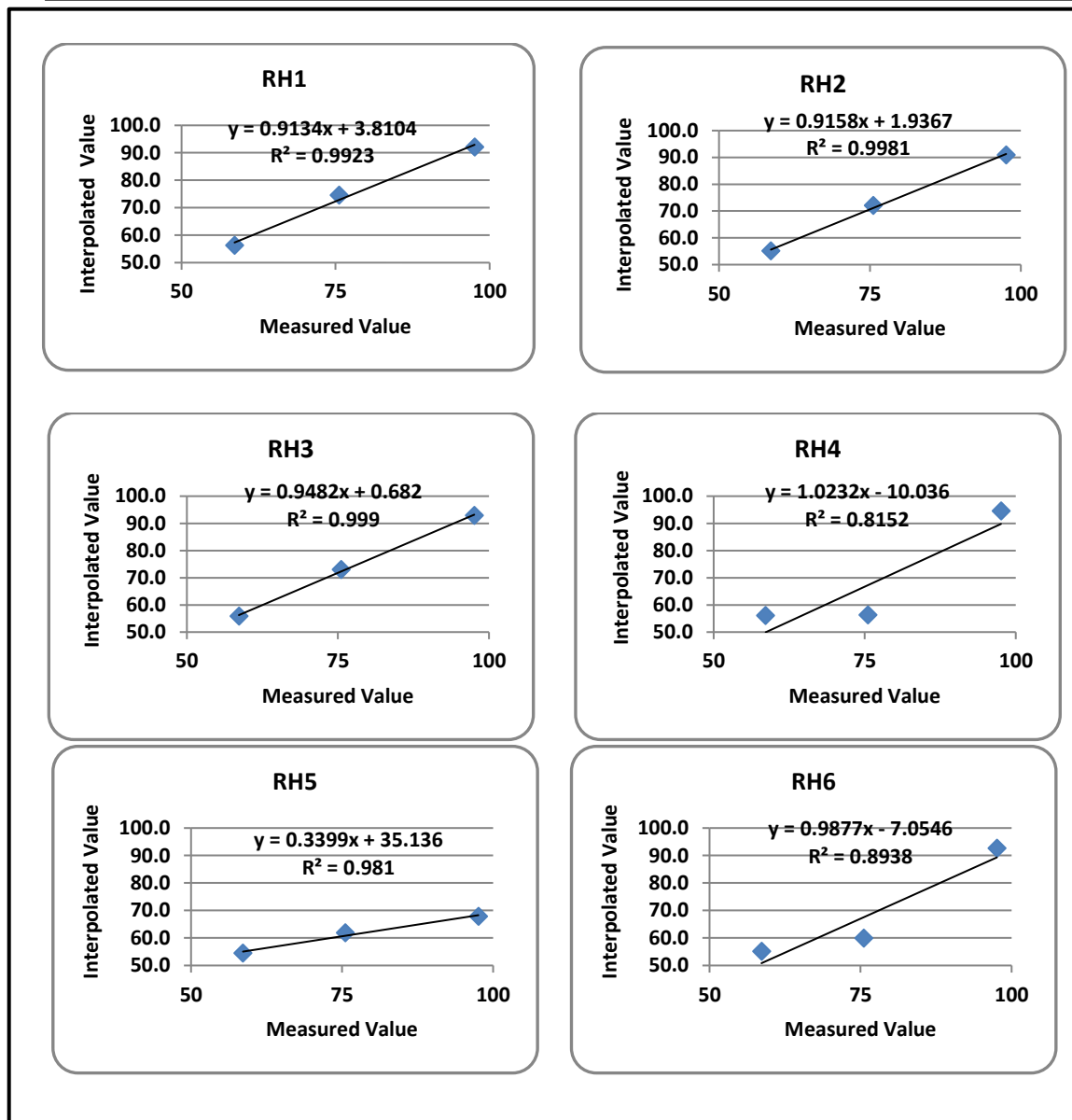


Figure 4-5 Regression line for each sensor

4.3.3 Check for the Temperature Sensors

Temperature sensors' readings were calibrated using a hotplate, a thermometer and ice packs (see Figure 4-6). All sensors were connected to the data logger and the Triax data recording software. Sensors were placed at different heights to avoid contact and minimise interaction. The temperature of the hotplate was gradually increased up from 22 °C (room temperature) to 29 °C and switched off after 45 minutes when they reached the ambient temperature (ambient temperature of 22 °C controlled by the room thermostat) within 45 minutes. Ice cubes were used to bring down the temperature

surrounding the sensors to 7 °C. The whole observation period was around 3.5 hours and the data were recorded every 5 minutes.

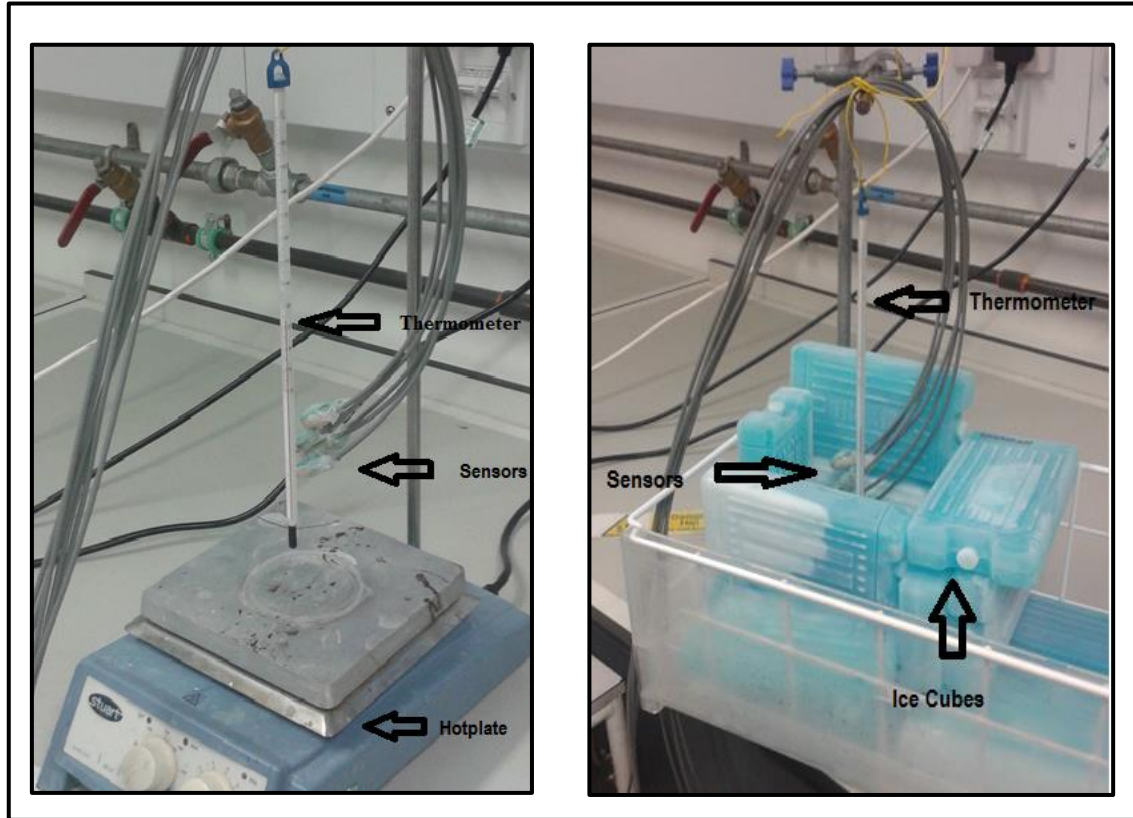


Figure 4-6 Temperature sensor calibration using hotplate and ice cubes

Given the configuration used in Figure 4-6, sensors had to be set at in different positions or distances from the ice cubes. Sensors that were closer to the ice pack read lower temperatures than sensors further away. This was the case with temperature sensors T2 and T3, where a lower temperature was measured when compared to T1, T4 and T6.

Figure 4-7 shows all temperature sensors (T1, T2, T3, T4 and T6) and the thermometer reaching stable ambient temperature readings after 2 hours before cooling starts. The average values of each cooling and heating state were compared to the thermometer values, showing a good agreement.

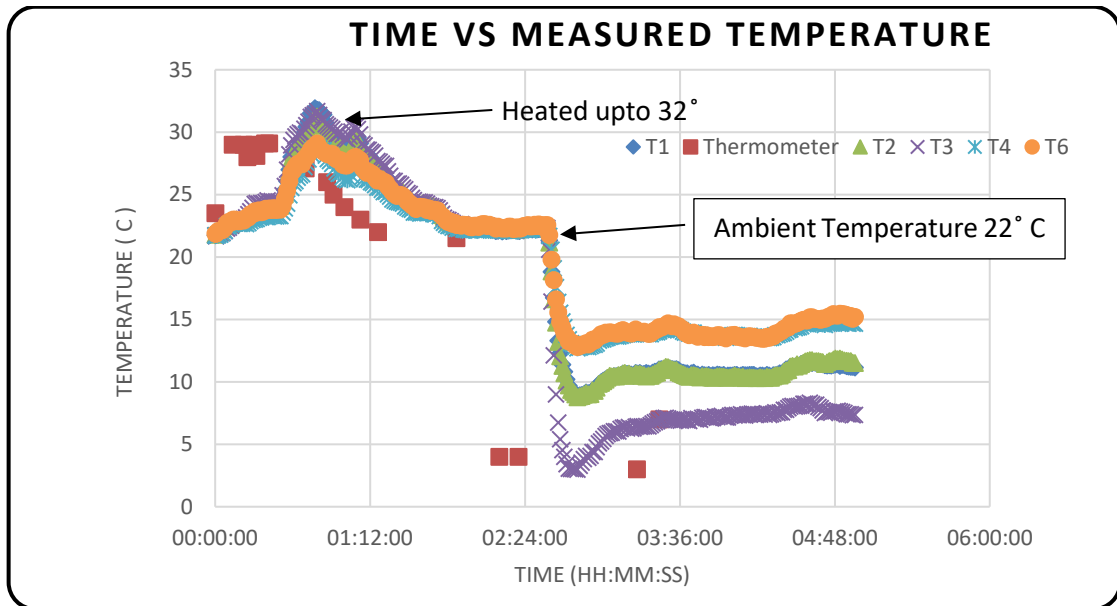


Figure 4-7 Thermometer and sensor temperature during calibration

4.4 Experiment # 1 Set-Up

A wall, made of mortar and brick, was available in the Geotechnical Lab, at UCL and shown in Figure 4-8. Figure 4-9 show cross-section of the location of sensors and source of water.

The available brick and mortar wall was instrumented with six sensors (humidity/temperature) to measure relative humidity and temperature. Sensor RH5 was mounted on the top of the test wall. Due to the malfunction of this sensor, the reading from this sensor was not used in this experiment. The sensors were embedded into holes drilled within the brickwork, to provide an estimate of the *in situ* relative humidity and temperature at each point.

Water was sprayed on the test wall using a small pump connected to a piping system; the wetting process was limited to 15 minutes to avoid any damage to the sensors.

Sensor readings were recorded at different time intervals over a period of 380 hours (around 16 days). Since readings can vary considerably when taken from various locations within the test wall (cooler near the bottom and warmer near the top) sensors were positioned in different locations, as shown in Figure

4-8, to ensure that different areas were measured accurately. At the same time, a series of images of the drying process were captured and analysed using a thermal camera and associated software (Research I.R Max) in order to understand the correlation between temperature and relative humidity.

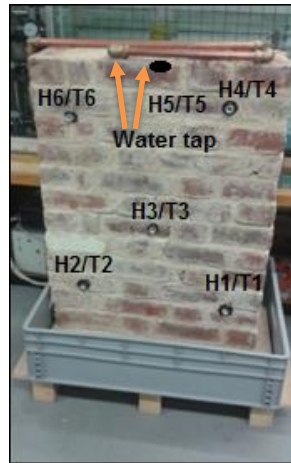


Figure 4-8 Location of sensors and source of water

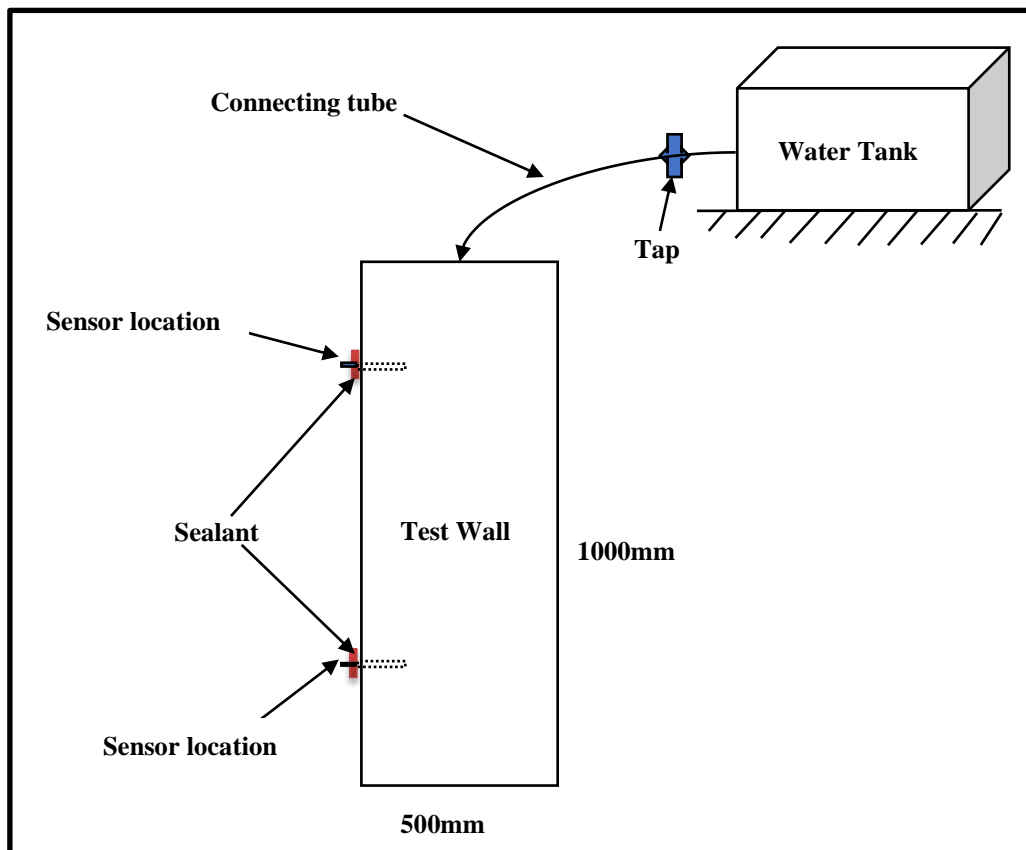


Figure 4-9 Cross section of location of sensors and source of water

4.4.1 Thermal Imaging Camera

The camera used for the test wall was a FLIR A645, which is a research-grade camera. Thermal sensitivity of 0.08°C coupled with a 640×480 pixel display, provides accurate, high-resolution 16-bit thermal images in real-time (www.flir.com/thg). The camera required a certain distance between the object and camera position to capture the entire face of the test block with its regular lens. The distance between the camera and the test wall was 1.65m.

4.4.2 Data Acquisition

A few reference thermograms were captured before the wall had been wetted. During the wetting process, the moisture gained access through capillary action at the various openings in the test wall. Water was spread from the water tank, which was placed back of the wall and connected through the pipe. The water was at the same temperature as the wall (22°C). It was leftover to equilibrate the temperature together with the wall for longer than 24 hours.

The FLIR A645 camera was connected to the laptop computer *via* research IR Max software that allows the camera to be controlled, and images were collected and stored on the computer. Humidity/temperature sensors inserted into the wall and connected to a data logger were recorded using the Triax software. At the beginning of the observation, sensor data (humidity/temperature) were recorded every 1 minute for two hours after that the observation frequency was decreased to 30 minutes. A high rate of measurement (every 1 minute) was applied during the wetting process and low frequency (every 30 minutes) of measurement was applied during the drying process.

4.4.3 Data Analysis

The FLIR Research IR Max Software was used to analyse the captured thermograms. The software is capable of visualizing thermal patterns and enables viewing, pre- and post-recording and storing images at high speed.

Sensor readings were recorded before wetting the wall in order to obtain the inside wall reference values for temperature and relative humidity. The ambient temperature was 21° C throughout the observations (room temperature was set by a thermostat).

The temperature changes cause a thermal gradient in the wall during the wetting and drying processes and the heat transfer, as a result of these gradients, occurs in the brick and the mortar. The heat transfer in the brick and mortar is time-dependent; thermal gradients may be reduced when temperature changes are less rapid.

Every thermographic surface point corresponded to a colour-coded temperature interval with a temperature resolution of 0.1 °C can be seen on

Figure 4-10 This colour palette gave an intuitive physiological impression of cold (black to blue) and warm (red to white) temperatures. Figure 4-10 shows that the top of the wall had a slightly higher temperature than the bottom.

This experiment analysed the profiles of temperature and relative humidity in the test wall made of brick and mortar samples and the associated evaporation fronts. Evaporation fronts showed the drying process relating to the corresponding moisture profiles and moisture profiles for different temperature values were obtained.

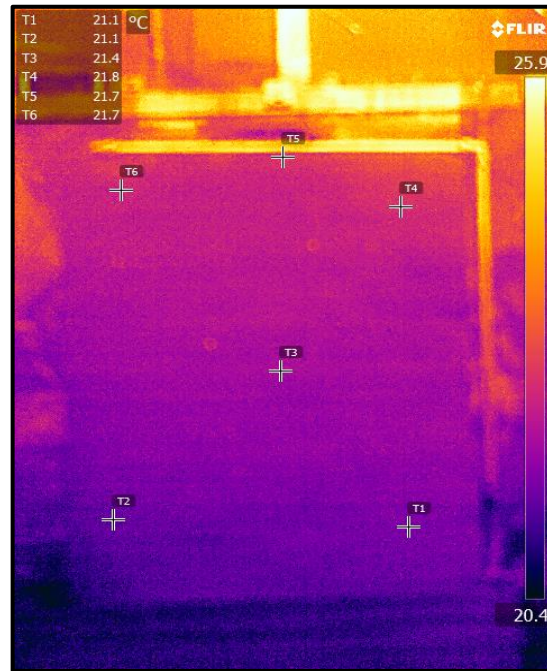


Figure 4-10 Reference image (before wetting the wall)

Figure 4-11 shows the thermographic image that was taken on January 6th, 2015 at 11.50 am immediately after wetting the wall and shows different temperature values on the wall. Wet areas are relatively cold and clearly visible in this thermogram as dark blue and dry areas are light pink/orange. The average surface temperature of the wall dropped from 21.1 °C to 16.2 °C during the 15 minutes of wetting process.

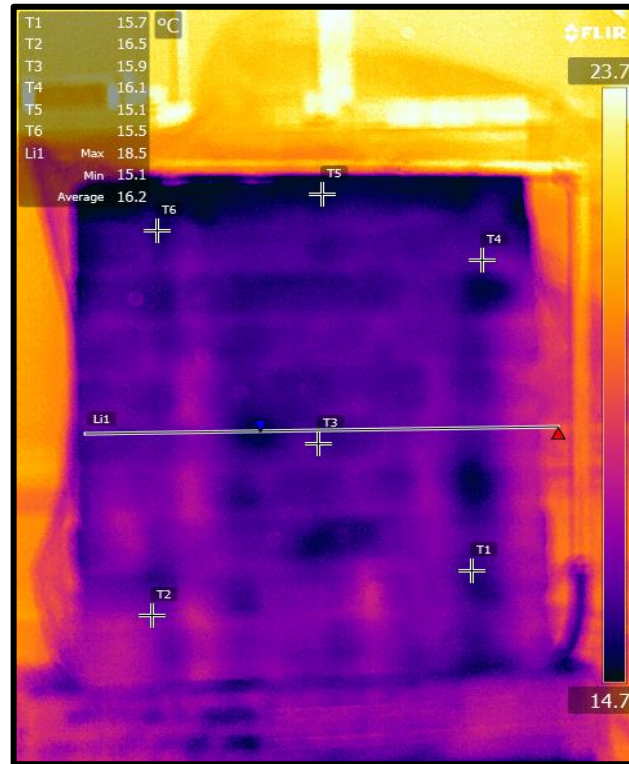


Figure 4-11 Image taken after wetting the wall with tap water

Figure 4-12 shows the change in relative humidity, inside the test wall over a period of 380 hours. According to the manufacturer, these sensors must not be exposed to higher humidity for a prolonged time. To avoid damage to the sensors, they were removed from the test wall and placed outside (top of the wall) for a few minutes at 170, 193, 239 hours and 308 hours. During this time, readings dropped to the lab humidity (26.6 %), as can be seen in the figure. Once re-inserted into the wall the readings went back to the higher values of humidity previously measured (80% and 97%). This indicates that the relative humidity sensors were not damaged by the exposure to high moisture.

Sensor H3 was removed because in its place a pipe, to simulate seepage in the wall, was inserted for experiment 2. All other sensors were placed inside the test wall and the relative humidity of these sensors increased gradually after wetting the wall, varying between 80% and 97% over a longer period (380 hours). However, the surface temperature of the test wall reached the ambient temperature within 18 hours after wetting of the test wall.

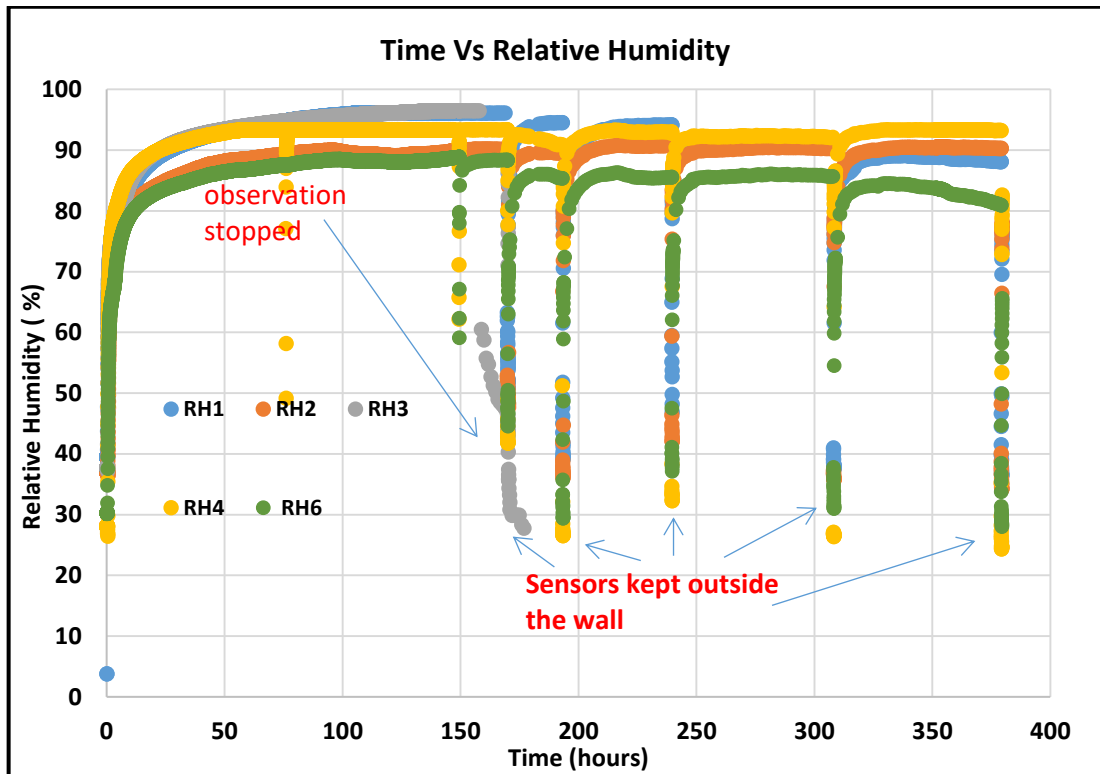


Figure 4-12 Relative humidity changes with time during before wetting, during wetting and drying process

Data were analysed in three different phases such as before wetting (for reference values), during wetting and then drying. To determine the correlation between sets of measurements, the relative humidity and temperature measured by the temperature sensor and thermal camera were plotted against each other.

4.4.3.1 Before Wetting

In order to get reference values of all sensors (relative humidity/temperature) observations were performed for 10 minutes before wetting, at the same time thermograms were captured using the thermal camera. The following figures have been drawn using those observed values.

Figure 4-13 and Figure 4-14 show that the relative humidity surrounding sensors RH1, RH2, RH3, RH4 and RH6 was stable during the first 10 minutes of the observation and reached values of 40%, 37%, 37.71%, 28% and 30.35% respectively. At the same time, the temperature inside the wall around sensor

T1 was between 20.6 °C and 20.7 °C, around sensor T2 was between 20.65 °C and 20.75 °C, around T3 was between 20.8 °C and 20.9 °C, around T4 was between 21.17 °C and 21.25 °C and T6 was between 21.30 °C and 21.44 °C. The surface temperature observed by the thermal camera at the location T1 was between 21.10 °C and 20.20 °C, T2 between 21.10 °C and 20.10 °C, T3 between 21.40 and 20.70, T4 between 21.80 °C and 20.70 °C and T6 was 21.7 °C and 21.30 °C. These values indicate that at the beginning of the experiment the temperature measured by the temperature sensors and humidity was stable inside the test wall and at the same time the thermal camera is showing changes in temperature. All the temperature and relative humidity sensors had similar behaviour in all 5 locations during this observational period.

The thermal camera had a variation of ± 1 °C in static measurements. This can be seen in

Figure 4-13. In order to obtain better precision in a steady condition, readings must be averaged over a greater period, which was not done here. Thermal cameras have a self-calibrating mechanism that can change a reading by as much as 2 degrees; however,

Figure 4-13 does not show that mechanism in action.

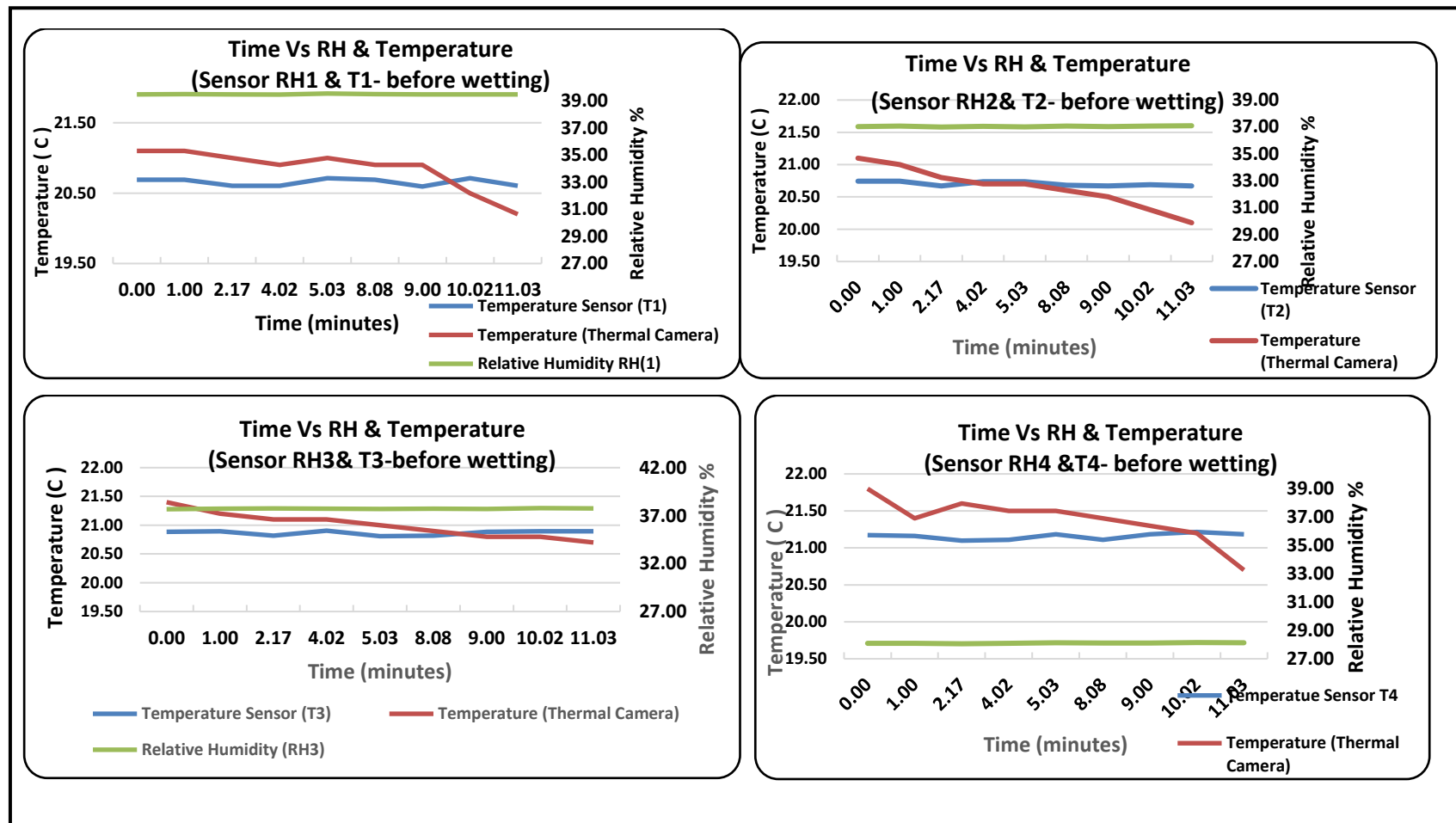


Figure 4-13 Relative humidity sensors (RH1, RH2, RH3 & RH4), Temperature sensors (T1, T2, T3 & T4) and Temperature measured by Thermal camera before wetting

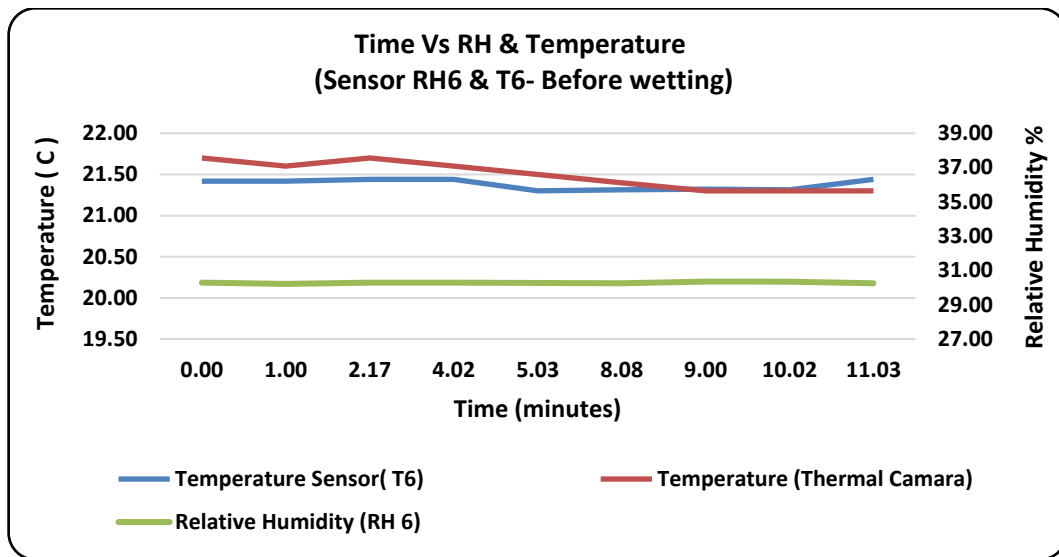


Figure 4-14 Relative humidity sensors (RH6), Temperature sensor (T6) and Temperature measured by the thermal camera

4.4.3.2 During Wetting

The observations made were recorded during the wetting process, and the surface temperature of the wall was observed using a thermal camera. The following figures illustrate changes in temperature and relative humidity during 15 minutes of wetting the wall.

Figure 4-15 and Figure 4-16 show that during the first 15 minutes of the wetting process, the surface temperature measured by the thermal camera varied at T1 location between 15.70 °C and 17.30 °C, T2 location between 16.5 °C and 17.30 °C, T3 location between 15.90 °C and 17.10 °C, T4 location between 16.10 °C and 17.5 °C and T6 location between 15.50 °C and 16.80 °C. During the wetting process temperature measurement at T1 location shows larger changes in temperature from 17.30 °C to 15.70 °C. This was due to more water poured closer to that sensor.

At the same time the inside wall temperature, measured by temperature sensors began to drop, T1 location between 20.71 °C and 18.91 °C, T2 location between 20.55 °C and 19.47 °C, T3 location between 20.46 °C and 19.11 °C,

T4 location between 20.73 °C and 19.52 °C and T5 location between 21.27 °C and 20.27 °C. The temperature dropped because of the capillary suction effect of the porous material of the brick and mortar, which absorbed water molecules quickly and trapped them inside the wall.

The relative humidity sensors have a fast wetting response, responding to a change from 59.24 % to 68.04% at RH1, 36.53% to 51.62% at RH2, 55.81% to 66.93% at RH3, 35.46% to 61.72% at RH4 and 41.95% to 54.09% at RH6.

The temperature drops as the humidity inside the wall increases. Therefore, there is a reduction in the amount of water in the external surface and an increase in the water inside the wall. This can be seen by the changes in temperature and moisture measurements.

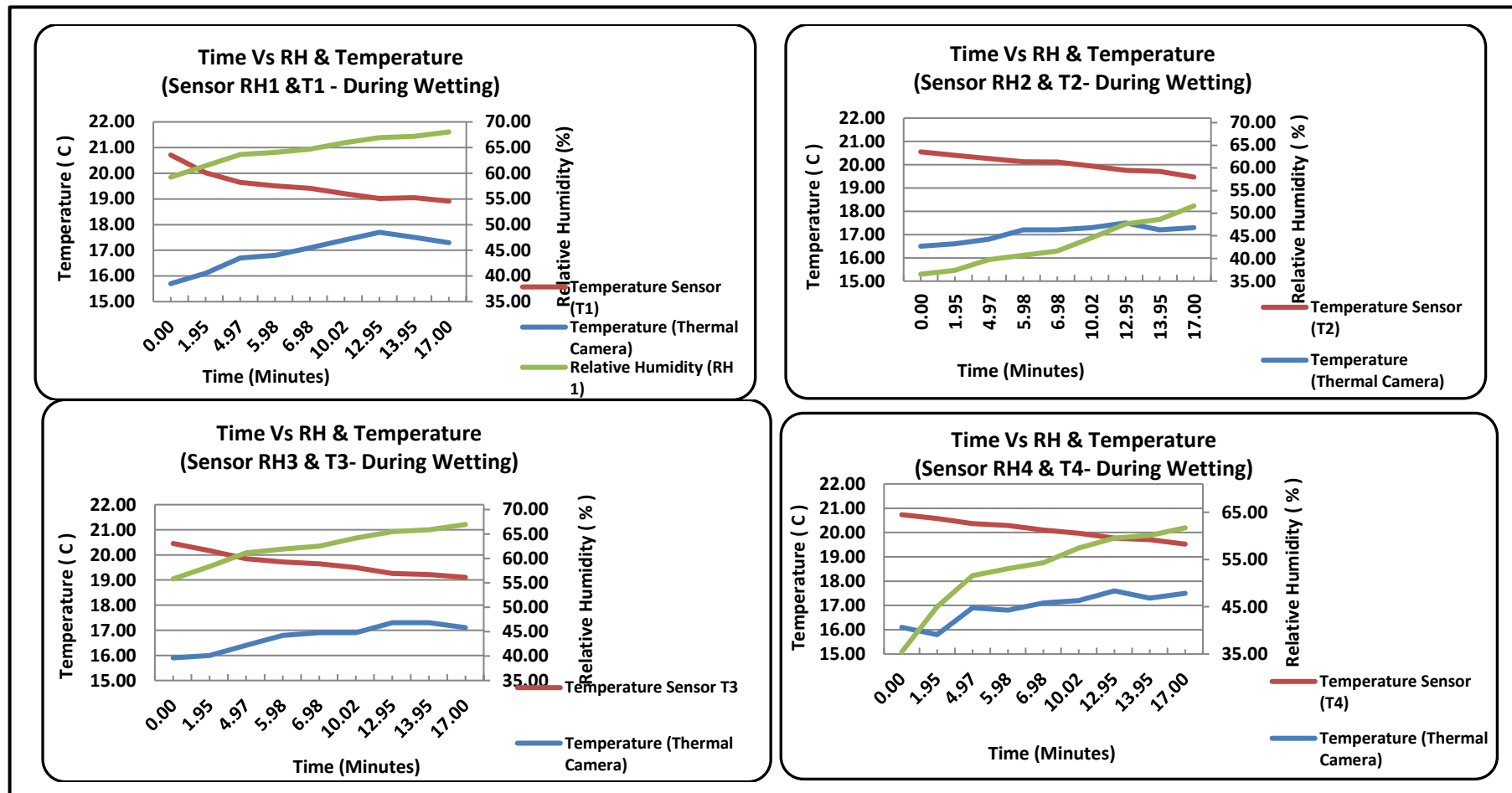


Figure 4-15 Relative humidity sensors (RH1, RH2, RH3 & RH4), temperature sensors (T1, T2, T3 & T4) and temperature measured by thermal camera during wetting

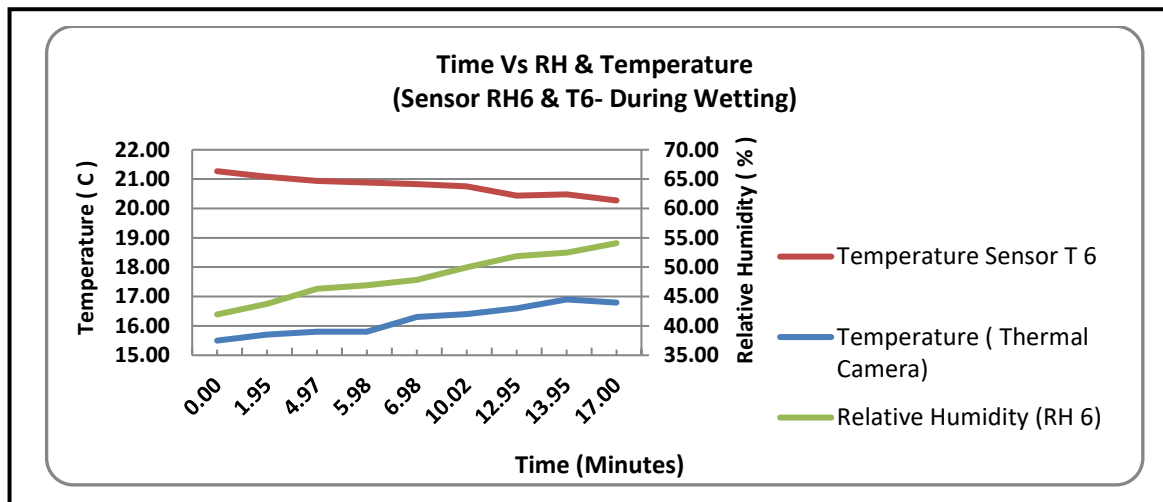


Figure 4-16 Relative humidity sensor (RH6), temperature sensor (T6) and temperature measured by the thermal camera during wetting

4.4.3.3 Drying

At the beginning of the drying process, it was observed that temperature increases slowly and tends towards eventual stabilization. The relative humidity increases due to the brick's inner layers, becoming saturated and then starting to dry slowly. While the temperatures increase, the relative humidity reduction is due to evaporation of the first layer of water, which allows small amounts of air to enter the space where the sensor is located. At the beginning of the drying process, the temperature gradients into the brick are large and decrease as the drying progresses. Temperature gradients disappear when the equilibrium conditions are achieved between the ambient humidity and moisture of the brick (Cortes, 2013).

Sensor H3/T3 was unplugged to install a 16mm diameter pipe at that location for experiment # 2. Early removal of the H3/T3 sensor did not affect the end results of this experiment because of the availability of data for other sensors. Therefore, only 143.92 hours of data were available.

Figure 4-17 and Figure 4-18 show data after 245 hours of the drying process and drying times at surface temperatures measured by the thermal camera and the inside temperature which was measured by the temperature sensors. It is clear that the moisture evaporates faster on the surface of the wall, hence

the increase in the temperature is faster than on the inside of the wall. Once the wall starts drying on the inside, the moisture in the sensor location reduces, however, the temperature seems to increase at a faster pace whilst the moisture is reaching a limiting value above the 95 or 97%. Suddenly the rates change, and the temperature starts increasing at a faster pace with the moisture reducing. This seems to be a trend in the system, as all sensors show the same behaviour.

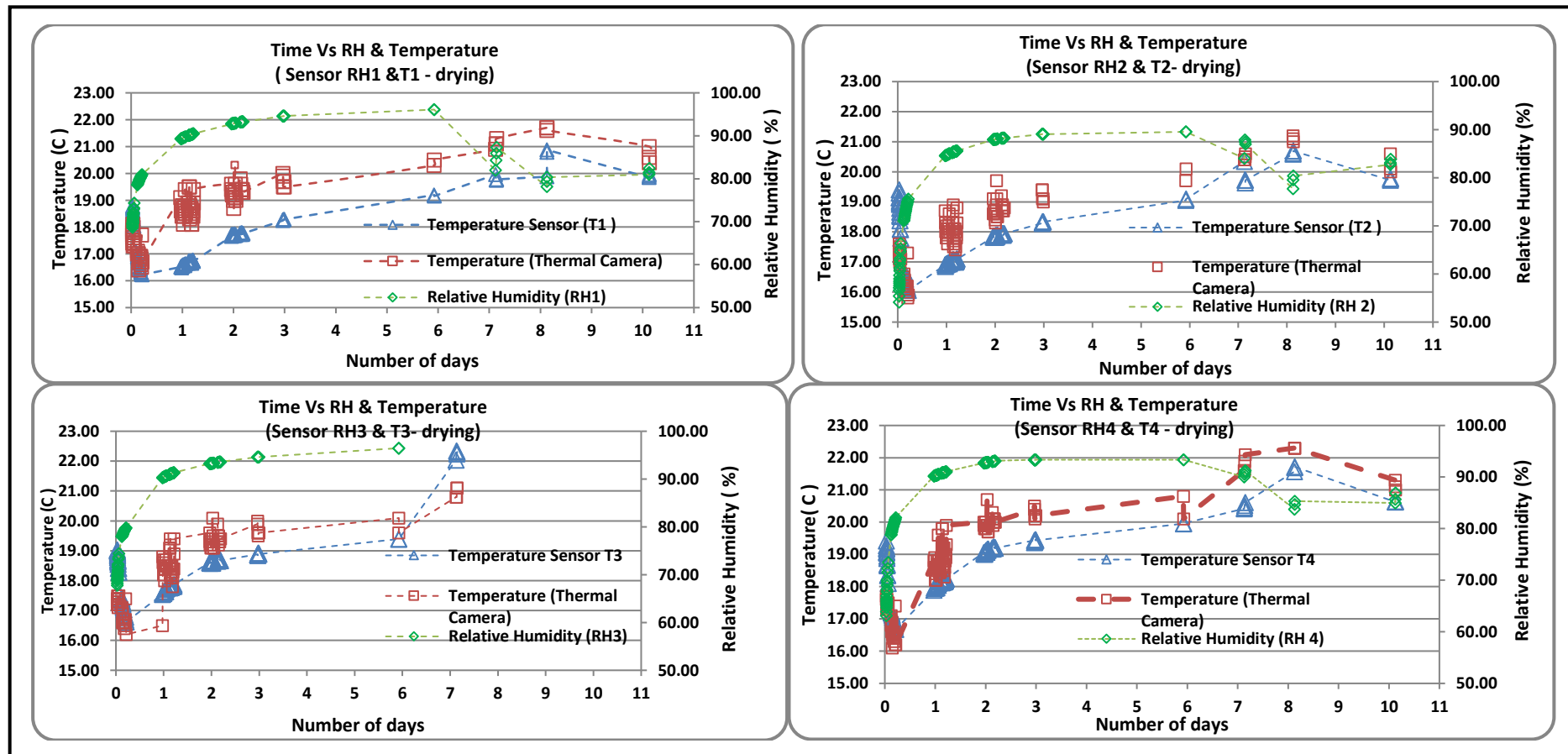


Figure 4-17 Relative humidity sensors (RH1, RH2, RH3 & RH4), temperature sensors (T1, T2, T3 & T4) and temperature measured by thermal camera during drying

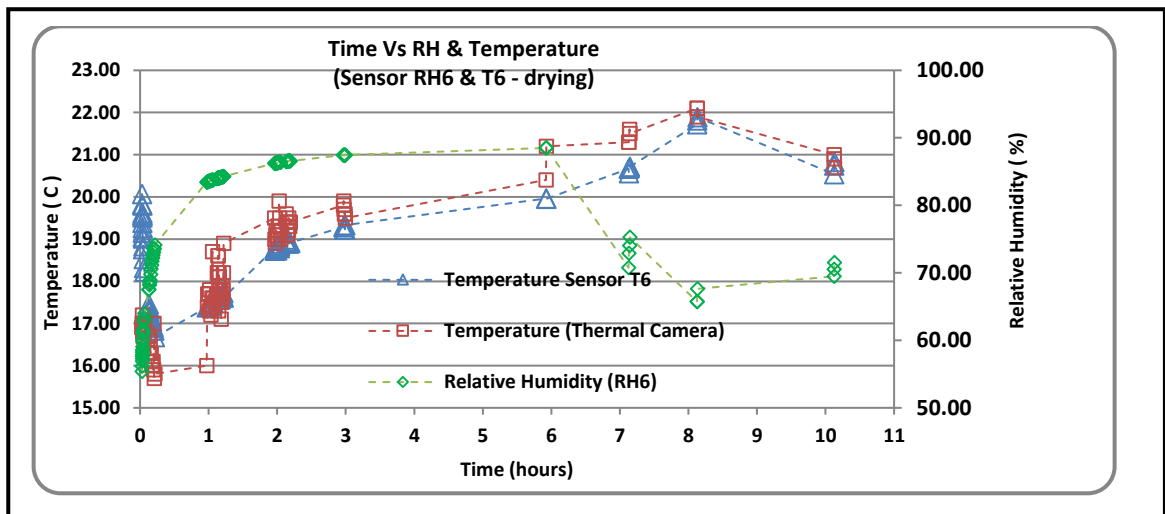


Figure 4-18 Relative humidity sensor (RH6), temperature sensor (T6) and temperature measured by the thermal camera during drying

These data are tabulated in Table 4-5 and the following abbreviations are used in the table.

TST1- Temperature Sensor T1

TC1- Thermal Camera measurement at Surface T1

RH1 (%) - Relative Humidity 1

Table 4-5 Temperature Sensor, Thermal Camera and Relative Humidity measurements during drying

Date	Time	Time (Hours)	TST1	TC1	RH1 (%)	TST2	TC2	RH2 (%)	TST3	TC3	RH3 (%)	TST4	TC4	RH4 (%)	TST6	TC6	RH6 (%)
06/01/2015	12:10:05	0.029	18.79	17.60	68.68	19.40	17.60	54.14	19.01	17.30	67.81	19.42	17.70	63.16	20.07	16.90	55.41
07/01/2015	11:30:10	24.001	16.57	18.80	89.44	16.94	18.20	84.69	17.58	18.50	90.43	18.00	18.60	90.31	17.43	17.70	83.58
08/01/2015	11:30:02	48.001	17.73	19.00	92.91	17.84	18.40	87.97	18.62	19.10	93.30	19.10	19.80	92.83	18.73	19.00	86.26
09/01/2015	10:42:09	71.967	18.25	20.00	94.57	18.29	19.40	89.06	18.88	19.90	94.60	19.44	20.40	93.34	19.29	19.80	87.46
12/01/2015	09:36:05	143.922	19.19	20.30	96.10	19.05	19.70	89.54	19.40	20.10	96.48	19.95	20.80	93.36	19.96	20.40	88.49
13/01/2015	15:00:49	168.147	19.78	21.30	87.28	19.72	20.60	86.98	22.31	21.10		20.62	22.10	91.30	20.71	21.50	75.26
14/01/2015	14:32:05	192.127	20.79	21.70	79.34	20.63	21.20	79.58				21.70	22.30	84.74	21.82	22.10	65.74
16/01/2015	14:37:00	240.131	19.96	20.40	82.40	19.77	20.00	83.87				20.65	21.00	86.96	20.83	20.70	71.54

Table 4-5 shows step changes of temperature and relative humidity readings with the corresponding time intervals during 245 hours of the drying process. Comparison between temperature sensor readings and thermal camera readings indicated that drying occurred at a much faster rate at the surface than inside the wall as expected.

Relative humidity profiles (Figure 4-17 and Figure 4-18) show that RH increased gradually and reached maximum values of 96.10% at RH1, 89.54% at RH2, 96.48% at RH3, 93.36% at RH4 and 88.49% at RH6 and these were reached 144 hours after the drying process started. Table 5-5 shows the relative humidity increases and decreases during the time interval between 0.0 hours and 240 hours. This would be due to the brick's inner layers being saturated during the wetting process which then decreases while the temperature increases. This then began to increase (at 240.13 hours) because water vapour was travelling from the hotter to the cooler areas.

4.4.4 Experiment # 1 Conclusion

The following conclusions can be drawn regarding the use of relative humidity, temperature sensors and thermography.

- The data showed that the relative humidity was stable inside the wall before wetting, at that time surface temperature (measured by the thermal camera) was very close to ambient temperature (21 ° C). All the temperature and relative humidity sensors showed similar behaviour in all 5 locations before wetting.
- During the wetting, the temperature reduces quickly because of the water at the surface. As the water permeates through the wall it reaches the voids of the brick material and moisture values increase very quickly, followed also by a reduction in temperature in the order of 1 ° C (minimum) in all sensors.
- The surface dries very quickly and it can be seen by the change in temperature measured with the thermal camera. In the inner part of the wall, temperatures start rising slowly whilst the moisture is still increasing. Once the moisture reaches equilibrium and starts dropping a much larger rate of increase in temperature is seen.
- The surface temperature of most parts of the wall quickly reached an ambient temperature of 21 ° C at 240hrs after the wetting process. Data

indicated that drying occurs at a much faster rate at the surface than inside the wall because of overhead Air-Conditioning (AC) which was operating 24 hours in the lab, the AC system helps with the drying. However, the conditions are constant so that observations are independent of the boundary conditions since this did not change.

- This experiment showed that integration of moisture, temperature sensors and the thermal camera could be used to detect moisture inside a wall and water on the surface more effectively than other methods (e.g. laser scanner). Compared to other defects, active seepages (running water) have occurred more in several areas on the LUL network. Therefore, this technique could be used to detect water ingress/seepage effectively.

4.5 Experiment # 2 Set-Up

The purpose of this experiment was to simulate water seepage through a brick wall, using a thermal camera and moisture meter to detect the advancement of the saturation front. A constant head of water was applied inside of the wall at the H3/T3 location (see Figure 4-19) by using a 16mm diameter tube pipe attached to a tank located above the wall (Figure 4-19 and Figure 4-20) at 1.2m above the floor level in order to provide adequate water pressure at the wall. The wall was initially dry and surface thermograms were captured every 10 minutes. At the same time, a moisture meter (Figure 4-21) was used to measure the moisture content at different locations on the test wall; these are shown in Figure 4-22. The instrument has two prongs and when measuring moisture, the prongs must be inserted into the test material. The material being measured must be selected from the menu before measurements are attempted.

Moisture meter specifications were:

- Parameters - % material moisture contents, temperature °C °F
- Accuracy- Conductivity measurement $\pm 2\%$

- Temperature $\pm 1^{\circ}\text{C}$
- Resolution 0.1%, 0.1 $^{\circ}\text{C}$, 0.1 $^{\circ}\text{F}$
- Measurement range: - 0.0%- 95.7 %, -10 $^{\circ}\text{C}$ to +50 $^{\circ}\text{C}$

The water source is located by referring to the region with the highest moisture content. For passive thermography, signs of water seepage can be identified by locating the cooler region on the thermal image. Passive thermography test materials are naturally at a different temperature depending on their emissivity and radiant energy. Figure 4-19 shows the water tube connected between the water tank and the test wall through the water tap. Figure 4- 20 shows the back of the test wall with the 16mm diameter water pipe attached to the test wall through a drilled hole.

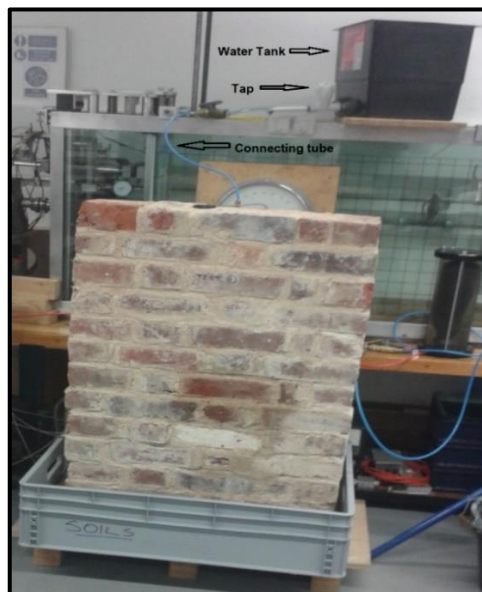


Figure 4-19 Front side of the test wall



Figure 4-20 Backside of the test wall

Figure 4-21 shows the moisture meter which was used to measure wall moisture content.



Figure 4-21 Moisture meter

4.5.1 Data Analysis

Thirteen locations (X,1,2,3,4,5,6,7,8,9,10,11,12) were chosen (see Figure 4-22) on the wall for moisture, and temperature measurements using thermograms. Representative thermograms and the corresponding photographs are shown in Figure 4-23 through Figure 4-32 at different time intervals. The suspected wet areas were relatively cool compared to the dry brick and clearly visible in a

thermogram as dark blue areas. These figures showed that moisture regions were clearly identifiable from that of the dry areas.

Each sensor location was superimposed on thermograms, which were recorded between 9.25 am and 1 pm. Then, using the point measurements tool in Research I.R max, the temperature of the pixels closest to the measurement point were determined. From one epoch to the other, it is likely that a variation in the location of the point existed; however, when a measurement was performed in the middle of the brick, care was taken to ensure that no measurements were taken near the edges of the brick. A similar approach was used for points in the mortar.

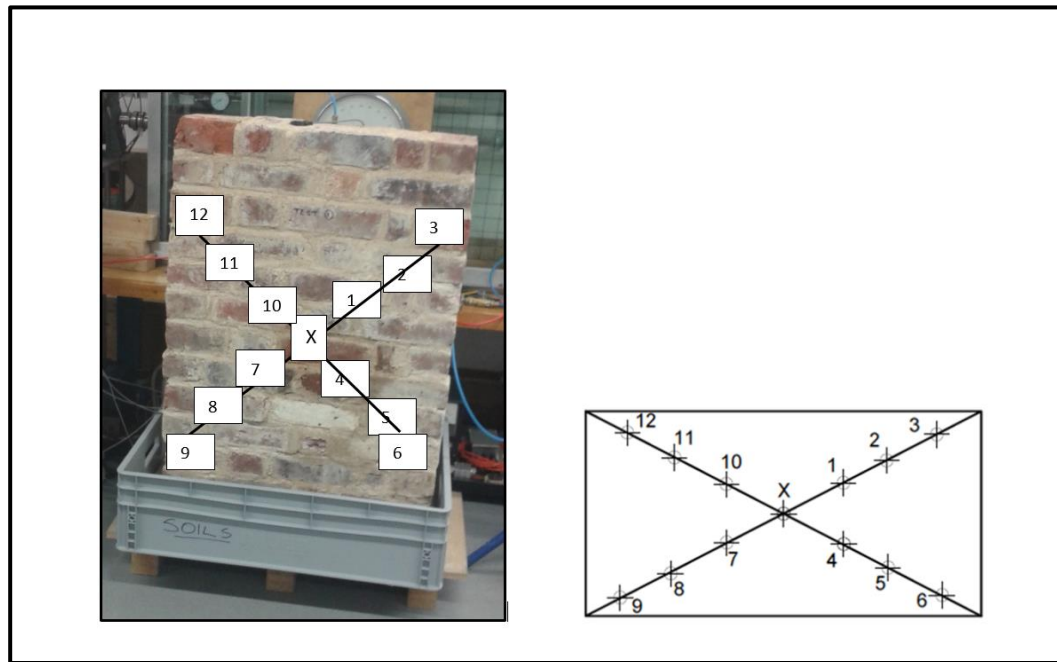


Figure 4-22 Schematic diagram of moisture measurements on the wall

Table 4-6 shows moisture measurement locations on the wall.

Table 4-6 Moisture measurement locations on the wall

Locations	Brick	Mortar
X	✓	
1	✓	
2	✓	
3	✓	
4	✓	
5	✓	
6		✓
7	✓	
8	✓	
9		✓
10	✓	
11	✓	
12		✓

Dampness is hazardous before it can be seen on the surface and materials do not become visibly damp and do not feel wet to the touch until they are quite damp. Thus, dampness is hazardous long before it can be detected unaided. This is why it is essential to use a moisture meter for surveying for damp, and making judgments about its severity. Figure 4-25 shows that the unaided eye could not identify dampness; however, a clearer indication of the sign of moisture was obtained by thermography as shown in Figure 4-26.

The temperature of the water seepage area of each thermogram was measured using FLIR Research I.R Max software. Measured values were used to calculate temperature differences in each location during the 3 hours and 35 minutes wetting process. The temperature differences are too small to locate water ingress visually, but the thermograms make it evident.



Figure 4-23 Visual image @ 9.25 am

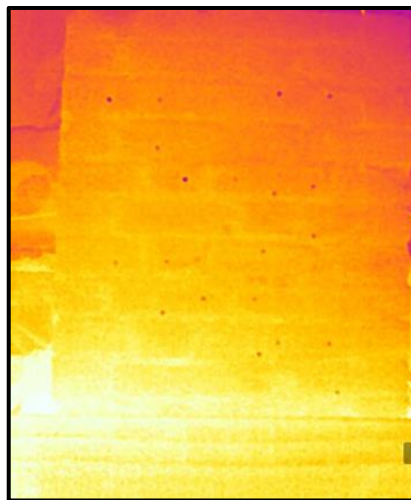


Figure 4-24 Thermography image @ 9.25 am



Figure 4-25 Visual image @ 9.50 am

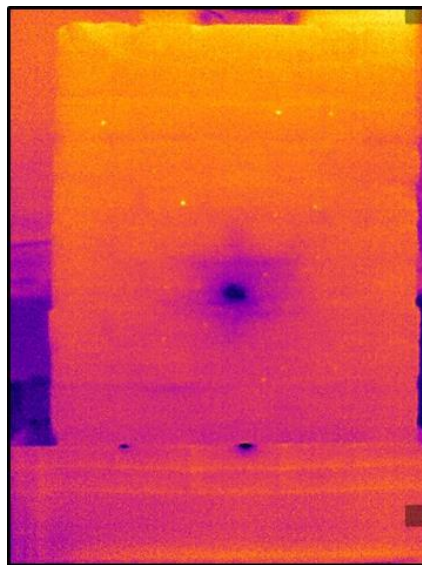


Figure 4-26 Thermography image @ 9.50 am



Figure 4-27 Visual image @ 10:15 am

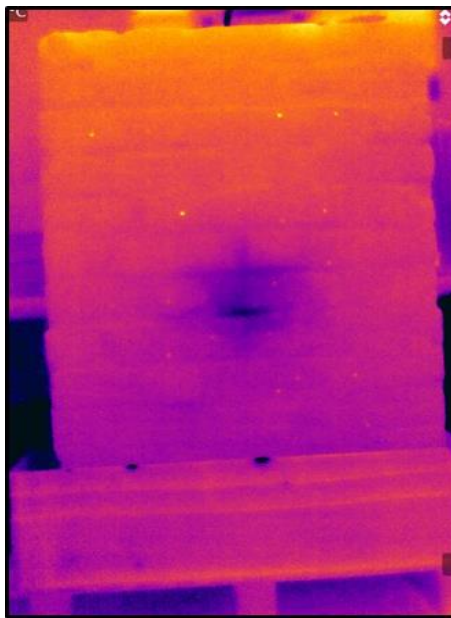


Figure 4-28 Thermography image @ 10:15 am



Figure 4-29 Visual image @ 12:00 pm

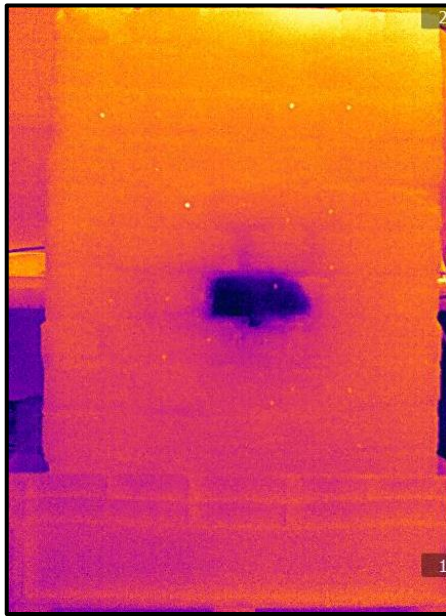


Figure 4-30 Thermography image @ 12:00 pm

The precise location of moisture can be identified using the moisture meter. The precise location is essential to assessing the risk of accumulated moisture. But water seepage locations should investigate to determine exactly where to place the moisture meter. Although the thermograms cannot quantify moisture content,

they are very useful in locating suspect areas. A thermal camera can guide the use of moisture meters during an observation. Figure 4-30 and Figure 4-32 show that excessive moisture appears as a darker pattern in the thermogram, indicating lower surface temperatures in areas with elevated moisture. Based on those patterns, suspect areas can be located, and then confirmed and quantified by using a moisture meter.



Figure 4-31 Visual image @ 13:00pm

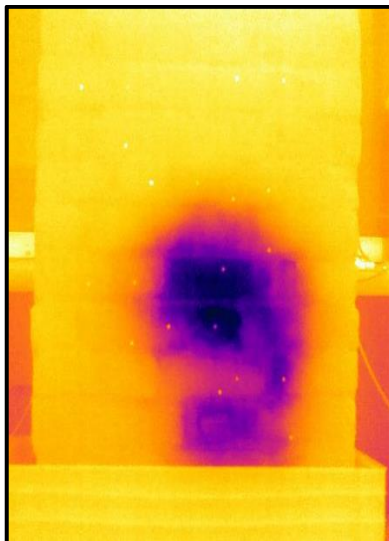


Figure 4-32 Thermography image @ 13:00 pm

Figure 4-33, Figure 4-34 and Figure 4-35 show the variation of moisture content at different locations over a period of 3 hours and 35 minutes of the wetting process. The maximum value of 12.60 was reached at the location of X and a minimum value of 2.80 reached at location 11. These values indicate that moisture content varies widely over short distances.

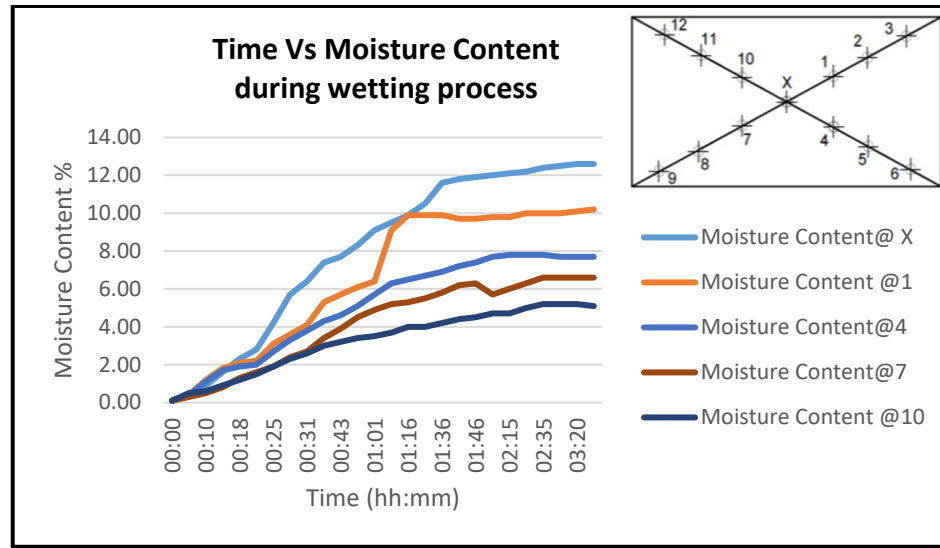


Figure 4-33 Moisture measurements @ X, 1, 4,7,10 locations

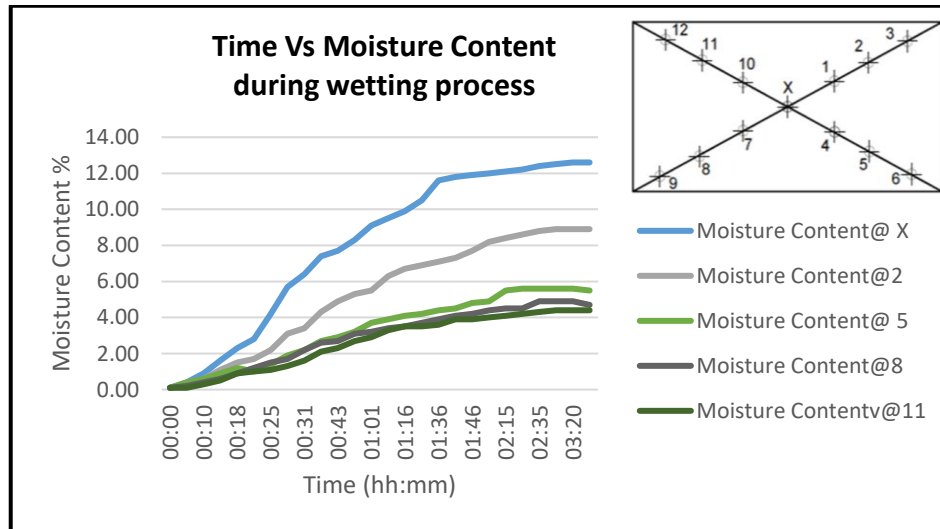


Figure 4-34 Moisture measurements @ X, 2, 5,11,8 locations

Figure 4-36 shows the maximum moisture content reached at each location over a period of 3 hours and 35 minutes of the wetting process. Furthermore, maximum

moisture content varies widely over short distances and the moisture content at one location (e.g., @ 1), does not mean that the moisture content of that same material, even 5cm away (e.g., @ 3) will have the same. The maximum moisture changes depend on the materials (e.g., brick and mortar) and distance from the water path.

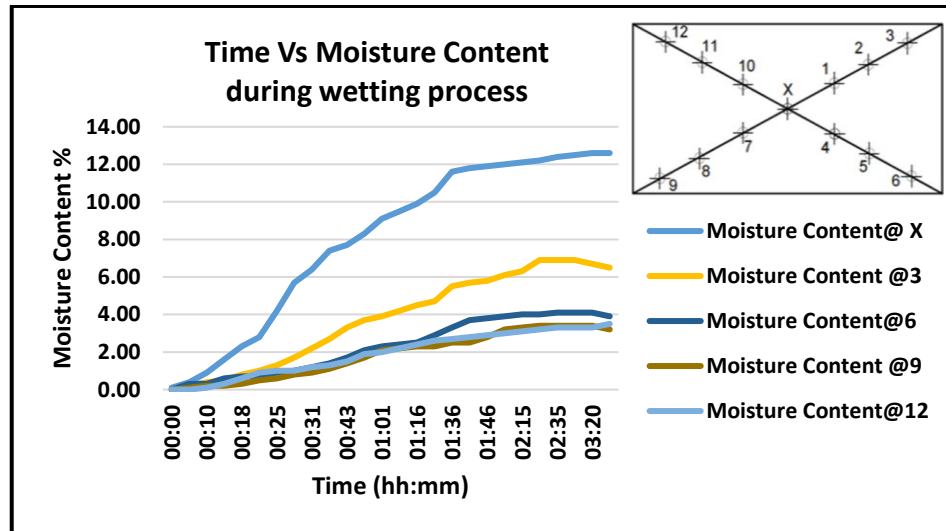


Figure 4-35 Moisture measurements @ X, 3, 6,9,12 locations

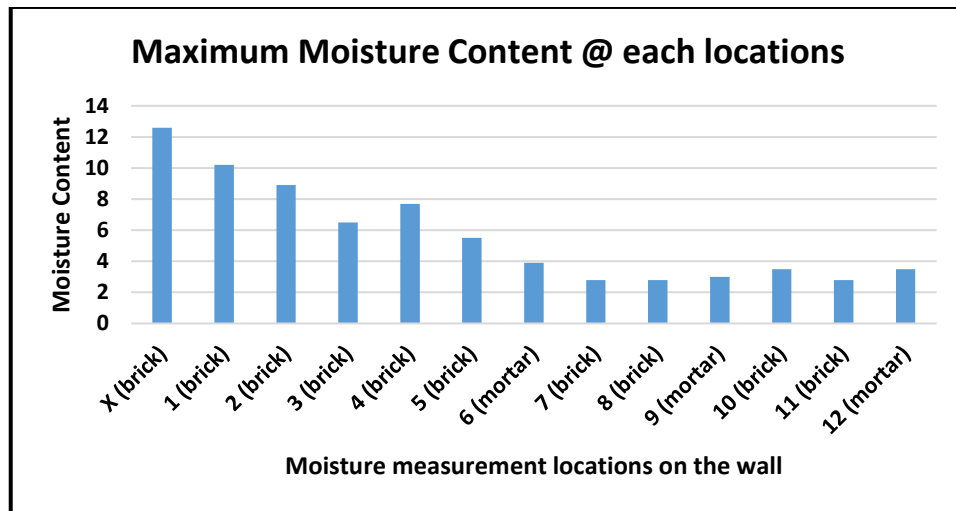


Figure 4-36 Maximum moisture content @ each location

Figure 4-37 shows the variation of moisture contents at different locations on the bricks of the test wall over the surface temperature differences. The graph shows

that the moisture content has a similar behaviour i.e increase in moisture with the reduction of temperature in at all the points measured. The maximum values reached, however, are different. This is attributed to the variation in the brick density in the measurement area.

Equation (4.2) shows the regression line of Figure 4-37.

$$\text{Moisture content (Y)} = -2.1588 * (\text{reference temperature} - \text{observed temperature}) \quad (4.2)$$

The brick wall used in this experiment was initially used to study the behaviour of old structures. Therefore, the bricks used were in the order of 200 years old, and as a consequence, a quality control was not very good, as these are likely to be of different porosities. During this research, the porosity of the bricks was not studied. According to Esbert et al. (1997), old clay bricks from that period show porosity values ranging between 15% and 40%. This is likely to be because of the large variation in moisture content, as seen in Figure 4-37.

Modern bricks are likely to have a much smaller range of porosity given the highest quality control, lower presence of impurities and constant firing temperature.; therefore, a much lower variation in moisture content. The calibration procedure remained the same and only one regression line was used here in this application, as it would be impossible to know the location of different porosity bricks.

The surface temperature measured by the thermal camera depends on the emissivity of the materials. Therefore, during the wetting process, for every point where the moisture meter was used, the test wall had two different combinations of emissivity values; mortar and water (0.87 and 0.96 emissivity's respectively) and brick and water (0.93 and 0.96 emissivity's respectively). The brick calibration equation of Figure 4-37, equation (4.2) was used to convert surface temperature

measurements performed with the thermal camera to a moisture content map. The advantage of this procedure is the ability to assess dry parts of the test wall.

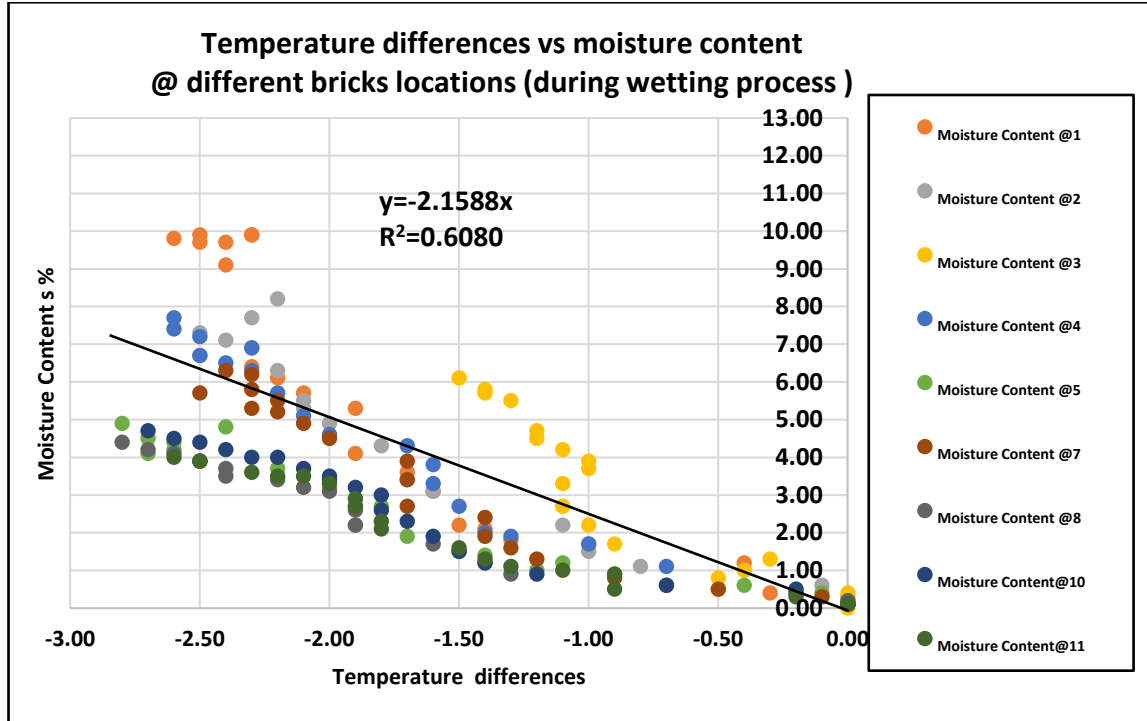


Figure 4-37 Variation of moisture content at different brick locations over surface temperature differences.

Figure 4-38 shows a variation of moisture contents at different mortar locations on the test wall over the surface temperature differences. The data collected for the mortar show that the 3 locations selected have a similar behaviour, indicating that the mortar is more uniform than the bricks and shows a better correlation between temperature and moisture. It is also clear that the mortar is less porous than the bricks as the maximum moisture content achieved is around 3 to 4%.

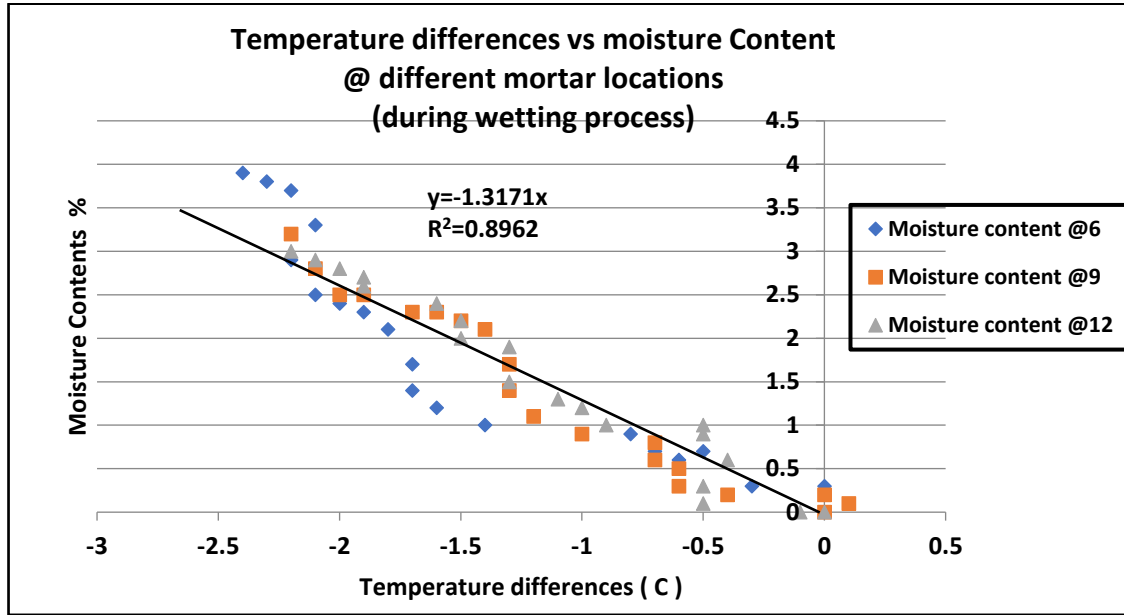


Figure 4-38 Variation of moisture content at different mortar locations over surface temperature differences

In Figure 4-39 to Figure 4-43, the horizontal and vertical axes are in pixels because exporting data from thermograms, yield a spreadsheet with temperature values in cells and coordinates in pixels. By choosing an adequate initial temperature and applying equation 4.1 to the exported spreadsheet, the temperature values were converted into moisture content. These operations were performed in Excel. Figure 4-39 to Figure 4-43 show the contour plots created in MATLAB of the evolution in moisture content due to the seepage on the test wall at different epochs. A scale was determined through the length of features in the tunnel, i.e. the drip tray dimensions.

Figure 4-39 shows the variation of moisture content in the test wall at 9.25 am before water is released from the header tank. A dry brick temperature of 21.7°C was used as a reference temperature to calculate the temperature differences of the wall at 9.25 am. This figure can be used to establish whether the moisture content is higher towards the water path (e.g. the place where the water tube touches the wall). At the beginning of the observation surface, moisture level almost dry.

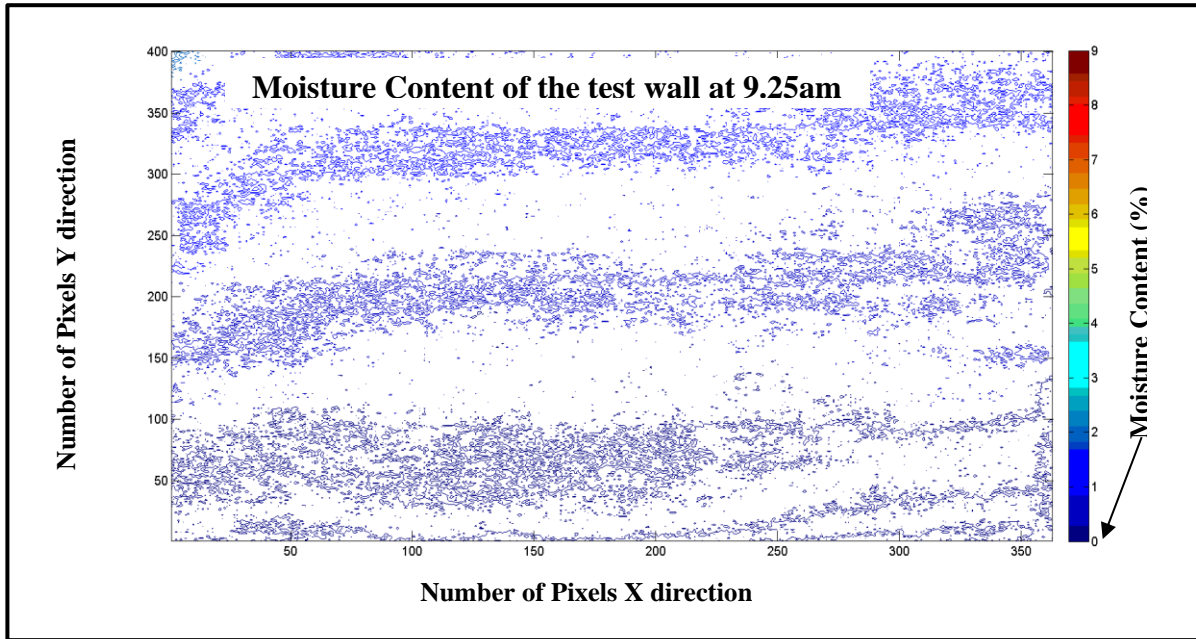


Figure 4-39 Moisture Content of the test wall at 9.25am

Figure 4-40 shows the variation of moisture content in the test wall at 9.50 am after water is released from the header tank. A temperature of 21.6°C was selected as an average dry brick temperature of the test wall at 9.50 am in order to calculate the temperature difference of the wall at that time. This figure shows nearly 3% moisture content occurred closer to the water tube marked by the light blue contours.

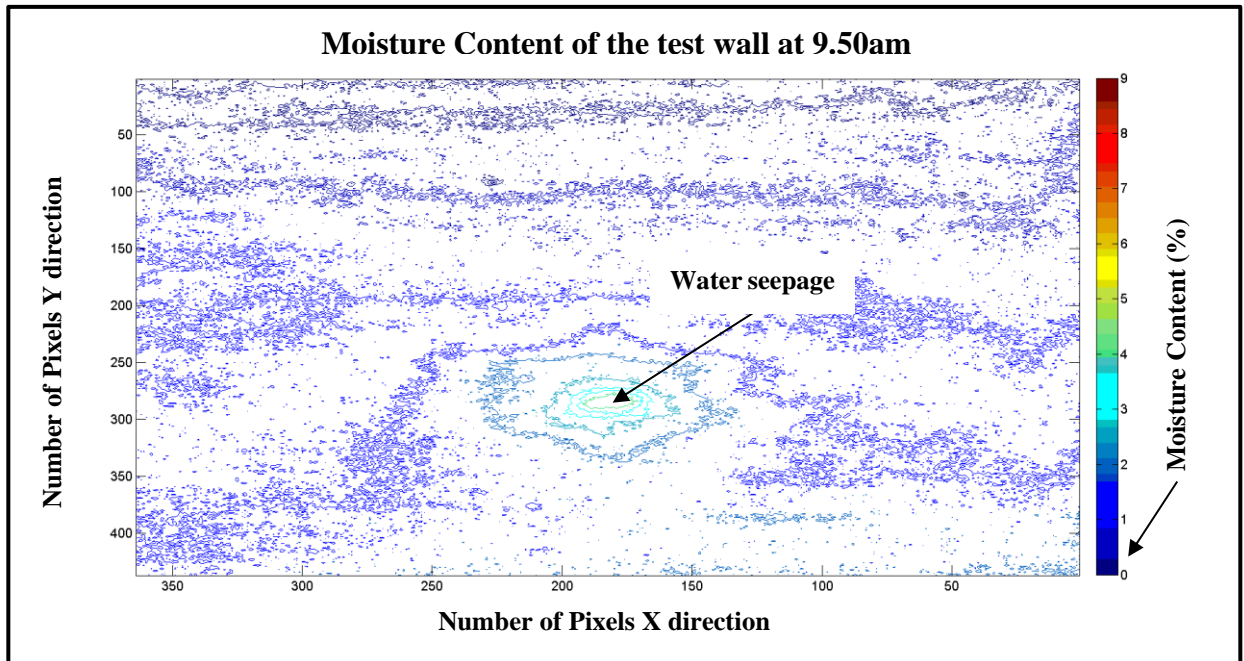


Figure 4-40 Moisture Content of the test wall at 9.50 am

Figure 4-41 shows the variation of moisture content in the test wall at 10.15 am. A temperature of 21.6 °C was selected as an average dry brick temperature of the test wall at 10.15 am in order to calculate the temperature difference of the wall at that time. This figure shows nearly 3.5% of moisture content occurred closer to the water tube marked by the light blue contours.

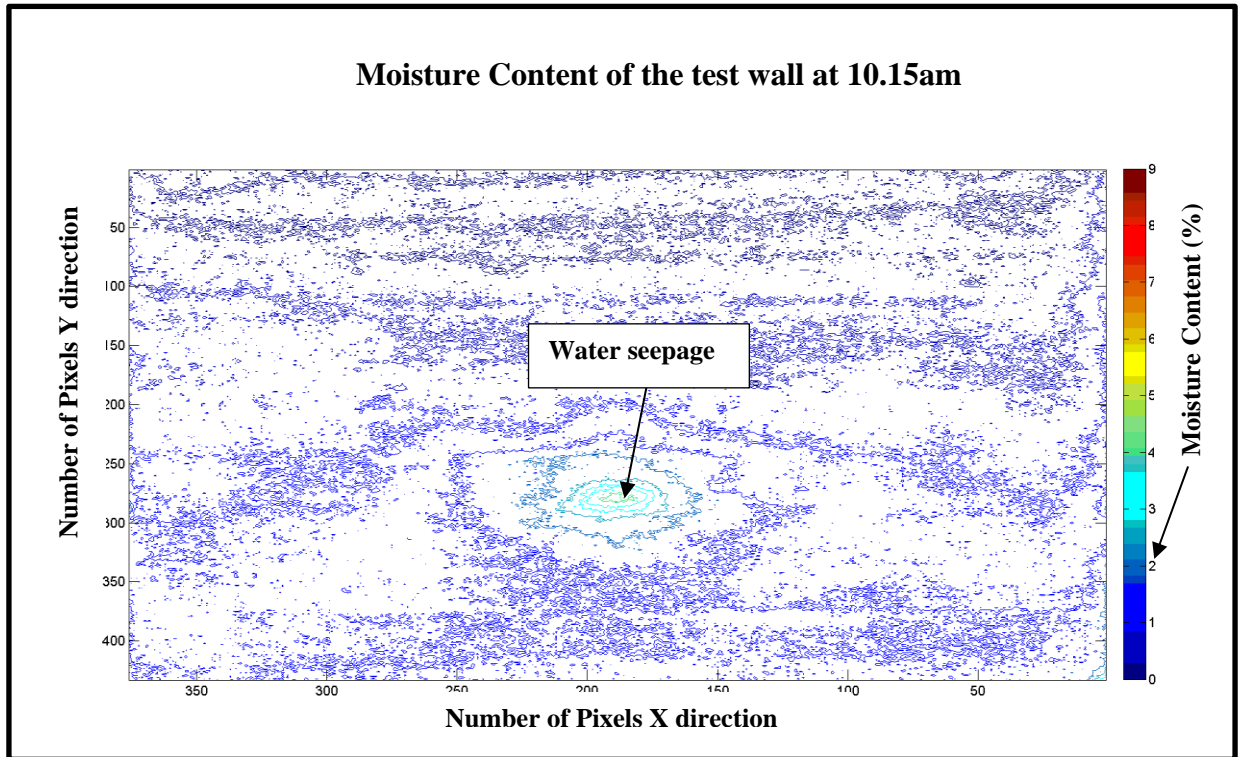


Figure 4-41 Moisture Content of the test wall at 10.15 am

Figure 4-42 shows the variation of moisture content in the test wall at 12.00 pm. A temperature of 21.9°C was selected as an average dry brick temperature of the test wall at 12.00 pm in order to calculate the temperature difference of the wall at that time. Points of equal moisture contents are shown by the contour plot, using the colour code to the right of the figure. Surface contours show that the surface moisture level reduced when the distance from the water source increased. Contour diagrams can be used to show different levels of moisture content during the wetting process. This figure shows nearly 7% moisture content occurred closer to the water tube marked by the light orange contours.

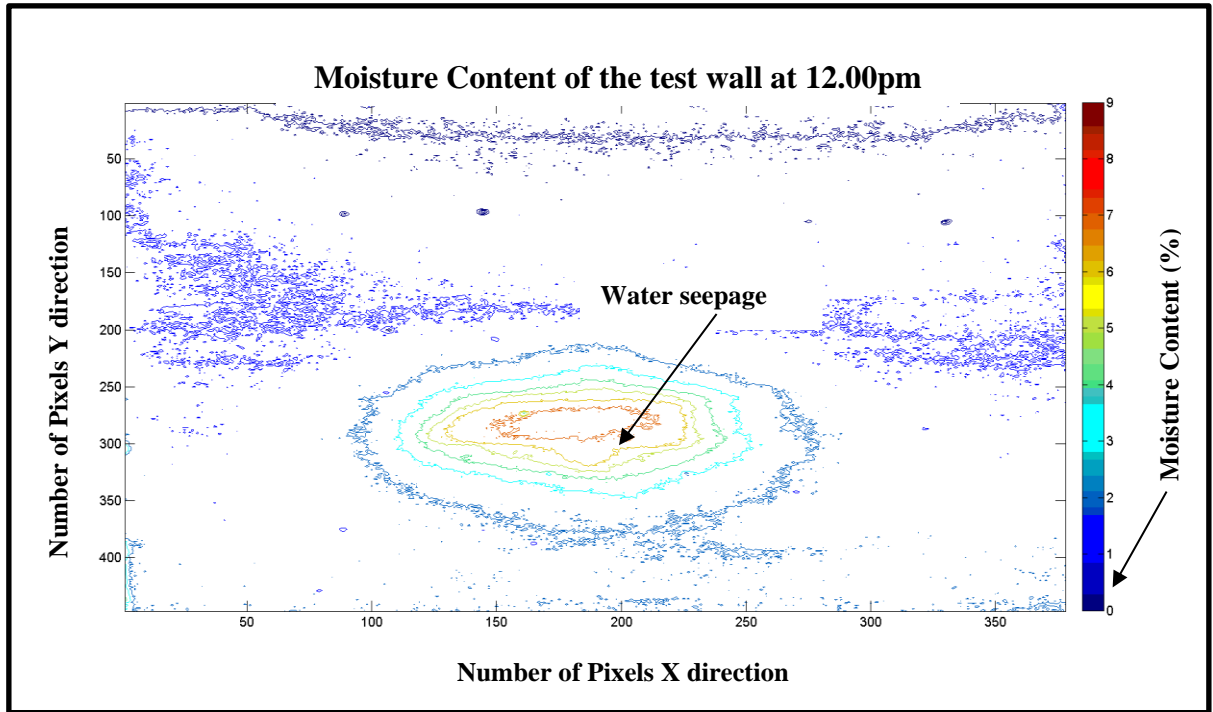


Figure 4-42 Moisture Content of the test wall at 12.00 pm

Figure 4-43 shows the variation of moisture content in the test wall at 1.00 pm. A temperature of 22.2 °C was selected as an average dry brick temperature of the test wall at 13.00 pm in order to calculate the temperature difference of the wall at that time. This figure shows that nearly 9% of moisture content occurred closer to the water tube marked by the light brown contours.

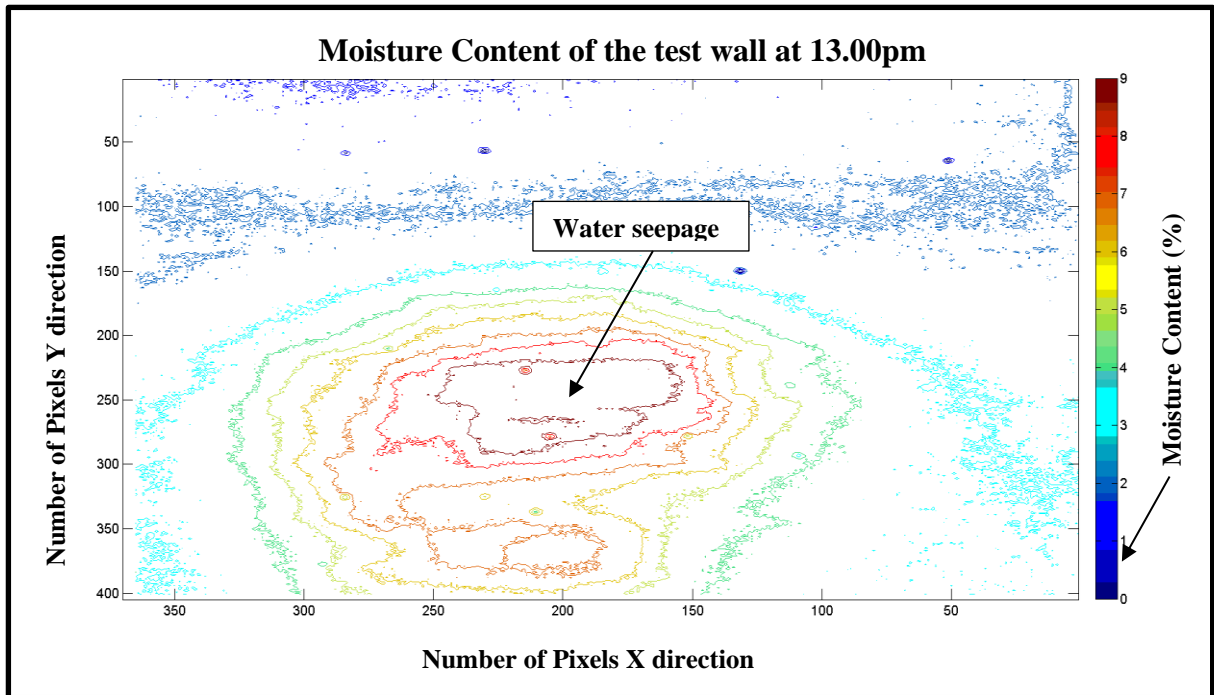


Figure 4-43 Moisture Content of the test wall at 13.00 pm

4.5.2 Experiment #2 Conclusions

The experiment demonstrated that infrared thermography, calibrated against measurements of moisture content, is an effective way to detect moisture anomalies in structural elements. The thermographic analysis represents the cheapest, most advantageous and quickest technique to be used to detect moisture anomalies.

The laboratory experiments have shown that once a seepage occurs in a brick wall, the temperature reduces. Therefore, it is possible to identify active seepages by measuring the rate of reduction in temperature. The opposite is also true, i.e. when the temperature increases towards the temperature of a drywall inactive seepages can be identified.

Figure 4-39 to Figure 4-43 shows that contour plots are a better way of visualising the moisture content and help to decide in what areas intervention is needed if the water reaches the saturation moisture content and may cause damage to the assets.

4.6 Thermography Site Trial

4.6.1 Introduction

A site trial of Infrared Thermography (IRT) was carried out during engineering hours on 18th and 19th of December 2015 with the aim of determining active water seepages on the tunnels of the District line. This site trial was incorporated with Euroconsult's annual brick tunnels laser inspection. The primary objective of this site trial was to identify active water seepage in the brick tunnels as well as test the system in a configuration that would allow the survey to be done from an engineering train, at the survey speed of 12km/h.

Thermography results were not validated with visual inspection because visual inspection could not identify small temperature differences to locate water ingress as accurately as thermograms. The temperature difference of 0.01 ° C can be measured using a thermal camera.

During the two site trial days, 99 sections of brick tunnels were scanned using a thermal camera. However, in this report, only the data from tunnel sections TL41, TL58 and TL77 were processed to identify thermal anomalies associated with water ingress and validate their location using Euroconsult's laser scanner images.

4.6.2 Water Ingress/Seepage into London Underground Assets

The majority of London Underground bridges and structures assets, as well as all of the Deep Tube Tunnels (DTT) assets, are constructed below the ground surface and are often vulnerable to seepage. Water seepage is due to rainwater, groundwater, water from damaged utilities and percolating through the ground. LUL acknowledge that if the structure or tunnel is built below the groundwater table, there is more of a chance that water will ingress into the structure due to the poor water tightness (G1417, 2013).

Tunnels and structures tend to “weep and seep” and LUL usually manages them effectively through the controlled diversion of seepage into drainage systems. However, there will be instances where the seepage, if left untreated, can cause structural deterioration of the asset itself and can cause damage and deterioration of ancillary structures and equipment. Additionally, seepage can have a detrimental effect on the aesthetic appearances at stations. It could also have an impact on the operational railway because of seepage affecting track, signalling, and power and communication systems (G1417, 2013). Currently London Underground performs a routine visual inspection to identify water seepage in the tunnel lining. The action to repair or control water seepage is typical as a result of the visual inspection evaluation.

In some cases, seepage into tunnels and structural assets could result in the ingress of ground (particularly with non-cohesive soils) as well as water. Such seepages have the potential to form voids behind the structure causing eccentric loading and instability. It could also cause ground settlement. Water ingress may also create health and safety risks to LUL staff and railway users.

Usually, LUL performs damp surveys (e.g. measuring moisture content, relative humidity, and temperature) and visual inspections to identify areas of water ingress. As a part of the survey, they use dye testing as well to identify a water path. Geotechnical information such as borehole logs and historical reports are also used to analyse the local strata. Most of the LUL’s civil assets were built on London clay. The Lambeth Group is between London clay (low permeability) and a chalk aquifer reduces the water reaching the surface and consequently causes pressure to build up underneath the London Clay. As this groundwater pressure increases on the clay, the low permeability of the clay pushes up and can also result in groundwater tracking along with the interface between more permeable layers. When the asset’s waterproofing fails around this interface, this often results in what appears to be concentrated points of ingress. Furthermore, LUL’s historical reports show that in some cases, ingress of water is mainly caused by surface water runoff primarily from rain (e.g. active ingress was witnessed during

the heavy rains). A dye penetration test performed by a contractor showed that when the road gullies are blocked, surface water from the roads and pavements can easily penetrate the underground structures when its water tightness failed. Leaking water mains (e.g. Thames water mains) could also influence the groundwater movement in local areas. As a consequence of these issues, temporarily active water ingress might appear within the assets (LW1341, 2012).

4.7 Scanning Methodology

The engineering train was driven smoothly through the tunnel without exceeding the target speed of 12Km/h to achieve expected results (without any noise in the captured data). To obtain useful data, the inspection was performed in places where suspicion of water seepage existed. The inspection was carried out using a locomotive and a flat wagon. A metal frame was assembled on the flat wagon, serving as a base to which the following equipment was fixed: six laser-camera units, one Lidar scanner (both from Euroconsult) and the Thermal camera-FLIR A 645 (see Figure 4-44). The laser scanner configuration was used to survey half of the sections (separated by the middle of the crown) for each run of brick tunnels known as TL sections. The thermal camera, however, was positioned to capture the haunch area of the tunnel, as according to the visual inspection reports, it is the area where the highest number of issues relating to water ingress takes place. The thermograms created by this scanning system represent the surface temperature distribution based on the emissivity value of the surface.

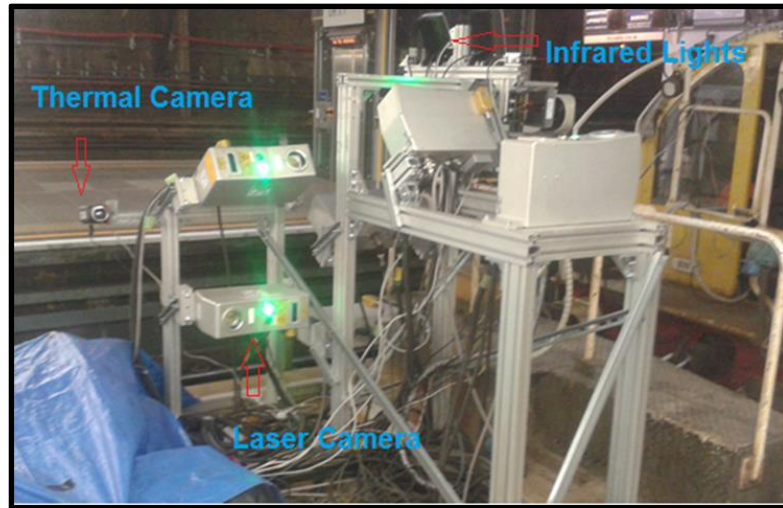


Figure 4-44 Metal frame with Thermal, Laser cameras and infrared red lights on a flat wagon

4.8 Method- Detection of Water Seepage/Ingress

Mapping the radiant temperature pattern can assist in the identification of thermal anomalies. These thermal anomalies allow for the detection of the presence of moisture or seepage zones on tunnels (surface cooling can be detected due to the water evaporation). In recent years, infrared thermography has been widely used in engineering applications due to the technological development of portable, cost-effective, thermal cameras and fast measurement and processing of digital images (Barla et al., 2015). For the tunnel lining inspection, thermally cold spots in the images usually indicate of areas of moisture (White et.al, 2014).

The tunnel walls are at different temperatures due to groundwater presence. Due to this variation, it is easy to identify spots of water infiltration on a thermogram. Certain geological models can help to identify probable water ingress places (e.g. if the tunnel passes under the water table the tunnel may be affected more than a tunnel above the water table). Results showed that moisture anomalies could always be seen as colder areas. The camera used to capture the thermal images were not capable of focusing clearly because of the movement of the train. In order to compare the results from the thermal camera with the results from Euroconsult images with prominent features (e.g. drip tray, cables) were chosen.

The approach is based on a contrast between temperatures in the captured thermograms to identify brick saturation.

4.9 Data Analysis

The data were captured in video format using the Research I.R Max software to identify possible thermal anomalies. An IR image source file contains the raw data with information about an object's temperature and emissivity. The recorded parameters are user configurable. Water seepage areas can be detected as relatively colder/dark areas when compared to the same surrounding material. This means that larger temperature differences in an assessed area present brighter contrast levels in the image (Kastberger and Stachl 2003).

Given that the inspection train travels at a constant speed of 12Km/h (3.3m/s) and the camera is capable of 6 frames per second (one frame every 0.167sec), at the highest resolution, whilst one frame is being captured, the train will have travelled approximately 0.5m. Therefore, each pixel of the frame will have a temperature value influenced by the temperature of a small length of the tunnel in a horizontal direction, which should be less than 0.5m if we consider the time taken to acquire and process the image or one frame.

To study the areas of interest, thermal pictures with at least 50% overlap were stitched together using the FLIR Tools+ software to create a larger image with more details. The areas for comparison were selected based on fixings attached to the wall. Thermograms showing drip trays (metal containers fixed on certain tunnel areas to collect water dripping from the surface) were selected as the areas that were easily identifiable on the thermal image data set and the Euroconsult's laser scanner data. Other fixed points on the tunnels (e.g. nameplates) were also used to identify the images.

The approach in creating the moisture contours map was similar to the approach followed for the wall experiment (section 4.5), where the temperature difference between the dry and wet brick wall was calculated and later transformed into

moisture content based on the equations determined previously (equation 4.2), using Excel, whilst MATLAB was used to plot the contours.

4.10 Tunnel 58 (TL58)

Tunnel 58 is located between Paddington and Edgware Road station and is 162m in length. Figure 4-45 shows the drip trays and a seepage area identified by the thermal camera in three consecutive frames. The drip trays are located between 127m and 128m from Paddington station to Edgware Road station.

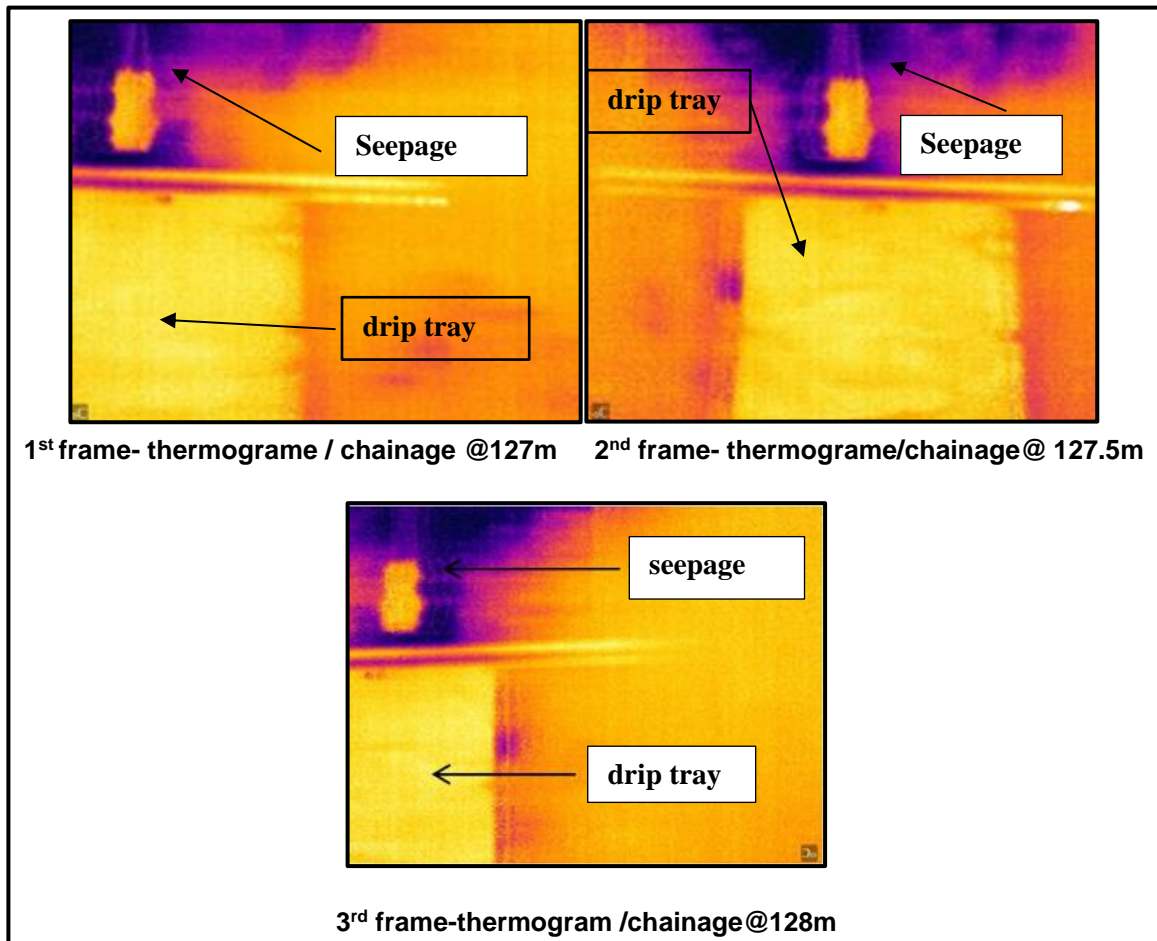


Figure 4-45 TL58 drip tray and water seepage location (between 127m and 128m) between Paddington and Edgware Road station

Figure 4-46 shows a panorama view (stitched frame 1,2 and 3 shown in Figure 4-46) with temperature measurements that easily identify features such as the drip tray, cables and the water seepage area in the TL58 tunnel section. The temperature measurements correspondent to lines Li1 and Li2 on the figure were plotted in Figure 4-47.

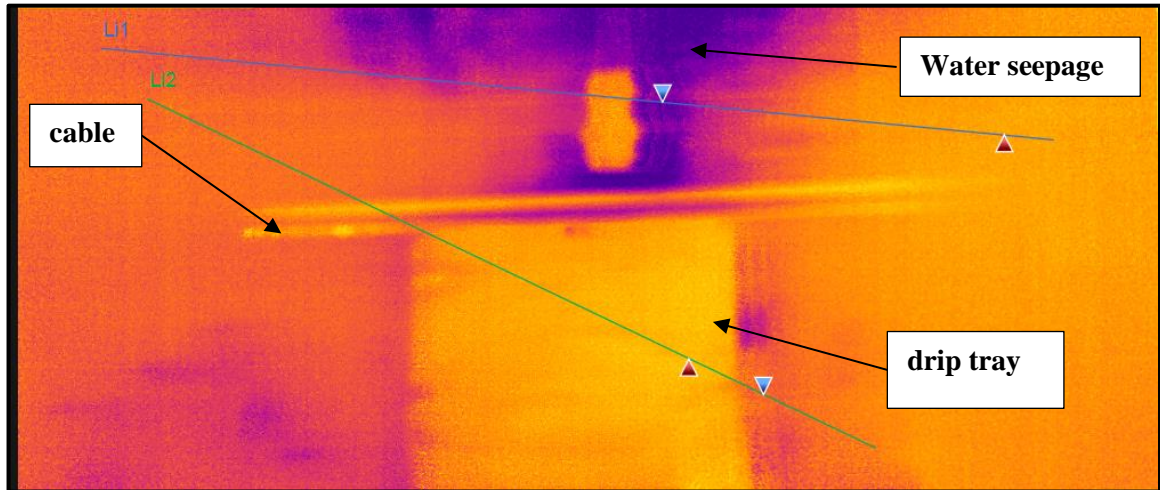


Figure 4-46 TL58 drip tray, cable and water seepage between Paddington and Edgware Road stations at chainage 127-128m

Figure 4-47 shows the temperature of different objects along the tunnel section at chainage 127-128m.

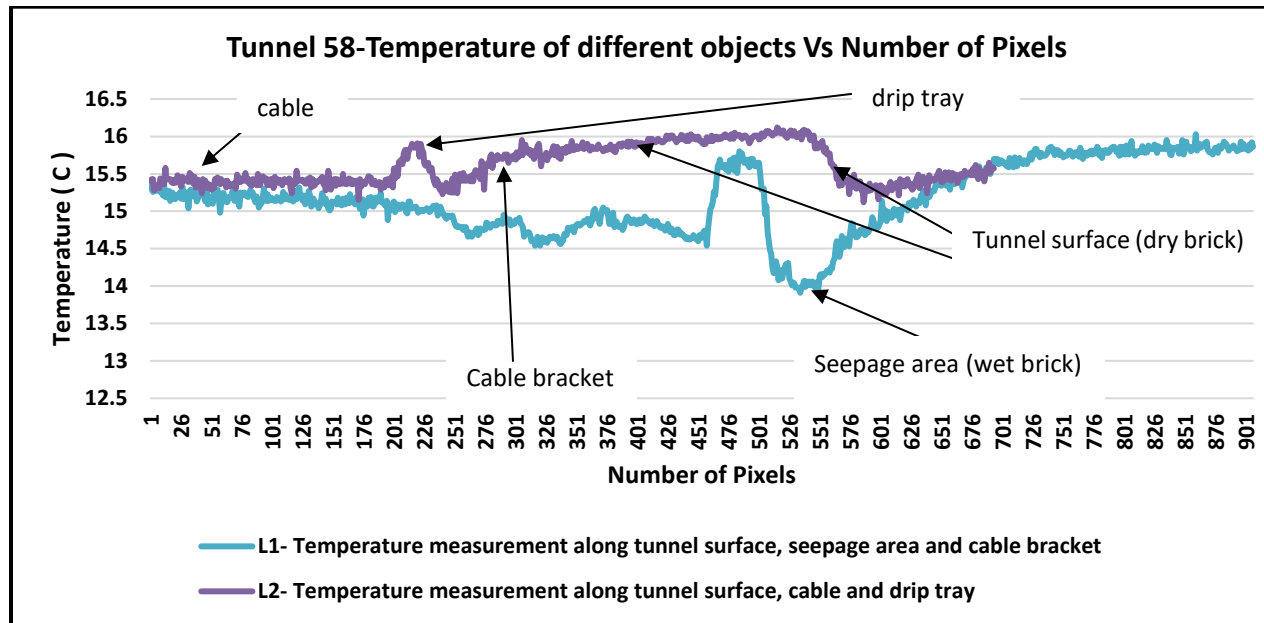


Figure 4-47 TL58 temperature of different objects between Paddington and Edgware road-stations between chainage 127-128m

In order to capture the changes in temperature of the bricks, the emissivity used is around 0.95, a standard value for thermal cameras. The highest temperature was recorded along the drip tray because it is made of metal and, as such, has a much lower emissivity than the standard value selected, therefore the temperature determined by the camera will be higher than the real temperature of the material.

The aims on this experiment were;

- To determine the temperature of the dry brick. Identify cooler areas on the brick as these are an indication of water.
- Identify other features that could be checked, like light bulbs and cable brackets.

Temperature measurements along the seepage area are lower than other objects of the tunnel. The temperature of the tunnel surface varied between 14.9 °C and 15.5 °C. The temperature of the cables is similar to the temperature of the drip tray and the dry tunnel lining surface. This same phenomenon was observed in the brick wall experiment (see section 4.5).

Equation (4.3) below, was used to convert the surface temperature to create the moisture map (see Figure 4-48). This equation was derived from the lab test (see section 4.5) and 15 °C was selected as an average dry brick temperature for tunnel58 (TL58)

Moisture content = $-2.1588 * (\text{reference temperature} - \text{observed temperature})$ (4.2)

The following assumptions were made when converting the tunnel's surface temperature into moisture content using equation (4.2).

- The porosity of bricks in tunnel sections TL41, TL58 and TL77 are the same as the bricks used in the wall in the lab test (see section 4.5) to derive the equation (4.2).
- The emissivity value is the same to all materials in the tunnel.
- It was assumed that temperatures higher than the reference temperature (obtained from dry brick temperature) were generated by different materials, therefore, temperatures higher than the reference temperature were disregarded as the presence of moisture reduce the temperature of the bricks.

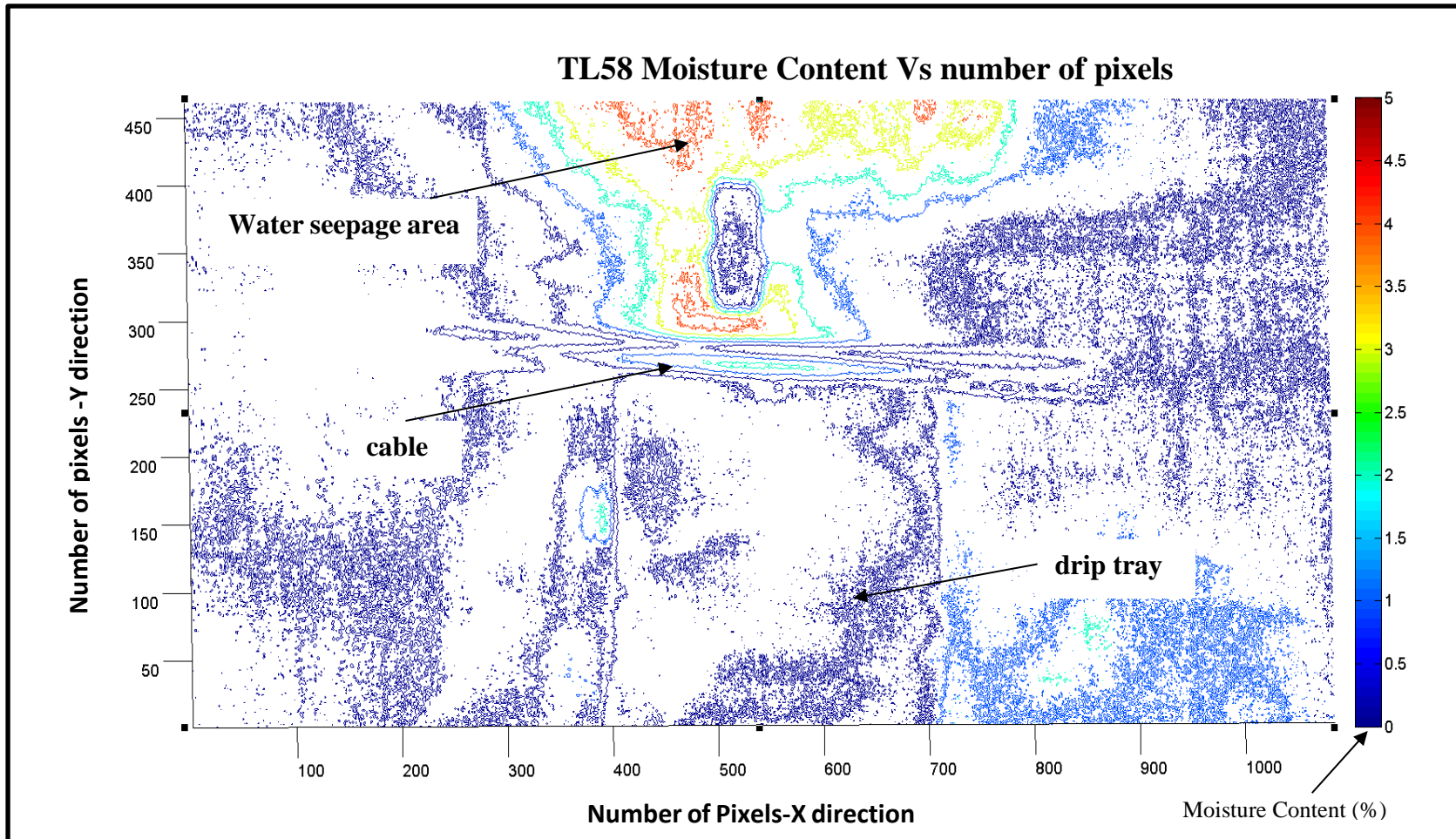


Figure 4-48 TL58 Moisture content vs. the number of pixels between chainage 127m and 128

When converting the temperature variations in moisture content, it is clear where the areas of larger moisture content where maintenance should be concentrated.

4.11 Tunnel 41 (TL 41)

Tunnel 41 (TL41) is 656m long and is situated between White Chapel and Stepney Green stations. Data from the 2015 laser inspection were used to locate, between chainage 90m and 96m - eastbound the features identified in the thermographic images, such as drip trays and cables. Figure 4-49 shows the drip trays (indicated in the picture) and seepage (dark rectangular area immediately below the drip trays shown by blue rectangular), as identified by the 2015 laser inspection performed by Euroconsult, between White Chapel and Stepney Green.

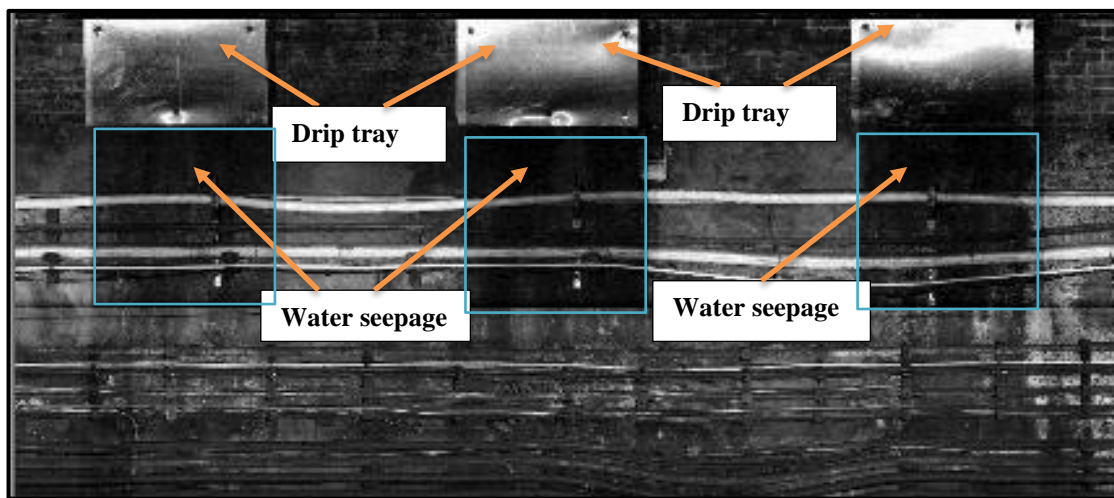


Figure 4-49 TL 41 drip trays between 90m and 93m Eastbound laser scanner 2015 inspection

Figure 4-50 shows the thermal image of Figure 4-49 between White Chapel and Stepney Green stations (eastbound). This figure shows the location of cables, the drip trays and the location of water in the brick lining. It is likely that the lower temperatures are due to the drip trays as shown by the vertical pattern, than a seepage through the bricks. This probably indicates a blockage on the drip tray drainage system or that it does not have enough capacity to drain the water

seeping through the brick lining. These results show that thermal images can provide not only information about seepage through the lining but identify if a water seepage control method is performing adequately.

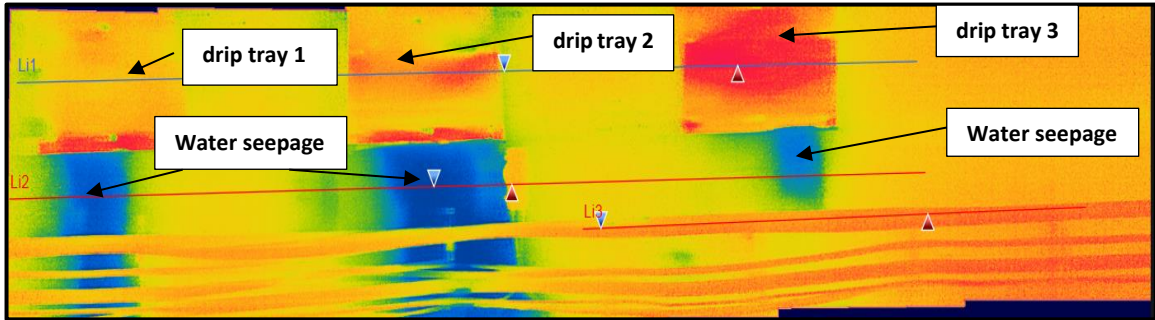


Figure 4-50 TL41 thermogram panorama view between chainage 90m and 93m (Eastbound)

The values of temperature determined by lines Li1, Li2 and Li3 on Figure 4-50 were plotted on Figure 4-51, showing temperature measurements of different objects between chainage 90 and 93. Again, the temperature of the drip trays were higher than in other places, given the material characteristics. It is also noticeable that the electric cables have higher temperatures, as expected given the dissipation of heat in the presence of a current. The temperature below drip tray 2 was lower than drip trays 1 and 3. This value could indicate that there is a larger overflow at location 2 compared to 1 and 3, potentially showing that the seepage in location 2 is larger than in the other locations.

Furthermore, Figure 4-51 shows significant temperature differences (2°C) between the water overfilled area and that of the tunnel surface.

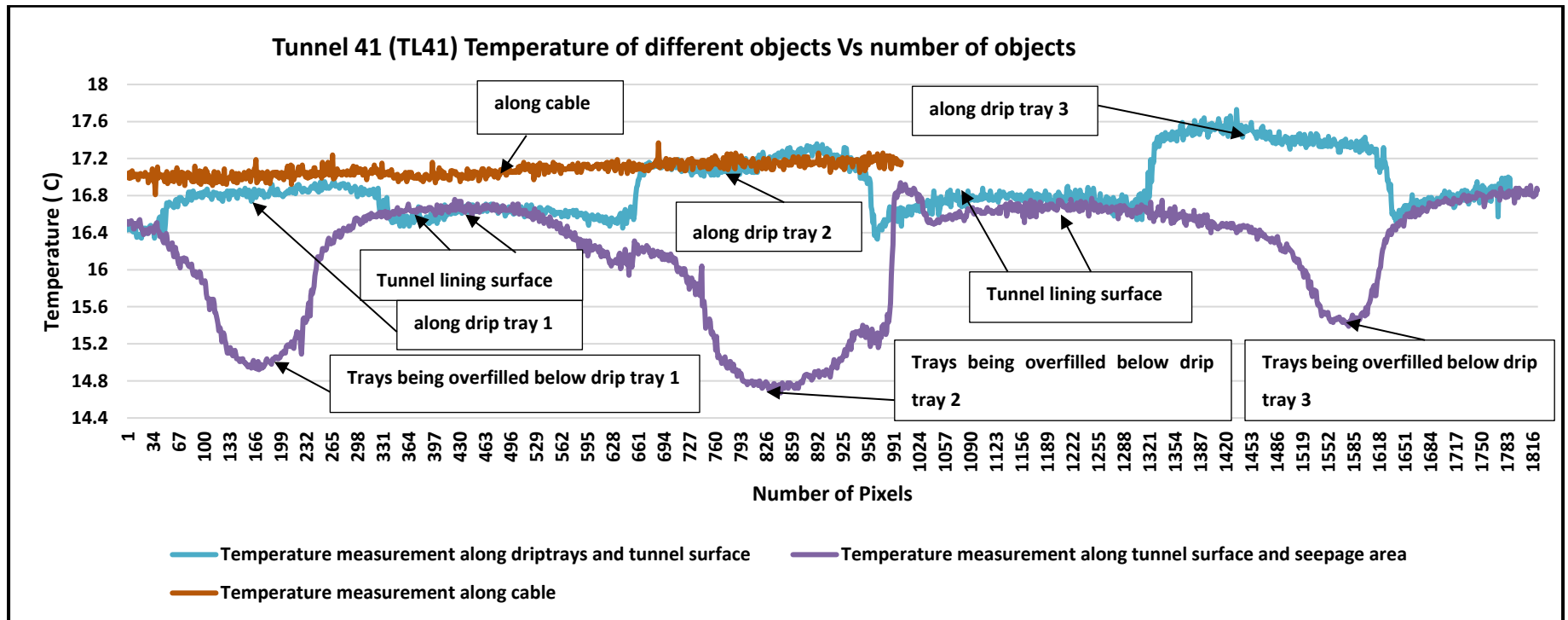


Figure 4-51 TL41 temperature measurements of thermograms on different objects between chainage 90m and 93m (East bound)

Figure 4-52 shows the surface moisture level of the different objects of TL41. The average dry brick temperature of 16.6°C was measured from the thermogram between chainage 90m and 93m as a tunnel temperature to calculate surface temperature differences. The equation [3.1] was used to convert the temperature differences into level of surface moisture. As lower temperatures were an indication of water in the tunnel, temperatures higher than the dry brick were disregarded and appear as 0% moisture.

Figure 4-52 also shows that moisture levels below the drip trays were higher than 6% with drip tray 2 showing values around 8%. Furthermore,

Figure 4-52 clearly indicates that higher moisture levels were observed below the drip trays because the trays were overfilled. The surface moisture level of the tunnel lining can be calculated and compared with different epochs using thermography inspection.

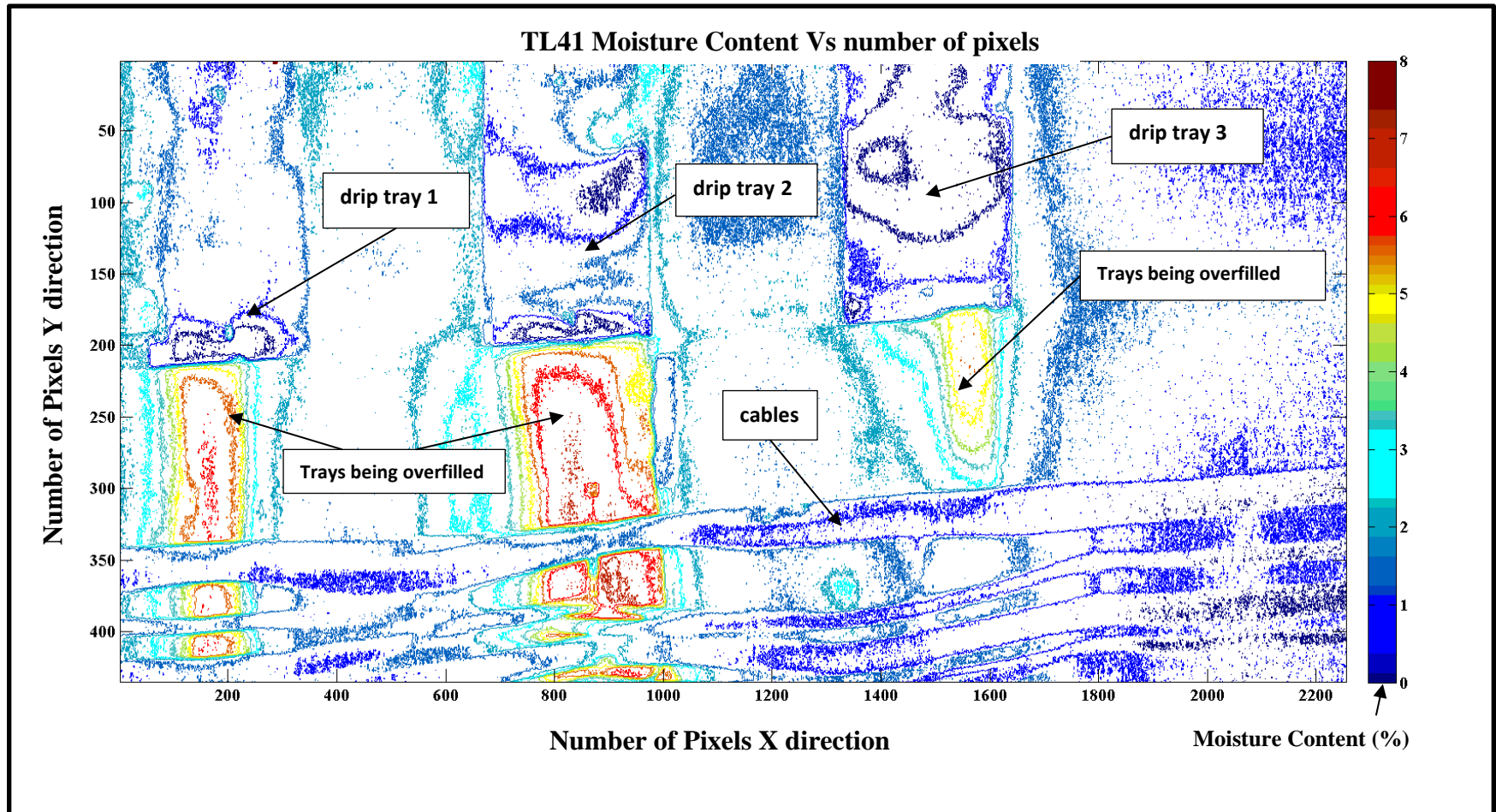


Figure 4-52 TL41 Moisture content vs the number of pixels between chainage 90m and 93m

4.12 Tunnel (TL 77)

Tunnel 77 (TL77) is 303m long and is situated between Liverpool Street and Aldgate stations. Figure 4-53 shows the TL77 drip trays and water seepage locations between chainages 16m-20m, identified by the Euroconsult surveying of 2015. The picture shows clearly the 2 sets of drip trays as well as cables and other fixtures in the wall.

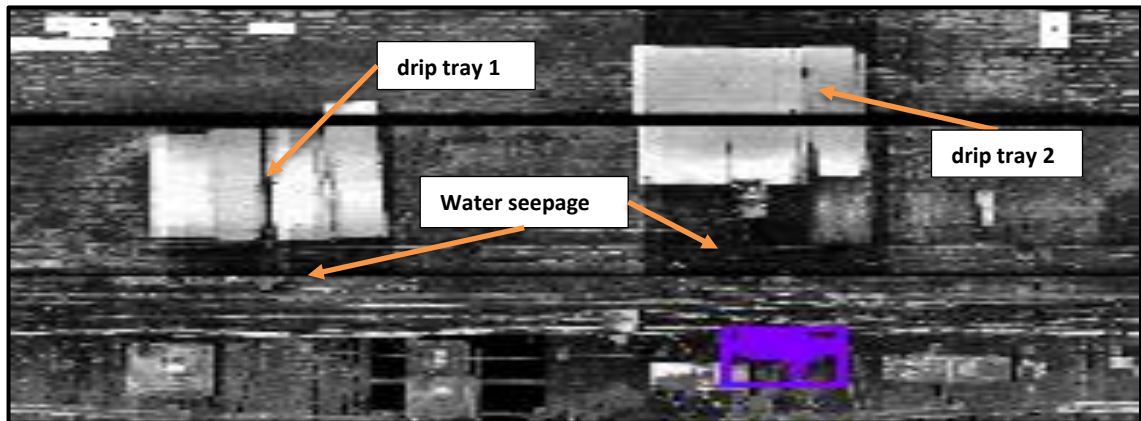


Figure 4-53 TL7 drip trays and water seepage locations between chainages 16m-20m (between Liverpool Street and Aldgate stations -Eastbound) - 2015 Laser Inspection

Again, the drip trays were used as a feature to identify the correct area from the thermal data collected. Figure 4-54 shows the result of stitching the pictures correspondent to the scene. Significant temperature differences were observed in the areas where water ingress has been detected (below the drip tray 1 and 2).

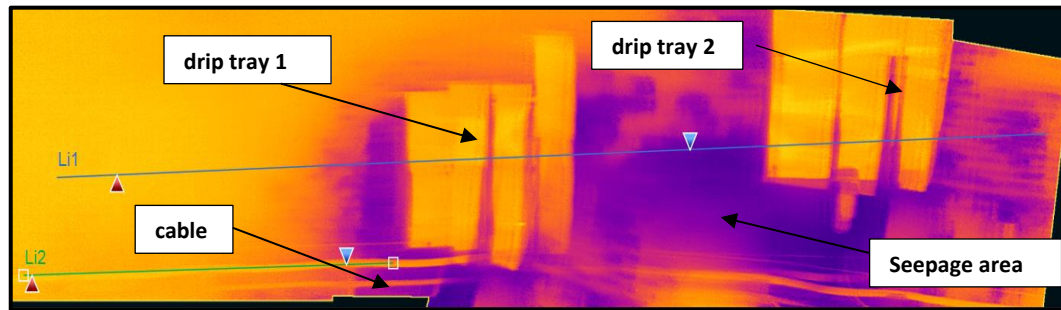


Figure 4-54 TL77 thermogram panoramic view between chainage 16m and 20m (southbound)

Temperature lines Li1 and Li2 were defined and the temperature along these lines was plotted in Figure 4-55. These lines go through different objects and the temperature variation caused by not only the seepage, but also different materials can be seen. Figure 4-55 shows the temperature measurements of different objects (drip tray, cable, tunnel surface and seepage area). The beginning of Li1 was used to identify the temperature of the dry bricks. It is also worth mentioning that the drip trays are at a temperature similar to the bricks and are surrounded by areas of lower temperatures attributed to higher moisture content of the bricks.

The analysis of the data is shown in Figure 4-56 where the temperature is transformed in moisture content on TL77, between chainage 16m and 20m. The average dry brick temperature of 17.2 °C, from Li1, was selected as a dry tunnel temperature, allowing the calculation of the surface temperature differences. The figure shows that the moisture levels around the drip trays are above 6%, whilst above and in the between the drip trays, areas with 9% can be identified. The results indicate that it is likely that another drip tray would be needed in the middle to collect water from the region with higher moisture content.

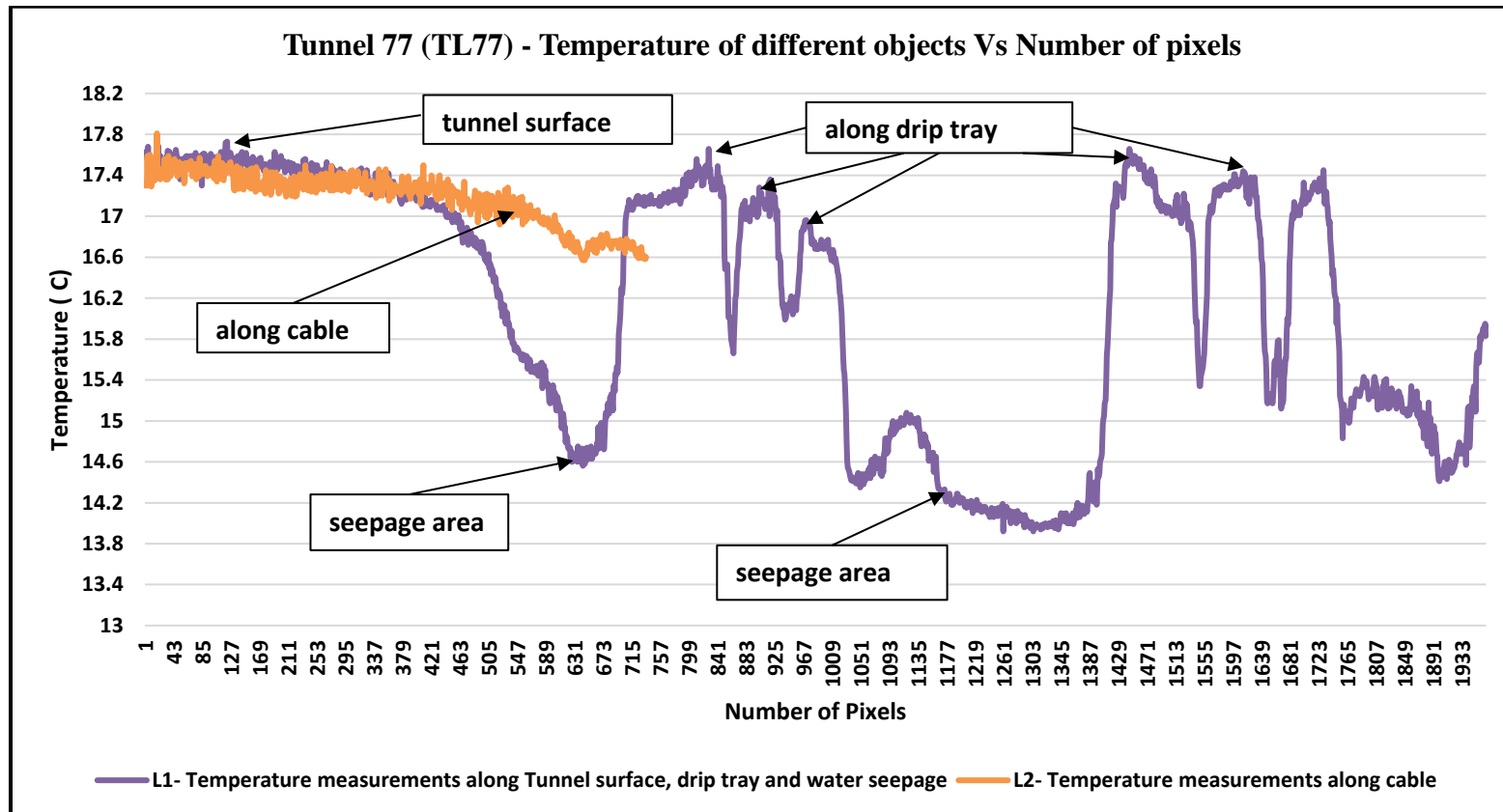


Figure 4-55 TL77 temperature measurements of thermograms on different objects between chainage 16m and 20m (southbound)

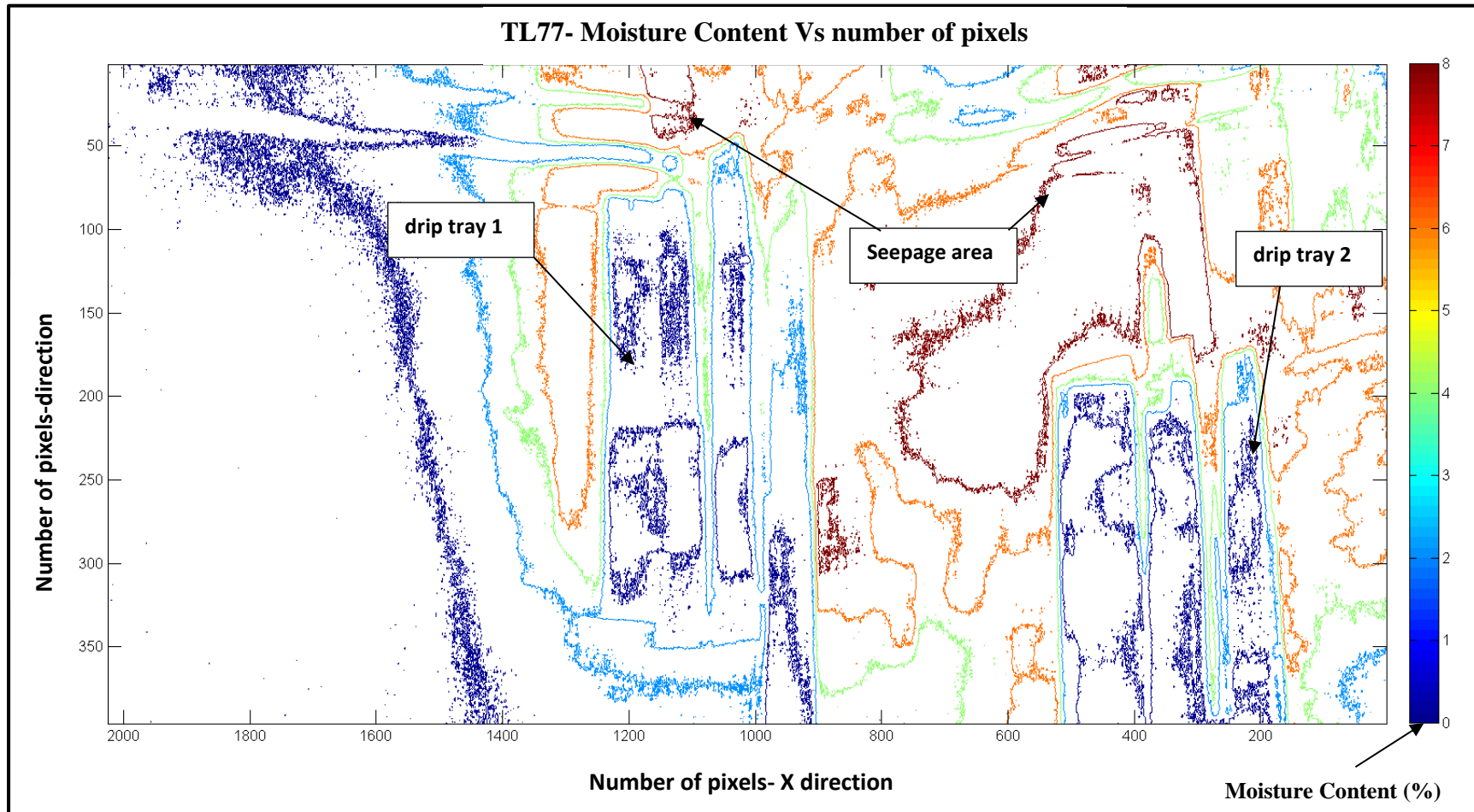


Figure 4-56 TL77 Moisture content vs the number of pixels between chainage 16m and 20m

4.13 Thermography Site Trial Conclusion

This trial showed that a combination of the laser scanner and thermography can be used synergistically to provide infrastructure owners/managers with a comprehensive and efficient method of monitoring water seepage and use proactive maintenance.

The following conclusions were drawn based on the results of the tunnel thermal survey.

- Brick moisture content can be identified by a contrast of temperatures in a thermogram and, by understanding this relationship, contours of moisture content can be plotted, indicating areas of active seepage.
- LUL relies on visual inspections to determine the location of water ingress in tunnels, however, given the conditions of a tunnel, this is a difficult task as seepage is only noticeable by the naked eye when it is already established. Thermographic inspections can be performed in any environment and provide measurements even at very low moisture contents (less than 3%), allowing a more accurate location of the defect. Also, light is not required, and a thermal camera could be used in the dark or on any automated system.
- This site trial proved that Infrared Thermography is a much more suitable technique to identify water seepage in brick tunnels than laser scanners. A comprehensive data set could be obtained by attaching thermal cameras to normal trains allowing the data collection to be done at any time on a tube line. Comparing different epochs would allow asset managers to react before a seepage is established, potentially eliminating the risk of system disruption caused by water ingress in tunnels.
- The results have also shown that the thermal camera could be used to monitor other features in the tunnel, such as location of brackets to hold

the cables, determine if light bulbs need replacement and check the performance of drip trays.

- During this site trial, large quantities of data were acquired but were not analysed due to time constraints. Therefore, this site trial was a proof of concept of an automated way of data analysis and interpretation.

Chapter 5. Case Study - HC3 Underbridge North East Wing Wall Monitoring

5.1 Introduction

In the railway industry, it is common practice to monitor deformation using surveying techniques or a total station and prisms where a network of points is observed manually or by an automatic system (point-based measurements) allowing pre-defined points to be monitored and trends defined. New technologies such as TLS and CRP are becoming common surveying techniques that allow high levels of automation and the quick surveying of the whole structure without an interruption of services. These technologies, combined or not, allow for the identification of many defects that only a visual inspection could identify. The downside is the large amount of data generated, rendering the process slow and creating data visualisation problems but, with advances in computer power, it is foreseen that this problem will soon be overcome.

The primary objective of this case study was to assess the possibility of using the terrestrial laser scanner (TLS), close-range photogrammetry (CRP) as a measuring tool to identify defects in structures, such as loss of bricks and extent of cracking, as well as excess movement due to external actions. The TLS and CRP data were compared to Total Station (TS) surveys of the area to determine if the deformation of particular points of the structure was accurate. This indicated the quality of the captured data. Furthermore, this chapter demonstrates the steps followed by the author in defining adequate procedures to carry out surveying, using TLS and CRP, as well as demonstrating the possibilities of such techniques in determining the change in the shape of the whole structure, which is difficult to do when only discrete points are being used, as is the case with a TS survey. In order to test these technologies a wing wall, located on the North-East Wing of the HC3 Underbridge, was chosen.

5.2 Structural Health Monitoring (SHM)

Over the past few decades, structural health monitoring (SHM) has been an important field of structural engineering, and a significant amount of research has been conducted in this field. With the support of various sensors, such as temperature measuring devices, inclinometers, and accelerometers all deployed on a structure, its health condition can be determined. A warning signal can be promptly announced by the developed diagnostic theories when the structure exceeds its safety margin (Cheung, *et al*, 2007). Systems for SHM, assessment of structural performance and damage identification have been used mostly for critical infrastructure assets, in which significant capital investments and large losses, due to failures and breakdowns, justify the investment in structural monitoring systems (Farrar & Worden 2007). The data acquired by these systems are the starting point to develop strategies to reduce operational and maintenance costs as well as to improve performance and quality. These types of investments are now easier to substantiate given the advancements in sensing technologies that reduce fabrication and installation costs, thereby increasing reliability (Delgado *et.al*, 2016).

To assess their physical and functional performance, bridges and other structures require frequent inspections during their operational life. The value computed in design and the assumptions made during the structural modelling may vary from the actual structural response. This may be due to various reasons, such as environmental loading (e.g. earthquakes and winds), the live load on bridges and structures and the variation in structural materials and structural properties of members and joints. The assessment of deformation, deflection, vibration level and concrete cracking give the best indication of the integrity of the structure (Zhao and Han, *et.al*, 2016).

Regular inspections are performed to assess the condition of an asset. During an inspection, the inspector identifies structural safety, any likely future problems and also determines any maintenance needs. Visual inspections cannot be performed frequently due to asset location, height and sometimes the requirement to close lanes for traffic. Despite this, frequent

inspection/monitoring of bridges and structures are necessary to assess their safety and serviceability (Park *et al.*, 2007).

Structural Health Monitoring systems can be expensive, particularly when installation (survival rate) and maintenance costs are added. In embedded monitoring (contact monitoring), the system network of sensors that are embedded (permanently attached) into the structure that measure monitoring parameters such as stress, temperature, acceleration and vibration are monitored over time. An embedded monitoring system is invasive, where drilling or glueing of the target or sensor is required. This can result in safety and timing issues during installation as well as subsequent maintenance. Additionally, embedded monitoring systems typically consist of a complex set of various types of sensors and other devices and software, which requires professional installation and monitoring (Zhao and Han, *et.al*, 2016). High accuracy, low cost and easy to integrate into data acquisition sensors are a vital part of SHM. In a wired monitoring system, maintenance and replacement cost are likely to occur, reducing reliability between sensors and data acquisition (Bao and Li, 2016)

To overcome this difficulty, non-embedded monitoring (non-contact monitoring) methods (e.g. laser scanner, photogrammetry and thermography) of inspection start to gain attention as a part of the maintenance procedure. In a non-embedded monitoring system, the monitoring parameters are observed without touching the structures. An optical non-contact technique is used, due to its ability to measure a surface without the need of physically touching or probing the object. Table 5-1 shows the advantages and disadvantages of the embedded and non-embedded monitoring system.

Table 5-1 Comparison between embedded and non-embedded monitoring system

Embedded Monitoring System		Non-Embedded Monitoring System	
Advantage	Disadvantage	Advantage	Disadvantage
Monitors processes and assets accurately, reliably and continuously	Requires professional installation and maintenance	Rapidly used for large areas of structure (area information)	No real-time information, data needs to be post-processed for informed decision making
Collects and processes asset data in real-time	Maintenance and replacement costs are higher	Cost-effective, fast and reliable	Requires a minimum distance between target and instrument, e.g. difficult to monitor party walls when surrounding area is constructed
	Inspection required to touch the inspectable part of the asset	Inspection can be performed for non-tangible parts of the asset	
	Requires a substantial maintenance	Requires less maintenance	
	Only discrete information is obtained, no information about surrounding area of the structure		

Table 5-2 shows how the technology for monitoring infrastructure assets has been changing in the last sixty years, with the introduction of new sensors and methods based on laser scanners and image correlation.

Table 5-2 Technology for monitoring infrastructure (Mazzanti, 2016)

Stressmeter						
Levelling			Continuous Monitoring			
Theodolite			US standards	Early Warning Monitoring	European Standards	Digital Image Correlation
Extensometer	Vibration Monitoring		Total Station	GSM data transmission	Laser Scanner	Drones
Piezometer	Submarine Monitoring	Datalogger	Time Domain Reflectometry	Fibre Optics technology	Multi-parametric borehole systems	Web based data management
Load cell	Inclinometer	Laser distance-meter	In place inclinometers	GNSS Technology	Interferometric Radar technology	Wireless monitoring
1950s	1960s	1970s	1980s	1990s	2000s	2010s

In the existing or current methodology, sensors (e.g. strain gauges, tiltmeters, crack meters, accelerometers and extensometers) or survey targets are placed in several locations on the structures for the assessment of the structural safety and reliability. These sensors must be installed, maintained, and frequently recalibrated to produce reliable and repetitive results. The data must be processed and interpreted to obtain reliable information which may be complicated and time-consuming, sometimes out of the control of the Structural Engineer.

Before deploying any sensors or data interpretation, the following questions must be answered (Mair, 2015):

- What sensors are needed to measure the performance of structures and assets?
- How can they be made robust?
- How can the data be analysed to give reliable, meaningful results?

The questions above must be answered taking into account the fundamental requirements of today's structural inspections that are listed below:

- Knowledge of the current condition of the structure

- Early detection and monitoring of critical areas
- Documentation of damage development
- Basis for the timely planning of construction measures
- Realistic maintenance budget planning
- Need for a systematic inspection strategy

5.3 Site Location and Description of Structures

The north-east wing wall investigated in this case study is located just outside of Ladbroke Grove Station (Figure 5-1). Wing walls support the underbridge M176/HC3 between Ladbroke Grove and Westbourne Park Stations. Underbridge HC3 carries the Hammersmith and City Line over the B450/Ladbroke Grove carriageway. The bridge is close to residential dwellings, amenities and the A40 carriageway overbridge. Access to the underside of the structure can be gained via the B450, Ladbroke Grove.

The bridge HC3 is a single span structure that carries the Hammersmith and City Line from east to west spanning approximately 9m over a single carriageway section and pavements of Ladbroke Grove Road.

The bridge deck comprises three plate girders with perpendicular concrete planking supported on concrete bearing shelves capping the brick abutments at each end. The abutments are clad in corrugated PVC from the bearing shelf level to approximately 0.60m above the pavement level where stainless-steel cladding continues to the pavement level.

The parapet wall of the bridge measures approximately 2.30m from the bridge deck level and comprises riveted steel sheets. The wing walls are vertical and flush with the abutments, and form party walls with adjacent buildings and properties.

The North-West wing wall comprises a 2.42m wide and approximately 4.23m high rendered brick section abutting onto an access door to Ladbroke Grove Station. The South-West wing wall includes a 4.23m high brick section dropping to a height of 3.05m before abutting onto the main entrance to

Ladbroke Grove Station. The brick section of the north-east wing wall is approximately 7.05m wide and approximately 4.50m high, topped with a galvanized steel palisade fence. The south-east wing wall comprises a 1.80m wide and 4.30m high brick section, abutting onto a lower section of the retaining wall of more recent construction, separated by a rubber-sealed joint (Intrusive Survey and Ground Investigation Report LUL, 2014).



General View of Southern Elevation



General View of Northern Elevation of bridge HC3 showing part of the A40 Bridge.



General View of the east abutment and southeast wing wall.



General view of the east abutment northeast wing wall.



General view of the west abutment and southwest wing wall.



General view of bridge soffit

Figure 5-1 Multiview of Abutment and Wing wall

5.3.1 Principal Inspection Report

The last Principal inspection report for the north-east wing wall was carried out on 21/06/2013. The element abutment scored 95.83%, whilst the element deck scored 90%; indicating that both bridge elements were in good condition.

The recommendations from the principal inspection report are as follows:

- The old standing diagonal crack in the north-east wing wall was previously reported as hairline. There has been a change since the principal inspection of 22/05/2009, where the crack has become displaced by 11mm, measured by the crack meter (see Figure 5-2). Therefore the crack must be monitored.
- Minor vegetation by the south-east bearing
- Minor vegetation by the north-west bearing

5.4 Geology and Reason for Monitoring

The geology of the wing wall and bridge location was established using the British Geological Survey (BGS) 1:50 000 scale map reference no. 270 South London – Solid and drift geology, and confirmed on the BGS 'Geology of Britain Viewer' website showing the area to be underlain predominantly by the London Clay Formation (Intrusive Survey and Ground Investigation Report LUL, 2014).

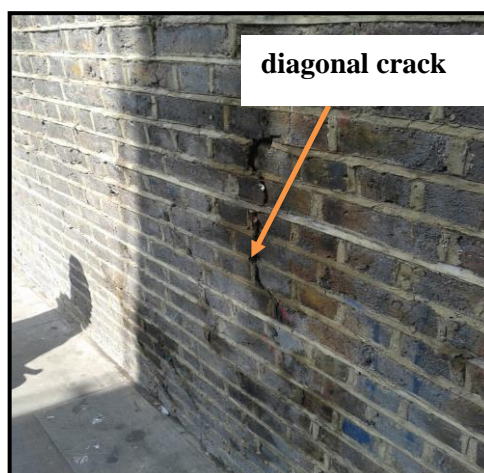


Figure 5-2 Diagonal crack to the northeast wing wall adjacent to the east abutment (LUL, principal inspection report 2013)

The intrusive survey and ground investigation report 2014 described a vertical crack with approximately 1-10mm aperture, approximately 1.0m in length in the lower portion of the north-east wing wall. This crack was still visible on a site visit (November 2015) and no repair work was performed.

The feasibility report for the prevention of bridge strike (LUL, 2013), intrusive survey and ground investigation report (LUL, 2014) and principal inspection report, 2013 recommended the need to monitor this crack and the wall movement. Crack development, mortar loss in joints and wall deformation can result in dangerous situations for road users and surrounding structures. Therefore, a monitoring regime was established by a London Underground structural maintenance team. Initially, the use of a TLS was suggested by the LUL Survey Manager. Then, close-range photogrammetry and total station survey were utilised by the researcher as a part of this work. Details of data collection for the different epochs are shown in Table 5-3.

Table 5-3 Data collection for the different epochs

Epoch	Date	Instrumentation	Data Captured by
1	March-15	Laser Scanner- P20	LU- Survey Team
2	June-15	Laser Scanner- P40	LU- Survey Team
3	Sep-15	Laser Scanner- P40	LU- Survey Team
4	Dec-15	Total Station- Leica TS-06 Flexline	Researcher
		Digital Camera-D700	
5	Jan-16	Total Station- Leica TS-06 Flexline	Researcher
		Digital Camera-D700	
6	Feb-16	Total Station- Leica TS-06 Flexline	Researcher
		Digital Camera-D700	
		Laser Scanner- P40	LU- Survey Team
7	March-16	Digital Camera-D700	Researcher
		Laser Scanner- P40	LU- Survey Team
8	April-16	Digital Camera -D700	Researcher
		Total Station	LU- Survey Team
		Laser Scanner- P40	LU- Survey Team

Epoch	Date	Instrumentation	Data Captured by
9	May-16	Digital Camera-D700	Researcher
10	June-16	Digital Camera-D700	Researcher
		Total Station	LU- Survey Team

5.5 Total Station Survey

A TS consists of a theodolite with a built-in distance meter (distancer), and so it can measure angles and distances at the same time. The latest TS has an opto-electronic distance meter (EDM) and electronic angular measurements. The slope distance, horizontal distance, vertical, and horizontal angles can be measured using a TS. Then, the horizontal distance, the height difference, and the coordinates are calculated automatically, and all measurements and additional information can be recorded (Zeiske, 2015). In land surveying, TSs are used to produce topographical maps and detailed surveys for various applications. For engineering surveying applications, TSs are used for deformation measurements and setting out work.

Figure 5-3 shows an automatic total station (ATS) real-time monitoring system which was used by a monitoring contractor at the Bank station capacity upgrade programme. This type of continuous monitoring set up requires a weatherproof casing without interruption of the targets line of sight. This system measures the absolute displacement of the targets. This motorized total station can be controlled remotely, using remotely operative software to track the targets and do the measurements without the need for manual intervention. The software can manage measured monitoring points, auto calculation and self-correction (Huang *et al* 2006). However, maintaining real-time monitoring systems (e.g. ATS) and their accessories (e.g. data logger, dial-up connection to connect to the server and continuous power supply) are costly to provide a reliable monitoring solution.



Figure 5-3 Total Station on fixed location for deformation monitoring (image from Geodata)

5.5.1 Targets

Highly reflective materials such as glass must be used as targets to get a high return signal when measuring distances using a TS. Electromagnetic waves generated by the TS travel through the atmosphere to the reflective prism or target and are reflected back to the instrument in order to calculate the distance. Targets and reflectors come in a variety of colors, sizes and angles to suit most kinds of monitoring applications. A sample of targets are shown in Figure 5-4, where different types of prisms are on the top row and retroreflective targets are shown on the bottom row (Soni, 2016).



Figure 5-4 Examples of prism (top) and retroreflective targets (bottom) used with total stations (Soni, 2016)

Recent case studies in the literature and industry have shown that the application of the TS in deformation monitoring of structures, bridges and tunnels have increased dramatically over the last decade. Kuhlman and Glaser (2002) performed manual monitoring, using TS in the reflector-less mode, to monitor bridge deformation every six years and they had detected movements and change in the shape of the bridge to millimetre levels of accuracy.

Automatic Target Functionality (ATF) and precise target positioning of the TS was researched by Cosser et al. (2003) and Psimoulis and Stiros (2007) for automatic dynamic monitoring of bridges. Due to the rate at which measurements were made ($\sim 1\text{Hz}$), Cosser et al. found that it was possible to carry out slow dynamic deformation monitoring. However, Psimoulis and Stiros used a new generation of TS with better ATR capabilities (e.g., measurements of up to 3Hz) to perform dynamic monitoring more frequently.

5.5.2 Reference framework

Survey control points were selected of known locations that define a local reference frame in which all other measurements can be referenced to define the wall coordinate system in three axes. The X-axis was selected as a horizontal line parallel to the base of the wing wall; the Y-axis is perpendicular to the base and positive towards the wall. The Z-axis is selected as a vertical line determined by the vertical axis of the instrument at the occupied station. Assume the TS is at point "A" with a known coordinate (X_A, Y_A, Z_A), the coordinates of any target point (B) can be determined precisely from the instrument position A (See Figure 5-5) (Mosbeh et al., 2005).

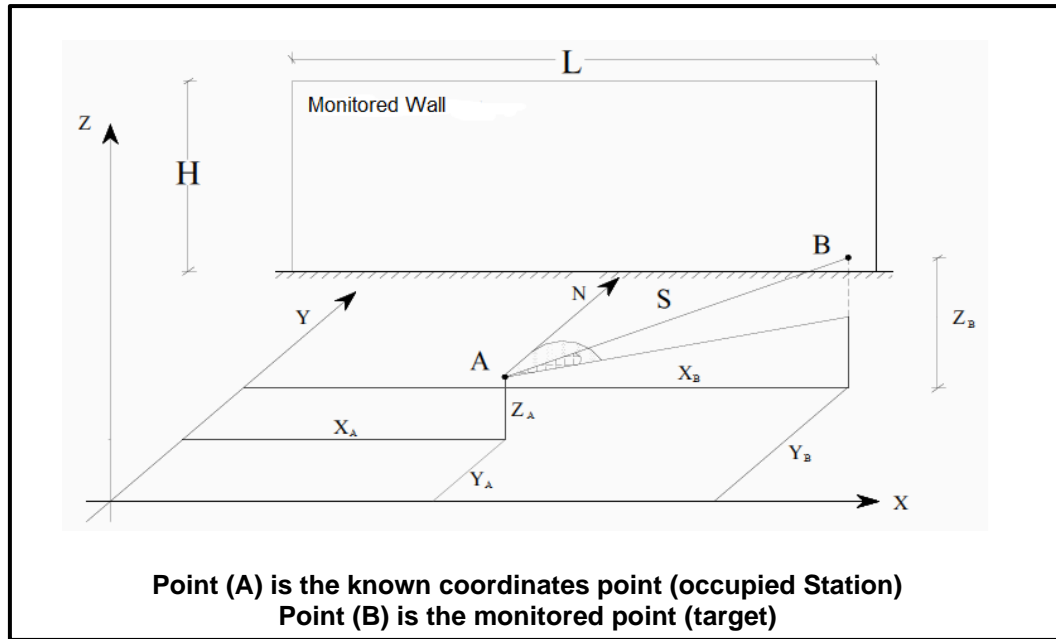


Figure 5-5 Local reference framework

Using a sufficient number of discrete points on the wing wall, displacements can be determined in all three directions. For example, at time (t), there is a specific position of point $P_t (E_t, N_t, H_t)$ whereas at time ($t+\Delta t$), the position of the same point is $P_{t+\Delta t} (E_{t+\Delta t}, N_{t+\Delta t}, H_{t+\Delta t})$. Displacement ($\Delta E, \Delta N, \Delta H$) can be obtained by the difference between the coordinates at time (t) and ($t+\Delta t$) resulting, in a distance (d) between P_t and $P_{t+\Delta t}$ given by equation 5-1.

$$d = \sqrt{\Delta E^2 + \Delta N^2 + \Delta H^2} \quad (5-1)$$

5.5.3 Total Station Monitoring Setup

London Underground's Survey team established two ground control points named M177-20 and M177-21 on the pavement, close to the wing wall, using GPS observation and linked to the Ordnance Survey Coordinate reference system. Due to a limited line of sight to survey all the targets fixed on the wall another ground control point (GCP1) was established in front of the wing wall using a total station (Leica FlexLine TS06). Traverse adjustments were not required due to the small numbers (three) of ground control points required for observing the targets. The Total Station- Leica FlexLine TS06 (see Figure 5-6) measured coordinates of these targets directly in radiation method (see Figure 5-7).

Manual monitoring was established, and observations were taken from December 2015 until June 2016.



Figure 5-6 Total Station - Leica FlexLine TS06

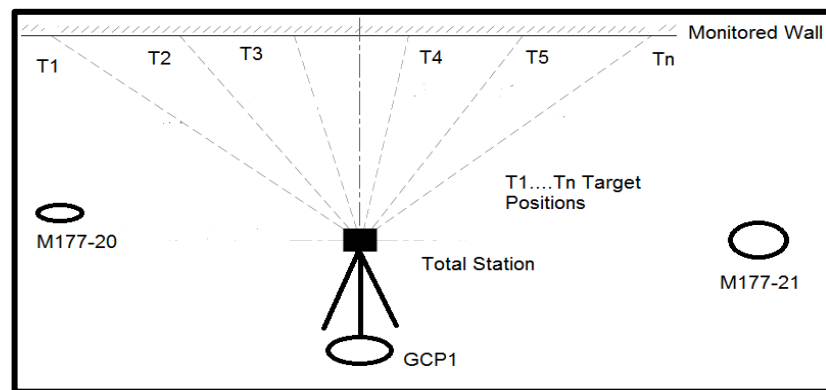


Figure 5-7 Measurements of targets using Total Station Radiation method

Each target was observed twice, and the average was obtained as a final coordinate of the target for a particular epoch. Data were stored in the internal memory of the TS and downloaded in a dxf format. The Coordinates were exported to Excel using AUTOCAD-2015 for deformation analysis. At the end of the closing shot, foresight and a backsight of the Ground Control Points was performed and the error differences between the observed and known values were checked to ensure the instrument orientation had not slipped.

5.6 Terrestrial Laser Scanner (TLS)

The terrestrial laser scanner is a measurement technique that has been developed to obtain a large number of 3D coordinate points (point clouds) and texture information quickly (Zhang, 2008). For each point in the point cloud, two angles are recorded together with a distance measurement. Additionally, the intensity of the reflection is recorded, and, for some types of scanners, the RGB-value of the reflection are captured, however, the intensity is not a calibrated value. The original intensity values are rescaled such that the final values resemble a black and white photo of the scanned scene (Soudarissanane *et al.*, 2007).

The engineering applications of the TLS ranges from cultural heritage documentation to crime scene investigation, but also traditional land surveying tasks such as the construction of as-built models and deformation monitoring (Shan and Toth, 2009). A more practical advantage is that no access to the area of interest is necessary, which is very useful for surveying hazardous locations, such as railroads or busy traffic junctions (Lindenbergh, 2010; Shan and Toth, 2009).

Several researchers performed case studies to quantify the benefits of using TLS as a measuring tool to monitor/inspect structures. For example, Monserrat and Crosetto (2008) showed that creating a surface mesh/polynomial using different epochs of point clouds can be used to identify deformation of structures. This technique could be a solution for the limited precision of TLS single points compared to TS measurements; particularly important in the case of deformation measurements.

TLS was used by Laefer *et al.* (2014) to identify cracks that were 5mm wide with a precision of 1mm of the masonry wall using the plane fitting technique. By combining TLS and strain gauge measurements Soni *et.al* (2015) showed that millimetre levels of precision could be achieved, and that sub-millimetre deformation could be detected. Furthermore, they have shown TLS to be invaluable for capturing a larger volume of surface information of the railway arches in order to identify wall movement more precisely than the TS.

Gordon *et al.* (2005) and Park *et al.* (2007) performed case studies on steel beams and showed the benefits of using TLS as a monitoring/inspection tool for a wide variety of structures. They showed that TLS instruments can be used to measure small deformations (less than 3mm).

Nuttens *et al.*, 2014; Alba and Scaioni, 2010; Puente *et al.*, 2012 showed that TLS technology has the capability (higher accuracy and speed of data acquisition) to perform deformation monitoring of structures. The collected data can then be used to construct digital, two-dimensional drawings or three-dimensional models, useful for a wide variety of applications. Laser scanners are line-of-sight instruments, so to ensure complete coverage of a structure, multiple scan positions may be required (Huseyin *et.al*, 2008). The quality of the 3D data captured by a laser scanner depends on radiometric and geometric properties of the surface under observation. However, due to rapid changes in technology, manufacturers have produced laser scanners that are more accurate, faster and affordable to capture 3D data.

According to Park *et.al.* (2007), there are several advantages in using a TLS in structural health monitoring and these include:

- (a) No in-situ instrumentation or sensors installation required
- (b) No difficulties to reach structures or structural members
- (c) Independence of natural light sources
- (d) No wiring and installation costs

The laser scanner technology can be divided into two categories, such as static and kinematic (see Figure 5-8 and Figure 5-9).

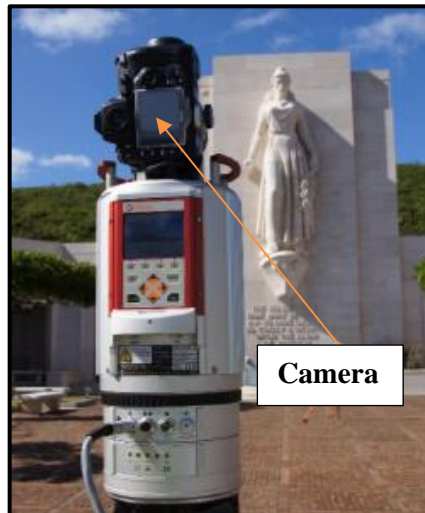
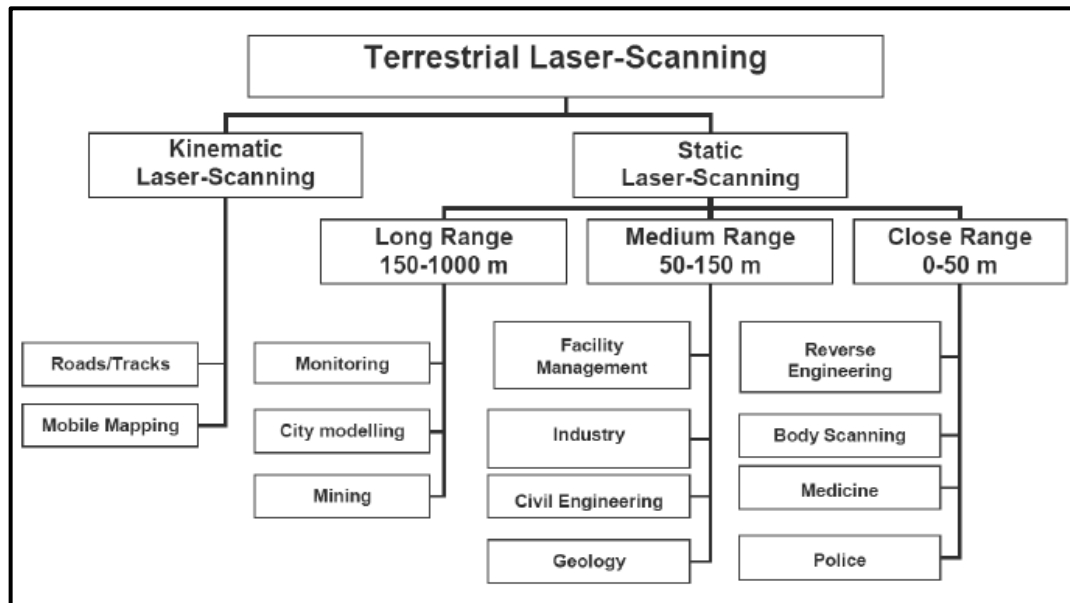


Figure 5-8 Static Laser Scanner (Mazzanti, 2016)



Figure 5-9 Kinematic Laser Scanner (Mazzanti, 2016)

In static laser scanning, the scanner is kept in a fixed location during the data acquisition. Data acquired by this method has high precision and dense point information. When the scanner is mounted on a moving platform, it is called a kinematic laser scanner. These systems require additional sensor systems such as an inertial navigation system (INS), GPS and an odometer to identify the trajectory of the laser scanner. Due to these additional sensor requirements, the system is more complex and expensive (Huseyin *et al.*, 2008) compared to static laser scanners. Figure 5-10 shows different scanner types and their applications.



**Figure 5-10 Overview of scanner types and applications
(Ingensan, 2006)**

5.6.1 Principles of Laser Scanning

Three techniques are commonly used to measure the distance between the scanner and an object: triangulation-based, pulse-based and phase-based measurements as shown in Figure 5-11. Most of the used laser scanning systems are pulse-based or phase-based (Wehr, 2008).

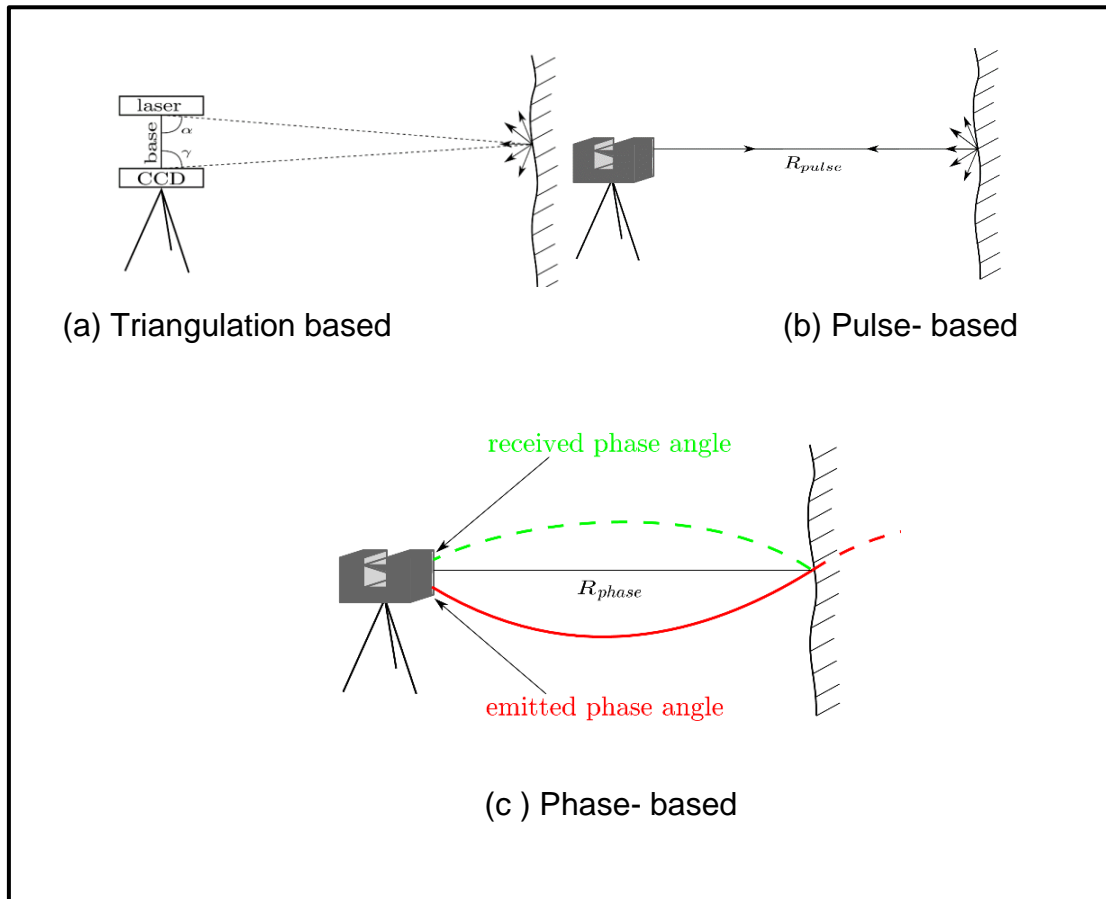


Figure 5-11 The principle of laser range measurement: (a) Triangulation measurements (Boehler and Marbs (2002) (b) Pulse distance measurements, after Boehler and Marbs (2002) and (c) Phase difference distance measurements, after Van Ree (2006)

(a) Triangulation-based

In the triangulation-based method the distance between the laser and the recording unit, a CCD (charge-coupled device) camera, and two angles α and γ , formed by laser, camera and object, are used to calculate the distance between instrument and object. Within this triangle, the base and the angles α and γ are known; the range is computed using this triangle. Triangulation-based systems are suitable for small ranges (below 10 m) since the length of the base is limited (Boehler and Marbs, 2002).

(b) Pulse-based

For the pulse-based method, distance measurement is based on the two-way travel time (t) of the signal. With known speed of light (c), the distance R pulse is calculated (Figure 5-11 b):

$$R_{\text{pulse}} = 1/2ct \quad (5.2)$$

The maximum range of the pulse-based systems is several hundreds of meters and depends on the emitted amount of energy.

(c) Phase-based

Finally, for the phase-based method, the instrument measures the phase shift between the emitted and returned signal (Figure 5-11c). The emitted laser signal is modulated with two or three harmonic waves.

The measured phase difference, θ is proportional to the travelling time, t :

$$t = \frac{\theta}{\omega} \quad (5.3)$$

with ω the angular frequency of the harmonic wave that is used to modulate the signal (Wehr, 2008).

Combining equations (5.2) and (5.3) leads to the phase-based range R_{Phase} (Wehr, 2008):

$$R_{\text{Phase}} = \frac{c}{t} \frac{\theta}{\omega} \quad (5.4)$$

Using the propagation law of variances (Teunissen, 2000), the accuracy of the phase-based range measurement is:

$$\sigma^2 R_{\text{phase}} = \left(\frac{c}{2\omega}\right)^2 \sigma_{\theta}^2 \quad (5.5)$$

From eq. (5.5), it follows that the variance of the range measurement depends on the variance of the phase difference measurement, provided that c and ω are constant. The smaller the angular frequency ω is, the higher the accuracy. Therefore the signal with the highest frequency determines the accuracy of the range measurement.

The accuracy achieved with pulse-based and phase-based systems is similar, but the measurement frequency differs. For pulse-based systems, the next pulse can only be emitted when the previous signal has returned. For phase-based systems, the measurements are taken continuously resulting in a higher measurement frequency. Depending on the goals of the survey the most suitable scanner can be chosen.

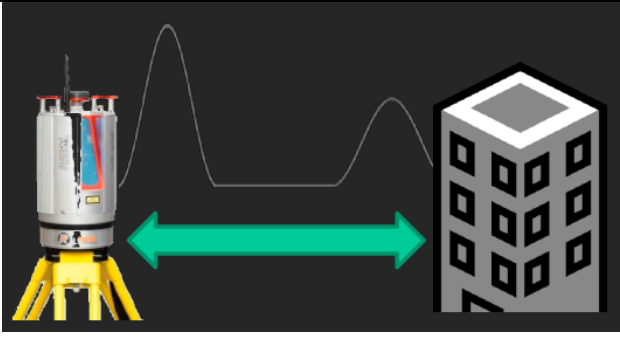
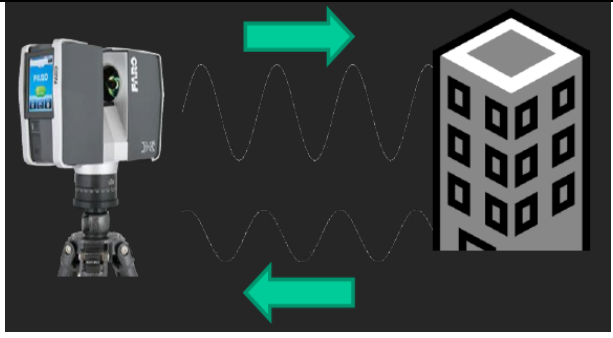
Time of Flight (pulse based)	Phase Shift (phase based)
	
Good Range (1m-6Km)	Low maximum range (<500m) Slightly more precise
Multiple target capability	Can have ambiguous
Expensive option	Economical option

Figure 5-12 Comparison between Time of Flight and Phase Shift scanners (Mazzanti, 2016)

5.6.2 Error sources of laser scanning points

Laser Scanner measurements are subject to errors. Each measurement has a unique standard deviation, depending on various factors. For a laser scanner, four categories of errors are defined that contribute to the individual point quality (Soudarissanane et al., 2008). These will be discussed below.

(a) Scanning geometry

According to (Soudarissanane et al., 2007), the range and the incidence angle are determined by the scanning geometry, which results from the standpoint of the laser scanner with respect to the scene. For pulse and phase-based scanners, the accuracy decreases with an increasing range as the returned

signal is weaker and the footprint is larger for larger distances. The incidence angle is the angle between the incoming laser beam and the normal to the surface. If the incidence angle is larger, the footprint of the beam on the object is larger, which makes the precise determination of the phase difference more difficult. For good results, the incidence angle should not exceed 75° .

(b) Surface properties

The signal interacts with the surface depending on the bidirectional reflectance distribution function (BRDF). The BRDF of a surface gives the ratio of the incoming to the outgoing radiance for a certain wavelength (Rees, 2001), i.e. it describes the scattering properties of the surface.

Clark and Robson (2004) showed that the colour of the surface influences the range measurement. The effect of the surface colour on the signal depends on the wavelength of the laser. The roughness of the surface determines the type of reflection. Smooth surfaces result in specular reflections, where the signal is reflected away from the laser scanner for larger angle of incidences. Rough surfaces result in diffuse reflections, where the signal is scattered in many directions and only a limited amount of the signal returns to the laser scanner.

(c) Instrument calibration and properties

Mechanical instrument errors contribute to the errors in the measurements. Small offsets of the mirror centre propagate in the measurements, as well as aberrations in the rotation mechanism, which influences the angular increments and thus the angular measurements (Lichti, 2007). Calibration of the instrument gives insight into these errors.

(d) Environmental conditions

The emitted signal is affected by environmental conditions such as temperature, atmosphere and illumination. The instrument performs best within a certain temperature range. Furthermore, systematic errors can be present in the data due to internal heating of the instrument. The atmospheric conditions, for example, humidity or air pressure, influence the propagated speed of light, however, this can be neglected for short ranges because the

errors generated are very small. In this case study distance between the test wall and the instrument position was 1.2 m (short-range), therefore, the atmospheric conditions are negligible. Steam and/or dust can cause additional refraction of the signal, which results in erroneous measurements. Illumination is an influencing factor as well if the frequency of the light is in the same band as the laser signal's frequency band and if the radiation is strong when compared to the laser signal. In this case, the measurements will contain larger errors (Boehler and Marbs, 2003).

5.6.3 TLS Survey Planning

Currently, there is no standard method for planning terrestrial laser scanning surveys. However, survey planning should be performed to minimize cost, maximize output and finish work on time. According to Huseyin et al. (2008), in general, a survey plan should include.

- Goal and objectives of the scanning
- Available instrument model
- Precise identification of the scanning location
- Mode of transportation of the scanner, accessories and personnel
- Data management (store, process and archive)
- Deliverables (2D drawings or 3D model)

5.6.4 TLS Instrumentation

London Underground Limited has used two types of scanners during the laser survey. They are a Leica P20 and a Leica P40 (see Figure 5-13). Scanner P20 was used to perform the data acquisition of the first epoch (30/03/15), thereafter the P40 scanner was used. Table 5-4 shows a comparison between the P20 and P40 laser scanners.



Figure 5-13 P20 and P40 3D Laser Scanning Product Specification Comparison (www.leica-geosystem.com)

Table 5-4 Comparison of Scanners parameters

	Range	Laser Class	Type	Laser Spot Size	Max Scan Rate	Positional Accuracy	Field of View	On-Board Storage	Integrated Camera	Sample Scan
P20	120 m	Class 1	Time of Flight / WFD	N/A	1 million pts/sec	4.5mm (0.4-25m range) 9mm (25-50m range)	360° x 270°	256GB HDD	Yes	3 min 22 sec
P40	270m	Class 1	Ultra High speed Time of Flight	N/A	1 million pts/sec	3 mm at 50 m; 6 mm at 100 m	360° x 290°	256GB HDD	Yes	N/A

Further information regarding the comparison of other parameters can be found on the manufacturer's website.

5.6.5 TLS Data Collection

The London Underground Survey team carried out the scanning of the wing wall using the Leica P20 and P40 scanners in six epochs. Both scanners are time-of-flight scanners and when compared to the P20, the P40 operates in ultra-high-speed time of flight, has a longer range (270m) and a higher positional accuracy. Due to high precision, P40 data were used as a baseline to compare other epochs of data.

The scanner position needs to be planned carefully to cover the scan area with a minimum number of scanner positions to scan the wing wall. The scanner position was set-up in between two ground control points. The wall was in the range of 4m from the scanner and point spacing of 4mm (set by the instrument). The scanning was performed on six separate epochs (see Table 5-3).

Heritage and Large (2009) showed that a detailed point cloud requires a high-density of points however this is obtained at the cost of a much larger scanning time. Therefore, the level of detail needs to be decided or estimated before starting any scanning work. When pressing the control button, scanners start to move from the starting point and capture point cloud data. The whole scanning process was fully automated and the operator can predefine the horizontal/vertical angle range required to be scanned.

The captured point cloud data were saved through the connected laptop, and they were visualized in 3D on the computer screen. This has provided a real-time overview of the area already scanned, and any missing points can be recaptured immediately to avoid costly re-visiting of the site. When using the internal memory of the scanner to store data, it cannot be viewed in real-time. To achieve higher accuracy in the registration phase, three artificial targets, known as T101, T103 and T104 were measured precisely using the TS (see Figure 5-14 to Figure 5-16).

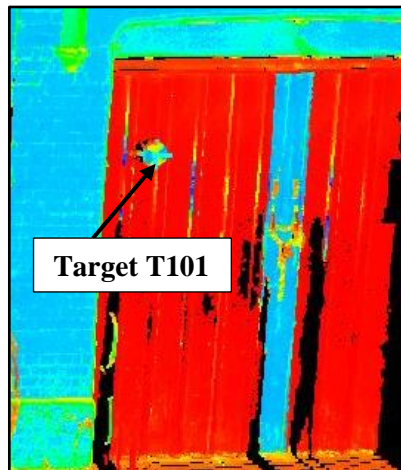


Figure 5-14 Target T101 fixed on the door –other side of the road (point cloud image)

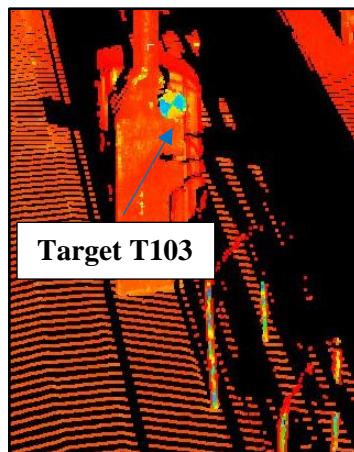


Figure 5-15 Target T103 fixed on the Lower part of CCTV (point cloud image)

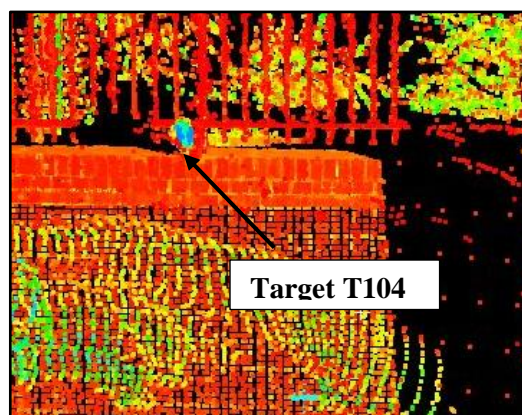


Figure 5-16 Target T104 top left of the Wing wall (point cloud image)

These targets were fine scanned to obtain a higher accuracy when determining their centre position during post-processing of the data. The wall was scanned from a single location. Therefore, multiple scanning positions were not required.

However, to increase the data accuracy the scanner height (changed height of the tripod) was changed after finishing the first scan and a second scan was performed. The point cloud colours are based on the intensity of the scan and is automatically allocated by the software Cyclone when processing the point cloud.

After the acquisition of the TLS data, several processing steps are required before a change detection or deformation analysis can be carried out. These processing steps consist of registration and segmentation of the data. The registration process has a large influence on the final quality of the point cloud.

5.6.6 Registration and Geo-Referencing

During the registration process, point clouds captured in the different scanner set-ups were transformed to the same coordinate system using geo-referencing. For geo-referencing, the targets need to be surveyed using a TS. To perform an accurate registration, at least three targets need to be at a common location between two scans. However, more than three targets minimized the errors when performing a least-squares optimization. Errors in the registration process propagate in the final point cloud and influence the ability to detect deformations. A registration with an accuracy in the order of magnitude of a few millimetres is therefore required.

5.6.7 Cyclone - Data Processing

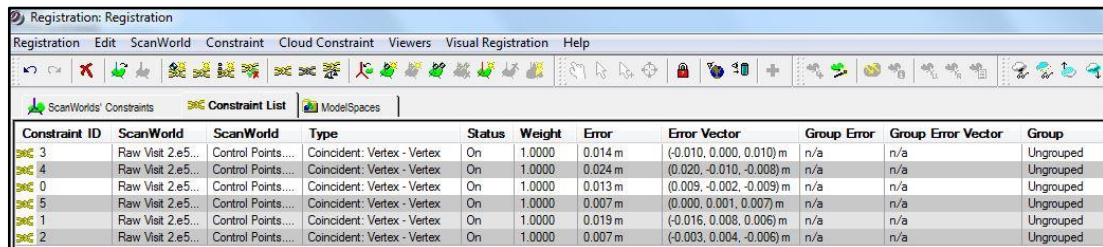
The laser scanner data were processed using the software Leica Cyclone version 9.1. Before processing the noise data (people in the line of sight of the scanner) were removed. The following processing steps were followed.

- 1. Creating Database:** A database was created before importing any raw data into Cyclone software. The created database (*.imp) can be seen in Cyclone Navigator.
- 2. Importing Scan Data:** Raw data were imported into the created database in the E57 file format. Each scan is shown as a Scan-World (Cyclone's database structure) without any specified orientation or

coordinate system. Four major parts of the Scan-World are control space, model space, scans and images. If an integrated camera (digital camera embedded to laser scanner) is used to capture a field of view of the scanner during the scanning, the image can be imported into the image folder.

- 3. Target Identification:** The centre of each target was identified automatically by using a specific function of the Cyclone software. This part is important for the target-to-target registration process. In target-to-target registration, at least three targets need to be matched between two Scan-Worlds to register the scans. During the data processing of epoch two, the automatic detection of targets, done by the software, failed. Therefore, a manual insertion of the target was performed by selecting the centre point and the vertex. These points were selected and labelled according to the symbology used during the TS survey. Finally, the vertex was copied to the control space.
- 4. Import Total Station Data:** The coordinates (measured by the TS) of all the control points were imported into Cyclone as a CSV file format before starting the registration process (registration process can be found in section 5.6.6).
- 5. Adding Data to Registration:** Then total station data and each Scan-World were imported for registration, and control point data were set as home Scan-World.
- 6. Adding Constrain:** In a subsequent step, constraints were added automatically using the auto-add constraint function in the constraint menu. At this stage, the measurement column does not show any errors. To compute the errors accumulated by the whole process, the scans need to be registered and the “Register” command was selected under the “Registration Menu”.

- 7. Finding Errors:** Once the registration was completed, the error vector column appears with different error values (see Figure 5-17) for each registered scan. Constraints with higher error value were examined by opening Scan-World. The errors were fixed manually, or the target was not included in the registration. After disabling the higher error value constraint or target, the project was re-registered.



Constraint ID	ScanWorld	ScanWorld	Type	Status	Weight	Error	Error Vector	Group Error	Group Error Vector	Group
3	Raw Visit 2.e5...	Control Points...	Coincident: Vertex - Vertex	On	1.0000	0.014 m	(-0.010, 0.000, 0.010) m	n/a	n/a	Ungrouped
4	Raw Visit 2.e5...	Control Points...	Coincident: Vertex - Vertex	On	1.0000	0.024 m	(0.020, -0.010, -0.008) m	n/a	n/a	Ungrouped
0	Raw Visit 2.e5...	Control Points...	Coincident: Vertex - Vertex	On	1.0000	0.013 m	(0.009, -0.002, -0.009) m	n/a	n/a	Ungrouped
5	Raw Visit 2.e5...	Control Points...	Coincident: Vertex - Vertex	On	1.0000	0.007 m	(0.000, 0.001, 0.007) m	n/a	n/a	Ungrouped
1	Raw Visit 2.e5...	Control Points...	Coincident: Vertex - Vertex	On	1.0000	0.019 m	(-0.016, 0.008, 0.006) m	n/a	n/a	Ungrouped
2	Raw Visit 2.e5...	Control Points...	Coincident: Vertex - Vertex	On	1.0000	0.007 m	(-0.003, 0.004, -0.006) m	n/a	n/a	Ungrouped

Figure 5-17 Constraint list after registering

- 8. Fixing Errors:** - After the re-registration, constraints were rechecked using the registration, diagnostic tool, to understand if the re-registration was within the acceptable limits (<3mm).
- 9. Adding Cloud Constraint:** - Cloud Constrains are the sufficient overlapping area within the scan-world. Adding cloud constraint can optimise (see Figure -5-18) the registration process. Once the auto-cloud constrain is finished, the process is completed, and the software shows all added constraints and their error values.

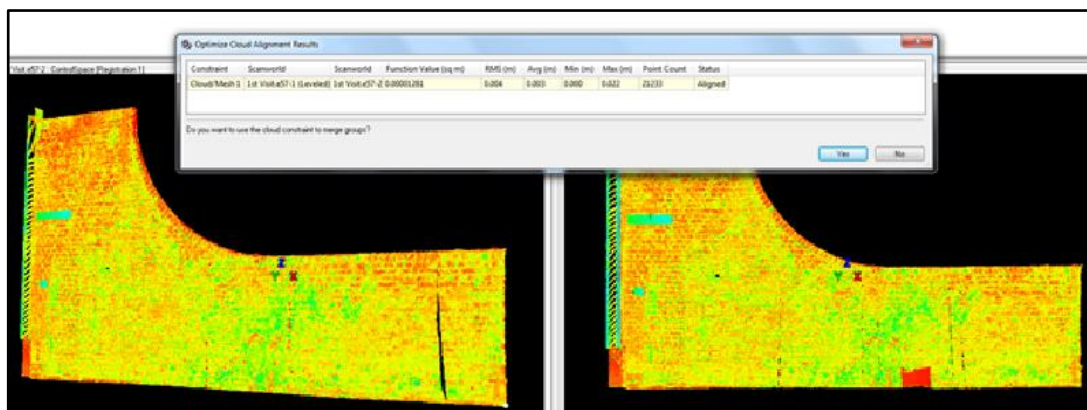


Figure -5-18 Optimize cloud alignment results

10. Freezing and creating Model-space

To create the final registered point cloud, the registration needs to be frozen and nothing can be changed. If there is a need to add any additional constraint, the Model space from the previous registration has to be deleted and the point cloud re-registered using the new constraint.

11. Exporting Data: - The final data were exported into an E57 file format for deformation analysis.

5.7 Close Range Photogrammetry (CRP)

Photogrammetry “*encompasses methods of image measurement and interpretation in order to derive the shape and location of an object from one or more photographs of that object*” (Luhmann et al., 2014).

Two primary classifications of photography used in the science of photogrammetry, are terrestrial and aerial. Terrestrial photogrammetry deals with photographs taken with a camera located on the surface of the earth. The camera may be hand-held, mounted on tripods, or suspended from towers or other specially designed mounts. The term “Close Range Photogrammetry” is generally used for terrestrial photographs having object distances of up to about 300m (Luhmann et al., 2014). In Aerial Photogrammetry, aerial photographs are taken by the air-borne vehicle and primarily used for producing topography and contour maps.

Close-range photogrammetry (CRP) is a passive sensor technology widely used for deformation monitoring applications. With the rapid development of computer processing technology, data storage capacity and digitized image recording and processing systems, CRP has entered a fully digitalized era with great potential for engineering applications. One advantage of photogrammetric techniques is that deformations can be detected by a device that is not in contact with the object (Tasci, 2013).

CRP is a technique that has many advantages, a few of which are:

- It is a non-contact technique that is capable of measuring difficult-to-access structures
- It is less labour-intensive compared to the terrestrial laser scanner and can be used rapidly
- It records a large amount of geometric information in a short period by acquiring images using low-cost cameras
- It allows revisiting the visual records and performing additional analysis at a later time
- It can be used as a convenient tool for routine measurement applications

Using a low-cost digital camera, a number of overlapping pictures can be used to create a 3D point cloud. 3D surfaces and textures can be created using point clouds, and the information can be applied to deformation monitoring of bridges and structures (Jiang et al., 2008). TS data need to be integrated with CRP measurement to produce scaled and geo-referenced point clouds. Using the CRP technique, data can be collected rapidly from a mobile camera and point clouds can be generated for deformation monitoring. The image quality and the geometry of the network influence the quality of point clouds generated from natural features. The image quality solely depends on the illumination of an area of interest at the time of photography. Compared to TLS, the CRP technique is twenty times cheaper and one-tenth of the cost of a single total station used in surveying (Soni, 2016).

Currently, wire strain gauges or inductive displacement transducers are used to measure displacement and deformation. These techniques have high precision; however, only point-wise and one-dimension measurement can be monitored, and they do not provide surface information or a large number of measurement points to detect cracks during only loading. Maas (1992), Hampel (1997) and Luhmann (2000) showed that CRP is a viable solution for complete surface measurements because it allows automatic measurements of two and three-dimensional displacement fields, deformations, and defects.

Luhmann *et al.* (2013) showed that Close Range Photogrammetry (CRP) can be applied for deformation monitoring, especially in access and time-constrained environments.

Soni *et.al* (2015) used CRP and a TLS for structural monitoring of a railway arch in London Bridge Station. A CRP survey was carried out during one of the epochs to compare the system to the TLS. The results showed that the point cloud quality was comparable to TLS. However, this process was very time consuming and required intensive processing power. Due to CRP being a passive method of survey, the quality of the data cannot be evaluated (for example missing gaps of the surface) until the end of the workflow.

Previous research (Tasci, 2013) using the CRP method, compared measurements and reflector-less total station measurements, used to perform deformation measurements on a steel arch bridge. The behaviour of the steel arch bridge was also compared with numerical results generated by using the finite element method (FEM). By comparing these methods and processing the data obtained from photographs taken during the test being carried out in the laboratory, the authors showed that all the methods agree in terms of detecting displacements. This reveals that photogrammetry can be used as a surveying technique, especially when a quick and accurate analysis is required.

Detchev *et al.* (2011) had used consumer-grade digital cameras and projectors for the deformation monitoring of structural elements. They had conducted experiments using multiple digital cameras and projectors on a stable metal frame, in order to detect deflections in concrete beams caused by a hydraulic actuator. After performing a semi-automated photogrammetric reconstruction of the visible beam surfaces and of the full surfaces of almost all the metal plates, it was shown that sub-millimetre precision for the estimation of the beam deflections could be achieved in object space.

This study looks not only to detect movement of the wing wall using CRP but also rapidly using CRP as an inspection tool to measure defects (e.g. crack propagation) and forecast their trends.

The theory of photogrammetry is beyond the scope of this thesis, and hence not discussed further, but it is available in other references such as Dowman (2001), Cooper and Robson (1994).

5.7.1 Digital Camera

The camera is the backbone in any photogrammetry-based measurement technique. The Nikon D700 (see Figure 5-19) digital camera equipped with a 24mm lens was used to capture digital images, this camera uses a CMOS type of image sensor.



Figure 5-19 Nikon D700 Digital Camera

As stated by David et al. 2006:

“The significant difference between the CCD (charge-coupled device) and CMOS (complementary metal-oxide-semiconductor) sensor is that the CCD processes pixels in sequence while the CMOS transforms light into electrons simultaneously in the picture elements (i.e., pixels). As a result, the CMOS consumes less power and operates at a higher speed than the CCD sensor. However, CMOS sensors are considered more susceptible to noise resulting in lower quality images than CCD sensors which produce high-quality, low-distortion images”.

5.7.2 Artificial Target Selection

The artificial targets (manual monitoring prisms) were installed by the route maintenance contractor on the wing wall to provide a reference frame to point clouds created by the photogrammetry and terrestrial laser scanner. Duration of monitoring (the wing wall was demolished at the end of August 2016) and cost of a target were considered before selecting the targets. The black and white targets which are automatically identified by 'Cyclone' laser scanner software for geo-referencing were not installed due to their higher cost than the silver retro targets. Therefore, the silver retro target was selected and fixed with screws and plugs into the wall. The dimension of the target is "plaquette size: 75 x 60mm with a 30 x 30mm silver retro target" (see Figure 5-20).



Figure 5-20 Silver Retro Target

Eight targets were placed on the wing wall. The red circles on Figure 5-21 show the location of the targets on the wall. Two reference targets 5 and 10 (10 is not shown in the figure) were placed in a stable position, outside the predicted impact zones and another stable point was selected on the metal beam. Due to the private properties around the wing wall, it was difficult to select more control points outside the impact zone. These reference points were considered as a stable location for each epoch of observation.

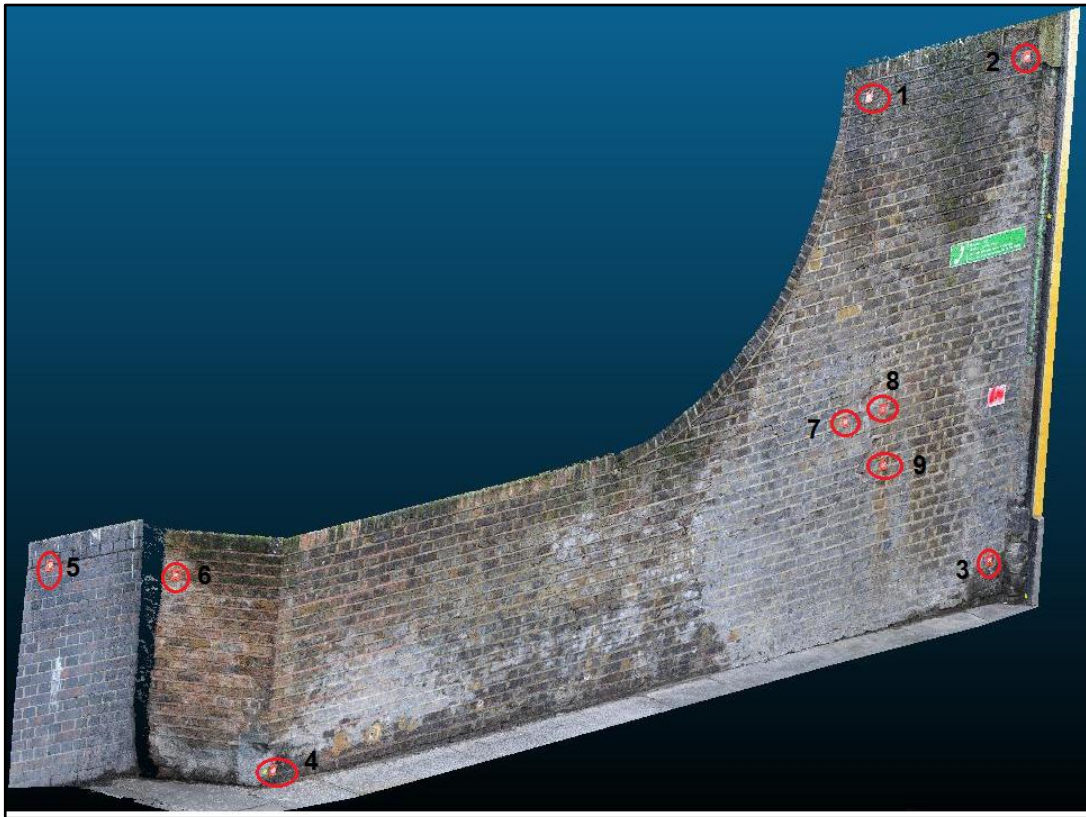


Figure 5-21 point cloud obtained from the CRP and locations of the nine monitoring targets (red circles)

After setting them up, their coordinates were measured precisely by using a Total Station (Leica Flexline TC 06). Point cloud data were scaled using target coordinates that had been observed using the TS to obtain the accurate dimensions of the wall.

5.7.3 Photogrammetry Data Capturing

A series of overlapping images (minimum 70%) were captured using a Nikon D700 digital camera. A wide-angle lens was used to capture images, this type of lens provides a larger area coverage, and fewer images are required to cover the whole wall. Due to sufficient natural light, a camera flash has not been used for the exposure.

The following setting of the camera were used in each epoch of data capture.

- focus (manual set at ∞)
- white balance (automatic)

- ISO rating -1000
- drive mode -single
- exposure mode -automatic
- picture quality- best
- image format- TIFF

The following scenarios have to be considered while capturing the photos to create point clouds.

- Always capture more photos than required to avoid a further site visit (time-consuming and costly)
- Agisoft- Photoscan can only reconstruct geometry from at least minimum two camera locations
- Do not try to capture the whole area in a single image frame and missing parts can be provided in the overlapping photo
- To achieve the best quality of image the light source is important. However, it should not be in the camera field of view and always avoid using flash. The flash allows to determine the location of the target easily. It would illuminate the target and determine their centres in an easy way

Figure 5-22 shows the best way to capture the photos as well as what not to do.

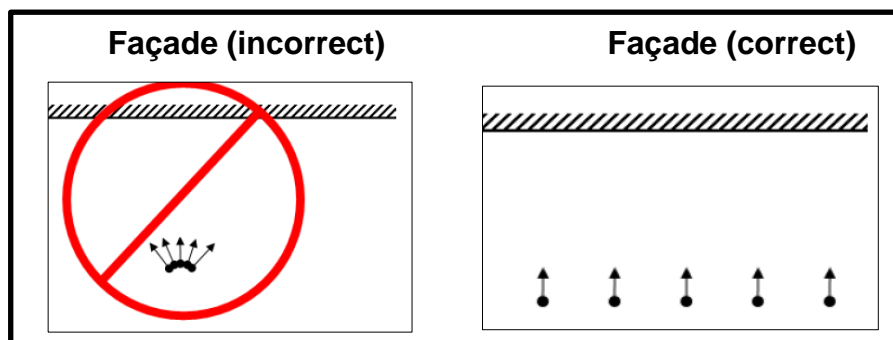


Figure 5-22 Photo capturing method for 3D point cloud construction
(www.Agisoft.com)

5.7.4 Data Processing

The commercial software package Agisoft-PhotoScan was used to process the images, to generate the dense point clouds and surface meshes of the HC3-wing wall. For multi-view 3D construction, Agisoft-Photo scan is an affordable solution. 'It uses structure from motion (SfM) and dense multi-view 3D reconstruction algorithms to generate 3D point clouds of an object from a collection of arbitrarily taken still images (Koutsoudis et al., 2013)'. Structure from Motion approach requires multiple pictures of an object or scene from more than one camera position (James and Robson, 2012).

The following processing steps were followed to create a 3D point cloud and texture surface mesh. For detailed information about each processing step and parameter, setup refers to the Agisoft Photo scan user manual.

5.7.5 Camera calibration

The process of determining the optical and geometric characteristics of a camera is called calibration (David et al., 2006). The calibration must be carried out for a project to be accurate so that the camera parameters are known.

The camera parameters consist of;

- f_x, f_y -focal length in x and y dimensions measured in pixels.
- C_x, C_y - Principal point coordinates, i.e. coordinates of lens optical axis interception with sensor plane.
- Skew-Skew transformation coefficient.
- k_1, k_2, k_3, k_4 - Radial distortion coefficients.
- p_1, p_2 - Tangential distortion coefficients.

The Agisoft- Photoscan estimates camera calibration parameters automatically using Brown's model for lens distortion. Therefore, manual calibration should not be needed if the user used standard optical lenses and a highly redundant image network. During the data processing, the Agisoft-Photoscan's algorithm performed auto-calibration using image EXIF (exchangeable image file format) camera information which can be found in

the images (Thoeni et.al, 2014). The camera calibration parameters are shown in Figure 5-23.

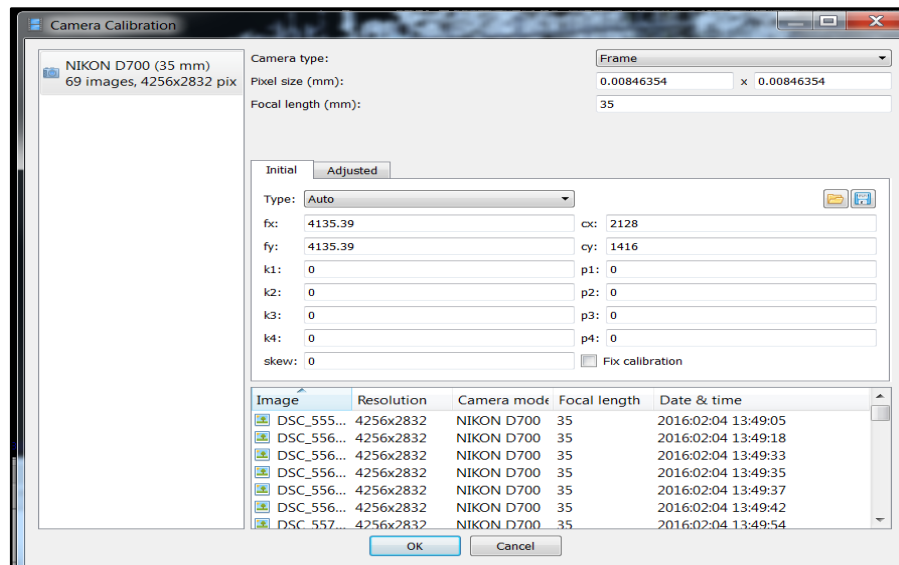


Figure 5-23 Automated camera calibration parameters generated by Agi-Soft

- **Loading Images**

The images were initially downloaded from the camera to the computer. Before loading photographs into Agisoft-PhotoScan, captured photos were carefully examined and selected for those suitable for 3D point cloud/model reconstruction. Poor quality images such as out of focus, poor illumination, shadows to be removed from captured images before loading. Then raw images in TIFF format were imported into Agisoft Photo Scan, as these are the best quality images since no compression algorithm was applied. The following image formats can also be imported into AgiSoft Photo scans: JPEG, TIFF, PNG, BMP, PPM, Open EXR and JPEG Multi-Picture Format (MPO). Photos can be loaded using the “Add photo” icon. Loaded photos can be viewed in the workspace pane with their flags (NC: not calibrated, NA: not aligned) and unwanted photos can be removed any time before aligning the photos.

- **Aligning Photos**

After the photographs had been loaded into Agisoft-Photo Scan, the first step of the photogrammetry analysis was aligning photos according to their overlapping. The alignment process iteratively refines the external and internal

camera orientations and camera locations through a 'least-squares solution'. Then software builds a sparse point cloud model. Poor image quality photos were removed before aligning, otherwise, it will influence the alignment results. Agisoft-Photoscan is capable of analysing image quality based on the sharpness level of the picture. Agisoft has a function to set two different accuracy settings for the alignment process such as 'low' and 'high'.

Low accuracy- initial estimation of the camera location and less processing time.

High accuracy- more accurate camera position and much more processing time.

In addition, several parameters controlled the photo-alignment procedure; detailed information can be found in the Agisoft user manual.

- **Point Cloud Generation**

Based on the estimated camera positions, the Agisoft-Photoscan software calculates depth information for each camera position to be combined into a single dense point cloud. The "build dense point cloud" command can be selected from the workflow menu. Desired reconstruction parameters can be selected from the build dense cloud dialog box. Quality and depth filtering are the two major parameters that can be set for point cloud generation. Higher quality settings can be used to obtain more detailed and accurate geometry, but require a longer time for processing. In this research higher quality option has been used.

- **Building Mesh**

PhotoScan supports several reconstruction methods and settings, which help to produce optimal reconstructions for a given data set. The following parameters were selected to build the mesh.

- **Surface type:** Arbitrary surface type can be used for modelling of any object. Therefore, this surface type was selected.
- **Source data:** Source data has to be selected for the mesh generation procedure. The dense cloud setting was selected to

generate high-quality output based on the previously reconstructed dense point cloud.

- **Polygon count:** Polygon count allows specifying the maximum number of polygons in the final mesh. Suggested values as being high, medium and low. These values are based on the number of points in the previously generated dense point cloud. The medium value was selected during the processing.
- **Interpolation:** Interpolation should be enabled to obtain accurate results and fill holes automatically. Sometimes some holes can still be present in the model and are to be filled in the post-processing step.

5.8 Change Detection and Deformation Analysis

A small variation on the surface of the wing wall is called deformation, and this can happen due to either new objects in the scene or removed objects. The distinction between changed and unchanged surfaces is based on an identification of corresponding segments.

The process of identifying differences of an object by observing it at two epochs is called change detection (Singh, 1989). During the change detection, objects or areas where changes occurred in the point cloud, are identified. In deformation analysis, the changed surfaces in a scene are investigated in more detail. The deformations that are to be found are in the order of magnitude of the point accuracy, but also in the same order as the noise. The registration of the point clouds influences their accuracy and therefore the possibility to detect deformations. Accurate registration is thus an important step. The available deformation methods can be divided into three different categories:

- point-to-point-based
- point-to-surface-based
- surface-to-surface-based

5.8.1 Point-to-point-based deformation

Deformation monitoring using a total station, measures fixed points at different epochs. The coordinates of these points are compared to find deformations. With a laser scanner, it is uncertain whether the same point is sampled at two different epochs. Furthermore, the point density of an object can vary as it is scanned from multiple standpoints. A direct point-to-point comparison is therefore not favourable. An approach of a pointwise comparison of the points for a deformation analysis is to use the range images. If the scans are taken from different standpoints, the scans are transformed to the same standpoint. Per point, represented by a pixel in the range image, the distance is calculated by subtracting the range value of that pixel in the other range image. Instead of the question of whether a change occurred, the range difference is now used to quantify the deformation. Problems arise when the point density varies or when areas are occluded. For a point-to-point-based comparison, corresponding points need to be identified. Besides the fact that the exact origin of the laser reflection is not known, this method does not fully use the high point density. It is possible to use the local neighbourhood of points to estimate points with redundancy. Furthermore, different point densities for the two-point clouds influence the results. Tsakiri et al. (2002) used retro-reflective targets that are placed on the object. These targets are scanned during multiple epochs, and for each target, the centre is calculated. Results show that deformations below 0.5 mm can be detected using TLS and targets. However, the accuracy achieved by traditional surveying is even higher (Tsakiri et al., 2006).

5.8.2 Point-to-surface-based deformation

To avoid the problems related to the point-to-point approach, one of the point clouds is represented by a surface (usually the reference point cloud) and the distance, perpendicular to the surface to each of the points of the second point cloud is calculated. This method has many advantages over the point-to-point comparison as the surface is calculated and is an average of the reference point cloud. The calculated differences are analysed using a gaussian distribution and the distance is usually assumed to be the average of all the

measurements, therefore eliminating the problems related to point cloud density and noise.

5.8.3 Surface to surface-based deformation

The surface to surface-based deformation method consists of computing the distance between two surfaces and both point clouds are represented by a surface. The disadvantage of this is that further processing is required compared to the other comparison techniques.

5.9 Data Analysis and Results

TS data were used to geo-reference both CRP and TLS to obtain absolute movements rather than relative movement. On the other hand, if TS only is used, a few points could be recorded instead of the complete surface information, obtainable from either CRP or TLS. Compared to TLS, CRP requires more processing time from an office to obtain point clouds from the images. The trend of defect changes and the wall movement was compared between different epochs of observations. This site trial has generated significant volumes of data and created the additional task of how to visualise changes and report their significance to the LUL route manager who is responsible for making a decision in a timely manner.

5.9.1 Comparison between Total Station (TS), Terrestrial Laser Scanner (TLS) and Close-Range Photogrammetry (CRP)

In February 2016, TS data were used as reference coordinates/baseline of each target to calculate the relative movements of targets for other epochs. General movement trends are described using a sufficient number of discrete point displacements (d_n):

$d_n (\Delta x \Delta y \Delta z)$ for n = point number ($n=8$ for this site trial)

Point displacements were calculated by differencing coordinates for the most recent survey campaign (f), from the coordinates obtained at a reference time (i), according to the equation below:

$$\Delta x = X_f - X_i \text{ is the X coordinate displacement} \quad (5.6)$$

$$\Delta y = Y_f - Y_i \text{ is the Y coordinate displacement} \quad (5.7)$$

$$\Delta z = Z_f - Z_i \text{ is the Z coordinate displacement} \quad (5.8)$$

Each movement vector has magnitude and direction expressed as point displacement coordinate differences. Collectively, these vectors describe the displacement field over a given time interval.

$$|d_n| = \sqrt{\Delta x^2 + \Delta y^2 + \Delta z^2} \text{ is the magnitude of the 3D displacement.} \quad (5.9)$$

Table 5-5 shows the 3D displacement of each target compared between February 2016 reference data. These data were plotted and are shown in Figure 5-26 and Figure 5-27 to compare the performance and limitations of each system (e.g. CRP, TLS and TS).

Table 5-5 3D Displacement of targets computed by TS measurements

Target	3D Displacement (mm)			
	Feb16-Dec15	Feb16-Jan 16	Feb16-April 16	Feb16-June16
1	7	7	5	5
2	8	9	7	3
3	9	4	4	4
4	3	10	2	4
6	10	10	6	8
7	2	4	4	5
8	10	11	9	5
9	7	6	7	6

To directly compare the results from TLS and CRP to the TS monitoring, an attempt to extract the discrete information from the surface model around each target (prism) was made. The direct comparison of the target locations (e.g. target coordinates) measured between the TS and the scan data could not be performed due to the 4mm point spacing of the point cloud that did not allow the determination of the centre of the target in the point cloud. Therefore, the

local plane fitting method to the TLS and CRP was applied to compare them to the TS dataset.

A small portion of the point cloud data, closer to each target and for each epoch, was segmented (see Figure 5-24) and a plane was adjusted to the segmented point cloud using the Cloud Compare software. The February 2016 laser scanner data were used as a reference point (baseline), and plane fitting was performed on this using Cloud Compare (CC) software.

There is a function in Cloud Compare that allows the “cloud-to-mesh comparison” where the fitted plane is the mesh. This uses the reference model/mesh as a baseline to compute the distance between the point cloud and the mesh (baseline). This function outputs the distances of the plane and the mesh as a Gaussian distribution, displaying a colour coded surface displacement map and a histogram of the residuals from the reference mesh to the cloud. The Gaussian mean (e.g., 4mm shown in Figure 5-25) was considered as the distance between the mesh and the point cloud for that particular area.

Figure 5-25 provides an example of the output when comparing the 3D deviation between the baseline and other point clouds, with the scale shown in meters.

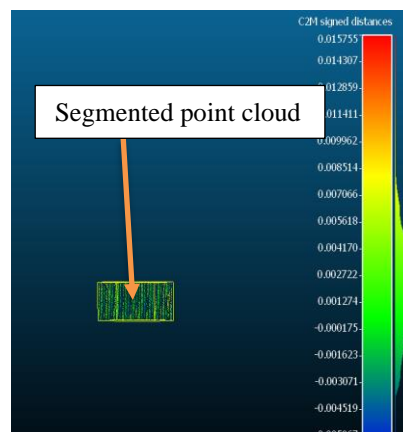


Figure 5-24 Segmented point cloud for plane fitting

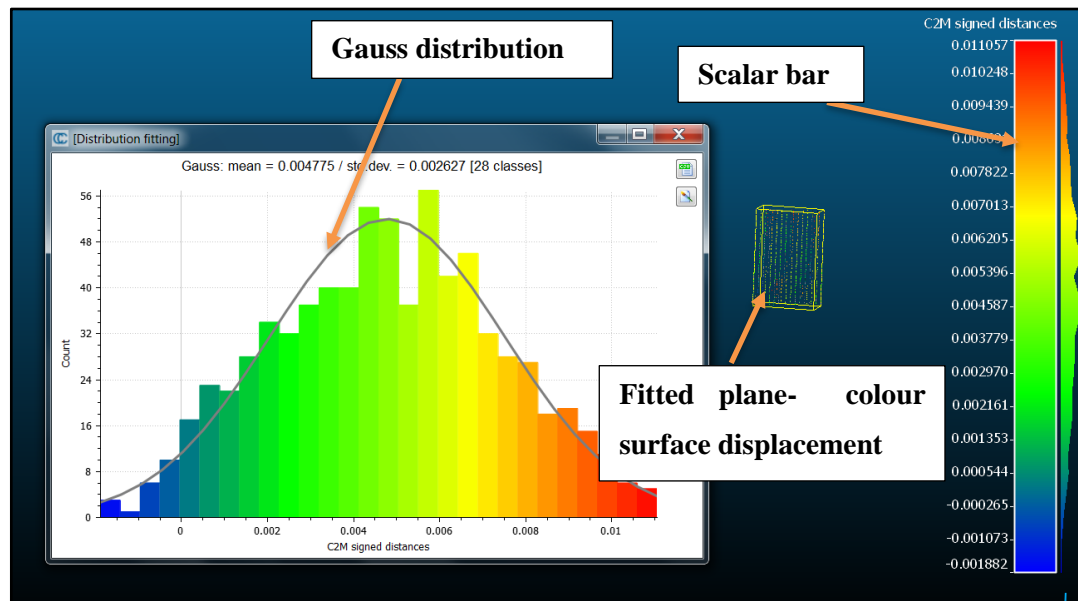


Figure 5-25 Colour surface displacement and histogram output from distance comparison in Cloud Compare

Figure 5-26 and Figure 5-27 show the time series of monitoring target locations, using the gaussian mean for CRP and TLS and the calculated coordinates for the TS. Each instrument uses its readings from Feb 16 as the baseline, given that this was the first common date from every instrument collected.

The objective of this analysis was to establish how well deviation/deformation could be measured and to test the capabilities of using TLS and CRP, by comparing the results with TS. Before deploying any new system, such as TLS and CRP for structural monitoring, there needs to be a way of validating the performance of the new system against the actual performance of a known method (e.g. Total Station Survey).

The results from these figures show that the deviations obtained by TS and TLS are within 1mm to 2mm variations in all target positions. Similarly, the deviations obtained by TLS and CRP are within 1mm to 3mm variations in all target positions. However, Target 8 measured on April 16 showed a much greater difference of 7mm. The author believes this to be an anomaly but cannot precisely say how this occurred.

Another observation was that CRP and TLS are almost always below the TS values. However,

Figure 5-26 and Figure 5-27 show that TLS and CRP have a similar precision to TS in most of the target locations, except target 8, as this was closer to the crack.

Results show that millimetre level accuracy can be achieved in deviation/deformation analysis through plane fitting techniques. However, the wall was not a plane surface if we consider the whole section. Therefore, in section 5-10, an analysis mesh was created to compare the whole section of the wall between the baseline and inter epochs.

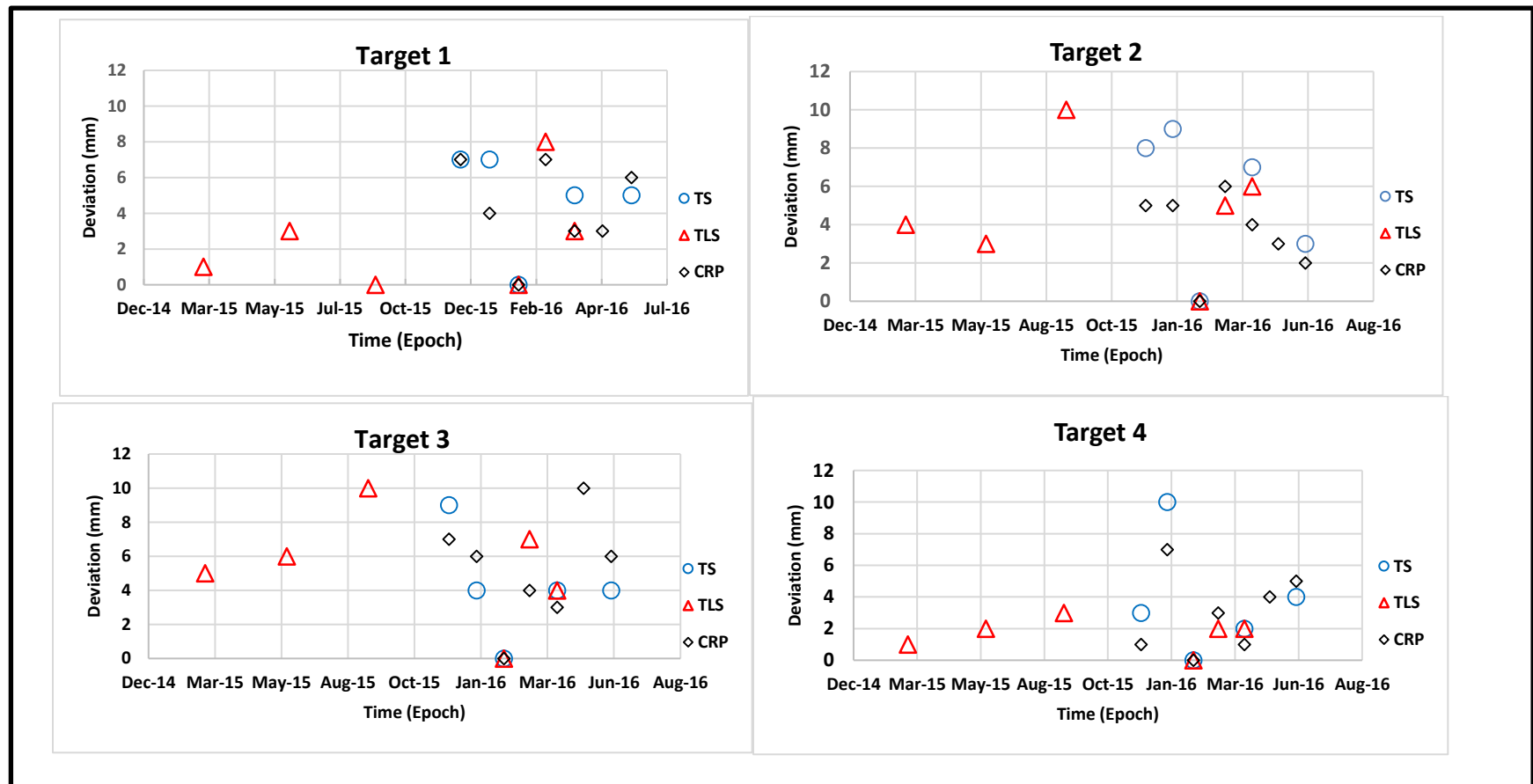


Figure 5-26 Comparison between TLS, CRP and TS of measuring deviation/deformation at Target points 1,2,3 and 4

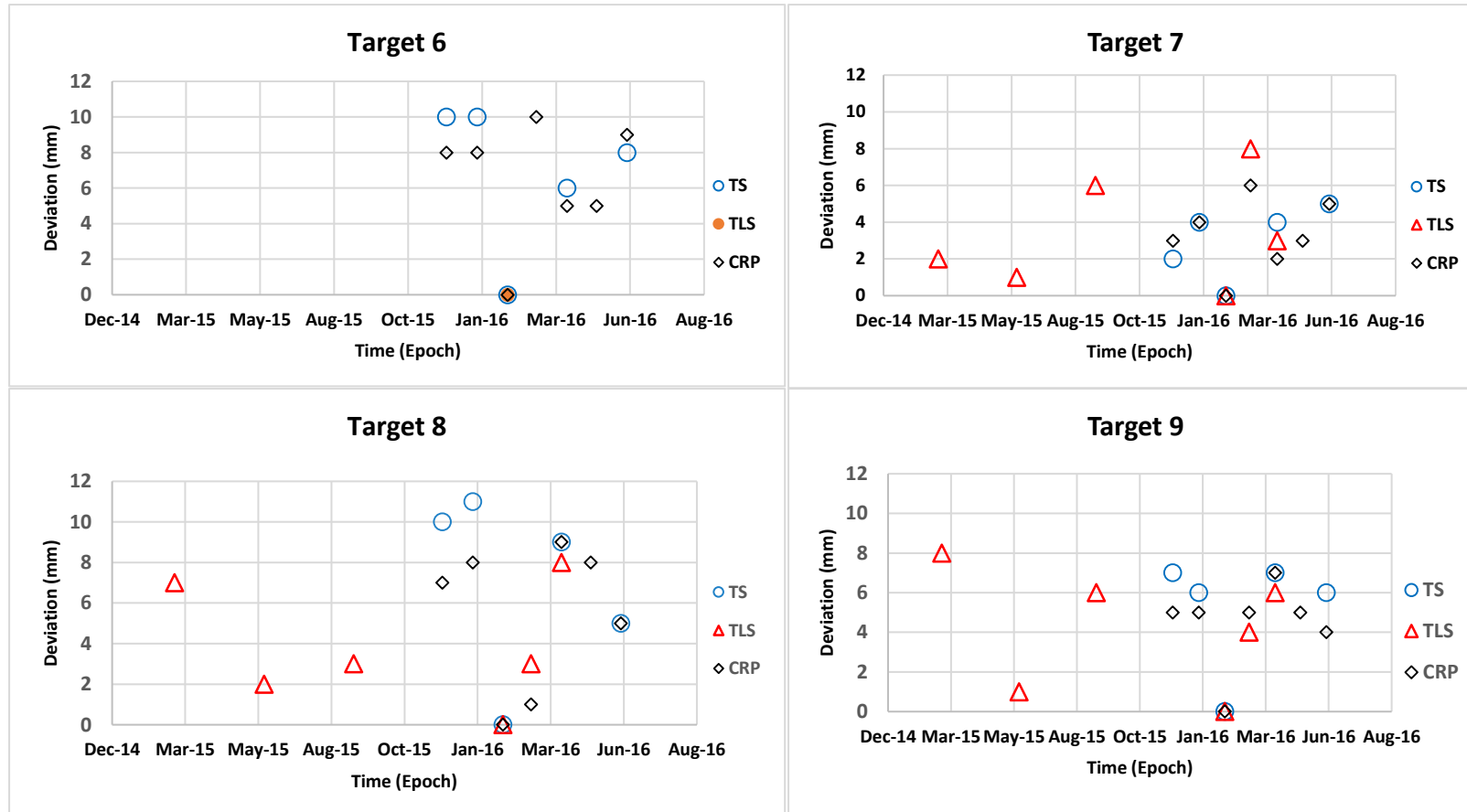


Figure 5-27 Comparison between TLS, CRP and TS of measuring deviation/deformation at Target points 6,7,8 and 9

5.10 Point Cloud Comparison in Cloud Compare

Point cloud data generated by the laser scanner and close-range photogrammetry were imported into the Cloud Compare software, to identify the wall movements between epochs. Cloud Compare is an open-source software capable of comparing 3D point clouds in between two epochs or in-between point cloud and meshing data. To achieve a better comparison between two-point clouds, they must be aligned using Cloud Compare's ICP (iterative closed point processing) algorithm or georeferenced by using TS data. For perfect alignment, an overlap between the two-point clouds is required. Before performing the alignment and registration of two-point clouds, noise (refers to moving objects in the area such as a pedestrian) and point clouds outside of the area of interest must be removed, otherwise, registration could be degraded (Girardeau-Montaut, 2011). This task was performed in Leica's "Cyclone" software, for laser scanner point clouds and "Agisoft- Photoscan" software for the point clouds created using digital photos. The point cloud captured by the Leica P40 scanner (March-16) was considered as the baseline for model comparison because of the accuracy and density. The cleaned point clouds were imported to Cloud Compare in a (*. pts) file format and, when importing, XYZ RGB, scalar-field and intensity were enabled.

After the data alignment, the cloud to mesh comparisons were performed. Deviation analysis was performed to calculate the distance between the two models. Before applying any local models in cloud compare, approximate deviation distance between two data sets were computed. Then local models such as least square planes and the height function were applied to increase the accuracy of the computed distance between two data sets (Girardeau-Montaut et al., 2005). Girardeau-Montaut, 2012 showed that the Height Function model is more accurate when compared to Least Square Planes because it is computed using more points. However, this model is not suitable for a noisy reference cloud. Before processing the deviation analysis, both points/mesh data were cropped to the same dimensions to remove any boundary effects. The comparison result is a coloured point cloud for each epoch showing the deviation about the reference

TLS and the previous epoch of point cloud data. However, one of the software limitations is that the only way of providing numerical information of the deformation is through the coloured scale.

Figure 5-28 shows the non-suitable position of the scanner to capture the whole of the wall and the figure clearly shows a missing part of the wall. Due to non-availability of the point cloud data created by TLS, this portion of the wall was not compared with other epochs of TLS and CRP point cloud. However, point clouds created by CRP in different epochs were compared.

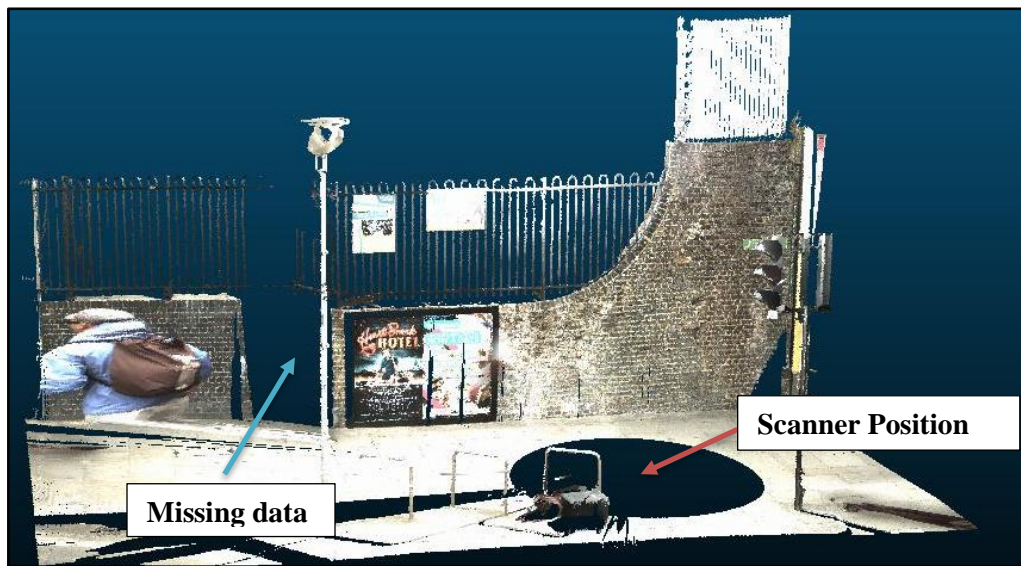


Figure 5-28 Non-suitable scanner position to scan the area of interest

5.11 TLS and CRP results

TLS and CRP provide complete surface information and area-based displacement/deviation maps to be computed. These maps were used for inter-comparison between different epochs. The deviation/deformation maps shown in Figure 5-29, Figure 5-30, Figure 5-31, Figure 5-32 and Figure 5-33 were created by comparing the meshed surface of the baseline point cloud (Feb16-TLS was considered as the baseline) and point cloud surfaces for each epoch of TLS and CRP in Cloud Compare (version 2.8.1) software. The deviation/deformation

shown are in “front-isometric” view for each of the epochs compared to the baseline. The scale of displacement analysed is -0.014m to +0.014m except, Figure 5-33; due to noise in the April 16 point cloud data, a scale value of -0.025m to +0.025m was used. The reference point cloud did not have noise (e.g pedestrian) therefore, when compared to noisy data, the software could not identify the corresponding point cloud and lead to erroneous results. The movements are shown in different colours to show the magnitude of the changes. A major limitation of Cloud Compare is that numerical values of deviation/deformation are represented through the colour coding map rather than a vector map.

5.11.1 TLS Results

Figure 5-29 to Figure 5-32 show the deviation maps computed between baseline and different epochs of TLS data. The colour scale used on the surface displacement map highlights a deviation or deformation of the wall. Results agree with the observations from the TS monitoring. The accuracy of the deviation map is dependent on the ICP registration between the epochs calculated by the Cyclone software. The majority of the errors came from the registration process as it seems that the alignment is normally done at the centre of the point cloud (lowest differences), whilst the edges of the point cloud tend to be where the largest differences were found.

The Gaussian mean and the standard deviation show that most of the wall deviates between 0mm and 3mm (shown in light green colour). The differences between the point clouds follow a normal distribution with a bell curve. However, the area closer to cracks deviated more than 14mm. The area shown in orange had deviations varying from 6-8 mm. Figure 5-33 shows a higher deviation value range of 9-12mm due to noise caused by a pedestrian in the April-2016 data and visible in the point cloud data.

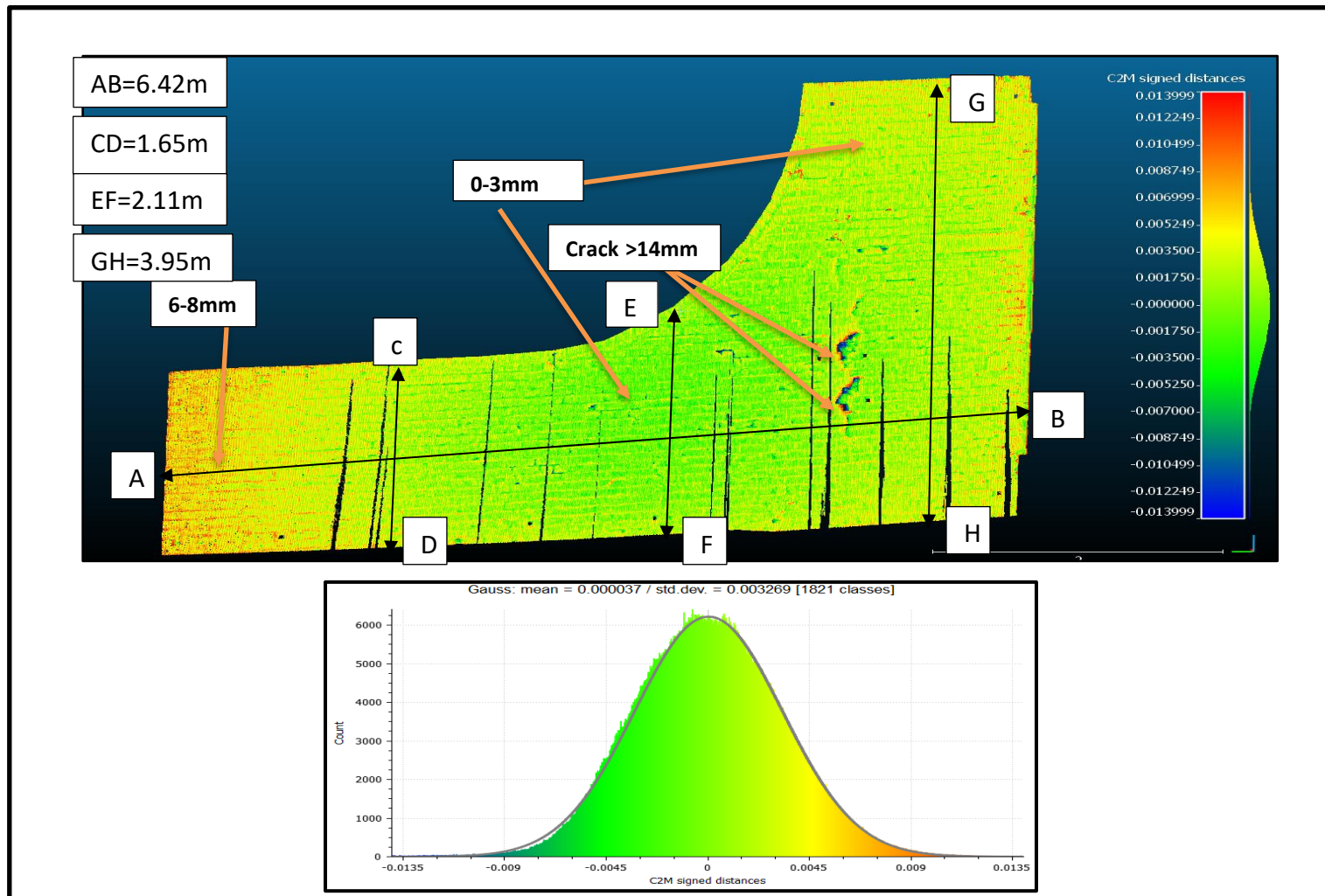


Figure 5-29 Deformation displacement map of the whole wall between Feb16 TLS and March-15 TLS (deflection in metres)

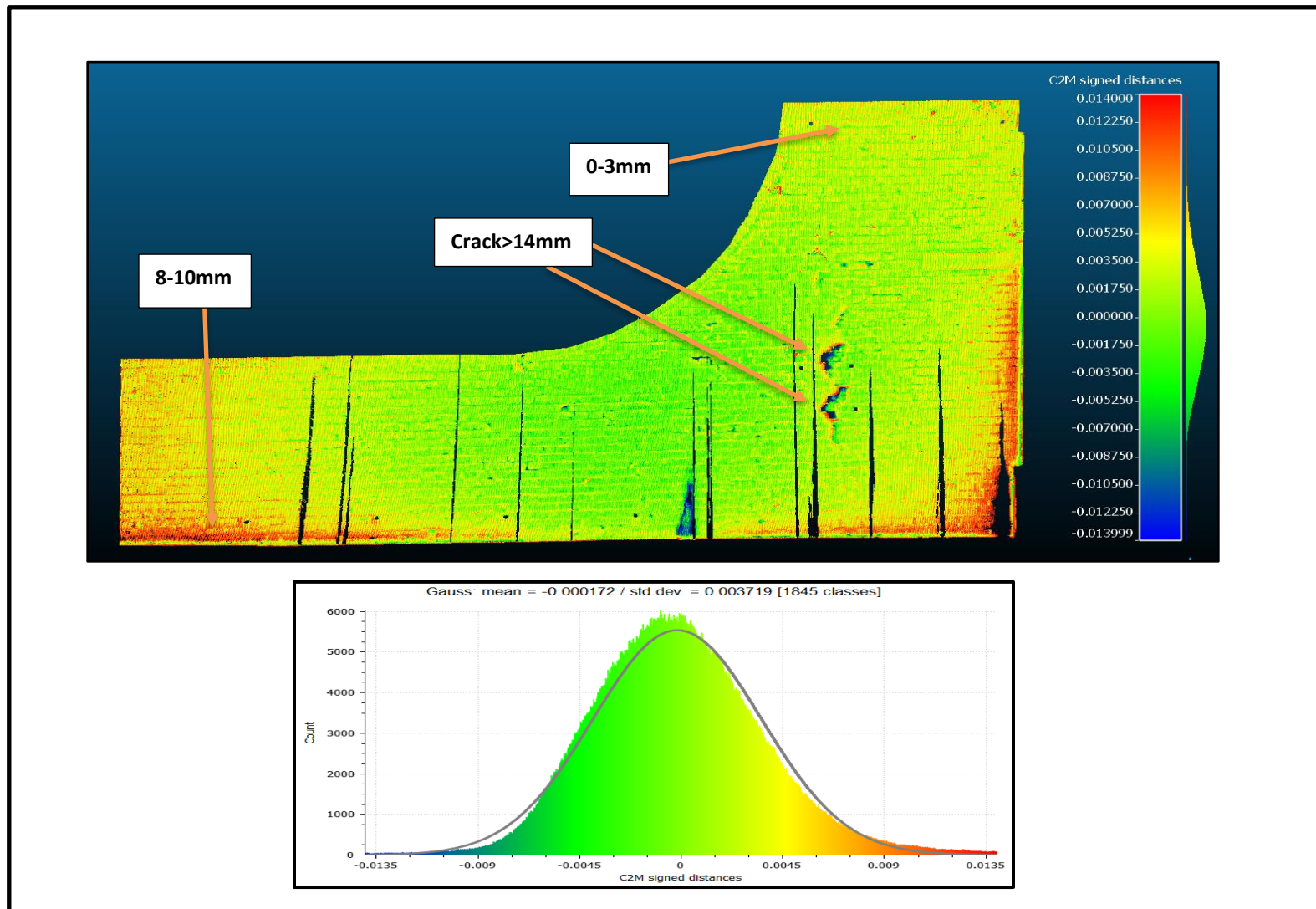


Figure 5-30 Deformation displacement map of the whole wall between Feb16 TLS and June-15 TLS (deflection in metres)

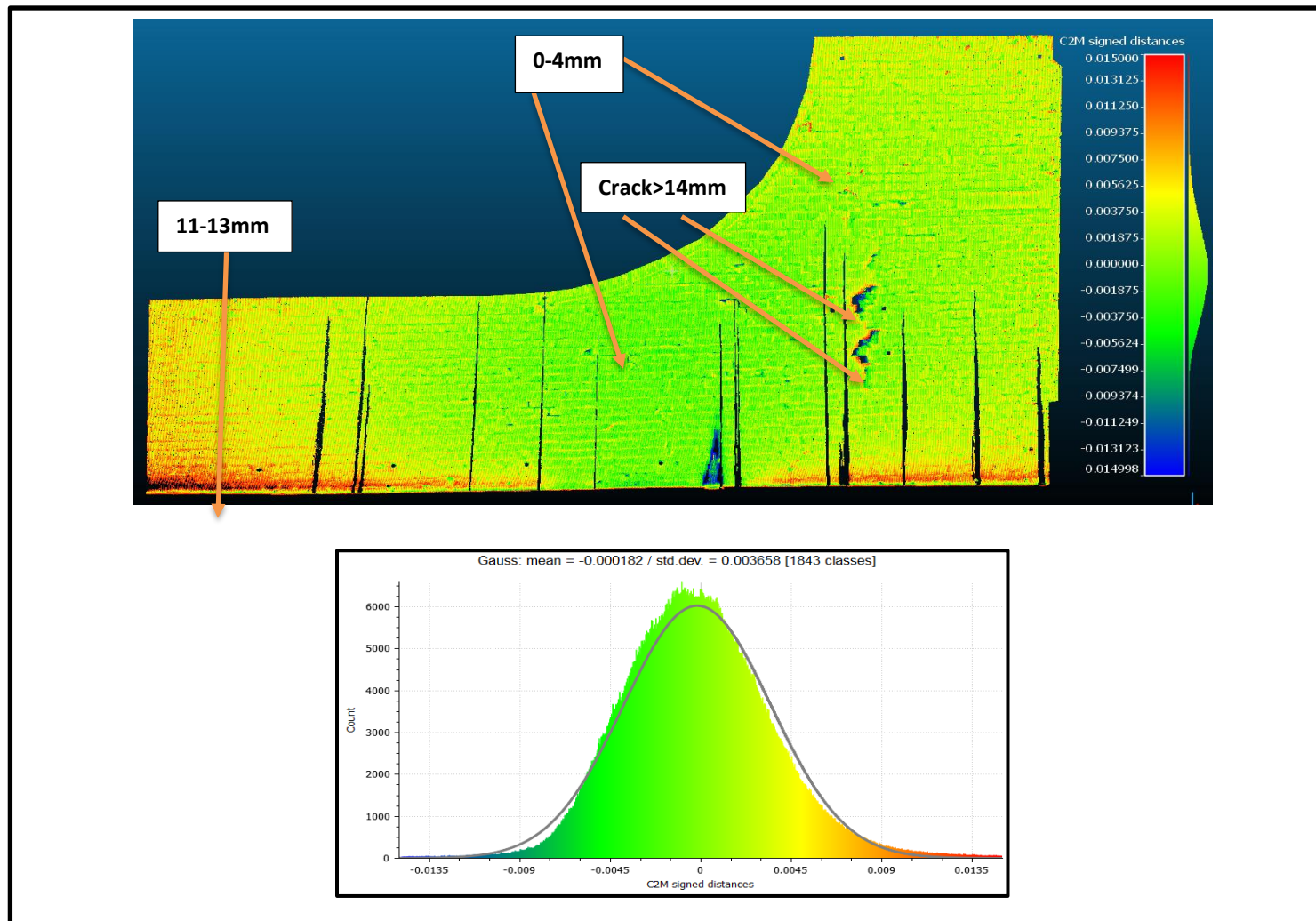


Figure 5-31 Deformation displacement map of the whole wall between Feb16 TLS and Sep-15 TLS (deflection in metres)

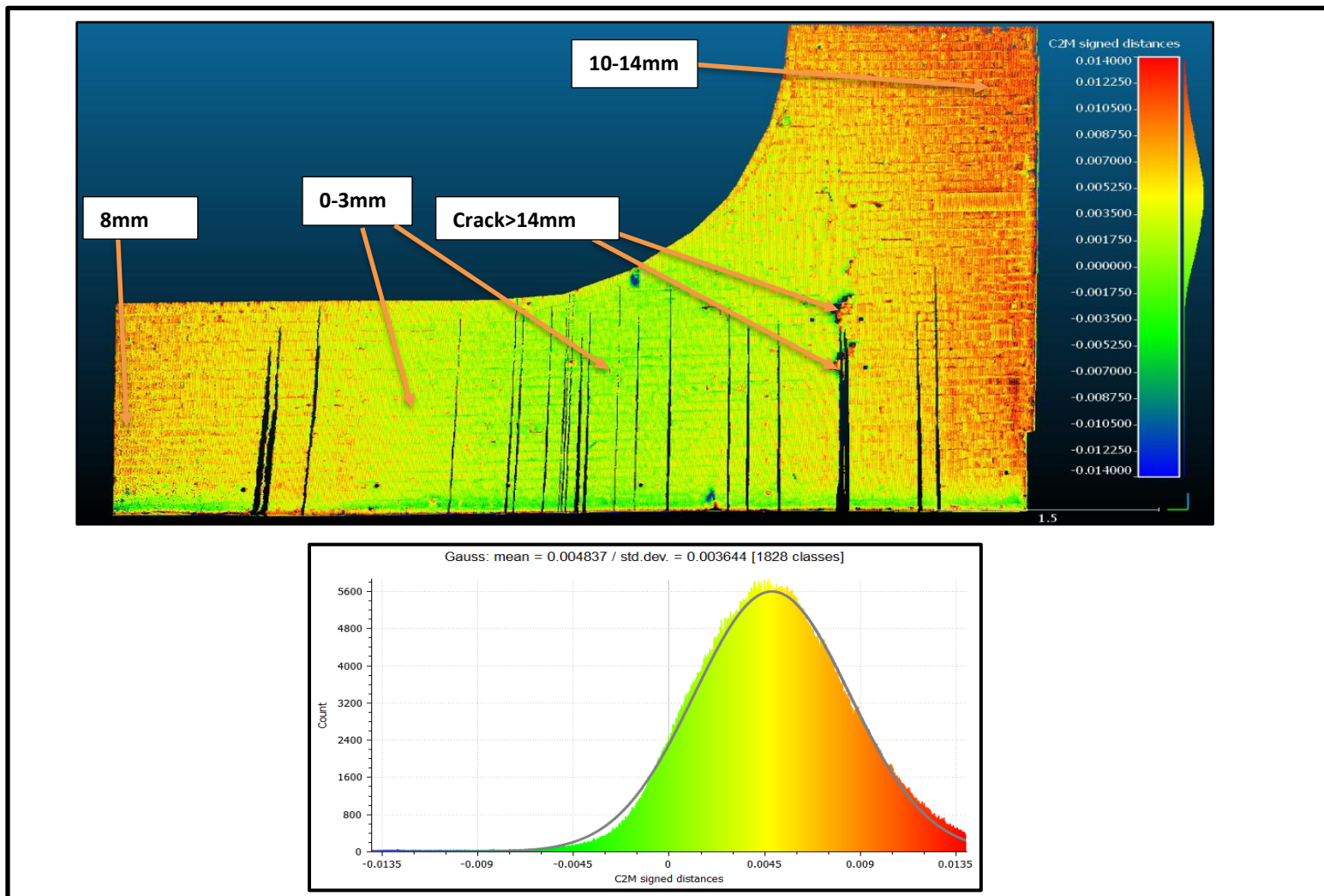


Figure 5-32 Deformation displacement map of the whole wall between Feb16 TLS and March-16 TLS (deflection in metres)

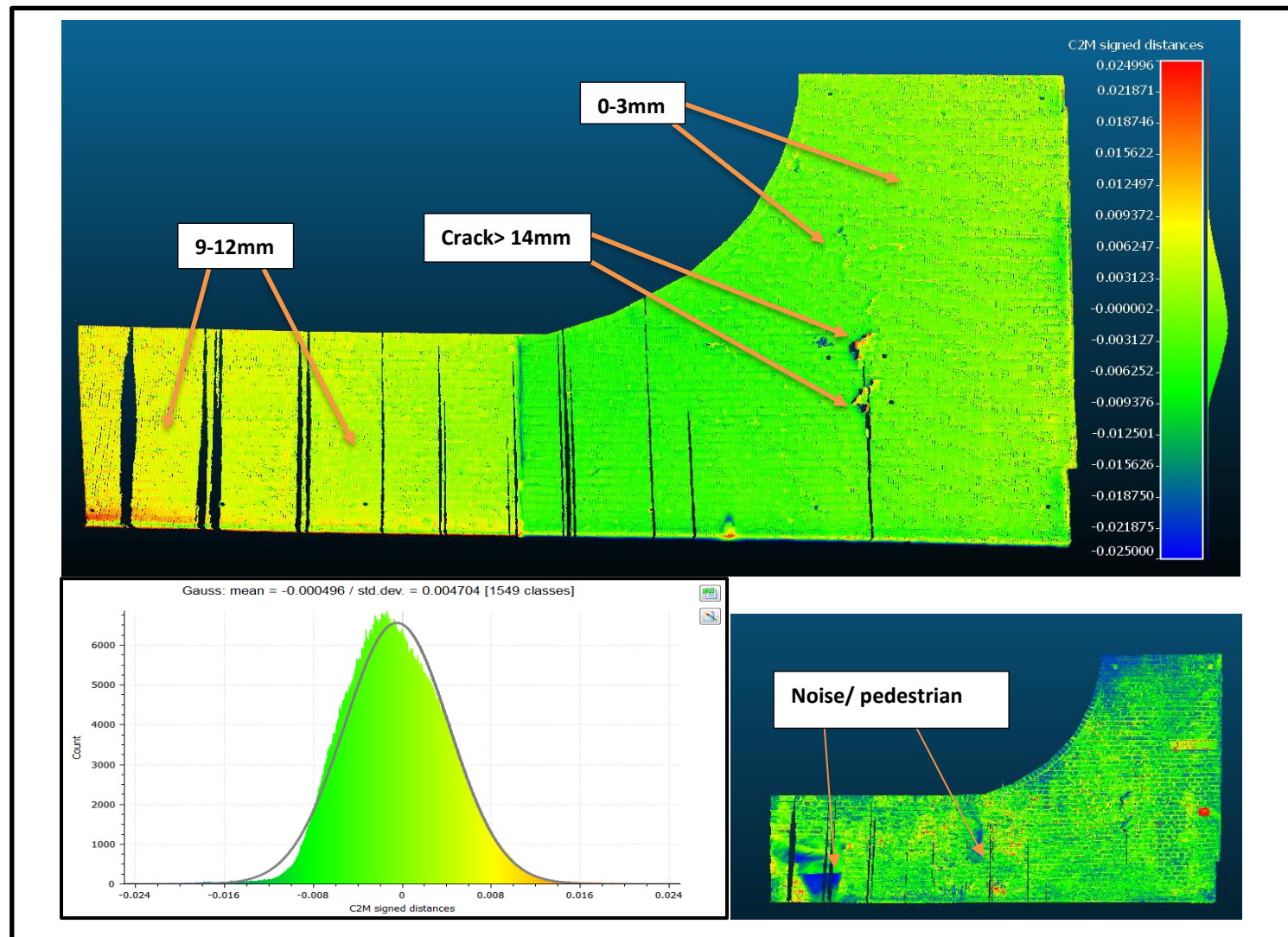


Figure 5-33 Deformation displacement map of the whole wall between Feb16 TLS and April-16 TLS (deflection in metres)

5.11.2 CRP Results

Figure 5-34 to 5-40 show deviation maps computed between the baseline (Feb 16 TLS) and the different epoch of CRP data. Furthermore, these figures show mean and standard deviations with the "theoretical" 95% confidence interval ($\text{mean} \pm 2\sigma$). Standard deviation expresses the variation from the mean value. Therefore, a low standard deviation refers to values which are close to the mean and oppositely, a high standard deviation indicates a bigger variation in comparison with the mean value. All the standard deviations in the figures are closer to their mean value and indicate that most of the point values are closer to the mean value.

The left side of the wall moved more than 14mm and Figure 5-34 shows this part was not captured by the TLS, except the baseline. Therefore, TLS comparison was not performed. Overall, many areas deviate by 0-5mm (yellow areas), and the mean deviation is around 1-4 mm. The crack and the vegetation area deviated more than 14mm.

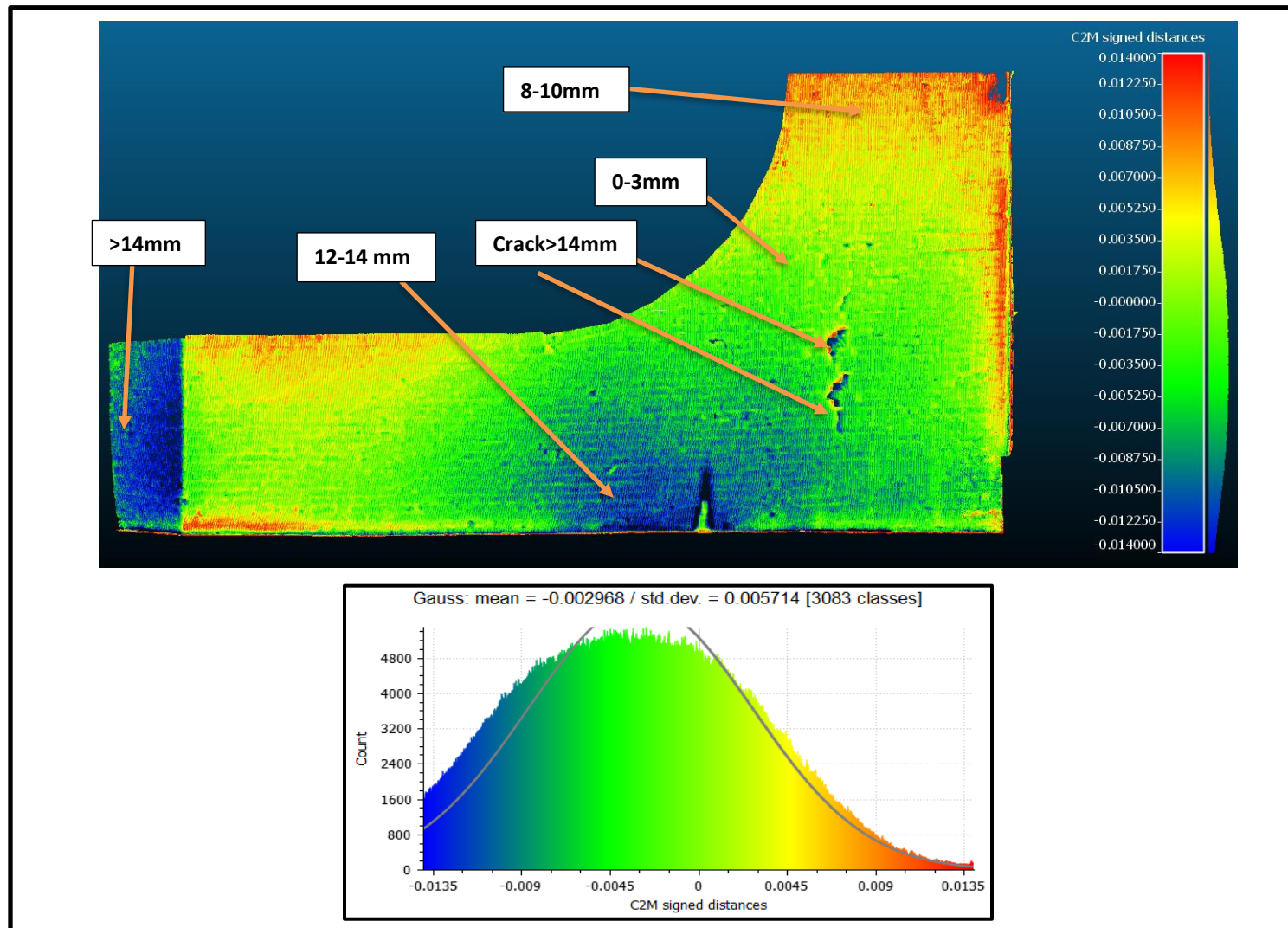


Figure 5-34 Deformation displacement map of the whole wall between Feb16 TLS and Dec-15 CRP (deflection in metres)

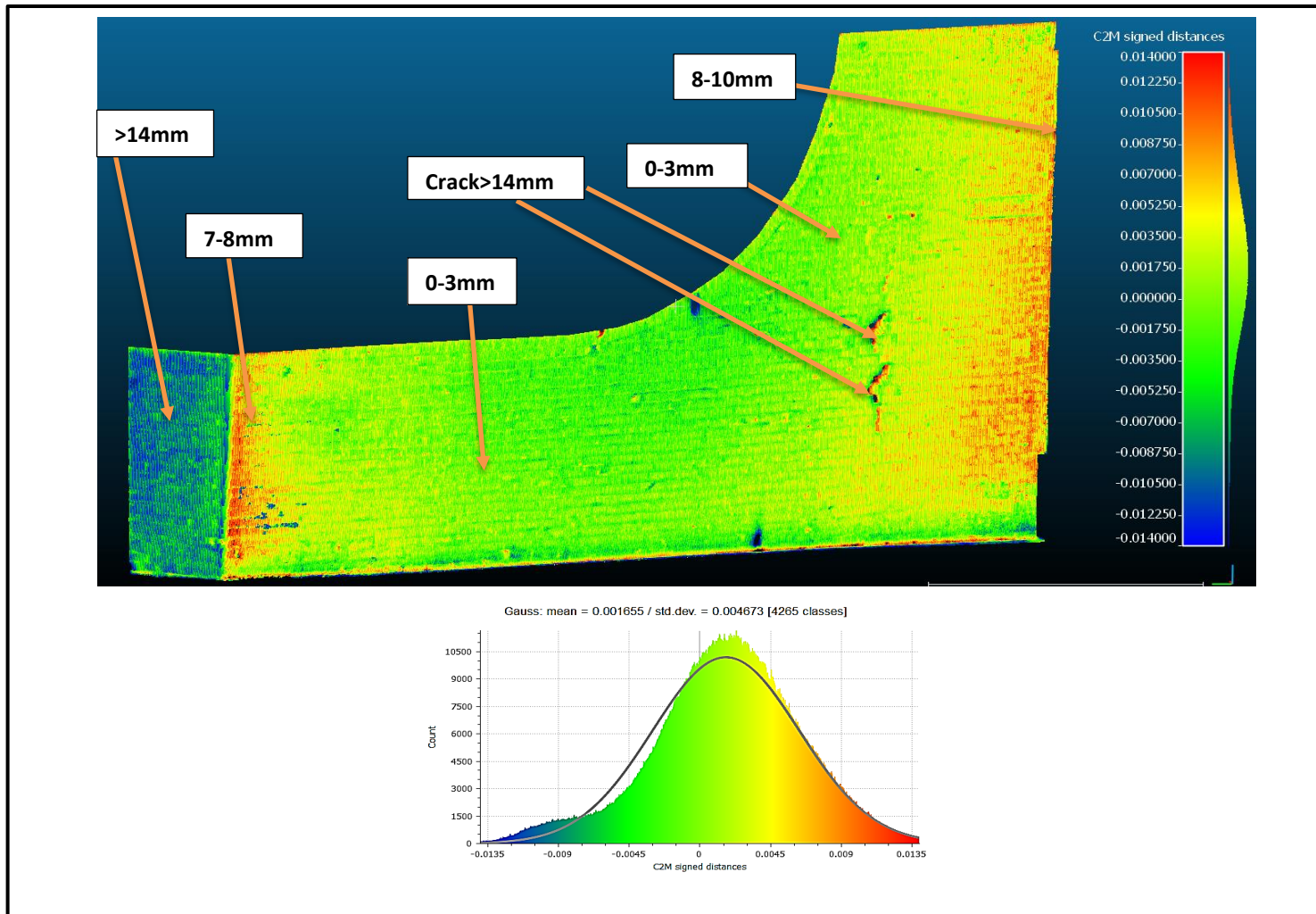


Figure 5-35 Deformation displacement map of the whole wall between Feb16 TLS and Jan -16 CRP (deflection in metres)

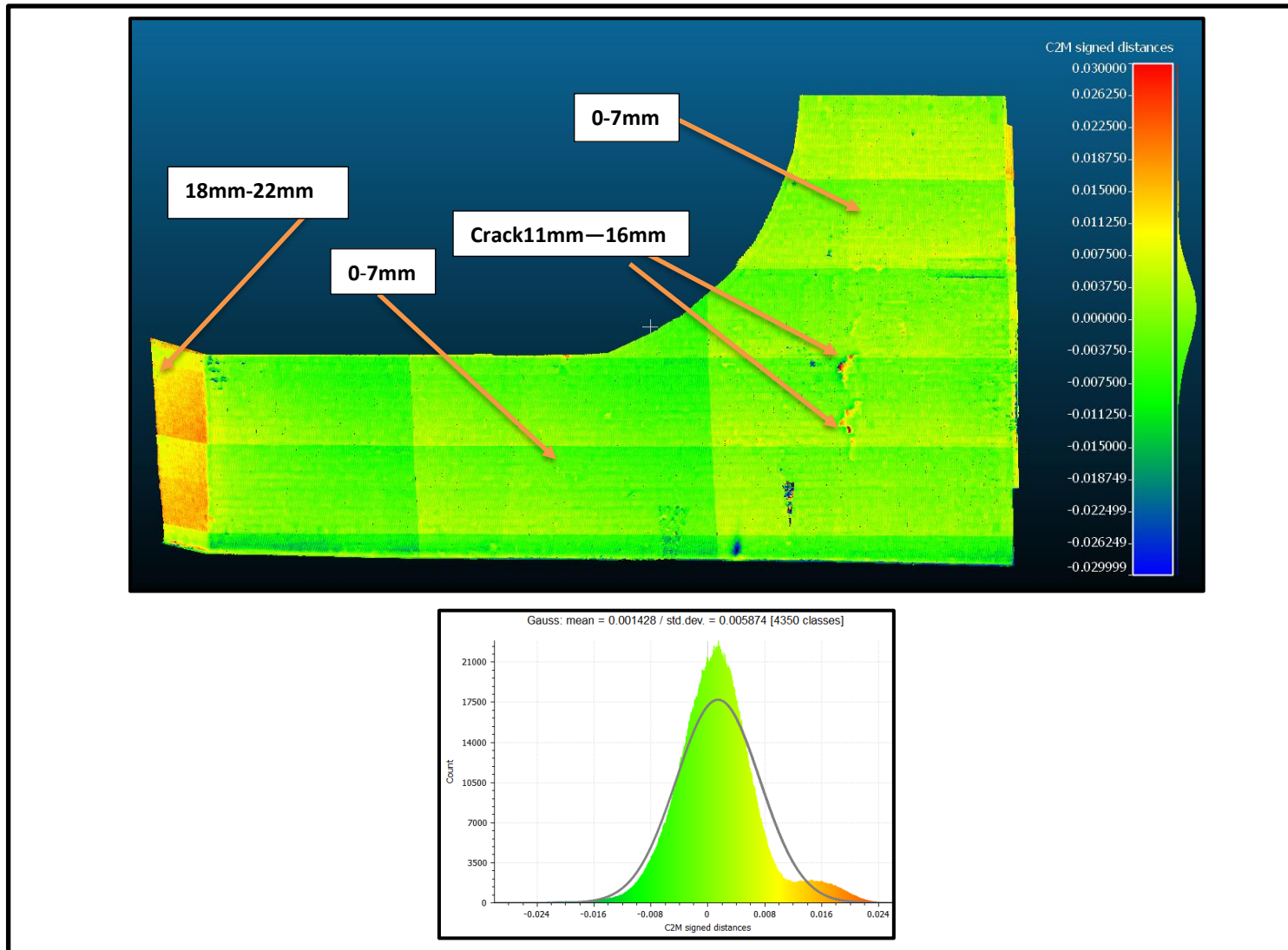


Figure 5-36 Deformation displacement map of the whole wall between Feb16 TLS and Feb-16 CRP (deflection in metres)

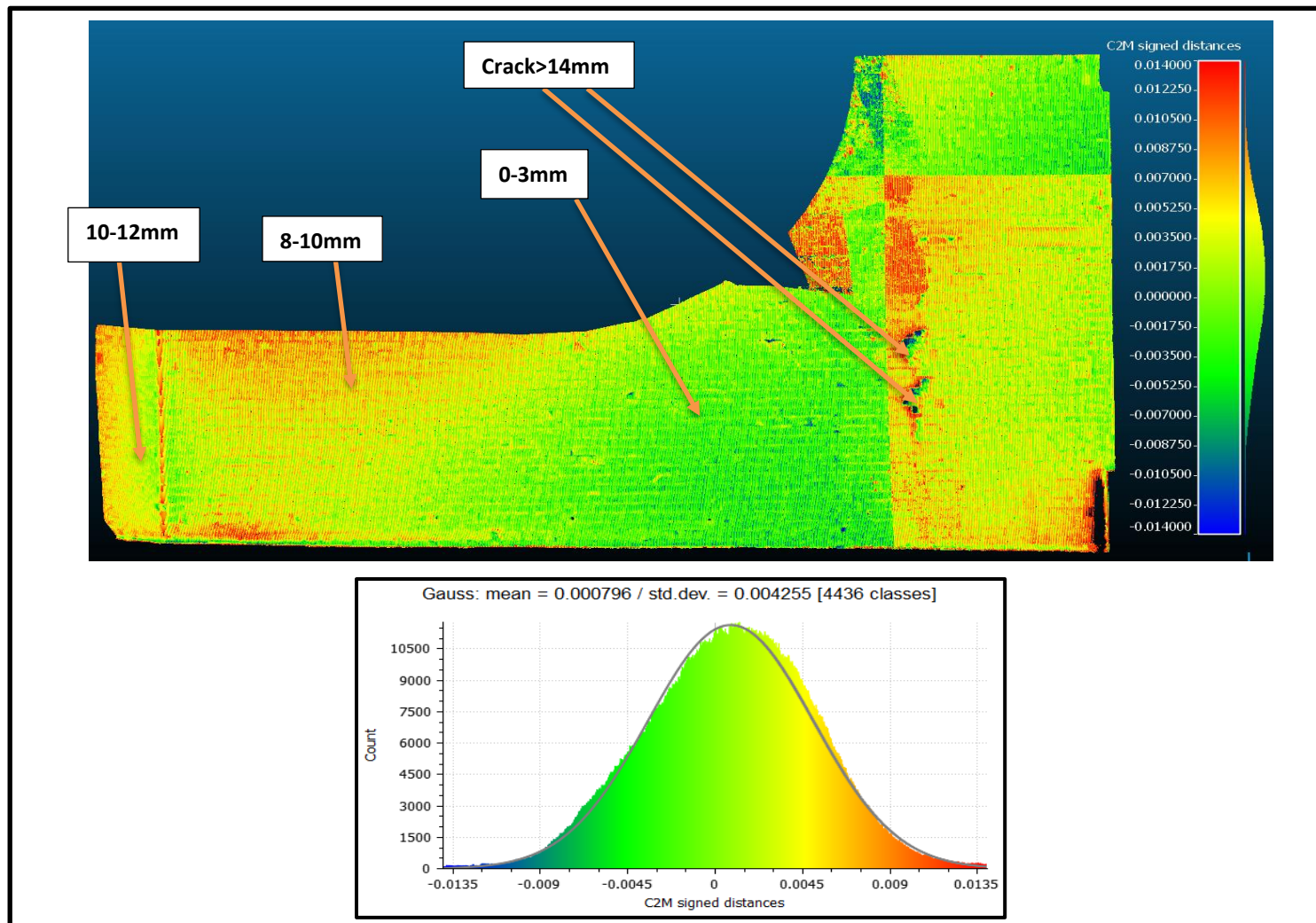


Figure 5-37 Deformation displacement map of the whole wall between Feb16 TLS and March-16 CRP (deflection in metres)

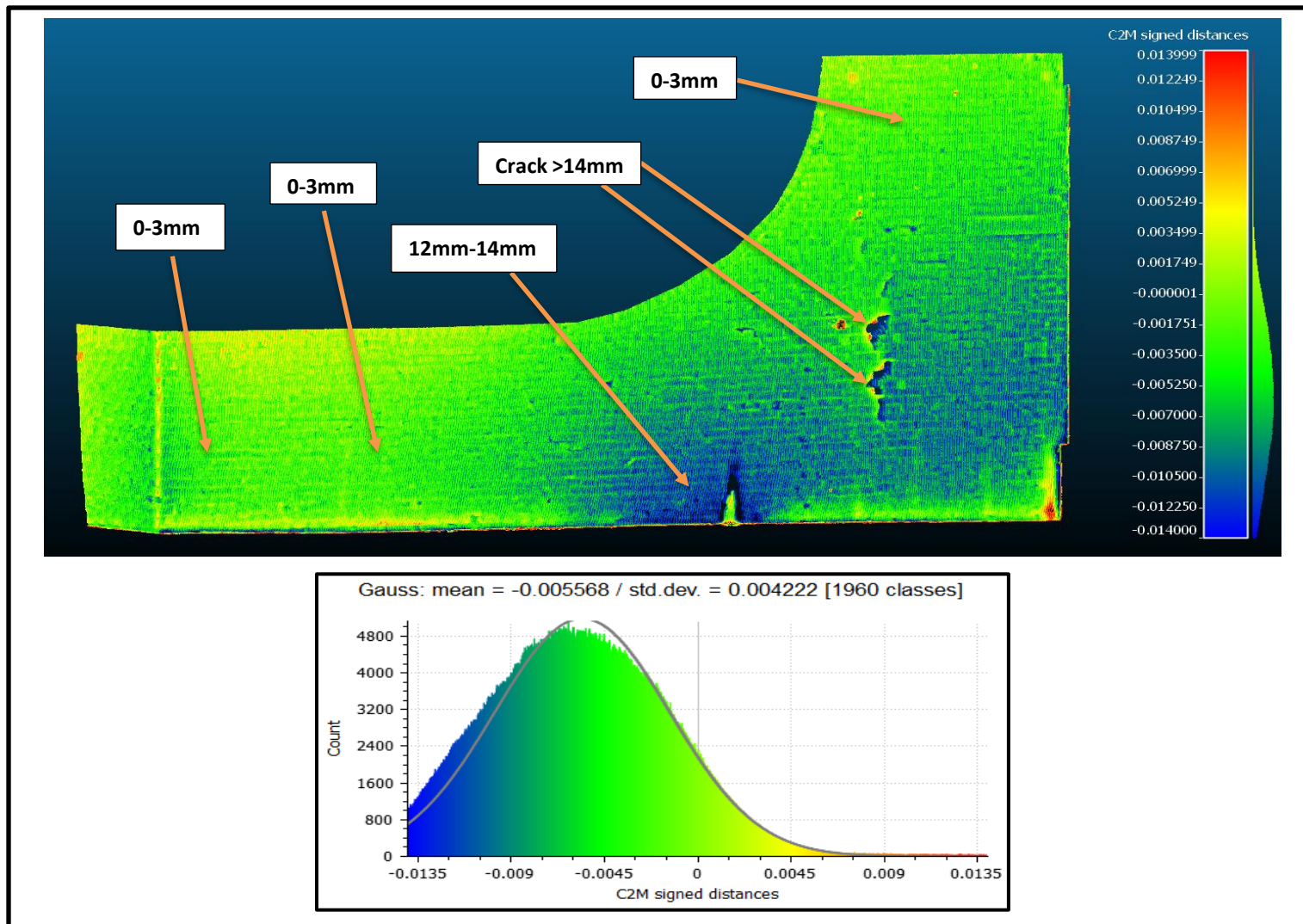


Figure 5-38 Deformation displacement map of the whole wall between Feb16 TLS and April-16 CRP (deflection in metres)

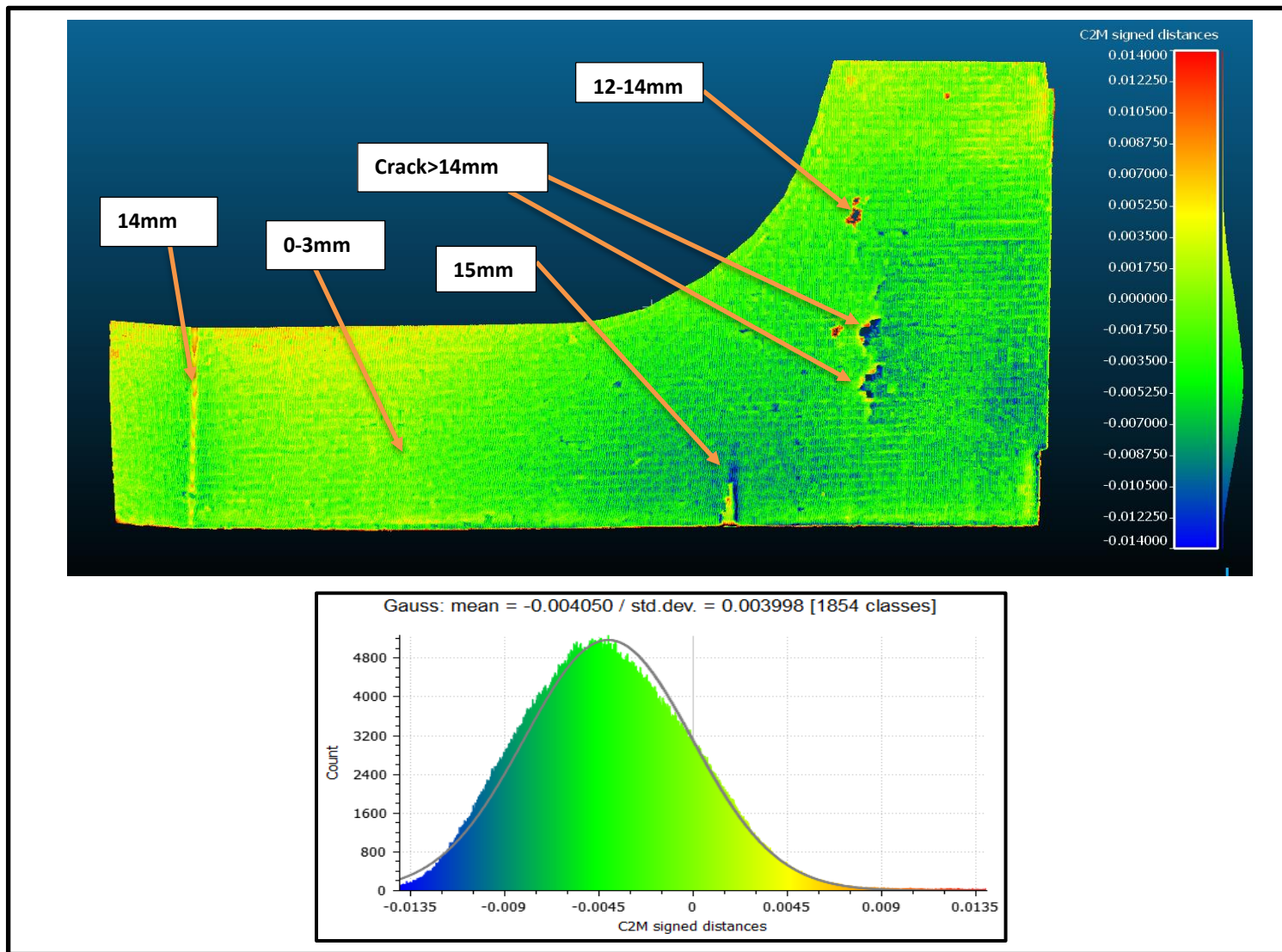


Figure 5-39 Deformation displacement map of the whole wall between Feb16 TLS and May-16 CRP (deflection in metres)

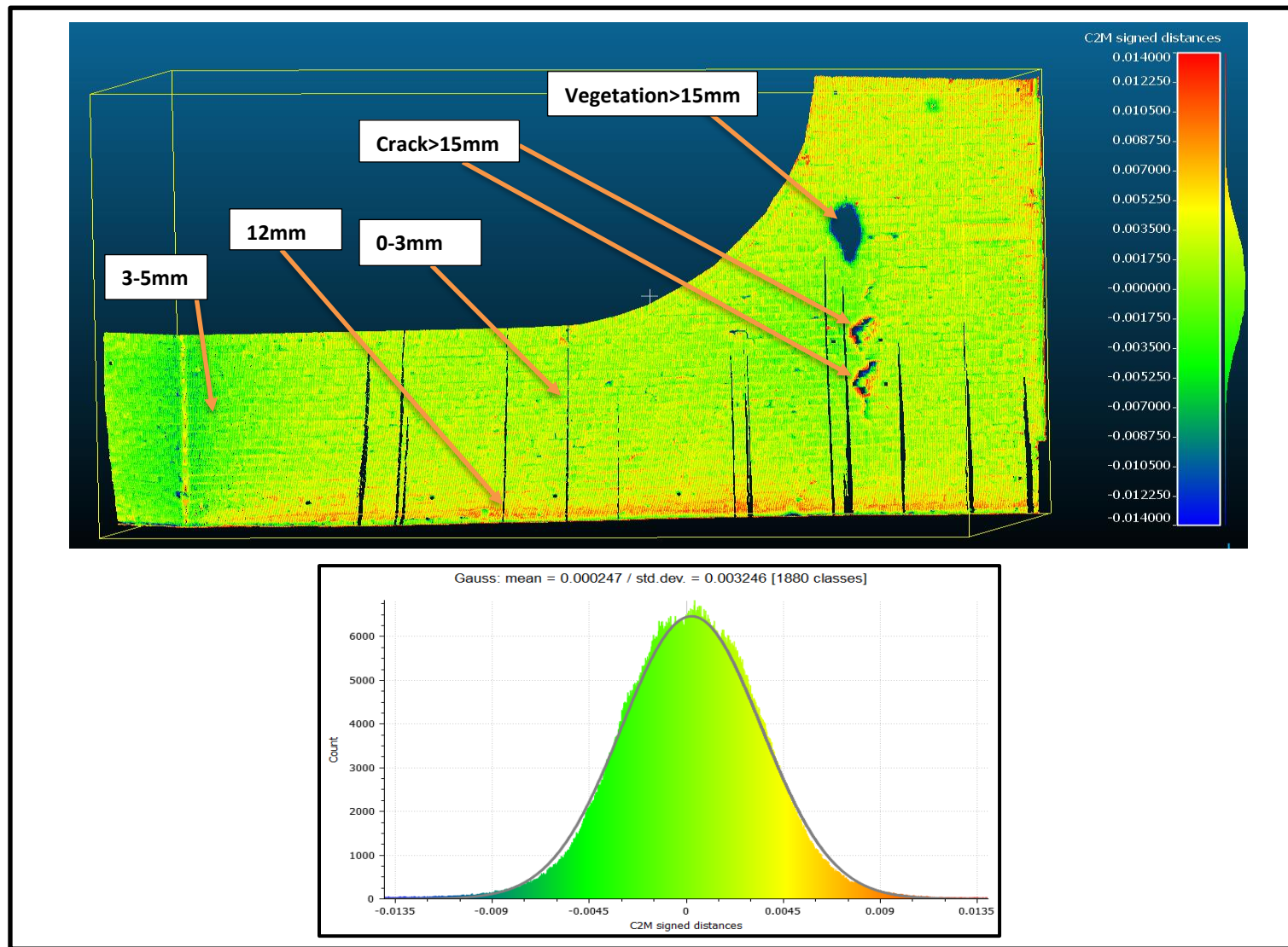


Figure 5-40 Deformation displacement map of the whole wall between Feb16 TLS and June-16 CRP (deflection in metres)

5.12 Further Analysis of Terrestrial Laser Scanner (TLS) and Close-Range Photogrammetry (CRP) data

Section 5.11 showed that the maximum wall movements occurred at the left side edge and the right-side bridge abutment. However, these movements were very small and likely to be due to:

1. Lack of control points outside of the area at the top of the wall
2. Discrepancies between registering/geo-referencing the laser scanner point cloud (geo-referenced by LUL) and photogrammetry point cloud (by the researcher). These cannot be avoided as it is a consequence of the accuracy of the surveying techniques.

Therefore, further analysis was performed in order to identify deformations of the wall and to check the accuracy of the point clouds. To carry out this analysis, strips of data were cut from the laser scanner and photogrammetry point clouds at three different locations identified as top, middle and bottom strip, shown as black lines in Figure 5-41.

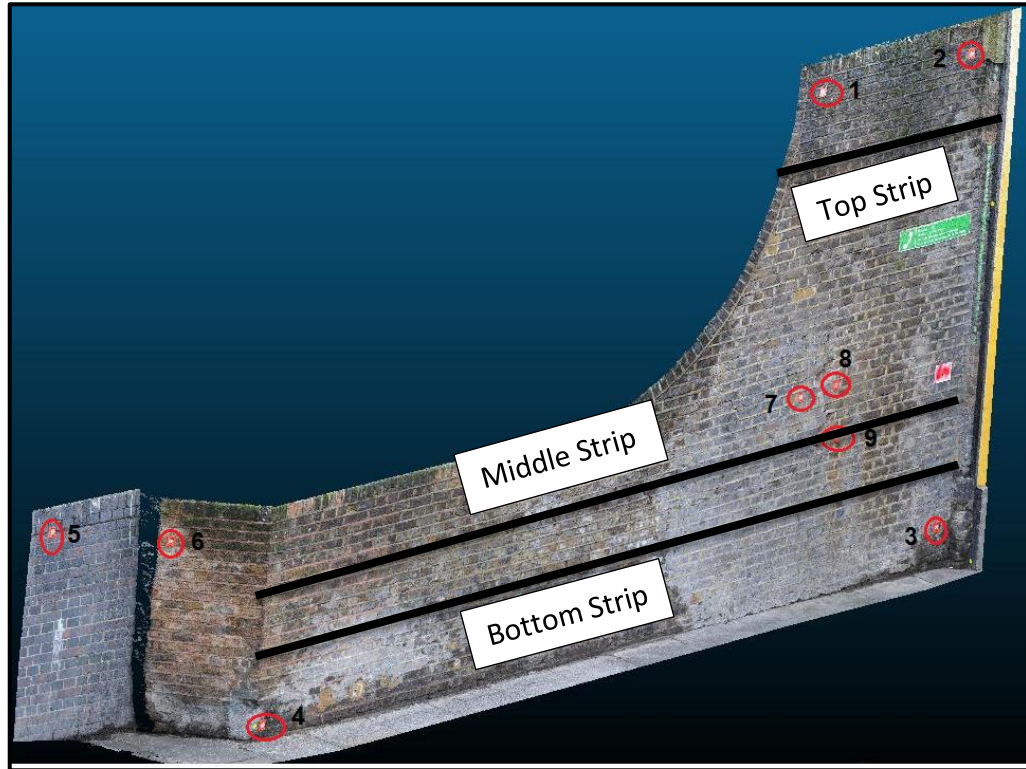


Figure 5-41 Location of the top, middle and bottom strips on the studied wall

The strips of data removed from the point clouds had a large number of points with 3D coordinates. However, since changes in the vertical axis are minimal, i.e. $\pm 1\text{mm}$, movements in the vertical direction were neglected. The values for the minimum Y and the maximum X coordinates were determined and used as the initial point or the zero coordinate.

As the Total Station had been determined by LUL to a reference grid based on the Ordnance Survey of Great Britain, it was necessary to convert the coordinates from the photogrammetry to the same reference grid. As such, each strip was plotted as a 2D graph, where the angle (θ) between a line passing through the outermost point and origin was measured. This angle was used to rotate the coordinates of the data points, using equations (5.10) and (5.11).

$$X = x\cos\theta - y\sin\theta \quad (5.10)$$

$$Y = y\cos\theta + x\sin\theta \quad (5.11)$$

Where:

x = initial coordinate in the X-axis on the horizontal plane

y = initial coordinate in the Y-axis on the horizontal plane.

θ = rotation angle

X = new coordinate in the horizontal axis

Y = new coordinate in the horizontal axis

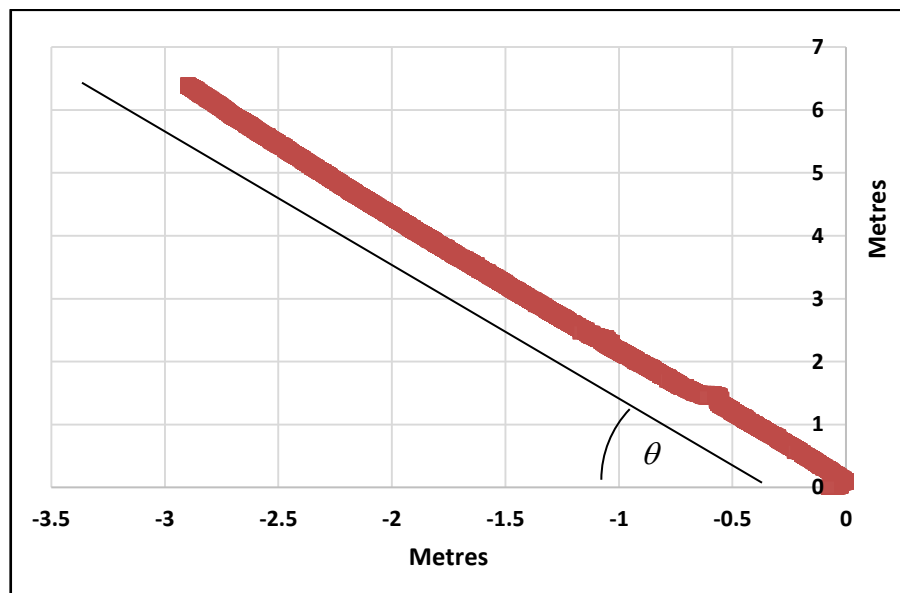


Figure 5-42 Determining the rotation angle

After the rotation of the coordinates of the strips, the new x- and y-coordinates were compared to the baseline values in order to understand the amount and form (shape) of rotations the structure had experienced.

5.12.1 Comparison of movements between top, middle and bottom strips of wall

The wall movements, determined by photogrammetry of June 2016 (the last epoch), for the three strips are plotted together and shown in Figure 5-43. The figure shows that the wall deformed towards the pavement with the bottom strip showing deformation of around 35mm, whilst the middle strip shows deformation of around 60mm. The raw data for each strip shows a scatter of around 15mm and it may be possible to reduce the scatter by filtering the data, however, this was not attempted here, so that the quality of the data, generated by both methods, can be appreciated. Also, filtering the data would smoothen drastic changes in shape; an example is a crack in the structure whereby, any filter applied here would mask the true depth of the damage. For the wall movements, the outside edge of the scatter has been used, i.e. the largest value. As changes in movement between surveys are required and provided that this outer edge is consistently used, this method is valid. However, with the improvements in the accuracy of measuring instruments, the scatter will reduce and therefore, the mid-point of the scatter should be used in future works. The figure also shows that the right side of the wall did not move much from the middle to the top strip, showing small movements from the bottom to the middle strip. This would appear to suggest that the right-hand side of the wall is significantly stiffer than the rest of the wall and, as a consequence, a crack (peak seen in the middle strip, depth of around 50mm) appeared at around -1.5m along the wall. A later site visit confirmed that behind the area of the wall of no movement, there is a buttress to the wall; a much more rigid structure, as seen in Figure 5-44. The buttress, being significantly stiffer than the wall, creates a discontinuity in stiffness, thereby causing the crack to occur at their junction.

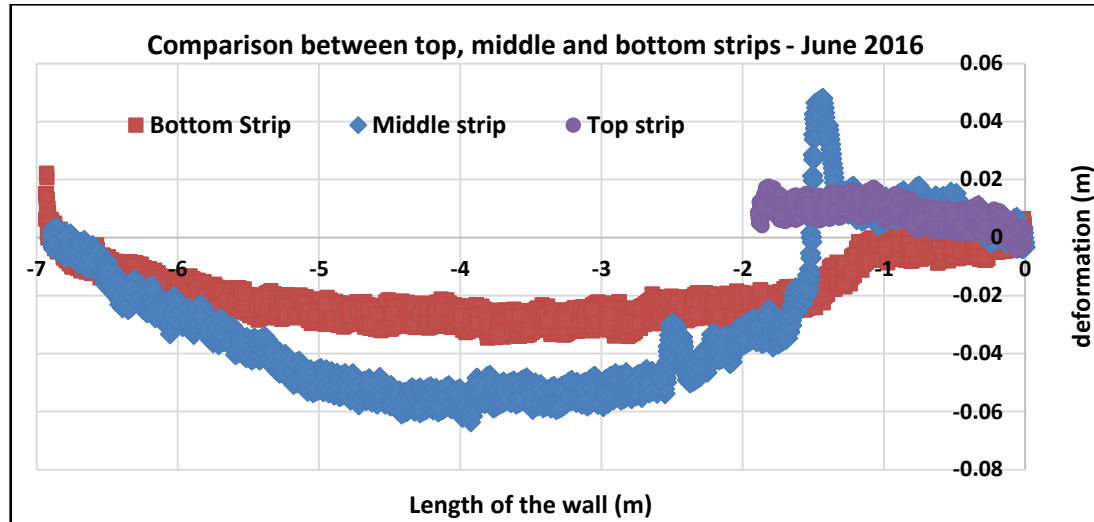


Figure 5-43 Comparison between top, middle and bottom strips for June 2016 (last epoch of Photogrammetry)



Figure 5-44 Abutment at the back of the wall

5.12.2 Comparing Terrestrial Laser scanner and Close-Range Photogrammetry point clouds

As commented upon earlier, the point clouds generated using the laser scanner were geo-referenced by LUL, whilst the point clouds generated using photogrammetry were geo-referenced by the author, using the same total station and control points used by LUL. Therefore, a comparison between the two forms of point clouds, for the same epoch is necessary to understand the accuracy and repeatability of the techniques. With this in mind, the point cloud created in March 2016 using the laser scanner is compared to the point cloud generated using photogrammetry on the same date. For this comparison, only the middle strip is used and the result can be seen in Figure 5-45.

Figure 5-45 shows that both point clouds have similar scattering, around 15mm, furthermore, they have the same shape and show that the wall has deformed towards the pavement by as much as 60mm. It is also possible to discern the depth of the crack, on both strips, with similar dimensions, i.e. around 60 mm. Unfortunately, the depth of the crack may not be accurate. However, cracks can also be determined by the abrupt change in the direction as seen in the figure. This observation is important as it means that measurements taken by LUL in March 2015 with the laser scanner, can be compared directly with the later work using the photogrammetry technique performed by the author.

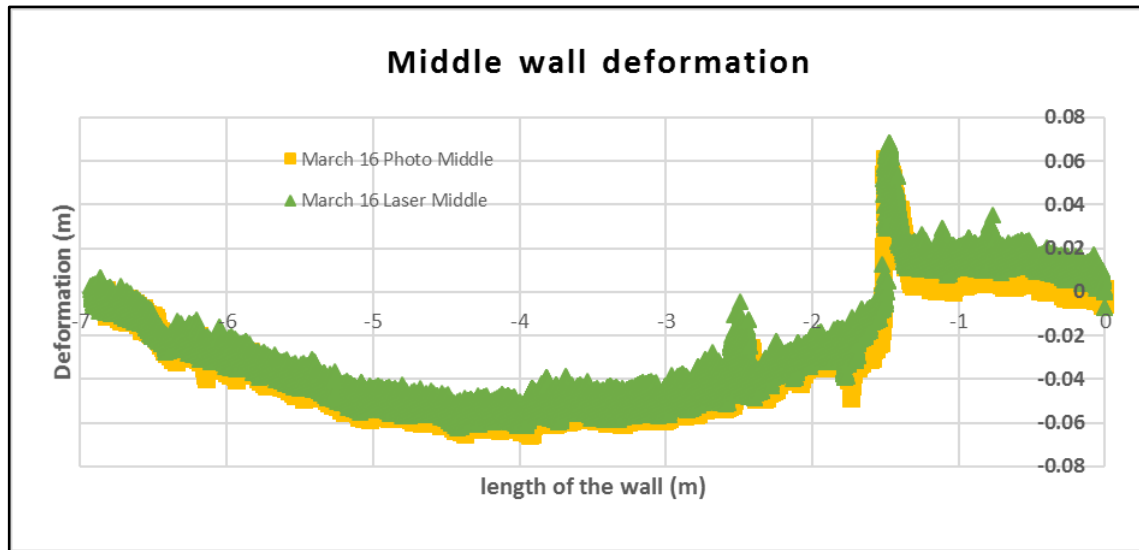


Figure 5-45 Comparison of the middle strip from laser scanner and photogrammetry

The results presented in Figure 5-45 also show that despite being obtained using different equipment and being geo-referenced by different persons, the point clouds are compatible and can be directly compared. The results also demonstrate that when comparing point cloud to point cloud or point cloud to plane (definition in section 5.8), a difference is likely to be seen given that there is a 15mm scatter in the strips. Therefore, direct comparisons between point cloud to point cloud should be avoided unless larger deformations are measured; hence, point cloud to plane is preferred.

5.12.3 Comparison between the first and last epoch of laser scanner and photogrammetry

Figure 5-46 compares the first and last epochs of the point clouds, for top, middle and bottom strips obtained by using laser scanner and photogrammetry. Figure 5-46 shows that for all epochs, the deformation of the bottom part of the wall is between 30 and 35mm, whilst for the middle, the difference shows between 60 and 65mm, and for the top, this difference is around 15mm. Comparing all 4

epochs in each figure showed a very small difference between the strips, these are likely to be related to small differences in the geo-referencing or the initial assumptions for the rotation of the strips. It is clear that the deformed shape occurred before the monitoring period and the wall has not undergone any deformation during the monitoring period.

The results are shown here demonstrate the potential of this technique to measure deformations in the shape of the structure, whether by laser scanner or photogrammetry. When analysing Figure 5.46, it was predicted that the behaviour implied a stiffer structure at the top strip of the wall than could be observed from the front of the wall; this was confirmed (Class A prediction¹) by a later site visit. It is clear that the use of these new technologies will require analytical skills not generally taught to those using more conventional surveying techniques. Hence, interpretation of movements will need a combination of skills and, most likely, different or retrained personnel.

¹ Terzaghi, K. (1943) Theoretical Soil Mechanics, John Wiley and Sons, New York, USA

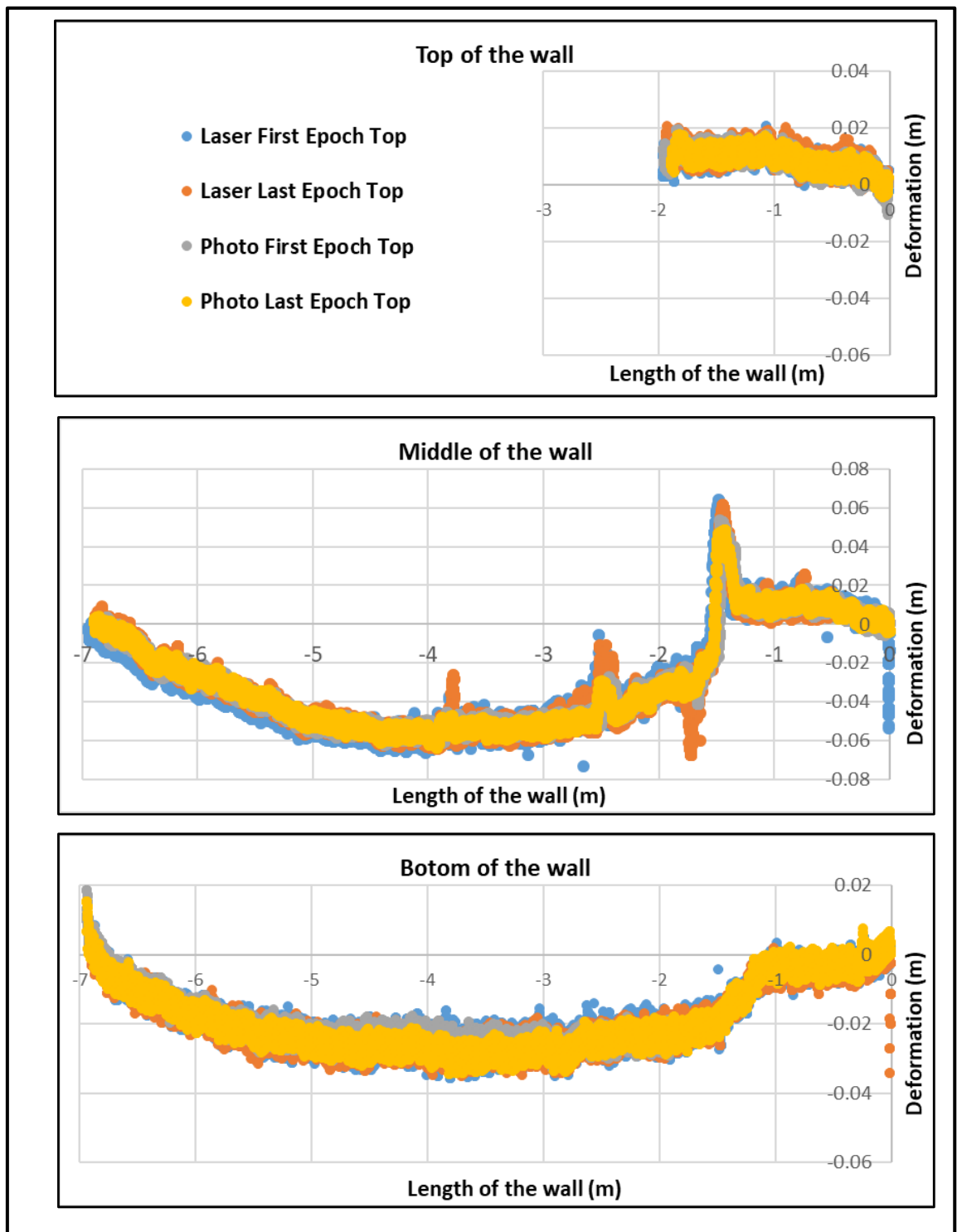


Figure 5-46 Comparison between the first and the last epochs of Laser scanner and photogrammetry: a) Top strip; b) Middle strip and c) Bottom strip

5.13 Conclusion

The case study presented in this chapter used different technologies to identify movement on the north-east wing wall to overbridge HC3. The results show that a 3D multi-view construction can be performed using close-range photogrammetry (CRP) and terrestrial laser scanning (TLS). The site trial also showed that CRP could produce a similar point cloud quality to the TLS systems. This demonstrates the potential for applying TLS and CRP for monitoring structures.

The results show that the wall movements measured by TS, TLS, and CRP systems were of similar magnitude. The movements computed from CRP and TLS were presented to the route manager through the colour deformation/deviation maps to assist in the decision to be made regarding the safety of the wall. TLS and CRP provided more detailed information about the change in wall shape when compared to TS which only provided discrete point information. The results are promising and show that their application could be justified in certain instances such as rapid inspection of large structures.

This case study indicates that LUL can easily implement this technology to rapidly inspect their buildings and structures to identify defects (e.g. crack, spalling, mortar loss in joints, face loss, and vegetation growth) and monitor their assets for deformation during the construction of assets nearby. There are commercial software available for change detection (in this research, open-source software was used) that could be customised to add auto data processing function and significantly reduce data interpretation and the decision-making time. Furthermore, TLS and CRP provide a non-destructive method to inspect infrastructure. Therefore, inspection can be performed quickly and rapidly with minimum access requirement.

Compared to TLS, CRP is cheaper and easier to use by untrained staff. However, data processing required a huge amount of time and large computer memory due to their passive behaviour.

Chapter 6. Conclusions and Future work

6.1 Introduction

This research was motivated by the concerns London Underground Limited has regarding the effectiveness of using visual manual inspections to determine the condition of its physical assets over the whole metro network to obtain rapid and detailed knowledge of the asset condition. It was focused on the application of new technologies to support LUL's civil asset management inspections, with the objective of increasing the speed and improve the accuracy when observing infrastructure conditions. Detailed conclusions were presented in each chapter and, in this summary, the main conclusions are reiterated, and future directions of research are suggested.

6.2 Conclusions

1. The gap analysis performed in Chapter 2 identified that visual inspections are not reliable as they are subjective and dependent on the inspector's ability to identify and score the defects. It is also a time-consuming process when the whole of the metro network requires inspection.
2. Chapter 3 discussed the case study of a brick tunnel on LUL Sub Surface Line (for the Circle, Hammersmith & City and District lines). The comparison was performed between visual inspections and Euroconsult's laser scans. This analysed showed that a direct comparison between two inspections' scores are inappropriate because the laser inspection does not capture all the defects mentioned in the Engineering Standard S1060. The laser survey system still requires manual intervention to complete the visual inspection report. Therefore, the laser inspection and the visual inspection methods are not mutually exclusive. The laser inspection system needs to be further developed to interpret/report the data automatically and satisfy the requirements mentioned in the Engineering standard S1060. In order to effectively

validate the laser inspection, both inspections should be performed at the same time.

3. The thermography chapter (chapter 4) has demonstrated, through the lab experiments, that it is possible to determine a relationship between moisture content and changes in the temperature, measured by a thermal camera, in brick walls. This relationship depends on the type of bricks and can be obtained in the laboratory to calibrate the thermal camera.

The site trial has demonstrated the potential of Thermography as a technique more suitable to identify water seepage in brick tunnels than a laser scanner system described in the previous chapter. A comprehensive data set could be obtained by attaching thermal cameras to normal trains, allowing the data collection to be done at any time on a tube line. Comparing different epochs would allow asset managers to react before a seepage is established, potentially eliminating the risk of system disruption caused by water ingress in tunnels. The data collected also revealed that this technique could be used to determine the condition of other assets that clearly appear in the thermal pictures, such as brackets, cable supports, broken light bulbs, etc. Furthermore, the thermographic analysis is one of the cheapest, easiest and relatively fast technique to apply in monitoring of these types of assets.

4. Chapter 5 a case study was presented used different technologies to identify movement on the North-East wing wall to overbridge HC3. The results show that a 3D multi-view construction can be performed using Close Range Photogrammetry (CRP) and Terrestrial Laser Scanning (TLS). The site trial also showed that CRP could produce a similar point cloud quality to the TLS systems.

In this research there were insufficient control points outside the impact area and, to achieve high precision results, adequate geo-referencing

points should be placed outside the anticipated impact areas. This is important to obtain the absolute movement of the wall, not just the deformed shape. This case study indicates that LUL can easily implement this technology to inspect rapidly their buildings and structures to identify defects. Photogrammetry and laser scanner inspections can be performed quickly and rapidly with minimum access requirements. It is clear that the use of these new technologies will require analytical skills not generally taught to those using more conventional surveying techniques. Hence, interpretation of movements will need a combination of skills and, most likely, different or retrained personnel.

6.3 Future work

This research has highlighted the benefits that can be obtained using new technologies. It also has highlighted areas where further research is required, in order to make these new technologies more efficient in the management of physical assets.

1. Currently, Euroconsult's Laser Scanner system does not capture drumminess (loosen bricks), mentioned on the engineering standard S1060. Therefore, further hardware and software need to be developed to identify drumminess automatically.
2. Euroconsult's Laser Scanner system acquires data in a kinematic mode and the laser is configured to point towards the tunnel surface, therefore the system does not report other problems that would be identified by an inspector, such as headwalls' defects. In order to identify these out of plane defects at the same time when collecting data on the tunnel surface, further research is necessary to determine for the possibility to installing additional scanners that could be focus towards headwalls and other areas of interest. In addition, the data collection method also needs to be changed from kinematic mode to mixture of static

(headwalls details can be acquired kinematic to static) and kinematic modes.

3. At present, Euroconsult's laser scanner system offers a more reliable and repeatable scoring system for certain defects, however, it does not replace completely the Principal Inspections. The laser survey system still requires manual intervention to complete the visual inspection report. Therefore, the laser inspection and the visual inspection methods are not mutually exclusive and need further development to identify and interpret defect categories mentioned on the inspection standards S1060.
4. Euroconsult has developed equations to calculate defects severity and extent using their computer vision algorithm. However, visual inspection assignment of scores for extent and severity depends on the ability of the inspector to interpret the data. Currently, visual inspection provides the Condition Score as the lowest element rating contained in the structure and is derived from the scoring system mentioned in the standard S1060. Due to these different scoring methods, further investigation must be performed to establish a unified scoring system that can be reproduced by the monitoring system and the inspector.
5. During this research, comparisons were performed between two inspection methods in different inspection periods. Euroconsult's inspections were performed in 2014 and 2015, but the visual inspection was performed in 2013. In order to validate the Euroconsult's results with the visual inspection, visual inspections also have to be performed at the same time.
6. During this research, creating the point clouds using photogrammetry involved manual processing such as selecting overlapping images and loading into the software; selection of several parameters to aligning

photos; creating the point cloud and generating the mesh. According to the Agisoft software manual, it should be possible to automate the above sequences by developing the coding, thereby saving significant time and cost.

7. The calibration of a camera must be carried out for the data to be accurate. This requires that the camera parameters (see section 5.7.5) are known. The Agisoft- Photoscan, which was used in this research, estimates camera calibration parameters automatically using Brown's model for lens distortion. Therefore, manual calibration was not performed because the Nikon D700, which was used to capture images, has used standard optical lenses and a highly redundant image network. However, in future, if different software or any other camera lens are used for structural monitoring work, camera calibration should be performed.
8. Close Range Photogrammetry techniques can be used for not only monitoring the condition of tunnels bridges and structures but also other assets such as bridges and structures, embankments and cuttings with that may have poor accessibility. Therefore, further work should be considered into the use of drones attached with multiple cameras, capturing photos and analysing and interpreting data automatically.
9. Some of Terrestrial Laser Scanner data shows a high noise level (e.g. pedestrians passing through when capturing data). There may be some benefit to in using filters to reduce the noise level in the scanner data, in order to reduce the scattering effect resolved displacements.
10. In order to highlight seasonal (drying epoch to understand if the seepage is active or inactive) variations of seepage, it would be necessary to perform thermography scans more than once a year. Hence thermography would have to be carried out at times other than

with the engineering train, currently, laser scanning is performed once a year.

11. Creating moisture maps, from the thermography site trials, was a manual procedure. It involved capture data in video format, identify drip trays and other prominent features; stitching overlapped snapshots to create panoramic views, export the temperature data to Excel in order to perform the conversion from temperature to moisture and finally, import the data to Matlab to create the moisture maps. Algorithms that automatically identify the seepage area (using temperature values) and the dry bricks in the thermal images, automating the above process need to be developed.
12. The bricks used in the lab test and the bricks used to build the SSL tunnel are different. Therefore, further work needs to be performed to derive an equation to convert from temperature measurement to moisture level using the actual bricks used to build a specific tunnel.
13. Thermal images could also be used to identify deflector plates, drip trays, tunnel number plates, cable brackets, light bulbs and cable malfunction (cold, no power, hot, power). Therefore, further work needs to be done to identify those features and interpret their condition automatically.
14. A large volume of data was captured during this research. Therefore, further work needs to be done to manage this data in a “big data” concept and produce algorithms to enable rapid decision making to be performed.
15. Currently, LUL maintains their assets based on a planned preventive or reactive maintenance strategy using visual inspection reports. This research has shown that using new technologies, the amount of

predictive maintenance can be increased whilst reducing reactive maintenance. For this, further research is need on the asset condition monitored with new technologies.

References and Bibliography

Agisoft PhotoScan Professional (version 0.9.0), <http://www.agisoft.ru> (12 January 2016).

Alba, M, and M Scaioni. 2010. "Automatic Detection of Changes and Deformation in Rock Faces by Terrestrial Laser Scanning." In Proceedings of the ISPRS Commission V Mid-Term Symposium 'Close Range Image Measurement Techniques, 11–16.

Avdelidis, N.P., A.Moropoulou, and P.Theoulakis (2003) 'Detection of Water Deposits and Movements in Porous Materials by Infrared Imaging' Infrared Physics & Technology, 6: 183-190

Amditis. A, J.G Victores, R.L.Taragan (2016), 'Integrated Robotic Solutions for Tunnel Structural evaluations and characterization Robo-spect EC proposals', SEE Tunnel:Promoting Tunneling in SEE Region" ITA WTC 2015 Congress and 41st General Assembly, Lacroma Valamar Congress Center, Dubrovnik, Croatia

BSI 2008. PAS 55:2008: The Specification for the Optimized Management of Physical Assets, Parts 1 and 2. British Standards Institute, London.

Bao.Y and H. Li (2016), 'Compressive sensing-based wireless sensors and sensor networks for structural health monitoring', School of Civil Engineering, Harbin Institute of Technology, Harbin, China. Proceedings of the International Conference on Smart Infrastructure and Construction ISBN 978-0-7277-6127-9.

Boehler, W. and A. Marbs (2002). 3D scanning instruments ,Institute for Spatial Information and Surveying Technology, FH Mainz, University of Applied Sciences, Germany.

Bisby, L. A., Take, W. A., and Caspary, A. (2007). "Quantifying Strain Variation in FRP Confined Concrete Using Digital Image Correlation." *1st Asia-Pacific Conference on FRP in Structures*, Hong Kong, China, 599-604.

Barreira, E., V.P. de Freitas, J.M.P.Q. Delgado and N.M.M. Ramos (2012) 'Thermography Applications in the Study of Buildings Hygrothermal Behaviour', LFC –Building Physics Laboratory, Civil Engineering Department, Faculty of Engineering, University of Porto Portugal

Balaguer, C. G. Victores, (2010) Robotic tunnel inspection and repair. In: *Technology Innovation in Underground Construction*. CRC Press, 2010, p. 445–460.

Balaguer, C., R. Montero, J. G. Victores, S. Martínez, and A. Jardón (2014), 'Towards Fully Automated Tunnel Inspection: A Survey and Future Trends', the 31st International Symposium on Automation and Robotics in Construction and Mining (ISARC 2014) 19

Blitz, J and G. Simpson (1996) *Ultrasonic methods of non-destructive testing*. Springer.

Barreira, E., and de Freitas, V., (2007) 'Evaluation of building materials using infrared thermography', *Construction and Building Materials*, 21[1] 218-224.

Busher, K.A., W. Wild, and H. Wiggensauser (1999) 'Moisture Measurements in building Materials by Amplitude- Densitive Modulation Thermography' , *Diagnostic Image Technologies and industrial Applications* , Munich Germany, June 1999. Bellingham: WA: International Society for optical Engineering, 1999. 34-43.

Bowers, K. (2014) 'Maintaining London Underground's tunnels', presentation NCE tunnelling summit London.

Carino, N (2001) 'The impact-echo method: an overview. In: Proceedings of the 2001 Structures Congress & Exposition. Washington, DC, American Society of Civil Engineers, 2001, p. 18.

Cheung, Moe M.S. Noruziaan. Bahman & Yang, C.Y. 2007. Health monitoring data in assessing critical behavior of bridges, *Structure and Infrastructure Engineering*, v3, n4, p325-342.

Carino, N (2001), 'The impact-echo method: an overview', In: Proceedings of the 2001 Structures Congress & Exposition. Washington, DC, American Society of Civil Engineers, 2001, p. 18.

Cheung, L. L. K., K. Soga, P. J. Bennett, Y. Kobayashi, B. Amatya and P. Wright (2010) 'Optical fibre strain measurement for tunnel lining monitoring', *Proceedings of the Institution of Civil Engineers Geotechnical Engineering* 163, GE3, 119–130

Chew. C (2004) 'Alliance Strategy for the inspection and assessment of BCV and SSL tunnel assessment' Metronet Rail –Internal Report – London Underground

Caffull,K., Sims,M., (2014), 'Predictive & Preventative Programme Strategy' Internal Report London Underground

Choi, S., and Shah, S. P. (1997). "Measurement of deformations on concrete subjected to compression using image correlation." *Experimental Mechanics*, 37(3), 307-313.

Corr D., Accardi M., Grahambrady L., and Shah S. (2007). "Digital image correlation analysis of interfacial debonding properties and fracture behavior in concrete." *Engineering Fracture Mechanics*, 74(1-2), 109-121

Clark, M.R., McCann, D.M., Forde, M.C. (2003), 'Application of infrared thermography to the non-destructive testing of concrete and masonry bridges',

Department of Civil and Environmental Engineering, School of Engineering and Electronics, University of Edinburgh, The King's Buildings, Edinburgh EH9 3JN, UK

Chields, K.W., G.E.Courville, and P.W Chields (1983) ' An Investigation of Factors Influencing Infrared Roof Moisture Surveys Using a Mathematical Model', *Thermosense VI [Orlando, FL, April 1983]* Bellingham: WA: International Society for Optical Engineering, 1983. 82-94

Cortes,L.L (2013) 'Moisture Transfer Analysis During Drying of Brick by Temperature and Relative Humidity Profiles' , *European Scientific Journal* November 2013 edition vol.9, No.33 ISSN: 1857 – 7881 (Print) e - ISSN 1857-7431

Cloud Compare (version 2.4), <http://www.danielgm.net/cc> (12 January 2017).

Cooper, M.A.R., and S.Robson (1994), 'Photogrammetric Methods for Monitoring Deformation': Theory, Practice and Potential 10th International Conference on Experimental Mechanics, Lisbon.

Cardenala. J , E. Mataa , J.L. Perez-Garciaa , J. Delgadoa , M.A. Hernandeza , A. Gonzalezb , J.R. Diaz-de-Teranb (2008), 'Close Range Digital Photogrammetry techniques applied to Landslides monitoring', *The International Archives of the Photogrammetry, Remote Sensing and Spatial Information Sciences*. Vol. XXXVII. Part B8. Beijing 2008

Clark, J. and S. Robson (2004). Accuracy of measurements made with a Cyrax 2500 Laser.

Christian,W (2004). *The Subterranean Railway*. Atlantic Books, London'

Destrebecq, J. F., Toussaint, E., and Ferrier, E. (2010). "Analysis of Cracks and Deformations in a Full Scale Reinforced Concrete Beam Using a Digital Image Correlation Technique." *Experimental Mechanics*. 51(6), 879-890.

Devrient, M. (2013) Giga Data, mega problem – or is it? CIRIA 6th Mini-Conference: Geotechnical issues in Construction.

Delatte, N., S. Chen, N. Maini, N. Parker, A. Agrawal, G. Mylonakis, K. Subramaniam, A. Kawaguchi, P. Bosela, S. McNeil, and R. Miller (2002), 'Application of Non-destructive Evaluation to Subway Tunnel Systems', Transportation Research Record 1845 Paper No 03-3269.

Detchev .I , A. Habib, M. El-Badry (2011), 'Estimation of Vertical Deflections in Concrete Beams through Digital Close Range Photogrammetry', International Archives of the Photogrammetry, Remote Sensing and Spatial Information Sciences, Volume XXXVIII-5/W12, 2011ISPRS Calgary 2011 Workshop, 29-31 August 2011, Calgary, Canada.

Dowman, I J(2001). Fundamentals of Digital Photogrammetry Close Range Photogrammetry and Machine Vision. Whittles Publishing, Scotland, UK, pp. 52-76.

David. V, Y.Tian and R.Jiang (2006) , 'Photogrammetry Applications in Routine Bridge Inspection and Historic Bridge Documentation' New Mexico State University Department of Civil Engineering Box 30001, MSC 3CE Las Cruces, NM 88003-8001

Delgado J.M.D, I. Brilakis and C. Middleton (2016), 'Modelling, management, and visualisation of structural performance monitoring data on BIM', University of Cambridge, Cambridge, United Kingdom. Proceedings of the International Conference on Smart Infrastructure and Construction.

Delgado J.M.D, I. Brilakis and C. Middleton (2016), 'Modelling, management, and visualisation of structural performance monitoring data on BIM', University of Cambridge, Cambridge, United Kingdom. Proceedings of the International Conference on Smart Infrastructure and Construction.

Edwards,R., P.Burns, C.Johnson, S.Male, M.Pilling, R.Rayner and J.Woodhouse (2010) 'Asset management in the rail and utilities sectors' in C.Lloyd(ed) , Asset Management Whole-life management of physical assets', Thomas Telford Limited , ICE publishing , 40 Marsh Wall, London E14 9TP.

Edwards,A.T., (2000) Comparison of Strain Gage and Fiber Optic Sensors on A Sting Balance In A Supersonic Wind Tunnel MSc thesis, Virginia Polytechnic Institute and State University.

Esbert RM, Ordaz J, Alonso J, Montoto M (1997) Physical properties of stone materials. Manual of Diagnosis and Treatment of Stone and Ceramic Materials, Col·legi d'Aparelladors i Arquitectes de Barcelona, pp 21–38

Euroconsult, Tunnelings system (2014) 'Inspection of brick tunnels and covered ways SSL London Underground Limited- Internal Report'.

Fourie1 C.J. and N.T. Zhuwaki1(2017) 'A Modelling Framework for Railway Infrastructure Reliability Analysis' South African Journal of Industrial Engineering December 2017 Vol 28(4), pp 150-160.

Fackler, M (2012), 'Nine Killed When Highway Tunnel Collapses in Japan', The New York Times.

Fujihashi, K., K. Kurihara, K. Hirayama and S. Toyoda (2005) 'Monitoring system based on optical fibre sensing technology for tunnel structures and other infrastructure', In Sensing Issues in Civil Structural Health Monitoring (Ansari F (ed.)), Springer, Dordrecht, 185–195

Frossel, F. (2006) 'Masonry drying and cellar rehabilitation'. Stuttgart: Fraunhofer IRB Verlag

Gavilán.M, F. Sánchez, J.A. Ramos and O. Marcos (2013), 'Mobile Inspection System for High- Resolution Assessment of Tunnels,' The 6th International Conference on Structural Health Monitoring of Intelligent Infrastructure Hong Kong.

Garcia L.J, S.M Quintero , Heine E, Ed,(2007), ' Application of Terrestrial Laser Scanning for Risk Mapping, Editorial Universidad Polytechnic de Valencia', Valencia, ISBN 978-84-8363-199-7.

Grinzato, E., and A. Mazzoldi (1991) ' Infrared Detection of Moist Areas in Monumental Buildings Based on Thermal Inertia Analysis' *Thermosense X111*[Orlando, FL, April 1991]. Bellingham: WA: International Society for optical Engineering, 1991.75-82

Gorjian,N., L. Ma, M.Mittinty, P. Yarlagadda, Y.Sun (2009) 'A Review on Degradation Models in Reliability Analysis' , Proceedings of the 4th World Congress on Engineering Asset Management Athens, Greece.

Gordon SJ, Lichti D et al (2005) Structural deformation measurement using terrestrial laser scanners, Curtin University of Technology

Girardeau-Montaut, D., (2011). CloudCompare: Cloud to Cloud Compare Workflow. online] Available at:
<http://www.danielgm.net/cc/forum/viewtopic.php?f=9&t=105>____(accessed 15 May 2013).

Girardeau-Montaut, D., Roux, M., Marc, R., & Thibault, G., (2005). Change detection on points cloud data acquired with a ground laser scanner. International Archives of Photogrammetry, Remote Sensing and Spatial Information Sciences, 36(part 3), W19

Gordon, S. J., D. Lichti, M. Stewart and J. Franke (2005) Structural deformation measurement using terrestrial laser scanners. In Proceedings of 11th International FIG Symposium on Deformation Measurements (p. 8)

Gerardo, W and J. W. Bryant (2006), Asset Management Data Collection for Supporting Decision Processes, U.S Department of Transportation Federal Highway administration.

Huang A.B., Lee J.T., Wang C.C., Ho Y.T., Chuang T.S (2013), 'Field Monitoring of Shield Tunnel Lining Using Optical Fiber Bragg Grating Based Sensors' Proceedings of the 18th International Conference on Soil Mechanics and Geotechnical Engineering, Paris.

Huseyin. C, H.Erwin, J.Luis, L.García, R.Poelman, and M.Santana (2008), Theory and practice on Terrestrial Laser Scanning Training material based on practical applications Flemish Agency of the European Leonardo Da Vinci programme

Hampel. U, H.G Maas (2003), 'Application of Digital Photogrammetry for Measuring Deformation And Cracks During Load Tests In Civil Engineering Material Testing', Institute of Photogrammetry and Remote Sensing, Dresden University of Technology, Germany

Hampel , U (1997) , 'Using digital close-range photogrammetry method for deformation and Crack width measurements of reinforced concrete structures' , . 34. Research Colloquium the DafStb , Institute of Structures and Materials , Technical University of Dresden at pp. 125-134

Hooper, R., R. Armitage, K.A. Gallagher and T. Osorio (2009), 'Whole-life infrastructure asset management: good practice guide for civil infrastructure', CIRIA C677, Classic Home, 174-180 Old street London

Jiang R, Jáuregui DVet al (2008) Close-range photogrammetry applications in bridge measurement: literature review. Measurement 41(8): 823–834

Jenkins, D.R., L.I. Knab, and R.G. Mathey (1982) 'Laboratory studies of Infrared Thermography in Roofing Moisture Detection '. Special Technical Publications, West Conshohocken: PA American Society for Testing and Materials, 207-220

Kominsky J, R.. , J. S, Luckino, T. F, Martin (2010) 'Passive Infrared Thermography—A Qualitative Method for Detecting Moisture Anomalies in

Building Envelopes' , Environmental Quality Management, Inc., 1800 Carillon Boulevard, Cincinnati, OH 45240

Küntz, M., Jolin, M., Bastien, J., Perez, F., and Hild, F. (2006). "Digital image correlation analysis of crack behavior in a reinforced concrete beam during a load test." *Canadian Journal of Civil Engineering*, 33(11), 1418-1425.

Koutsoudis, A., Vidmar, B., Ioannakis, G., Arnaoutoglou, F., Pavlidis, G., and Chamzas, C., (2013) 'Multi-image 3D reconstruction data evaluation. *Journal of Cultural Heritage*, 15(1), pp. 73–79.

Laurent.J, R. Fox-Ivey, F.S Dominguez and A.R Garcia (2014), 'Use of 3D Scanning Technology for Automated Inspection of Tunnels Proceedings of the World Tunnel Congress – Use of 3D Scanning Technology for Automated Inspection of Tunnels. Foz do Iguaçu, Brazil.

Lindenbergh.R , L.Uchanski, A. Bucksh and R.V.Gosliga (2011), 'Structural Monitoring of Tunnels Using Terrestrial Laser Scanning' , Delft Institute for Earth Observation and Space Systems, Delft University of Technology.

Luhmann T and Robson S (2013) Close-range Photogrammetry and 3D Imaging, De Gruyter.

Lichti, D. (2004). A resolution measure for Terrestrial Laser Scanners. In: The International Archives of the Photogrammetry, Remote Sensing and Spatial Information Sciences, Part XXX, vol. 34.

Lo, Tommy Y.and Choi, K.T.W. (2004), 'Building defects diagnosis by infrared thermography,' *Structural Survey*, Volume 22 • Number 5 • 2004 • pp. 259–263.

Ljungberg, S.A.(1995) “ Infrared Techniques in Buildings and structures: Operation and Maintenance” In *Infrared Methodology and Technology*, 211-252. Langhorne: PA: Gordon and Breach Science Publishers.

Loupos, K., A. Amditis, C. Stentoumis, P. Chrobocinski, J. Victores, A. Roncaglia, S. Camarinopoulos, V. Kalidromitis, D. Bairaktaris, N. Komodakis and R. Lopez (2014) Robotic Intelligent Vision and Control for Tunnel Inspection and Evaluation - The ROBINSPECT EC Project

Laefer DF, Truong-Hong L et al (2014) Crack detection limits in unit-based masonry with terrestrial laser scanning. *NDT E Int* 62:66–76

Lecompte, D, Vantomme, J, and Sol, H. (2006). "Crack Detection in a Concrete Beam using Two Different Camera Techniques." *Structural Health Monitoring*, 5(1), 59-68.

Lawler, J., and Keane, D. (2001). "Measuring three-dimensional damage in concrete under compression." *ACI Materials*, 98(6), 465-475.

Luhmann, T (2000). *Close Range - Fundamentals, Methods and Applications*. Herbert Wichmann Verlag, Heidelberg

Lindenbergh, R. (2010). *Airborne and Terrestrial Laser Scanning*, Whittles Publishing,
hfdst. 7, pag. 237–269.

Lamas P.F, Caramés T.M.F and Castedo L (2017) 'Towards the Internet of Smart Trains: A Review on Industrial IoT-Connected Railways', Department of Computer Engineering, Faculty of Computer Science, Universidade da Coruña,

Matias, L., Vilhena, A., Magalhães, A., Santos, C. P., and Veiga, R., (2008) 'Performance of masonry specimens in contact with salt water - Absorption by capillary rise and evaporation phenomena', *Proceedings of 1st International Conference on Construction Heritage in Coastal and Marine Environments*, Laboratório Nacional de Engenharia Civil (LNEC), Lisbon, Portugal.

Monserat O, Crosetto M (2008) Deformation measurement using terrestrial laser scanning data and least squares 3D surface matching. *ISPRS J Photogramm Remote Sens* 63(1):142–154

Mckibbins, L, R. Elmer and K. Roberts (2009), 'Tunnels: Inspection, assessment and Maintenance CIRIA C671 classic house, 174-180 old street, London EC1 9BP.

Maas, H.-G (1992), 'Robust Automatic Surface Reconstruction with Structured Light' IAPRS Volume XXIX, Part B5, pp. 709–713. Washington.

Mckibbins.L.,R.Elmer and K.Roberts (2009), 'Tunnels: inspection, assessment and maintenance' CIRIA C671, Classic House, 174-180 old street London EC1V 9BP

Mohamad, H., P.J. Bennett, K. Soga, et al. (2007a), 'Monitoring tunnel deformation induced by close-proximity bored tunnelling using distributed optical fiber strain measurements', Proceedings of the 7th International Symposium on Field Measurements in Geomechanics, ASCE Geotechnical Special Publication No 175,1–13.

Moyoa.P., Brownjohnb J.M.W, Sureshc. R., Tjinc S.C (2005), 'Development of fiber Bragg grating sensors for monitoring civil infrastructure,' Engineering Structures 27 1828–1834.

McCormick, N., and J. Lord (2012) 'Digital image correlation for structural measurements', Proceedings of the Institution of Civil Engineers Civil Engineering 165, Issue CE4, 185–190 Paper 1100040

Moore,.R (2014) 'Best Practice Principles and Asset Management Standards', ICE Transport Asset Management Conference London

Moore, R., and R. Parry (2010), 'London Underground Asset Management Policy and Strategy'.

Mosbeh R., A.Beshr, M. Elshiekh (2005), 'Using Total Station for monitoring the deformation of high strength concrete beams' School of Civil Engineering, Harbin Institute of Technology, Harbin 150090, China

Moss,N. (2014) 'Monitoring recent experience and future requirements' internal presentation , London Underground Limited.

Mair.R (2015), 'Cambridge Centre for Smart Infrastructure and Construction annual review report

Mazzanti.P (2016), 'International Course on Geotechnical and Structural Monitoring', POPPI,Tuscany Italy.

Nuttens, Timothy, Cornelis Stal, Hans De Backer, Ken Schotte, Philippe Van Bogaert, and Alain De Wulf. 2014. "Methodology for the Ovalization Monitoring of Newly Built Circular Train Tunnels Based on Laser Scanning: Liefkenshoek Rail Link (Belgium)." *Automation in Construction* 43: 1–9.

National Transportation Safety Board (2006), 'Ceiling Collapse in the Interstate 90 Connector Tunnel. Boston', Massachusetts.

Night Tube (2014) 'Future of the tube' Transport for London (<http://www.tfl.gov.uk/campaign/tube-improvements/the-future-of-the-tube/night-tube?intcmp=22069>; 10 January 2015).

Nuttens .T, A.De Wulf, L. Bral, B. De Wit, L. Carlier, M.De Ryck, D. Constales, H.De Backer (2010), 'High resolution terrestrial laser scanning for tunnel deformation measurements' , FIG Congress 2010 Facing the Challenges – Building the Capacity Sydney, Australia.

Puente I, González-Jorge H et al (2012) Deformation monitoring of motorway underpasses using laser scanning data. *ISPRS-Int Arch Photogramm Remote Sens Spat Inf Sci* 1:235–238.

Park H, Lee H et al (2007) A new approach for health monitoring of structures: terrestrial laser scanning. *Comput Aided Civ Infrastr Eng* 22(1):19–30.

Pfeifer N, Brieze C,(2007), 'Laser scanning –Principles and Applications, GeoSiberia 2007', International Exhibition and Scientific Congress.

Park H. S, H. M. Lee, H.Adeli and I. Lee (2007), 'A New Approach for Health Monitoring of Structures: Terrestrial Laser Scanning', *Computer-Aided Civil and Infrastructure Engineering* 22 (2007) 19–30.

Park H. S, H. M. Lee, H. Adeli, I. Lee (2007) 'A New Approach for Health Monitoring of Structures: Terrestrial Laser Scanning' *Computer-Aided Civil and Infrastructure Engineering*. Published by Blackwell Publishing, 350 Main Street, Malden, MA 02148, USA, and 9600 Garsington Road, Oxford OX4 2DQ, UK.

Poblete, A., and M. Acebes Pascual (2007) ' Thermographic measurements of the effect of humidity in mortar porosity' , *Infrared physics & Technology* 49: 224-227.

Parmar,.A, Andrews.J (2010) 'Civils Information Strategy for Whole Life Asset Management' London Underground Limited- Internal Report.

Parlikad,.A, (2014) 'Managing the value of assets - the foundations of smart infrastructure asset management', Cambridge Centre for Small Infrastructure and Construction Asset Management projects, University of Cambridge-Cambridge U.K.

Pocock,D., N.Shetty, A.Hayes and J.Watts (2014) ' Leveraging the relationship between BIM and asset management, ' *Infrastructure Asset Management-Volume1- Issue1*.

Puente, I, H González-Jorge, B Riveiro, and P Arias. 2012. "Deformation Monitoring of Motorway Underpasses Using Laser Scanning Data." *ISPRS-International Archives of the Photogrammetry, Remote Sensing and Spatial Information Sciences* 1: 235–38.

Rosina, E. and Ludwig, N., (1999) Optimal thermographic procedures for moisture analysis in building materials, Diagnostic Imaging Technologies and Industrial Applications, SPIE, Vol. 3827, Germany.

Prescott, R.R. and J. Andrews (2011) 'Review of Infrastructure Asset Management Methods for Networked Systems', Nottingham Transportation Engineering Centre, University of Nottingham, UK

Rosina, E., Ludwig, N., and Rosi, L., (1998) 'Optimal Environmental Conditions to Detect Moisture In Ancient Buildings': Case Studies in Northern Italy, Proceedings of Thermosense XX, pp.188-199, SPIE, Orlando, USA.
Rees, W. (2001). Physical principles of remote sensing. Cambridge University Press

Ravindran.G (2013), 'Evaluation of New Technologies to support asset management of metro systems', MRes Dissertation, Urban Sustainability and Resilience, Department of Civil , Environmental and Geomatics Engineering, University College London.

Roberts, L and R. Hollier (2007), 'Developing levels of service and performance measures creating customer value from community assets', National Asset Management Steering (NAMS) Group Thames, New-Zealand

Sansalone, M., N.J. Carino (1989) 'Detecting delaminations in concrete slabs with and without overlays using the impact echo method' , ACI Materials Journal, 86 (2), p. 175–184.

Scanner against surfaces of known colour. In: The International Archives of Photogrammetry, Remote Sensing and Spatial Information Sciences, Commission IV, Part B4, vol. XXXV: pag. 1031–1037.

Sumitro, S., T. Okamotoa and D. Inaudib(2004) 'Intelligent Sensory Technology for Health Monitoring Based Maintenance of Infrastructures' , 11th

SPIE's Annual International Symposium on Smart Structures and Materials, San Diego, USA

Sun. T (2014) 'Introduction to Fibre Bragg Grating Optical Sensing for Structural Health Monitoring', Cambridge Centre for smart Infrastructure and Construction; Engineering department University of Cambridge.

Sims. C (2014) 'Delivering cost-effective and smooth refurbishment programmes on ageing tunnels' NCE Tunnelling Summit, London

Sham, J. (2008), 'Infrared Flash Thermography (FT) for Building Diagnosis, Detection of Surface Cracks, Subsurface effects and water-paths in Buildings Concrete Structures,'

Soni. A., S. Robson and B. Gleeson (2015), 'Structural monitoring for the rail industry using conventional survey, laser scanning and photogrammetry', Department of Civil, Environmental & Geomatic Engineering, University College London, Gower Street, London WC1E 6BT, UK.

Soudarissanane, S., J. van Ree, A. Bucksch and R. Lindenbergh (2007). Error budget of terrestrial laser scanning: influence of the incidence angle on the scan quality. In: 3D- Nordost, Berlin, Germany.

Shan, J. and C. Toth (2009). Topographic Laser Ranging and Scanning. Taylor and Francis Group.

Soni.A, S.Robson and B.Gleeson (2015), ' Structural monitoring for the rail industry using conventional survey, laser scanning and photogrammetry' Department of Civil, Environmental & Geomatic Engineering, University College London, Gower Street, London WC1E 6BT, UK

Soni, A (2016), ' Non-contact monitoring of railway infrastructure with terrestrial laser scanning and photogrammetry at Network Rail' , Eng.D Thesis,

Department of Civil, Environmental & Geomatic Engineering, University College London, Gower Street, London WC1E 6BT, UK.

Farrar, C.R. and K.Worden(2007), 'An introduction to structural health monitoring. Philosophical Transactions of the Royal Society A: Mathematical, Physical and Engineering Sciences, 365(1851), pp.303–315.

Titman, David. J. 'Applications of Thermography in NDT of Structures'. NDT & E international, 2001: 149-154.

Teunissen, P. (2000). Adjustment Theory, an introduction. Delft University of Technology.

Thoeni.K., A. Giacomini, R. Murtagh and E. Kniest (2014), 'A Comparison of Multi-View 3D Reconstruction of a Rock Wall using Several Cameras and A Laser Scanner' The International Archives of the Photogrammetry, Remote Sensing and Spatial Information Sciences, Volume XL-5, 2014 ISPRS Technical Commission V Symposium, 23 – 25 June 2014, Riva del Garda, Italy

Tasci. L (2013), 'Deformation Monitoring in Steel Arch Bridges Through Close-Range Photogrammetry and the Finite Element Method,' Department of Geodesy and Photogrammetry (Geomatic) Engineering, Firat University, Elazığ, Turkey.

TfL (2012) 'Rail and Underground Annual Benchmarking Report'

Transit Asset Management Practices (TAMP) (2010), A National and International Review, U.S department of transportation federal transit administration.

The Institute of Asset Management (IAM) (2014) 'Asset Management – an anatomy' Version 2, St Brandon's House, 29 Great George Street, Bristol

Victoria J. Hodge, O'Keefe. S., Weeks.M, and Moulds.A (2014) 'Wireless Sensor Networks for Condition Monitoring in the Railway Industry': A Survey,' Transactions On Intelligent Transportation Systems

Woodhouse,.J, A.Thomson, and M.Sims (2013) 'Optimal Asset Management Decision Making', Decision support tools limited; Salvo user training London Underground.

Washer, G., Fenwick, R. and Nelson, S. (2013) 'Guidelines for the Thermographic Inspection of Concrete Bridge Components in Shaded Conditions', the 92nd Annual Meeting of the Transportation Research Board Columbia.

Washer, G. A., Fenwick, R. G., and Bolleni, N. K. (2009), 'Development of Hand-held Thermographic Inspection Technologies' Department of Civil and Environmental Engineering, University of Missouri – Columbia E2503 Lafferre Hall Columbia, MO 65211.

Woollett.J, R.Diment, H.Neaves and B.Aquila (2005) 'Spatially Enabling an Asset Management Database' Tube line- Internal Presentation- London Underground Limited.

Wehr, A. (2008). 'LIDAR Airborne and terrestrial sensors' Advances in Photogrammetry, Remote Sensing and Spatial Information Sciences: 2008 ISPRS Congress book.

Woodhouse, John (2001). 'An introduction to Asset Management'. Asset Management Processes and Tools.

Yu. S, (2007) "Auto inspection system using a mobile robot for detecting concrete cracks in a tunnel" Automation in Construction, 16 (3), p. 255–261

Zheng D.H, Yue DJ, Yue JP (2008) Geometric feature constraint-based algorithm for building scanning point cloud registration. Acta Geodaetica et

Cartographica Sinica 37(04):464–468 (in Chinese) 1208 Nat Hazards (2014) 70:1197–1208 123

Zhao. X , , R. Han, Y. Yu, H. Liu, Y. Ding, M.Li and J.Ou (2016) , ‘Smartphone based Cloud-SHM and its applications’ Proceedings of the International Conference on Smart Infrastructure and Construction ISBN 978-0-7277-6127

Zeiske .K (2015), ‘Surveying made easily’, Leica Geosystem.

STANDARDS/INTERNAL REPORTS

Assessing the condition of constructed assets. Asset and Building Policy, Department of Infrastructure, State of Victoria, Australia, 1996.

Asset Management Primer. US Department of Transportation, Federal Highway Administration, Office of Asset Management, December 1999.

Euroconsult (2016), ‘Tunnelings High Resolution Inspection Circle Line and District Line’ London Underground- Internal Report.

G1417 (2013), ‘Grouting to control seepage in Tunnels and Structures’, Transport for London , London Underground

LW1341 (2012), ‘Water ingress management study’, Transport for London, London Underground

P020 (2014), ‘Asset Management Policy’, Tfl management system Transport for London

R0438- Ellipse Equipment Register and Hierarchy (2012), ‘London Underground Limited Issue no:- A1

S1042 (2014) ‘Asset Condition Reporting (ACR)’, Transport for London, London Underground

S1055 (2012), 'Standard for Civil Engineering Deep Tube Tunnel' London Underground Limited

S1060 (2014) 'Standard for the Inspection of Bridges and Structures' London Underground Limited

Technical user manual (2009), 'For the application of standard Tunnel Repairs Design and Details Network Rail.

Highway Infrastructure Asset Management Guidance Document (2013), 'Highways Maintenance Efficiency Programme' Department for Transport-London.

International Infrastructure Management Manual Version (2.0), 2002.

W2822 (2014) 'The management system work instructions inspecting brick tunnels', London Underground Limited.

Whole Life Value (WLV) (2016) Supporting Material, TfL Asset Management Steering Group and TfL Value Group.

W2904 (2014) 'The Management System Work Instructions- Producing A Brick Tunnel Inspection Chart,' London Underground Limited

Metronet (2007), 'Civil Assets Whole Life cycle project', Internal Presentation London Underground.

Moore, R. and R. Parry (2010) 'London Underground Asset Management Policy and Strategy', London Underground Limited

Appendix A- Tunnel laser survey with severity scores- Euroconsult

		Cracking			Dampness			Joint Condition			Material Condition			OVERALL RATING
		E	S	Score	E	S	Score	E	S	Score	E	S	Score	
1	Aldgate - Tower hill													
	TL35	A	4	4	A	1	8	A	3	5	A	1	8	78,13%
	CW28	A	1	8	A	1	8	A	2	7	A	3	5	87,50%
	CW38	A	1	8	A	1	8	A	4	4	A	4	4	75,00%
2	Tower hill – Monument													
	TL33	A	1	8	A	1	8	A	1	8	A	1	8	100,00%
	CW37	A	1	8	A	1	8	A	1	8	A	1	8	100,00%
	CW36	A	4	4	A	1	8	A	4	4	A	1	8	75,00%
	TL32	B	4	3	A	1	8	A	3	5	A	2	7	71,88%
3	Monument - Canon Street													
	TL31	A	4	4	A	1	8	A	4	4	A	2	7	71,88%
4	Canon Street - Mansion House													
	CW27	A	1	8	A	1	8	A	4	4	A	1	8	87,50%
	TL30	A	1	8	A	1	8	A	3	5	A	1	8	90,63%
	CW26	A	1	8	A	1	8	A	1	8	A	1	8	100,00%
	TL29	A	1	8	A	1	8	A	3	5	A	1	8	90,63%
	CW25	A	1	8	A	1	8	A	4	4	A	4	4	75,00%
	TL28	A	1	8	A	1	8	A	1	8	A	1	8	100,00%
5	Mansion House – Blackfriars													
	TL26	A	4	4	A	1	8	A	2	7	A	1	8	84,38%
	CW24	A	4	4	A	1	8	A	2	7	A	1	8	84,38%
6	Blackfriars – Temple													
	TL24	A	1	8	A	1	8	A	2	7	A	1	8	96,88%
	CW23	A	3	5	A	1	8	A	2	7	A	1	8	87,50%
	TL23	A	1	8	A	1	8	A	2	7	A	1	8	96,88%
	CW22	A	4	4	A	1	8	A	2	7	A	2	7	81,25%
	TL22	A	4	4	A	1	8	A	2	7	A	4	4	71,88%
	CW21	A	1	8	A	1	8	A	1	8	A	2	7	96,88%
7	Temple – Embankment													
	CW20	A	4	4	A	1	8	A	3	5	A	2	7	75,00%
	CW19	A	4	4	A	1	8	A	2	7	A	2	7	81,25%
8	Embankment – Westminster													
	CW18	A	1	8	A	1	8	A	2	7	A	2	7	93,75%
	CW17	A	1	8	A	1	8	A	3	5	A	4	4	78,13%
	TL21	A	1	8	A	1	8	A	2	7	A	1	8	96,88%
9	Westminster – St James's Park													
	TL20	A	1	8	A	1	8	A	2	7	A	1	8	96,88%
	CW16	A	1	8	A	1	8	A	2	7	A	1	8	96,88%

		Cracking			Dampness			Joint Condition			Material Condition			OVERALL RATING
		E	S	Score	E	S	Score	E	S	Score	E	S	Score	
10	St James's Park – Victoria													
	CW15	A	4	4	A	1	8	A	2	7	A	2	7	81,25%
	TL19	A	1	8	A	1	8	A	3	5	A	1	8	90,63%
	CW14	A	1	8	A	1	8	A	2	7	A	2	7	93,75%
	TL18	A	1	8	A	1	8	A	3	5	A	1	8	90,63%
	TL17	A	4	4	A	1	8	A	4	4	A	4	4	62,50%
11	Victoria - Sloan Square													
	TL16	A	1	8	A	1	8	A	2	7	A	1	8	96,88%
	TL15	A	1	8	A	1	8	A	4	4	A	2	7	84,38%
	TL14	A	1	8	A	1	8	A	2	7	A	1	8	96,88%
	TL13	A	4	4	A	1	8	A	2	7	A	2	7	81,25%
	TL12	A	1	8	A	1	8	A	2	7	A	3	5	87,50%
12	Sloan Square - South Kensington													
	TL11	A	4	4	A	1	8	A	2	7	A	1	8	84,38%
	CW13	A	4	4	A	1	8	A	3	5	A	1	8	78,13%
	TL10	A	4	4	A	1	8	A	2	7	A	1	8	84,38%
	TL9	A	4	4	A	1	8	A	2	7	A	3	5	75,00%
	TL8	A	4	4	A	1	8	A	2	7	A	2	7	81,25%
13	South Kensington - Gloucester Road													
	TL7	A	1	8	A	1	8	A	1	8	A	1	8	100,00%
	TL75	A	4	4	A	1	8	A	3	5	A	2	7	75,00%
14	Gloucester Road- HS Kensington													
	TL6	A	1	8	A	1	8	A	2	7	A	1	8	96,88%
	TL74	A	1	8	A	1	8	A	4	4	A	1	8	87,50%
	TL73	A	4	4	A	1	8	A	2	7	A	3	5	75,00%
	CW58	A	1	8	A	1	8	A	2	7	A	2	7	93,75%
15	HS Kensington- Notting hill													
	CW57	C	4	2	A	1	8	A	3	5	A	1	8	71,88%
	TL72	A	1	8	A	1	8	A	2	7	A	1	8	96,88%
	CW56	D	4	1	A	1	8	A	3	5	A	1	8	68,75%
	TL71	A	4	4	B	1	7	A	2	7	A	4	4	68,75%
	TL70	A	4	4	C	1	6	A	2	7	A	2	7	75,00%
16	Notting hill – Bayswater													
	TL69	A	4	4	A	1	8	A	2	7	A	3	5	75,00%
	TL68	A	4	4	A	1	8	A	2	7	A	3	5	75,00%
	TL67	A	3	5	A	1	8	A	2	7	A	3	5	78,13%
	TL66	A	4	4	A	1	8	A	2	7	A	1	8	84,38%

		Cracking			Dampness			Joint Condition			Material Condition			OVERALL RATING
		E	S	Score	E	S	Score	E	S	Score	E	S	Score	
17	Bayswater – Paddington													
	CW55	A	1	8	A	1	8	A	2	7	A	1	8	96,88%
	TL65	A	1	8	A	1	8	A	2	7	A	1	8	96,88%
	CW54	A	1	8	A	1	8	A	1	8	A	1	8	100,00%
	TL64	A	4	4	A	1	8	A	2	7	A	1	8	84,38%
	CW53	A	1	8	A	1	8	A	3	5	A	2	7	87,50%
	TL63	A	1	8	A	1	8	A	3	5	A	2	7	87,50%
	TL62	A	4	4	A	1	8	A	2	7	A	1	8	84,38%
	TL61	A	1	8	A	1	8	A	2	7	A	1	8	96,88%
	CW52	A	4	4	A	1	8	A	3	5	A	2	7	75,00%
	TL60	A	1	8	A	1	8	A	2	7	A	1	8	96,88%
18	Paddington - Edward Road													
	TL59	A	1	8	A	1	8	A	2	7	A	2	7	93,75%
	TL58	A	4	4	A	1	8	A	2	7	A	2	7	81,25%
	TL57	A	1	8	A	1	8	A	2	7	A	2	7	93,75%
	TL55	A	4	4	A	1	8	A	2	7	A	2	7	81,25%
	TL54	A	1	8	A	1	8	A	2	7	A	4	4	84,38%
19	Edward Road - Baker Street													
	TL53	A	4	4	A	1	8	A	2	7	A	2	7	81,25%
20	Baker Street - Great Portland Street													
	TL51	A	1	8	A	1	8	A	4	4	A	1	8	87,50%
	TL110	A	4	4	A	1	8	A	2	7	A	4	4	71,88%
	TL109	A	1	8	A	1	8	A	4	4	A	1	8	87,50%
21	Great Portland Street - Euston Square													
	TL106	A	4	4	A	1	8	A	2	7	A	2	7	81,25%
22	Euston Square - King Cross													
	TL103	A	4	4	A	1	8	A	2	7	A	4	4	71,88%
	CW71	A	1	8	A	1	8	A	3	5	A	4	4	78,13%
	TL102	A	4	4	A	1	8	A	2	7	A	1	8	84,38%
	CW70	A	4	4	A	1	8	A	4	4	A	1	8	75,00%
	CW69	A	1	8	B	1	7	A	2	7	A	2	7	90,63%
	TL101	A	1	8	B	1	7	A	2	7	A	1	8	93,75%
23	King Cross - Farringdon													
	CW67	A	1	8	A	1	8	A	1	8	A	1	8	100,00%
	CW66	A	1	8	A	1	8	A	1	8	A	1	8	100,00%
	TL97	A	4	4	A	1	8	A	3	5	A	2	7	75,00%
	TL91	A	4	4	A	1	8	A	2	7	A	1	8	84,38%
	TL89	A	4	4	A	1	8	A	3	5	A	2	7	75,00%
24	Farringdon – Barbican													
	TL85	A	4	4	A	1	8	A	2	7	A	1	8	84,38%

(Euroconsult's Tunnelling's system,2014)

Appendix B: - Summary of Scores laser survey (2014) and visual inspection

Summary of Score Tables					
Sections	Route	Euroconsult's Assessment Date	Euroconsult Ratings	Visual Inspection Rating	Visual Inspection Assessment Date
1	Aldgate - Tower Hill				
	TL35	28/06/2014	78.13%	83.33%	16/03/2013
	CW28	28/06/2014	87.50%	81.94%	21/09/2012
	CW38	28/06/2014	75.00%	87.50%	11/05/2013
2	Tower hill- Monument				
	TL33	28/06/2014	100.00%	87.50%	27/09/2012
	CW37	28/06/2014	100.00%	87.50%	14/12/2011
	CW36	28/06/2014	75.00%	91.67%	25/11/2011
	TL32	28/06/2014	71.88%	87.50%	03/06/2014
3	Monument-Canon Street				
	TL31	28/06/2014	71.88%	87.50%	21/06/2013
4	Canon Street-Mansion House				
	CW27	28/06/2014	87.50%	79.79%	30/04/2013
	TL30	28/06/2014	90.63	87.50%	05/06/2013
	CW26	28/06/2014	100.00%	83.33%	30/04/2013
	TL29	28/06/2014	90.63%	90.62%	13/05/2013
	CW25	28/06/2014	75.00%	93.75%	03/05/2013
	TL28	28/06/2014	100%	87.50%	30/04/2013
5	Mansion House-Blackfriars				
	TL26	28/06/2014	84.38%	80.36%	14/08/2013

Summary of Score Tables					
Sections	Route	Euroconsult's Assessment Date	Euroconsult Ratings	Visual Inspection Rating	Visual Inspection Assessment Date
	CW24	28/06/2014	84.38%	91.67%	19/02/2009
6	Blackfriars- Temple				
	TL24	29/06/2014	96.88%	81.25%	29/08/2013
	CW23	29/06/2014	87.50%	87.50%	15/05/2013
	TL23	29/06/2014	96.88%	93.75%	08/11/2012
	CW22	29/06/2014	81.25%	87.50%	15/05/2013
	TL22	29/06/2014	71.88	84.38%	31/03/2010
	CW21	29/06/2014	96.88	100.00%	
7	Temple- Embankment				
	CW20	29/06/2014	75	68.75%	19/07/2013
	CW19	29/06/2014	81.25	87.50%	03/04/2013
8	Embankment-Westminster				
	CW18	29/06/2014	93.75	81.25%	03/07/2013
	CW17	29/06/2014	78.13	95.80%	15/02/2011
	TL21	29/06/2014	96.88	68.75%	19/04/2011
9	Westminster- St James's Park				
	TL20	29/06/2014	96.88%	80.36%	24/03/2011
	CW16	29/06/2014	96.88%	89.60%	14/02/2011
10	St James's Park - Victoria				
	CW15	29/06/2014	81.25%	81.25%	24/03/2014
	TL19	29/06/2014	90.63%	85.71%	31/03/2010

Summary of Score Tables					
Sections	Route	Euroconsult's Assessment Date	Euroconsult Ratings	Visual Inspection Rating	Visual Inspection Assessment Date
	CW14	29/06/2014	93.75%	87.50%	13/03/2012
	TL18	29/06/2014	90.63%	80.35%	12/05/2011
	TL17		62.50%	78.13%	11/05/2011
11	Victoria-Sloan Square				
	TL16	29/06/2014	96.88%	81.25%	07/06/2011
11	TL15	29/06/2014	84.38%	89.29%	21/06/2011
	TL14	29/06/2014	96.88%	75.00%	31/05/2011
	TL13	29/06/2014	81.25%	90.00%	01/04/2011
	TL12	29/06/2014	87.50%	71.87%	08/04/2011
12	Sloan Square- South Kensington				
	TL11	05/07/2014	84.38%	78.13%	15/09/2011
	CW13	05/07/2014	78.13%	89.60%	31/03/2011
	TL10	05/07/2014	84.38%	84.38%	16/05/2013
	TL9	05/07/2014	75.00%	88.75%	28/02/2011
	TL8	05/07/2014	81.25%	89.30%	29/04/2013
13	South-Kensington- Gloucester Road				
	TL7	05/07/2014	100.00%	75.00%	01/02/2014
	TL75	05/07/2014	75.00%	62.50%	13/07/2011
14	Gloucester Road-HS Kensington				
	TL6	05/07/2014	96.88%	65.62%	01/03/2013

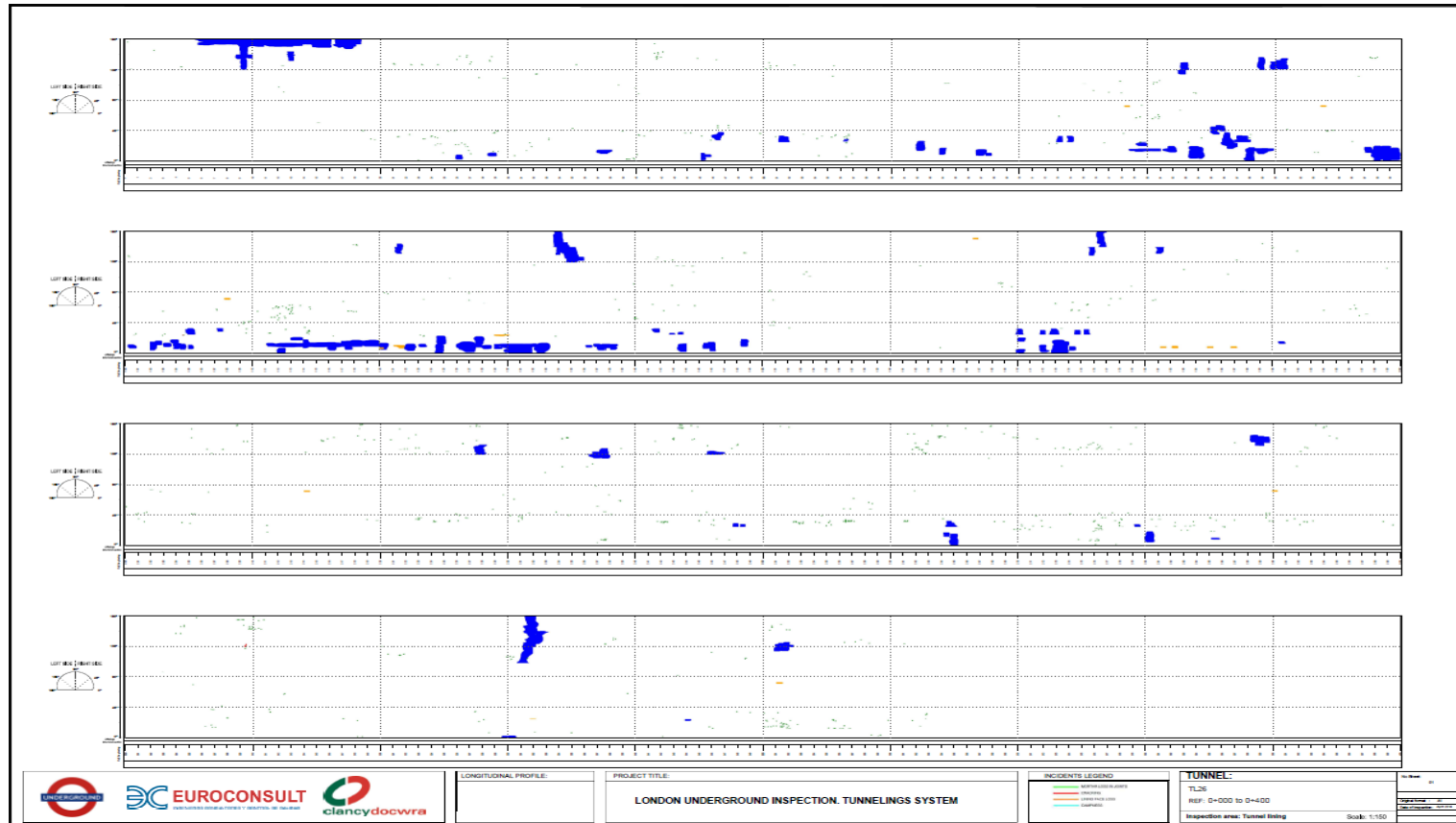
Summary of Score Tables					
Sections	Route	Euroconsult's Assessment Date	Euroconsult Ratings	Visual Inspection Rating	Visual Inspection Assessment Date
	TL74	05/07/2014	87.50%	78.12%	07/02/2013
	TL73	05/07/2014	75.00%	81.25%	25/02/2013
	CW58		93.75%	87.50%	04/05/2012
15	HS Kensington- Notting Hill				
	CW57	05/07/2014	71.88%	87.50%	05/05/2012
	TL72	05/07/2014	96.88%	84.38%	24/01/2012
	CW56	05/07/2014	68.75%	87.50%	04/04/2012
	TL71	05/07/2014	68.75%	71.88%	06/01/2009
	TL70	05/07/2014	75.00%	78.13%	25/03/2013
16	Notting Hill- Bayswater				
	TL69	05/07/2014	75.00%	81.25%	15/03/2012
	TL68	05/07/2014	75.00%	87.50%	28/03/2013
	TL67	05/07/2014	78.13%	81.25%	25/03/2013
	TL66	05/07/2014	84.38%	65.62%	01/03/2013
17	Bayswater- Paddington				
	CW55	05/07/2014	96.88%	91.67%	09/10/2013
	TL65	05/07/2014	96.88%	81.25%	18/05/2011
	CW54	05/07/2014	100.00%	87.50%	24/04/2014
	TL64	05/07/2014	84.38%	90.63%	08/06/2011
	CW53	05/07/2014	87.50%	75.00%	06/01/2009
	TL63	05/07/2014	87.50%	81.25%	06/01/2009
	TL62	05/07/2014	84.38%	84.38%	06/01/2009

Summary of Score Tables					
Sections	Route	Euroconsult's Assessment Date	Euroconsult Ratings	Visual Inspection Rating	Visual Inspection Assessment Date
	TL61	05/07/2014	96.88%	84.38%	06/01/2009
	CW52	05/07/2014	75.00%	75.00%	06/01/2009
	TL60	05/07/2014	96.88%	59.38%	10/05/2011
18	Paddington- Edward Road				
	TL59	06/07/2014	93.75%	83.92%	26/02/2013
	TL58	06/07/2014	81.25%	78.10%	28/08/2013
	TL57	06/07/2014	93.75%	71.08%	29/06/2012
	TL55	06/07/2014	81.25%	78.31%	13/08/2013
	TL54	06/07/2014	84.38%	87.50%	23/06/2012
19	Edward Road-Baker Street				
	TL53	06/07/2014	81.25%	46.88%	21/03/2013
20	Baker Street-Great Portland Street				
	TL51	06/07/2014	87.50%	84.38%	02/06/2012
	TL110	06/07/2014	71.88%	78.13%	15/09/2011
	TL109	06/07/2014	87.50%	84.38%	16/05/2013
21	Great Portland Street-Euston Square				
	TL106	06/07/2014	81.25%	81.25%	03/03/2014
22	Euston Square-King Cross				
	TL103	06/07/2014	71.88%	78.12%	22/01/2014
	CW71	06/07/2014	78.13%	87.50%	02/05/2012

Summary of Score Tables					
Sections	Route	Euroconsult's Assessment Date	Euroconsult Ratings	Visual Inspection Rating	Visual Inspection Assessment Date
	TL102	06/07/2014	84.38%	84.38%	20/09/2013
	CW70	06/07/2014	75.00%	75.00%	06/01/2009
	CW69	06/07/2014	90.63%	75.00%	24/04/2012
	TL101	06/07/2014	93.75%	81.25%	08/07/2013
23	King Cross- Farringdon				
	CW67	06/07/2014	100.00%	83.30%	07/09/2010
	CW66	06/07/2014	100.00%	91.67%	08/08/2013
	TL97	06/07/2014	75.00%	71.88%	09/10/2012
	TL91	06/07/2014	84.38%	88.75%	28/02/2014
	TL89	06/07/2014	75.00%	62.50%	05/09/2013
24	Farringdon- Barbican				
	TL85	06/07/2014	84.38%	80.36%	30/06/2011
25	Barbican- Moorgate				
	TL82	06/07/2014	78.13%	81.25%	09/07/2013
	CW75	06/07/2014	87.50%	77.50%	24/01/2012
26	Moorgate-Liverpool Street				
	CW62	06/07/2014	93.75%	89.06%	12/07/2013
	TL79	06/07/2014	78.13%	75.00%	01/02/2014
27	Liverpool Street- Aldgate				
	TL77	06/07/2014	100.00%	81.25%	02/08/2013
	CW61	06/07/2014	100.00%	75.00%	01/07/2011
	CW60	06/07/2014	100.00%	87.50%	02/09/2013

Summary of Score Tables					
Sections	Route	Euroconsult's Assessment Date	Euroconsult Ratings	Visual Inspection Rating	Visual Inspection Assessment Date
28	Aldgate -Aldgate East				
	TL76	06/07/2014	65.63%	83.93%	09/11/2013
	CW59	06/07/2014	75.00%	75.00%	29/06/2011
29	Aldgate East- White Chappel				
	TL37	06/07/2014	62.50%	75.00%	01/02/2014
	TL38	06/07/2014	71.88%	87.50%	03/04/2013
	CW30	06/07/2014	90.63%	66.67%	31/03/2010
	CW32	06/07/2014	84.38%	85.42%	19/05/2012
30	White Chappel-Stepney Green				
	cw33	06/07/2014	90.63%	87.50%	03/04/2014
	TL41	06/07/2014	75.00%	75.00%	06/03/2014
31	Stepney Green- Mile End				
	TL42	06/07/2014	68.75%	65.63%	18/12/2013
	TL43	06/07/2014	84.38%	79.17%	20/04/2013
32	Mile End- Bow Road				
	TL44	06/07/2014	71.88%	87.50%	15/04/2013
	CW35	06/07/2014	87.50%	81.25%	18/04/2013
33	Paddington- Edward Road				
	TL56	06/07/2014	84.38%	56.25%	05/03/2013
34	Tower hill- Aldgate East				
	CW29	06/07/2014	87.50%	87.50%	19/09/2012

Appendix C: - Tunnel Chart- Tunnel 26



Euroconsult's Tunnelling system (2014)

Appendix D: - Incidents identified by the laser survey for TL 26

Tunnel 26

Section	Meter	Type of incident	Extent(%)	Width	Depth	Severity
TL26	0	MORTAR LOSS IN JOINTS	0.0101	40.31	21.00	2
TL26	3	MORTAR LOSS IN JOINTS	0.0047	14.77	18.63	2
TL26	3	MORTAR LOSS IN JOINTS	0.0050	27.30	31.29	4
TL26	6	DAMP PATCHES	16.2592			N.A
TL26	9	DAMP PATCHES	4.8711			N.A
TL26	9	DAMP PATCHES	37.0626			N.A
TL26	12	MORTAR LOSS IN JOINTS	0.0050	15.92	15.23	2
TL26	12	DAMP PATCHES	0.8745			N.A
TL26	12	MORTAR LOSS IN JOINTS	0.0111	9.82	26.12	3
TL26	12	DAMP PATCHES	35.3688			N.A
TL26	15	MORTAR LOSS IN JOINTS	0.0126	12.50	58.61	4
TL26	15	DAMP PATCHES	26.9560			N.A
TL26	15	MORTAR LOSS IN JOINTS	0.0037	23.85	10.20	1
TL26	18	MORTAR LOSS IN JOINTS	0.0247	11.24	17.19	2
TL26	18	DAMP PATCHES	17.3641			N.A
TL26	21	MORTAR LOSS IN JOINTS	0.0009	17.34	18.84	2
TL26	21	MORTAR LOSS IN JOINTS	0.0186	11.77	13.84	1
TL26	21	MORTAR LOSS IN JOINTS	0.0211	29.33	20.60	2
TL26	24	DAMP PATCHES	1.1441			N.A
TL26	24	MORTAR LOSS IN JOINTS	0.0322	13.62	19.84	2
TL26	24	MORTAR LOSS IN JOINTS	0.0444	13.91	23.07	2
TL26	24	MORTAR LOSS IN JOINTS	0.0179	17.33	20.03	2
TL26	27	DAMP PATCHES	1.4460			N.A
TL26	27	MORTAR LOSS IN JOINTS	0.0128	18.53	9.70	1
TL26	27	MORTAR LOSS IN JOINTS	0.0450	17.52	14.81	1
TL26	27	MORTAR LOSS IN JOINTS	0.0045	15.28	15.87	2
TL26	27	MORTAR LOSS IN JOINTS	0.0358	23.04	22.48	2
TL26	27	MORTAR LOSS IN JOINTS	0.0141	33.90	16.27	2
TL26	30	MORTAR LOSS IN JOINTS	0.0147	13.63	25.34	3
TL26	30	MORTAR LOSS IN JOINTS	0.0163	11.23	60.77	4
TL26	33	MORTAR LOSS IN JOINTS	0.0147	13.83	18.60	2
TL26	33	MORTAR LOSS IN JOINTS	0.0094	13.58	16.32	2
TL26	36	DAMP PATCHES	2.8263			N.A
TL26	36	MORTAR LOSS IN JOINTS	0.0044	20.31	14.67	1
TL26	39	MORTAR LOSS IN JOINTS	0.0282	18.38	17.48	2
TL26	39	MORTAR LOSS IN JOINTS	0.0247	14.78	25.43	3
TL26	39	MORTAR LOSS IN JOINTS	0.0045	16.88	10.97	1
TL26	39	MORTAR LOSS IN JOINTS	0.0026	7.85	6.55	1
TL26	42	MORTAR LOSS IN JOINTS	0.0103	18.12	18.55	2
TL26	42	MORTAR LOSS IN JOINTS	0.0232	17.38	23.64	2
TL26	42	MORTAR LOSS IN JOINTS	0.0469	24.43	19.68	2
TL26	45	DAMP PATCHES	3.0452			N.A
TL26	45	DAMP PATCHES	2.7860			N.A
TL26	45	MORTAR LOSS IN JOINTS	0.0167	18.90	16.03	2
TL26	45	MORTAR LOSS IN JOINTS	0.0208	14.61	17.18	2
TL26	45	MORTAR LOSS IN JOINTS	0.0101	27.32	26.01	3
TL26	48	MORTAR LOSS IN JOINTS	0.0087	18.25	13.72	1
TL26	48	MORTAR LOSS IN JOINTS	0.0091	19.64	26.16	3
TL26	51	DAMP PATCHES	2.0864			N.A
TL26	51	MORTAR LOSS IN JOINTS	0.0077	8.78	16.78	2

Appendix D-List of incidents were identified by the laser survey-Tunnel-26

Section	Meter	Type of incident	Extent(%)	Width	Depth	Severity
TL26	51	MORTAR LOSS IN JOINTS	0.0277	24.83	21.77	2
TL26	54	MORTAR LOSS IN JOINTS	0.0261	21.23	9.50	1
TL26	54	DAMP PATCHES	0.0149			N.A
TL26	54	MORTAR LOSS IN JOINTS	0.0451	13.01	15.96	2
TL26	54	MORTAR LOSS IN JOINTS	0.0051	14.98	12.69	1
TL26	54	MORTAR LOSS IN JOINTS	0.0038	18.43	15.36	2
TL26	60	DAMP PATCHES	4.1167			N.A
TL26	60	DAMP PATCHES	2.1668			N.A
TL26	63	DAMP PATCHES	1.2099			N.A
TL26	63	MORTAR LOSS IN JOINTS	0.0110	22.85	11.35	1
TL26	63	MORTAR LOSS IN JOINTS	0.0160	10.87	28.54	3
TL26	66	DAMP PATCHES	4.4692			N.A
TL26	72	MORTAR LOSS IN JOINTS	0.0094	19.29	21.04	2
TL26	72	DAMP PATCHES	2.9542			N.A
TL26	72	MORTAR LOSS IN JOINTS	0.0103	19.78	20.50	2
TL26	72	MORTAR LOSS IN JOINTS	0.0069	47.79	7.44	1
TL26	75	MORTAR LOSS IN JOINTS	0.0033	26.71	16.97	2
TL26	75	MORTAR LOSS IN JOINTS	0.0061	21.01	37.84	4
TL26	75	MORTAR LOSS IN JOINTS	0.0044	15.47	15.62	2
TL26	78	DAMP PATCHES	8.3913			N.A
TL26	78	MORTAR LOSS IN JOINTS	0.0045	26.69	7.60	1
TL26	78	DAMP PATCHES	1.5418			N.A
TL26	78	MORTAR LOSS IN JOINTS	0.0169	16.55	14.15	1
TL26	78	MORTAR LOSS IN JOINTS	0.0384	20.89	29.30	3
TL26	78	MORTAR LOSS IN JOINTS	0.0032	9.62	26.48	3
TL26	78	LINING FACE LOSS	0.0580		5.02	1
TL26	78	MORTAR LOSS IN JOINTS	0.0033	9.69	10.10	1
TL26	78	MORTAR LOSS IN JOINTS	0.0045	21.20	17.20	2
TL26	81	DAMP PATCHES	15.9835			N.A
TL26	81	MORTAR LOSS IN JOINTS	0.0043	16.53	30.64	4
TL26	81	MORTAR LOSS IN JOINTS	0.0057	15.42	16.65	2
TL26	81	MORTAR LOSS IN JOINTS	0.0077	10.75	21.65	2
TL26	81	DAMP PATCHES	1.9852			N.A
TL26	81	MORTAR LOSS IN JOINTS	0.0151	15.80	15.76	2
TL26	81	DAMP PATCHES	6.0014			N.A
TL26	84	DAMP PATCHES	9.6558			N.A
TL26	84	DAMP PATCHES	13.0205			N.A
TL26	84	MORTAR LOSS IN JOINTS	0.0057	21.81	42.10	4
TL26	84	DAMP PATCHES	2.7154			N.A
TL26	84	MORTAR LOSS IN JOINTS	0.0139	21.32	11.23	1
TL26	87	DAMP PATCHES	13.2841			N.A
TL26	87	DAMP PATCHES	5.5709			N.A
TL26	87	MORTAR LOSS IN JOINTS	0.0084	20.46	8.24	1
TL26	87	DAMP PATCHES	3.1537			N.A
TL26	90	MORTAR LOSS IN JOINTS	0.0053	13.06	15.88	2
TL26	90	MORTAR LOSS IN JOINTS	0.0033	11.30	22.97	2
TL26	90	DAMP PATCHES	6.9000			N.A
TL26	93	MORTAR LOSS IN JOINTS	0.0064	14.02	23.47	2
TL26	93	MORTAR LOSS IN JOINTS	0.0320	20.27	41.97	4
TL26	93	LINING FACE LOSS	0.0832		15.85	2
TL26	93	LINING FACE LOSS	0.0532		5.81	1
TL26	96	DAMP PATCHES	24.2119			N.A
TL26	96	MORTAR LOSS IN JOINTS	0.0047	16.80	26.94	3
TL26	96	MORTAR LOSS IN JOINTS	0.0033	19.54	10.32	1
TL26	96	MORTAR LOSS IN JOINTS	0.0230	17.35	14.69	1
TL26	99	DAMP PATCHES	11.6071			N.A

Appendix D-List of incidents were identified by the laser survey-Tunnel-26

Section	Meter	Type of incident	Extent(%)	Width	Depth	Severity
TL26	99	MORTAR LOSS IN JOINTS	0.0023	11.02	25.57	3
TL26	99	MORTAR LOSS IN JOINTS	0.0051	13.21	32.13	4
TL26	99	MORTAR LOSS IN JOINTS	0.0061	19.14	25.18	3
TL26	99	MORTAR LOSS IN JOINTS	0.0060	25.20	17.52	2
TL26	102	CRACKING	0.0047	30.46	29.52	4
TL26	102	DAMP PATCHES	10.7878			N.A
TL26	102	MORTAR LOSS IN JOINTS	0.0080	12.91	22.79	2
TL26	102	MORTAR LOSS IN JOINTS	0.0055	11.22	19.11	2
TL26	102	MORTAR LOSS IN JOINTS	0.0052	10.60	21.38	2
TL26	105	DAMP PATCHES	1.3349			N.A
TL26	105	DAMP PATCHES	4.0118			N.A
TL26	105	MORTAR LOSS IN JOINTS	0.0095	17.34	29.06	3
TL26	108	MORTAR LOSS IN JOINTS	0.0354	21.14	24.36	2
TL26	108	MORTAR LOSS IN JOINTS	0.0054	11.24	24.30	2
TL26	108	LINING FACE LOSS	0.1333		2.70	1
TL26	111	DAMP PATCHES	18.0820			N.A
TL26	111	MORTAR LOSS IN JOINTS	0.0188	17.42	32.18	4
TL26	111	MORTAR LOSS IN JOINTS	0.1276	22.40	24.35	2
TL26	114	DAMP PATCHES	22.8243			N.A
TL26	114	MORTAR LOSS IN JOINTS	0.0033	39.42	17.44	2
TL26	114	MORTAR LOSS IN JOINTS	0.0658	16.13	25.31	3
TL26	114	MORTAR LOSS IN JOINTS	0.0108	26.08	24.72	2
TL26	114	MORTAR LOSS IN JOINTS	0.0019	13.49	20.68	2
TL26	117	DAMP PATCHES	26.4181			N.A
TL26	117	MORTAR LOSS IN JOINTS	0.0208	16.53	19.66	2
TL26	117	MORTAR LOSS IN JOINTS	0.0089	13.57	10.15	1
TL26	117	MORTAR LOSS IN JOINTS	0.0117	21.84	17.89	2
TL26	120	DAMP PATCHES	8.2142			N.A
TL26	120	LINING FACE LOSS	0.5061		5.31	1
TL26	120	MORTAR LOSS IN JOINTS	0.0078	18.39	14.20	1
TL26	120	DAMP PATCHES	1.6268			N.A
TL26	120	DAMP PATCHES	1.3891			N.A
TL26	123	DAMP PATCHES	10.0543			N.A
TL26	123	MORTAR LOSS IN JOINTS	0.0133	20.93	25.55	3
TL26	123	DAMP PATCHES	0.4227			N.A
TL26	123	MORTAR LOSS IN JOINTS	0.0037	24.93	60.90	4
TL26	126	DAMP PATCHES	22.5214			N.A
TL26	126	MORTAR LOSS IN JOINTS	0.0157	15.75	7.35	1
TL26	126	MORTAR LOSS IN JOINTS	0.0046	12.72	17.40	2
TL26	129	DAMP PATCHES	34.2108			N.A
TL26	129	LINING FACE LOSS	0.4115		7.74	1
TL26	129	MORTAR LOSS IN JOINTS	0.0039	16.53	24.01	2
TL26	132	DAMP PATCHES	11.4047			N.A
TL26	132	MORTAR LOSS IN JOINTS	0.0038	20.06	14.85	1
TL26	132	MORTAR LOSS IN JOINTS	0.0042	21.77	13.70	1
TL26	132	DAMP PATCHES	1.5629			N.A
TL26	132	DAMP PATCHES	3.2925			N.A
TL26	135	DAMP PATCHES	5.2746			N.A
TL26	135	DAMP PATCHES	22.7964			N.A
TL26	135	DAMP PATCHES	14.1549			N.A
TL26	138	DAMP PATCHES	2.2565			N.A
TL26	138	MORTAR LOSS IN JOINTS	0.0385	22.22	14.61	1
TL26	138	MORTAR LOSS IN JOINTS	0.0043	21.84	13.69	1
TL26	138	MORTAR LOSS IN JOINTS	0.0047	17.36	9.35	1
TL26	138	MORTAR LOSS IN JOINTS	0.0056	17.34	14.02	1
TL26	141	DAMP PATCHES	5.4033			N.A

Appendix D-List of incidents were identified by the laser survey-Tunnel-26

Section	Meter	Type of incident	Extent(%)	Width	Depth	Severity
TL26	141	DAMP PATCHES	2.3936			N.A
TL26	141	MORTAR LOSS IN JOINTS	0.0153	28.50	37.49	4
TL26	141	MORTAR LOSS IN JOINTS	0.0040	9.47	43.99	4
TL26	141	MORTAR LOSS IN JOINTS	0.0056	24.77	7.86	1
TL26	141	MORTAR LOSS IN JOINTS	0.0193	17.63	31.49	4
TL26	144	DAMP PATCHES	3.6098			N.A
TL26	144	MORTAR LOSS IN JOINTS	0.0055	23.33	19.53	2
TL26	144	MORTAR LOSS IN JOINTS	0.0381	9.40	18.79	2
TL26	147	DAMP PATCHES	2.2361			N.A
TL26	147	MORTAR LOSS IN JOINTS	0.0155	18.80	29.62	3
TL26	150	MORTAR LOSS IN JOINTS	0.0319	13.43	28.28	3
TL26	150	MORTAR LOSS IN JOINTS	0.0086	14.71	33.42	4
TL26	150	MORTAR LOSS IN JOINTS	0.0042	26.08	28.02	3
TL26	153	MORTAR LOSS IN JOINTS	0.0215	20.26	38.69	4
TL26	162	MORTAR LOSS IN JOINTS	0.0042	14.49	27.04	3
TL26	162	MORTAR LOSS IN JOINTS	0.0045	16.36	20.12	2
TL26	165	LINING FACE LOSS	0.0908		34.96	3
TL26	168	DAMP PATCHES	3.0171			N.A
TL26	168	DAMP PATCHES	3.0101			N.A
TL26	168	MORTAR LOSS IN JOINTS	0.0283	19.20	9.81	1
TL26	171	DAMP PATCHES	20.7128			N.A
TL26	171	DAMP PATCHES	5.8218			N.A
TL26	171	MORTAR LOSS IN JOINTS	0.0073	8.24	15.12	2
TL26	171	MORTAR LOSS IN JOINTS	0.0052	15.92	30.58	4
TL26	174	DAMP PATCHES	1.1051			N.A
TL26	174	DAMP PATCHES	1.8840			N.A
TL26	174	MORTAR LOSS IN JOINTS	0.0410	15.92	23.49	2
TL26	174	MORTAR LOSS IN JOINTS	0.0058	28.24	40.91	4
TL26	174	DAMP PATCHES	0.9932			N.A
TL26	177	MORTAR LOSS IN JOINTS	0.0090	24.09	20.40	2
TL26	177	MORTAR LOSS IN JOINTS	0.0142	22.98	17.06	2
TL26	177	MORTAR LOSS IN JOINTS	0.0033	19.90	33.34	4
TL26	177	DAMP PATCHES	6.2196			N.A
TL26	180	LINING FACE LOSS	0.3157		6.81	1
TL26	180	MORTAR LOSS IN JOINTS	0.0111	14.45	9.06	1
TL26	180	DAMP PATCHES	1.7499			N.A
TL26	183	LINING FACE LOSS	0.1257		3.75	1
TL26	183	MORTAR LOSS IN JOINTS	0.0095	32.71	37.54	4
TL26	183	MORTAR LOSS IN JOINTS	0.0057	9.98	22.41	2
TL26	186	LINING FACE LOSS	0.1506		7.69	1
TL26	186	MORTAR LOSS IN JOINTS	0.0084	16.44	13.81	1
TL26	186	MORTAR LOSS IN JOINTS	0.0051	16.36	10.94	1
TL26	186	MORTAR LOSS IN JOINTS	0.0045	13.87	53.67	4
TL26	186	MORTAR LOSS IN JOINTS	0.0040	21.32	74.40	4
TL26	189	DAMP PATCHES	0.3736			N.A
TL26	189	MORTAR LOSS IN JOINTS	0.0072	11.07	6.32	1
TL26	189	MORTAR LOSS IN JOINTS	0.0046	49.83	30.57	4
TL26	192	MORTAR LOSS IN JOINTS	0.0045	12.49	26.93	3
TL26	192	MORTAR LOSS IN JOINTS	0.0048	17.36	14.93	1
TL26	192	MORTAR LOSS IN JOINTS	0.0067	18.97	14.82	1
TL26	195	MORTAR LOSS IN JOINTS	0.0348	19.01	23.14	2
TL26	198	MORTAR LOSS IN JOINTS	0.0043	34.44	30.89	4
TL26	198	MORTAR LOSS IN JOINTS	0.0037	27.18	88.87	4
TL26	198	MORTAR LOSS IN JOINTS	0.0038	14.12	44.30	4
TL26	201	MORTAR LOSS IN JOINTS	0.0305	19.97	15.43	2
TL26	201	MORTAR LOSS IN JOINTS	0.0090	16.83	24.27	2

Appendix D-List of incidents were identified by the laser survey-Tunnel-26

Section	Meter	Type of incident	Extent(%)	Width	Depth	Severity
TL26	201	MORTAR LOSS IN JOINTS	0.0220	17.77	35.62	4
TL26	204	MORTAR LOSS IN JOINTS	0.0206	18.59	25.26	3
TL26	204	MORTAR LOSS IN JOINTS	0.0029	12.70	69.82	4
TL26	204	MORTAR LOSS IN JOINTS	0.0079	48.38	19.61	2
TL26	207	MORTAR LOSS IN JOINTS	0.0150	17.22	10.64	1
TL26	207	MORTAR LOSS IN JOINTS	0.0191	32.43	21.04	2
TL26	210	MORTAR LOSS IN JOINTS	0.0056	23.05	25.36	3
TL26	210	MORTAR LOSS IN JOINTS	0.0059	22.76	18.32	2
TL26	210	MORTAR LOSS IN JOINTS	0.0114	18.65	27.82	3
TL26	210	MORTAR LOSS IN JOINTS	0.0164	26.89	20.85	2
TL26	213	LINING FACE LOSS	0.0767		1.04	1
TL26	213	MORTAR LOSS IN JOINTS	0.0056	21.80	26.88	3
TL26	213	MORTAR LOSS IN JOINTS	0.0061	21.32	20.65	2
TL26	216	MORTAR LOSS IN JOINTS	0.0167	15.52	18.80	2
TL26	216	MORTAR LOSS IN JOINTS	0.0291	34.17	22.97	2
TL26	219	MORTAR LOSS IN JOINTS	0.0125	18.36	32.45	4
TL26	219	MORTAR LOSS IN JOINTS	0.0030	21.72	8.22	1
TL26	219	MORTAR LOSS IN JOINTS	0.0193	19.50	20.27	2
TL26	219	MORTAR LOSS IN JOINTS	0.0320	24.14	20.10	2
TL26	222	MORTAR LOSS IN JOINTS	0.0755	15.70	18.51	2
TL26	222	MORTAR LOSS IN JOINTS	0.0401	17.20	36.08	4
TL26	222	MORTAR LOSS IN JOINTS	0.0159	16.28	18.60	2
TL26	225	MORTAR LOSS IN JOINTS	0.0463	19.04	22.07	2
TL26	225	MORTAR LOSS IN JOINTS	0.0040	24.79	12.92	1
TL26	225	MORTAR LOSS IN JOINTS	0.0181	13.72	48.06	4
TL26	228	MORTAR LOSS IN JOINTS	0.0070	20.82	19.80	2
TL26	228	MORTAR LOSS IN JOINTS	0.0099	22.07	15.99	2
TL26	228	MORTAR LOSS IN JOINTS	0.0040	12.02	5.20	1
TL26	228	DAMP PATCHES	6.2719			N.A
TL26	228	MORTAR LOSS IN JOINTS	0.0043	25.14	21.29	2
TL26	228	MORTAR LOSS IN JOINTS	0.0167	28.37	34.16	4
TL26	231	MORTAR LOSS IN JOINTS	0.0335	15.17	20.57	2
TL26	231	MORTAR LOSS IN JOINTS	0.0030	15.23	28.09	3
TL26	234	MORTAR LOSS IN JOINTS	0.0097	18.37	13.47	1
TL26	234	MORTAR LOSS IN JOINTS	0.0058	16.98	26.49	3
TL26	234	MORTAR LOSS IN JOINTS	0.0313	20.19	22.93	2
TL26	237	MORTAR LOSS IN JOINTS	0.0238	11.55	17.21	2
TL26	237	MORTAR LOSS IN JOINTS	0.0108	15.04	37.72	4
TL26	237	MORTAR LOSS IN JOINTS	0.0320	16.62	48.90	4
TL26	237	MORTAR LOSS IN JOINTS	0.0083	10.70	8.82	1
TL26	237	DAMP PATCHES	4.7855			N.A
TL26	237	MORTAR LOSS IN JOINTS	0.0078	18.76	11.45	1
TL26	237	DAMP PATCHES	9.5060			N.A
TL26	237	MORTAR LOSS IN JOINTS	0.0040	17.27	14.58	1
TL26	240	MORTAR LOSS IN JOINTS	0.0675	16.54	24.91	2
TL26	240	MORTAR LOSS IN JOINTS	0.0092	13.01	22.96	2
TL26	240	MORTAR LOSS IN JOINTS	0.0042	24.77	28.14	3
TL26	243	MORTAR LOSS IN JOINTS	0.0182	19.09	22.04	2
TL26	243	MORTAR LOSS IN JOINTS	0.0047	18.38	29.11	3
TL26	243	MORTAR LOSS IN JOINTS	0.0125	20.53	44.21	4
TL26	243	MORTAR LOSS IN JOINTS	0.0754	17.74	26.29	3
TL26	246	MORTAR LOSS IN JOINTS	0.0062	11.09	23.81	2
TL26	246	DAMP PATCHES	1.2718			N.A
TL26	246	MORTAR LOSS IN JOINTS	0.0202	19.77	31.94	4
TL26	246	DAMP PATCHES	4.5801			N.A
TL26	246	MORTAR LOSS IN JOINTS	0.0207	18.23	19.41	2

Appendix D-List of incidents were identified by the laser survey-Tunnel-26

Section	Meter	Type of incident	Extent(%)	Width	Depth	Severity
TL26	252	MORTAR LOSS IN JOINTS	0.0663	17.99	26.85	3
TL26	252	MORTAR LOSS IN JOINTS	0.0081	10.87	33.88	4
TL26	255	MORTAR LOSS IN JOINTS	0.1046	15.01	34.35	4
TL26	255	MORTAR LOSS IN JOINTS	0.0175	25.00	17.12	2
TL26	258	MORTAR LOSS IN JOINTS	0.0209	20.72	33.51	4
TL26	258	MORTAR LOSS IN JOINTS	0.0058	22.88	20.37	2
TL26	261	MORTAR LOSS IN JOINTS	0.0202	12.80	17.74	2
TL26	261	MORTAR LOSS IN JOINTS	0.0029	10.68	20.84	2
TL26	261	MORTAR LOSS IN JOINTS	0.0879	21.99	30.56	4
TL26	261	MORTAR LOSS IN JOINTS	0.0117	10.93	20.01	2
TL26	264	DAMP PATCHES	5.5767			N.A
TL26	264	DAMP PATCHES	1.9377			N.A
TL26	264	MORTAR LOSS IN JOINTS	0.0061	22.35	8.52	1
TL26	264	MORTAR LOSS IN JOINTS	0.0443	16.57	18.75	2
TL26	267	MORTAR LOSS IN JOINTS	0.0094	21.94	27.31	3
TL26	267	MORTAR LOSS IN JOINTS	0.0102	22.27	30.03	4
TL26	267	MORTAR LOSS IN JOINTS	0.0039	17.91	39.21	4
TL26	267	MORTAR LOSS IN JOINTS	0.0205	14.77	18.06	2
TL26	270	MORTAR LOSS IN JOINTS	0.0159	23.56	20.75	2
TL26	270	MORTAR LOSS IN JOINTS	0.0317	14.42	19.49	2
TL26	270	MORTAR LOSS IN JOINTS	0.0347	12.88	24.45	2
TL26	273	MORTAR LOSS IN JOINTS	0.0161	22.27	28.14	3
TL26	273	MORTAR LOSS IN JOINTS	0.0038	16.62	22.98	2
TL26	273	MORTAR LOSS IN JOINTS	0.0049	13.99	38.55	4
TL26	273	MORTAR LOSS IN JOINTS	0.0254	25.72	26.89	3
TL26	276	MORTAR LOSS IN JOINTS	0.0474	13.45	27.71	3
TL26	276	MORTAR LOSS IN JOINTS	0.0995	17.20	23.50	2
TL26	276	MORTAR LOSS IN JOINTS	0.0468	17.06	22.95	2
TL26	276	MORTAR LOSS IN JOINTS	0.0028	16.41	28.11	3
TL26	279	DAMP PATCHES	5.5395			N.A
TL26	279	DAMP PATCHES	0.5919			N.A
TL26	279	MORTAR LOSS IN JOINTS	0.0345	17.25	38.52	4
TL26	279	MORTAR LOSS IN JOINTS	0.0055	16.43	68.52	4
TL26	279	MORTAR LOSS IN JOINTS	0.0399	23.08	21.87	2
TL26	282	MORTAR LOSS IN JOINTS	0.0081	20.61	19.09	2
TL26	282	MORTAR LOSS IN JOINTS	0.0274	18.45	13.61	1
TL26	285	DAMP PATCHES	0.3217			N.A
TL26	285	MORTAR LOSS IN JOINTS	0.0081	14.82	28.63	3
TL26	285	MORTAR LOSS IN JOINTS	0.0303	17.07	15.60	2
TL26	285	MORTAR LOSS IN JOINTS	0.0051	26.13	13.12	1
TL26	288	MORTAR LOSS IN JOINTS	0.0352	16.59	27.41	3
TL26	288	LINING FACE LOSS	0.0490		4.97	1
TL26	288	DAMP PATCHES	2.6972			N.A
TL26	288	DAMP PATCHES	4.1849			N.A
TL26	291	MORTAR LOSS IN JOINTS	0.0404	21.90	23.42	2
TL26	291	MORTAR LOSS IN JOINTS	0.0044	16.49	17.64	2
TL26	291	MORTAR LOSS IN JOINTS	0.0169	23.00	20.88	2
TL26	294	MORTAR LOSS IN JOINTS	0.0259	14.46	18.00	2
TL26	297	MORTAR LOSS IN JOINTS	0.0133	18.29	25.71	3
TL26	300	MORTAR LOSS IN JOINTS	0.0036	18.91	13.78	1
TL26	303	MORTAR LOSS IN JOINTS	0.0027	20.25	48.73	4
TL26	303	MORTAR LOSS IN JOINTS	0.0049	17.23	31.51	4
TL26	303	MORTAR LOSS IN JOINTS	0.0117	19.53	14.41	1
TL26	303	MORTAR LOSS IN JOINTS	0.0194	18.96	21.72	2
TL26	306	MORTAR LOSS IN JOINTS	0.0101	17.35	15.17	2
TL26	306	MORTAR LOSS IN JOINTS	0.0320	15.08	33.35	4

Appendix D-List of incidents were identified by the laser survey-Tunnel-26

Section	Meter	Type of incident	Extent(%)	Width	Depth	Severity
TL26	306	MORTAR LOSS IN JOINTS	0.0052	22.59	31.98	4
TL26	309	MORTAR LOSS IN JOINTS	0.0128	14.17	14.30	1
TL26	309	MORTAR LOSS IN JOINTS	0.0066	18.47	9.41	1
TL26	309	CRACKING	0.0573	25.15	18.82	4
TL26	309	MORTAR LOSS IN JOINTS	0.0811	13.68	16.94	2
TL26	312	MORTAR LOSS IN JOINTS	0.0063	18.58	48.62	4
TL26	315	MORTAR LOSS IN JOINTS	0.0074	16.53	21.61	2
TL26	318	MORTAR LOSS IN JOINTS	0.0135	17.30	12.23	1
TL26	318	MORTAR LOSS IN JOINTS	0.0149	16.08	37.19	4
TL26	321	MORTAR LOSS IN JOINTS	0.0042	21.68	61.80	4
TL26	321	MORTAR LOSS IN JOINTS	0.0331	25.44	19.55	2
TL26	321	MORTAR LOSS IN JOINTS	0.0106	9.39	15.55	2
TL26	327	MORTAR LOSS IN JOINTS	0.0218	22.40	12.70	1
TL26	327	MORTAR LOSS IN JOINTS	0.0113	20.76	75.53	4
TL26	330	DAMP PATCHES	0.9342			N.A
TL26	330	MORTAR LOSS IN JOINTS	0.0033	29.94	47.21	4
TL26	330	LINING FACE LOSS	0.0428		26.19	2
TL26	330	DAMP PATCHES	12.9134			N.A
TL26	330	MORTAR LOSS IN JOINTS	0.0466	16.92	22.78	2
TL26	330	DAMP PATCHES	17.3095			N.A
TL26	330	DAMP PATCHES	14.0836			N.A
TL26	333	MORTAR LOSS IN JOINTS	0.0065	18.36	15.74	2
TL26	333	MORTAR LOSS IN JOINTS	0.0214	18.49	35.10	4
TL26	333	DAMP PATCHES	7.3693			N.A
TL26	333	DAMP PATCHES	7.4328			N.A
TL26	336	MORTAR LOSS IN JOINTS	0.0049	14.54	14.42	1
TL26	339	MORTAR LOSS IN JOINTS	0.0094	22.25	33.16	4
TL26	339	MORTAR LOSS IN JOINTS	0.0143	12.90	19.42	2
TL26	342	DAMP PATCHES	0.1761			N.A
TL26	342	MORTAR LOSS IN JOINTS	0.0026	14.13	13.34	1
TL26	342	MORTAR LOSS IN JOINTS	0.0063	10.42	16.72	2
TL26	345	MORTAR LOSS IN JOINTS	0.0116	18.59	27.06	3
TL26	345	MORTAR LOSS IN JOINTS	0.0042	21.25	39.16	4
TL26	345	MORTAR LOSS IN JOINTS	0.0043			N.A
TL26	348	MORTAR LOSS IN JOINTS	0.0188	19.18	10.27	1
TL26	348	MORTAR LOSS IN JOINTS	0.0141	20.66	32.40	4
TL26	348	MORTAR LOSS IN JOINTS	0.0065	17.52	22.47	2
TL26	348	MORTAR LOSS IN JOINTS	0.0081	23.80	28.01	3
TL26	351	MORTAR LOSS IN JOINTS	0.0785	15.25	28.31	3
TL26	351	MORTAR LOSS IN JOINTS	0.0195	12.86	15.00	1
TL26	351	LINING FACE LOSS	0.1115		3.21	1
TL26	351	DAMP PATCHES	4.4658			N.A
TL26	351	DAMP PATCHES	9.9874			N.A
TL26	351	MORTAR LOSS IN JOINTS	0.0261	21.78	23.31	2
TL26	354	MORTAR LOSS IN JOINTS	0.0460	16.66	24.60	2
TL26	357	MORTAR LOSS IN JOINTS	0.0165	19.42	26.77	3
TL26	357	MORTAR LOSS IN JOINTS	0.0158	12.05	18.96	2
TL26	360	MORTAR LOSS IN JOINTS	0.0119	12.05	17.93	2
TL26	360	MORTAR LOSS IN JOINTS	0.0159	13.53	32.99	4
TL26	360	MORTAR LOSS IN JOINTS	0.0056	13.86	53.67	4
TL26	363	MORTAR LOSS IN JOINTS	0.0185	18.07	25.50	3
CW24	366	MORTAR LOSS IN JOINTS	0.1473	18.61	27.16	3
CW24	366	MORTAR LOSS IN JOINTS	0.1446	15.48	24.38	2
CW24	369	MORTAR LOSS IN JOINTS	0.0128	28.40	19.09	2
CW24	369	MORTAR LOSS IN JOINTS	0.0949	16.90	16.91	2
CW24	369	MORTAR LOSS IN JOINTS	0.2855	18.01	16.93	2

Appendix D-List of incidents were identified by the laser survey-Tunnel-26

Section	Meter	Type of incident	Extent(%)	Width	Depth	Severity
CW24	369	MORTAR LOSS IN JOINTS	0.0419	15.91	38.85	4
CW24	372	MORTAR LOSS IN JOINTS	0.0112	17.82	29.65	3
CW24	372	MORTAR LOSS IN JOINTS	0.0167	16.58	15.45	2
CW24	372	LINING FACE LOSS	0.0638		2.23	1
CW24	372	MORTAR LOSS IN JOINTS	0.1151	14.39	21.04	2
CW24	372	MORTAR LOSS IN JOINTS	0.1573	16.46	27.99	3
CW24	375	CRACKING	0.0064	12.65	34.09	4
CW24	375	MORTAR LOSS IN JOINTS	0.0609	18.32	36.27	4
CW24	375	MORTAR LOSS IN JOINTS	0.0968	19.93	44.02	4
CW24	375	MORTAR LOSS IN JOINTS	0.2128	15.23	21.32	2
CW24	375	MORTAR LOSS IN JOINTS	0.0680	22.69	23.51	2
CW24	378	DAMP PATCHES	4.5283			N.A
CW24	378	MORTAR LOSS IN JOINTS	0.0048	13.00	20.56	2
CW24	381	MORTAR LOSS IN JOINTS	0.0238	13.08	5.66	1
CW24	384	MORTAR LOSS IN JOINTS	0.1001	13.49	27.43	3
CW24	384	MORTAR LOSS IN JOINTS	0.0346	12.96	17.08	2
CW24	387	MORTAR LOSS IN JOINTS	0.1149	15.78	25.59	3
CW24	387	MORTAR LOSS IN JOINTS	0.0534	18.48	28.80	3
CW24	390	MORTAR LOSS IN JOINTS	0.0272	13.86	16.58	2
CW24	390	MORTAR LOSS IN JOINTS	0.0607	16.56	24.93	2
CW24	393	MORTAR LOSS IN JOINTS	0.0120	16.22	28.90	3
CW24	393	LINING FACE LOSS	0.1112		17.08	2
CW24	393	MORTAR LOSS IN JOINTS	0.0466	16.98	21.53	2
CW24	393	MORTAR LOSS IN JOINTS	0.0444	15.99	27.43	3
CW24	396	MORTAR LOSS IN JOINTS	0.3048	25.94	21.96	2
CW24	396	MORTAR LOSS IN JOINTS	0.0103	14.14	22.78	2
CW24	396	MORTAR LOSS IN JOINTS	0.0770	14.25	33.12	4
CW24	399	MORTAR LOSS IN JOINTS	0.0111	13.94	42.29	4
CW24	402	MORTAR LOSS IN JOINTS	0.3301	17.37	15.81	2
CW24	402	MORTAR LOSS IN JOINTS	0.0092	24.80	19.54	2
CW24	405	MORTAR LOSS IN JOINTS	0.0252	22.73	27.94	3
CW24	408	MORTAR LOSS IN JOINTS	0.1760	14.78	15.37	2
CW24	408	MORTAR LOSS IN JOINTS	0.0094	16.40	25.89	3
CW24	411	MORTAR LOSS IN JOINTS	0.1373	14.82	16.67	2
CW24	411	MORTAR LOSS IN JOINTS	0.0408	18.92	25.28	3
CW24	417	LINING FACE LOSS	0.1538		2.45	1
CW24	417	DAMP PATCHES	1.6367			N.A
CW24	420	MORTAR LOSS IN JOINTS	0.0053	16.18	7.24	1
CW24	420	MORTAR LOSS IN JOINTS	0.0274	17.15	23.41	2
#V_TRA	#V_ME T	#V_TIP	#V_EXT	#V_AN C	#V_PR O	#V_SEV